TETRAPHOSPHINE LINKERS FOR IMMOBILIZING CATALYSTS AND STUDIES OF POLYMER DEGRADATION MECHANISMS

A Dissertation

by

JOSEPH HUGH FRANKLIN BAKER

Submitted to the Office of Graduate and Professional Studies of
Texas A&M University
in partial fulfillment of the requirements for the degree of

DOCTOR OF PHILOSOPHY

Chair of Committee,	Janet Bluemel
Committee Members,	Hongcai Zhou
	Christian Hilty
	Jodie Lutkenhaus
Head of Department,	Simon North

December 2017

Major Subject: Chemistry

Copyright 2017 Joseph H. Baker

ABSTRACT

The overall goal of the first project of this thesis was to find ways to improve homogeneous catalysts and render them more recyclable and thus improve their lifetimes. One way to generate such superior catalysts is to whether them to solid, insoluble supports. The nature of the latter is crucial for the activities and lifetimes of the catalysts. Flexible linkers such as long alkyl chains allow contact of the catalysts with the surface and potentially their decomposition. Tetraphosphine linkers with rigid tetra*phenyl*element cores had been immobilized previously. The rigid nature of the scaffold ligands prevented interactions with the reactive surface and led to an immobilized Wilkinson's catalyst that could be recycled many times in a batchwise manner. In this new project, in order to test whether further increasing the distance between the immobilized catalyst and the surface would improve the lifetime of the catalysts, *biphenyl* spokes have been incorporated into the tetraphosphine linkers. The catalytic activity of these new catalysts compares favorably with that of previously used flexible linkers.

In the second project of this thesis polyetheretherketone (PEEK) polymers, which are utilized in applications of extreme service environments in the oil and gas industry, are studied. PEEK material is rather tolerant of high temperatures and pressures and chemically comparatively resistant. However, PEEK degrades quite rapidly in the commonly used $ZnBr_2$ containing completion fluids, in combination with the high temperatures and pressures needed for hydraulic fracturing. The degradation of the

polymer leads to machine parts breaking during the operation and results in costly delays in the drilling process.

Therefore, the main goal of the second project of this thesis was to elucidate the molecular mechanisms that lead to the degradation of the polymer, and to define the factors that influence these decomposition pathways.

Mechanistic studies after the identification of the small molecules produced, reveal the simultaneous occurrence of several decomposition pathways. The initial reaction in the PEEK polymer is the C-C bond cleavage at the ketone position. Subsequently, bromination by the $ZnBr_2$ in the completion fluids, other radical based decompositions, and hydrolysis under the acidic conditions take place.

DEDICATION

I would like to dedicate my thesis to my family, labmates and my advisor Dr. Bluemel. I could not have done it without any one of them.

ACKNOWLEDGEMENTS

I was fortunate enough to have a lot of help on the way to becoming a PhD. I first acknowledge my advisor Dr. Janet Bluemel. Regardless of the situation she has always had my back and did anything she could to help me through this PhD program.

I had the privilege of working with two undergrads. Kevin Dong helped run some catalysis experiments and he also assisted with syntheses. Scott Leyendecker also did some syntheses while he was working in the lab with me.

I had many many people help me with some of the analytical techniques I used for this dissertation. Dr. Howard Williams ran some NMR experiments on the cryoprobe. He always produced amazing data and later trained me to do the same with that instrument. Dr. Vladamir Bakhmoutov allowed me to be trained and to operate the solid-state NMR when I needed it and provided assistance when it was needed. Dr. Nattamai Bhuvanesh ran many crystals for me and was very patient as only one made it to this thesis. I also need to acknowledge Dr. Bo Wang for his mass spectrometry help.

I need to thank my fellow group members both current and those that have already graduated. Jackie and Rita both trained me in different areas while we were working together in the Bluemel lab.

Last I need to thank the members of APPEAL. Particularly Dr. Tim Bremner for his guidance throughout my time with APPEAL, and Dr. Hung-Jue Sue for his support, nominations for awards, and for allowing me access to his TGA and DSC.

CONTRIBUTORS AND FUNDING SOURCES

Contributors

This work was supervised by a dissertation committee consisting of the chair Professor Dr. Janet Bluemel, and Professors Dr. Hong-Cai Zhou and Dr. Christian Hilty of the Chemistry Department, and Professor Dr. Jodie Lutkenhaus of the Department of Chemical Engineering.

Some samples were provided to us from Baker Hughes for testing. All other work and work on those samples was completed by the student, under the advisement of Professor Dr. Janet Bluemel of the Department of Chemistry.

Funding Sources

The graduate study was supported by the Robert A. Welch Foundation under grant number A-1706, the National Science Foundation under grant numbers CHE-1300208 and CHE-0840464, and the APPEAL Consortium at Texas A&M University (Co-directors Dr. Hung-Jue Sue and Dr. Tim Bremner).

NOMENCLATURE

δ	chemical shift in ppm
λ	wavelength
^{29}Si	silicon nucleus (NMR)
^{13}C	carbon nucleus (NMR)
^{2}H	deuterium nucleus (NMR)
^{1}H	proton nucleus (NMR)
^{31}P	phosphorus nucleus (NMR)
^{1}H}	proton decoupled
^{31}P}	phosphorus decoupled
Å	Ångstrom
dpb	1,4-diphenoxybenzene
br	broad
Bu	butyl
COSY	COrrelation SpectroscopY (2D NMR)
CP	cross-polarization
CP/MAS	cross-polarization/magic angle spinning
CSA	chemical shift anisotropy
Cy	cyclohexyl

d	doublet (NMR), days
D	deuterium (^{2}H) atom
DCM	dichloromethane
DD	dipolar dephasing
DMSO	dimethylsulfoxide
D_2O	deuterium oxide
eq	equivalents, equatorial (NMR)
FID	free induction decay (NMR)
FT	Fourier Transformation
GC	gas chromatography
h	hours
HRMAS	high-resolution magic angle spinning
HSQC	heteronucular single quantum coherence spectroscopy (2D NMR)
Hz	Hertz
i	ipso
J	scalar coupling constant
IR	infrared
m	multiplet (NMR), medium (IR)
m	meta

MAS	magic angle spinning
Me	methyl
NCPh	benzonitrile
NMR	nuclear magnetic resonance
NOESY	Nuclear Overhauser Effect SpectroscopY (2D NMR)
o	ortho
p	para
Ph	phenyl
ppm	parts per million
py	pyridine
R	alkyl group
RT	RT
s	singlet (NMR), strong (IR)
t	triplet (NMR)
t	tertiary
tert	tertiary
TEM	transmission electron microscopy
THF	tetrahydrofuran
TMEDA	tetramethylethylenediamine

UV	ultraviolet
$\Delta\nu_{1/2}$	signal width at half height
Vis	visible
vs	very strong (IR)
w	weak (IR)

TABLE OF CONTENTS

LIST OF FIGURES

LIST OF SCHEMES

LIST OF TABLES

CHAPTER I

TETRAPHOSPHINES WITH TETRA(BIPHENYL)SILANE AND STANNANE CORES AS RIGID SCAFFOLD LINKERS FOR IMMOBILIZED CATALYSTS

1.1 Introduction

Catalysis represents one of the most central aspects of chemistry. Unfortunately, the "ideal catalyst"[1] with eternal lifetime, superior activity and total selectivity has still not been discovered. Therefore, different approaches have been investigated to improve the removal and recyclability of originally homogeneous catalysts. For example, one successful approach is based on biphasic catalysis using two liquid phases, one fluorous and one conventional organic phase, and controlling their miscibility via temperature under different conditions.[2] In another approach a rhodium catalyst could successfully be adsorbed on a teflon tape and reversibly released into solution for performing as a homogeneous catalyst.[3]

Our group and others have successfully pursued the immobilization of catalysts on solid supports via diverse linkers.[4] Optimally, an immobilized catalyst retains all the qualities of the homogeneous analog, while it allows for easy catalyst separation from the reaction mixture, batchwise recycling, or application in a continuous flow setting.

After experimenting with zirconium phosphate nanoplatelets[5] and various other oxides as support[6], silica[7] remains the most favorable support for immobilized catalysts. Silica can easily be modified with linkers incorporating ethoxysilane groups,[8,9] it

---

* Reproduced in part with permission from Baker, J. H.; Bhuvanesh, N.; Blümel, J. *J. Organomet. Chem.* **2017**, *847*, 193-203. https://doi.org/10.1016/j.jorganchem.2017.03.034
© 2017 Elsevier.

is mechanically robust, stable at higher temperatures, and settles within minutes after the reaction, so that the supernatant containing the products can simply be decanted. After washing the silica, the covalently bound immobilized catalyst can be used for the next catalytic run.

Using bifunctional phosphine linkers incorporating ethoxysilane groups, immobilized nickel catalysts for cyclotrimerization,[10] palladium and copper catalyst systems for Sonogashira reactions,[11] and rhodium catalysts for olefin hydrogenation[12] have been generated. All these catalysts showed unprecedented activities and lifetimes and could be recycled many times.

Nevertheless, some problems remain. For example, neighboring catalyst molecules on the surface can dimerize or agglomerate. Wilkinson's catalyst readily dimerizes already when stirred at room temperature in benzene,[13] and the dimer is catalytically not active. Accordingly, it was found that diluting the immobilized Wilkinson-type catalysts on the surface improved the catalytic performance substantially.[12b,12c] However, diluting surface-bound species entails a relative increase in the bulk of the support material, which is an unpopular scenario in industrial settings. Another, fatal problem arises when linkers decompose upon reaction with silica.[14] Additionally, phosphine linkers incoporating ethoxysilane groups can be transformed into the corresponding ethylphosphonium salts at higher temperatures, which are no longer able to coordinate to metal complexes.[15] The detachment of the catalyst complex from monodentate linkers, a general problem for immobilized catalysts which is typically classified as "leaching", leads to the gradual loss of metal complexes. We have investigated this issue using

palladium complexes by solid-state NMR and found that this problem can only be ameliorated by using favorable chelate linkers.[11a,11b] Finally, homogeneous catalysts that are tethered to the support via linkers with flexible alkyl chains can reach the support surface and decompose or form nanoparticles.[5,12a]

Recently, we have explored a rigid tetraphosphine linker system with tetraphenylelement cores[16] that successfully prevented rhodium catalysts from dimerization and kept the metal centers at a safe distance from the reactive silica surface.[17] Indeed, Wilkinson-type rhodium catalysts with unprecedented activity and selectivity could be obtained by using the rigid tetrahedral linker $[Sn(p\text{-}C_6H_4)PPh_2]_4$.[17]

In this contribution we extend the rigid linker theme and explore whether using the longer biphenyl instead of phenyl units will further improve the immobilized catalysts by preventing dimerization and decomposition by contact with the surface, as the distance between the substituents at the linker should increase from about 10 to 15 Å. For this purpose, diverse new tetraphosphines with tetra(biphenyl)element cores have been synthesized and fully characterized. They have been immobilized on silica and Wilkinson-type rhodium catalysts have been coordinated.

Selected linkers have been tested for their activity and recyclability in the important catalytic olefin hydrogenation[18] because there is already a substantial body of data on rhodium-catalyzed hydrogenation from our group.[12,17] A comparison with the hydrogenation results of other groups, using different catalytic systems, will be interesting as well.[19] Special interest in the work described here is placed on a linker

with a silicon atom at the core instead of a tin atom[17] in order to exclude the participation of the center atom of the linker in the catalytic hydrogenation.

Besides our application as linkers for immobilized catalysts, tetrahedral scaffold-type molecules are also of general interest in other fields. For example, they function as rigid structural elements for metal organic frameworks (MOFs),[20] porous organic and aromatic frameworks (POFs, PAFs)[21] and dendrimers.[22] Furthermore, they are of interest for studying photochemical effects,[23] and for materials chemistry in general.[24]

The most powerful method for characterizing amorphous solids is solid-state NMR spectroscopy.[25] It has been an invaluable tool for characterizing covalently bound linkers, catalysts, and supports, and recently the dynamics surface-adsorbed solid metal complexes could be determined by solid-state NMR analysis.[26] Silica as the support material is very advantageous for solid-state NMR studies as it does not interfere with the measurements as other supports do, for example, alumina containing quadrupolar nuclei,[6] or polymers producing ^{13}C NMR background signals.

In this contribution, new tetraphosphines with tetra(biphenyl)silane and -stannane cores will be synthesized, characterized, immobilized, and tested as linkers for immobilized Wilkinson-type rhodium catalysts for olefin hydrogenation.

1.2 Results and Discussion

1.2.1 Syntheses of Tetra(biphenyl)element Compounds

We have previously reported on tetraphosphines with tetraphenylmethane, tetraphenylsilane, and tetraphenylstannane cores.[16-17] In the following the syntheses of the analogs **1**-**7** (Scheme 1.1) with tetra(biphenyl)silane and -stannane cores are

described. Different strategies for syntheses of rigid tetrahedral aryl systems have been reported in the literature,[27] making use of multiple palladium coupling reactions and boronic acid derivatives, as well as Grignard reagents. For the sake of simplicity and to avoid multiple steps in the synthesis, our approach to the biphenyl systems was analogous to the successful previous syntheses of the tetraphenylelement compounds.[16-17]

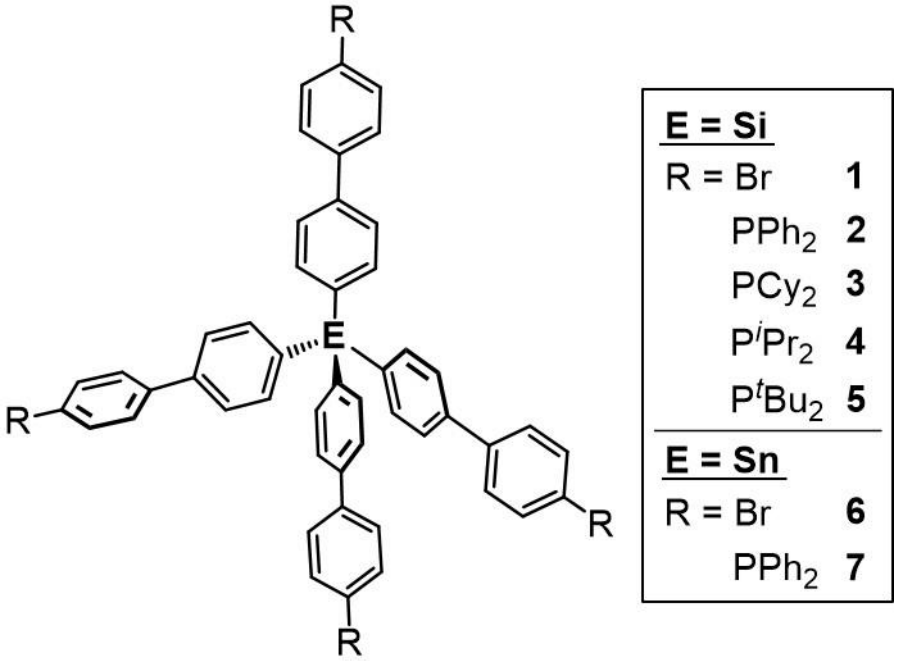

Scheme 1.1. Synthesized and characterized tetra(biphenyl)element compounds **1**-**7**.

Unfortunately, the syntheses of these tetra(biphenyl)element compounds proved to be more difficult as compared to the previously synthesized molecules with tetraphenylelement cores. When the syntheses of the tetrabromo compounds **1** and **6**, the

precursors for **2**-**5** and **7**, are pursued according to Scheme 1.2, the yields are not optimal.

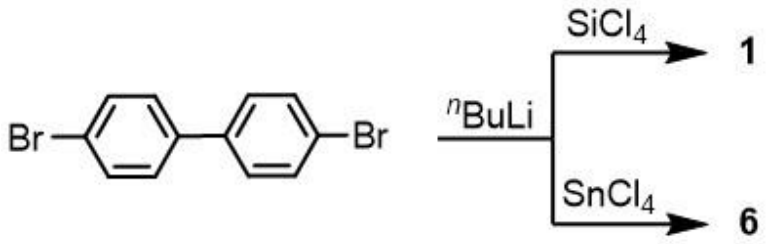

Scheme 1.2. Synthesis of **1** and **6**.

The reason for the lower yields is that 4,4'-dibromobiphenyl can not be monolithiated selectively.[28] In comparison, the monolithiation of 1,4-dibromobenzene is very selective and dilithiation does not even take place when applying an excess of four equivalents of *n*-butyllithium at room temperature (Scheme 1.3).[29] The monolithiation of 4,4'-dibromobiphenyl has been described in the literature and often used as a benchmark for the selectivity of a metalation reaction performed with an organolithium or Grignard reagent. However, even with the use of micromixers and temperatures as low as -78 °C absolute selectivity has not been achieved.[28b] Scheme 3 presents a typical distribution of mono- versus dilithiated dibromobiphenyl, as determined by quenching with methanol. This distribution has been reproduced in our hands, and the percentage of monolithiation of 4,4'-dibromobiphenyl is among the highest reported in the literature to the best of our knowledge.

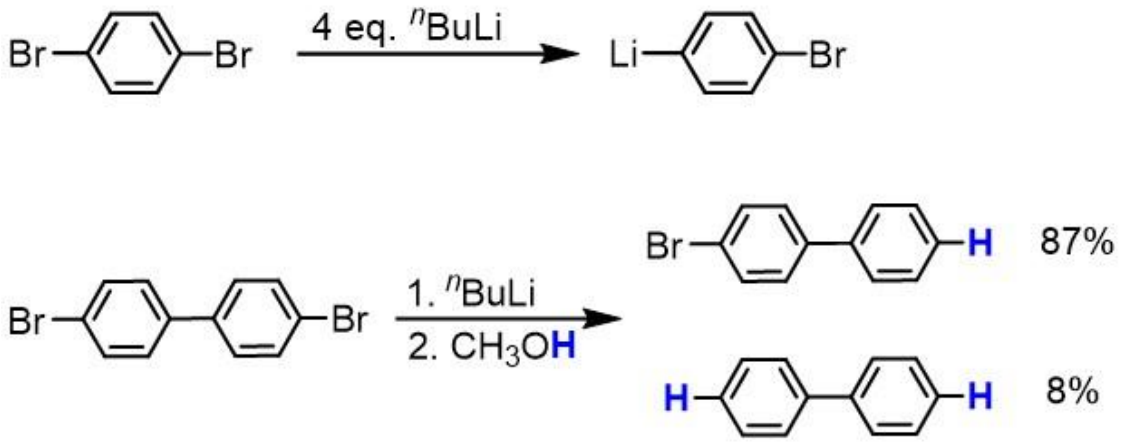

Scheme 1.3. Br/Li exchange products with 1,4-dibromobenzene and 4,4'-dibromobiphenyl (5% remaining starting material).

The lack of selectivity of the monolithiation of 4,4'-dibromobiphenyl is problematic considering that the dilithiated biphenyl can lead to oligomers when being reacted with $SiCl_4$ or $SnCl_4$ in the next step. This further reduces the yields substantially.

After numerous experiments aimed at ameliorating the outcome of the Br/Li exchange, it could be determined that the best approach was to remove the dilithiated byproduct from the reaction mixture prior to proceeding with the following synthetic steps. Fortunately, the dilithiated biphenyl precipitates out of diethyl ether while the monolithiated biphenyl is soluble in ether at room temperature. Therefore, the separation of the ether solution from the precipitate allows the isolation of the mono- and dilithium salts. Starting from the clean lithium salts limits the amounts of side products formed in subsequent reactions. In order to test the quality of the separation by the solubility in ether, the precipitate was quenched with water. The resulting ^{1}H and ^{13}C NMR spectra of the water-quenched precipitate show that it consisted of pure dilithium salt. The signals

in the spectra perfectly match the literature values for biphenyl.[30] The unoptimized yield of the isolated compound after the lithiation was 19%.

Removal of the dilithiated biphenyl prior to subsequent synthesis steps proved to be extremely beneficial for generating the tetrabromo compound **1** (Scheme 1). The compound was obtained with high purity in 88% yield. The product could be crystallized by slow evaporation of acetone producing clear needle-like crystals with high enough quality to subject them to single crystal X-ray analysis (Figure 1.1).[31] There are two distinct molecules in the unit cell which matches the ^{29}Si solid-state NMR spectrum of polycrystalline **1**, which shows two isotropic lines at -14.7 and -15.7 ppm, representing each molecule in the unit cell. This corresponds nicely with our earlier results on tetra(*p*-bromophenyl)silane.[17]

It is interesting to note the very obvious high degree of bending in the biphenyl spokes in the molecules that is most probably enforced by the strain of packing in the crystal lattice (Figure 1.1). In one case, the deviation from linearity amounts to 0.7 Å (Figure 1.1). This feature is reminiscent of the bending of the conjugated oligoacetylene chains described earlier in the context of "molecular wires".[32]

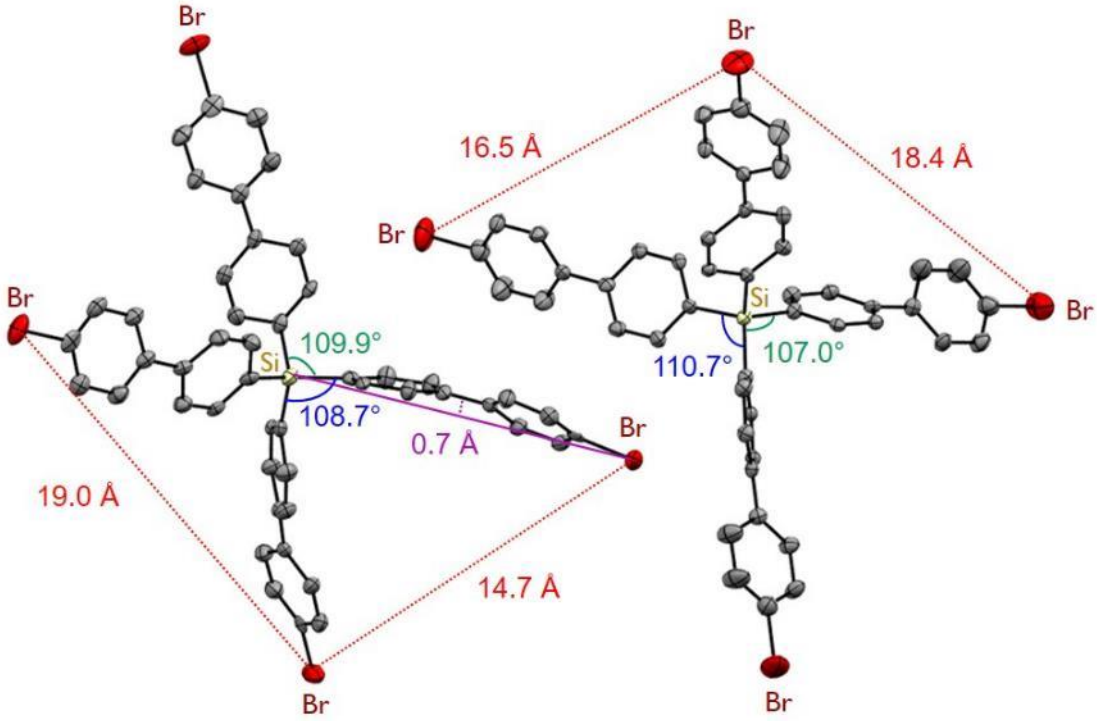

Figure 1.1. Single crystal X-ray structure of **1**. Two independent molecules are displayed.[31]

The bends in **1** create significant changes in the distances between the four bromine atoms in each molecule. The two that are bent towards each other are 14.7 Å apart, whereas the two that are bent away from each other are 19.0 Å apart. The bending even affects the lengths of the biphenyl units, for example, it shortens the length of one "arm" from 10.87 Å on the left to 10.84 Å on the right. It should be noted that in the only other literature known crystal structure of a tetra(biphenyl)silane[33] the bends are smaller. Due to the strains in the crystal lattice, the deviations from the ideal tetrahedral angle of 109.5° are substantial. For example, the right molecule in Figure 1.1 shows two deviating values of 107.0° and 110.7°. This leads again to very different distances

between the bromine atoms within one molecule, 18.4 versus 16.5 Å. The tight packing of the molecules within the crystal lattice results in a comparatively high density of the crystal of 1.58 g/cm^3. Finally, with respect to using these tetrahedral scaffolds as linkers for immobilizing catalysts, it should be noted that they will not clog the large pores of the silica used in the presented studies, which are on average 40 Å in diameter.

Four new tetraphosphines with tetra(biphenyl)silane cores (**2**-**5**) could be synthesized from **1** in high yields (Scheme 1.4). For the tetralithiation of **1** with ether as the solvent, the number of equivalents of ^{n}BuLi had to be increased to 20. This excess proved necessary because even 8 equivalents, an amount that had successfully been used previously with the tetraphenyl core linkers,[17] produced a mixture of starting bromides and phosphines after quenching the reaction with the chlorophosphines at -78 °C. The incomplete tetralithiation was proven by ^{13}C NMR after allowing the reaction mixture to warm to room temperature and stirring for 3 hours. Most diagnostic for this purpose was the ^{13}C NMR signal of the nucleus bound to Br at about 122 ppm. In THF the lithiation proceeds much more rapidly and a significantly smaller amount of ^{n}BuLi is needed, which is more atom economic and beneficial for the subsequent purification.

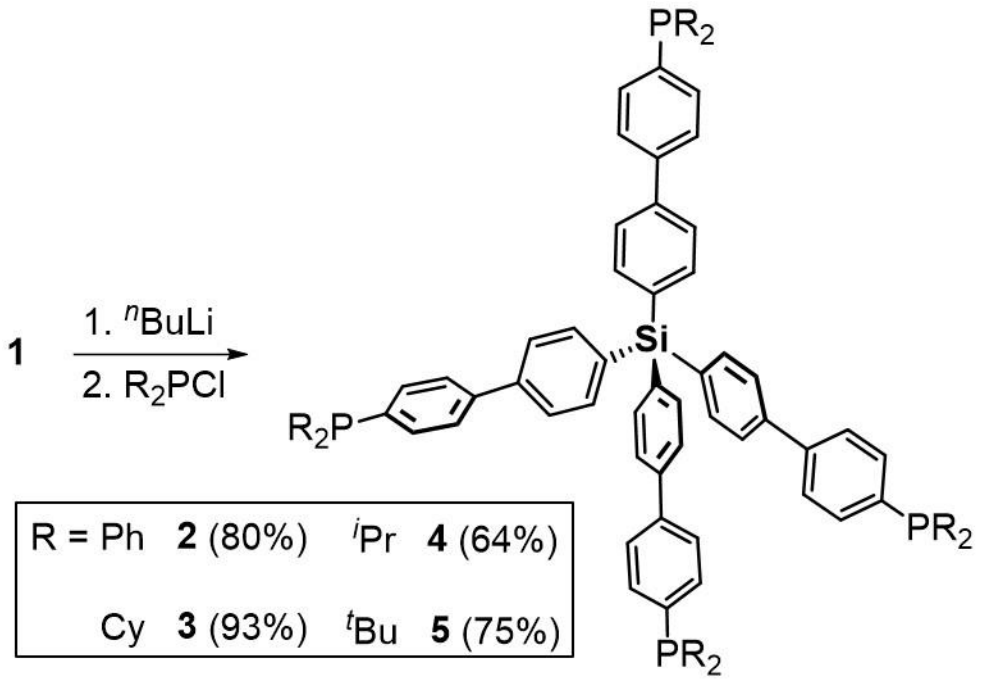

Scheme 1.4. Synthesis of the tetraphosphines **2**-**5**.

After quenching the tetralithium species with the corresponding chlorophosphines, the products **2**-**5** (Scheme 1.4) could easily be isolated in high purities and yields by removing the solvent, adding ethanol to the residue, filtering the suspension through a frit and thoroughly washing the solid product with ethanol. Figure 1.2 displays the solution ^{31}P NMR spectra of the tetraphosphines **2**-**5** in $CDCl_3$. Noteworthy is the absence of phosphorus-containing sideproducts, and that the phosphines are only moderately sensitive towards oxidation and can tolerate chlorinated solvents. Furthermore, there is only one signal for each tetraphosphine, confirming the symmetry of the compounds in solution. None of the signals shows any "fine structure" or additional signals, which would indicate the presence of triphosphines or diphosphines

from stemming from incomplete Br/Li exchange in the previous step of the synthesis (Scheme 4). It should also be noted that the tetraphosphines **2**-**5** are rather soluble in organic solvents, excluding the formation of oligomers.

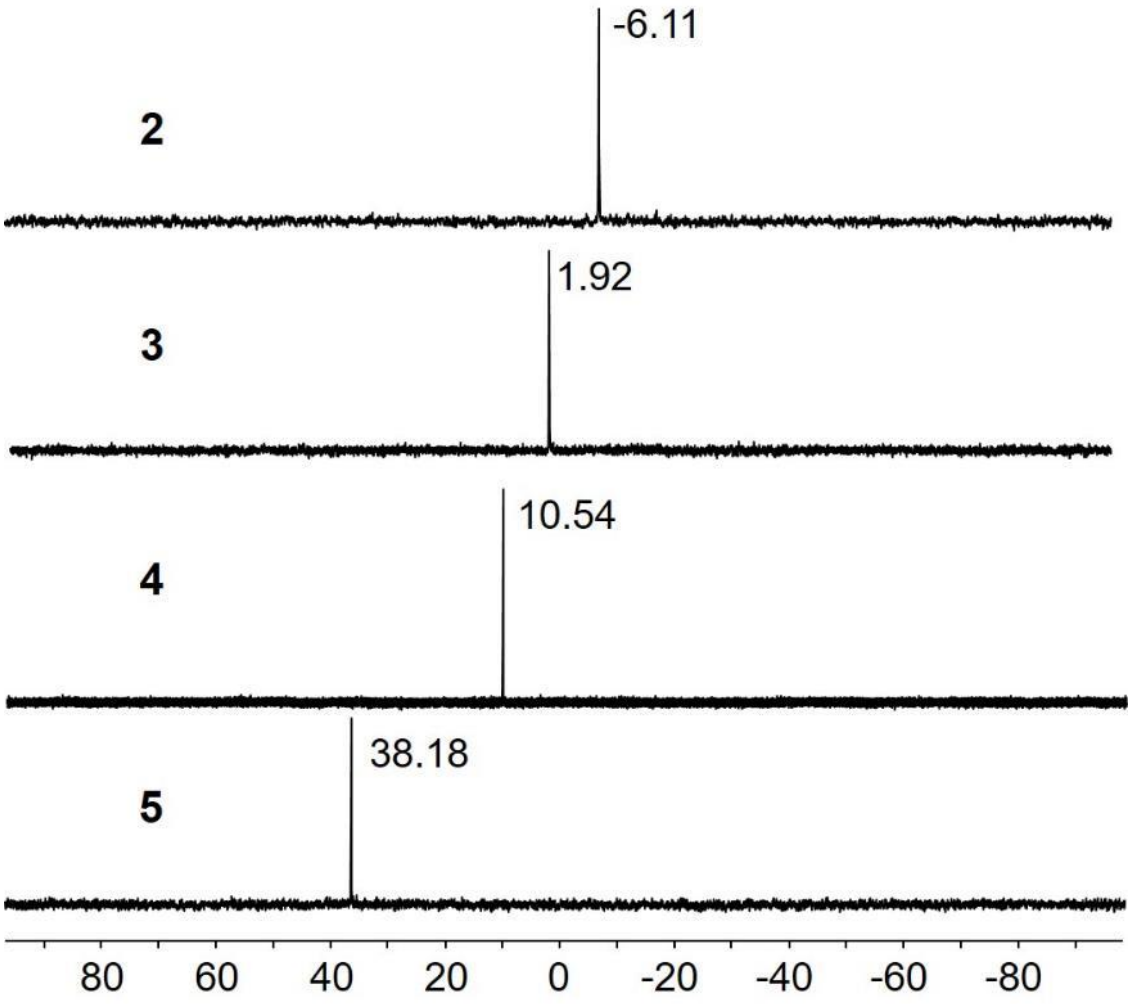

Figure 1.2. ^{31}P NMR spectra of tetraphosphines **2-5**. Numbers next to the signals correspond to the chemical shift values (ppm).

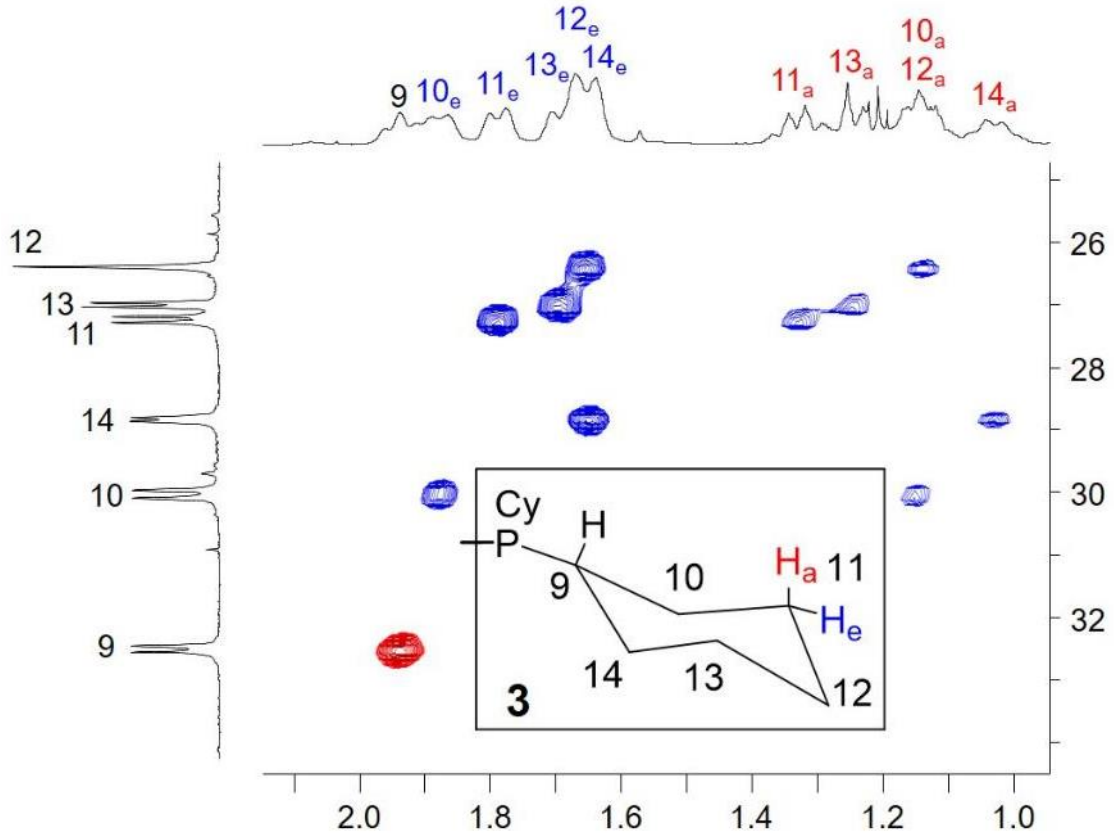

Figure 1.3. $^{13}C,^{1}H$ COSY NMR spectrum of **3** used for signal assignments in the cyclohexyl rings.

The signal assignments in the ^{1}H and ^{13}C NMR spectra are straightforward. They are based on the assignments of the tetraphosphines with tetraphenylelement cores reported earlier,[16-17] and on various two-dimensional techniques, such as $^{1}H,^{1}H$ COSY, and $^{13}C,^{1}H$ COSY NMR spectra. Figure 1.3 shows, for example, the COSY spectrum detailing the assignments of the cyclohexyl ring signals, which are additionally aided by the NMR study of $PhPCy_2$ reported in the literature.[34] Furthermore, especially with respect to distinguishing the signal sets of the two aryl rings in the biphenyl units, the [1-

$^{3}J(^{31}P\text{-}^{13}C)$ values are very helpful. The splittings of the carbon NMR signals due to $^{1\text{-}4}J(^{31}P\text{-}^{13}C)$ couplings can clearly be seen in the ^{13}C NMR trace in Figure 1.3.

1.2.2 Synthesis of Tetra(biphenyl)stannane Scaffolds

The synthesis of the tin compound **6** (Scheme 1.1) in analogy to **1** proceeded without difficulties. However, problems were encountered when trying to obtain the tetraphosphine **7** using the synthesis that was successful for **2**-**5** (Scheme 1.4). The main problem proved to be that a stoichiometric amount of ^{n}BuLi only led to incomplete Br/Li exchange. A twofold excess of ^{n}BuLi, however, resulted in the cleavage of the Sn-C bond and formation of dilithiated biphenyl. This is obvious, for example, when the tetrabromide **6** is treated with eight equivalents of ^{n}BuLi, the reaction is quenched with chlorodiphenylphosphine, and 4,4'-bis(diphenylphosphanyl)-1,1'-biphenyl is obtained as the sole phosphorus containing product (Scheme 5). The product has been identified unequivocally by ^{31}P and ^{13}C NMR spectroscopy and ESI MS. To corroborate the attack of the lithiating reagent at the tin center, tetraphenyltin has been subjected to the same treatment with ^{n}BuLi and chlorodiphenylphosphine, and Ph_3P was found as the sole phosphorus containing product by ^{31}P NMR. Therefore, tetralithiation of **6** is not a viable method for generating **7**, due to the Sn-C bond cleavage under these reaction conditions.

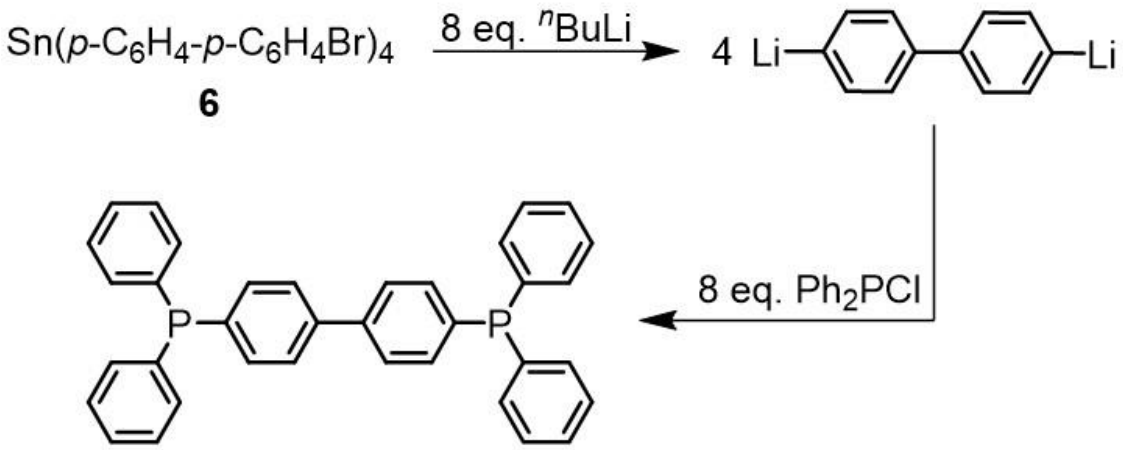

Scheme 1.5. Generating 4,4'-bis(diphenylphosphanyl)-1,1'-biphenyl by attempted tetralithiation of **6**.

Since the tetralithiation of **6** with the, according to experience, required excess of ^{n}BuLi[16-17] did not work, other approaches were tested. Unfortunately, addition of tetramethylethylene diamine (TMEDA) to activate the lithiating reagent[35] did not lead to the desired outcome even after varying the stoichiometries and reaction conditions. For example, using 4 equivalents of ^{n}BuLi only about 50% lithiation was observed. With 6 equivalents about 33% of arylbromides remained, besides decomposed material. Diagnostically most valuable in these attempts proved to be ^{13}C NMR that allowed to identify residual bromoaryl moieties by the *C*-Br signal at 121.8 ppm.

A more successful attempt to synthesize **6** is outlined in Scheme 1.6. In a first step, the phosphine **8** was prepared in high yields using the protocol for obtaining the clean monolithiated biphenyl described above. The lithiation of **8** with ^{n}BuLi had to be optimized next. Since triarylphosphines can undergo a P-C bond cleavage with an excess

of lithiating reagents, only one equivalent of ^{n}BuLi was used with **8**. The optimal conditions were identified as the solvent THF, a reaction temperature of -78 °C, and 1.25 equivalents of TMEDA with respect to ^{n}BuLi. After lithiation of **8** the quench of the reaction mixture with $SnCl_4$ leads to the tetraphosphine **7** (Scheme 1.6) in a respectable crude yield of 52%.

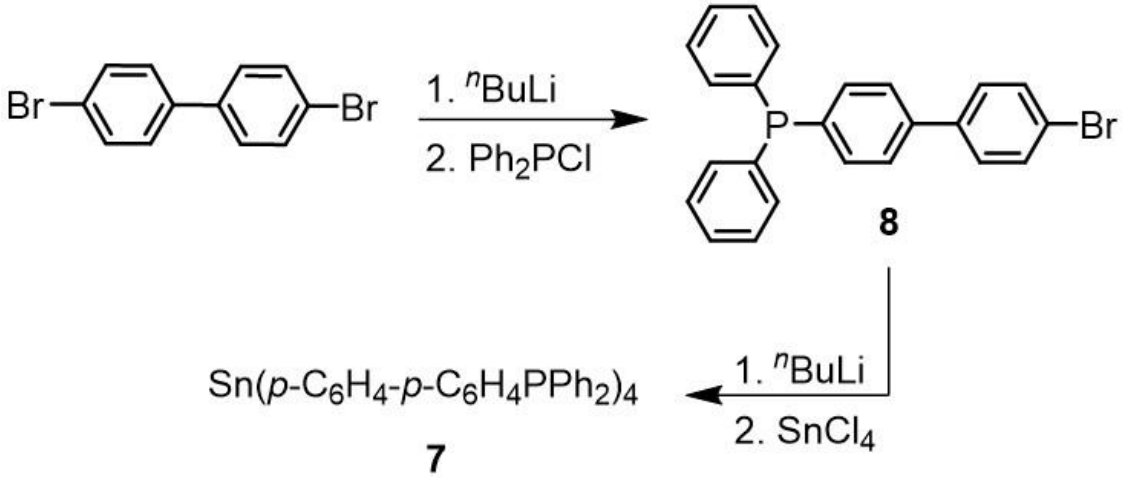

Scheme 1.6. Syntheses of the tetraphosphine **7** via phosphine **8**.

1.2.3 Immobilization of the Tetraphosphine Linkers

It has been described previously that phosphines form ethylphosphonium salts with siloxide counteranions in the presence of ethoxysilanes and silica.[15a,16-17] Alkylation of arylphosphines with chloroalkanes does not take place, for example, Ph_3P does not react with the silane used here, 3-chloropropyltriethoxysilane, in solution even if the components are stirred in toluene at 90 °C for several days.[29] Furthermore, ethoxysilanes do not react with arylphosphines in solution even under these harsh conditions. The

silica surface is needed to activate the ethoxysilanes in order for an ethylgroup to be taken up by the phosphine.[15b] Any di-, tri-, or tetraethoxysilane can form ethylphosphonium salts from phosphines in the presence of silica.[15a] As a precursor in the synthesis of other phosphine linkers, chloropropylethoxysilane is readily available in our lab and was used for the immobilization described here. While the transferred ethyl group clearly stems from the ethoxysilyl group, the siloxide counteranion could be associated with the silica surface, or the ethoxysilyl group. The latter is covalently linked to the surface via the residual ethoxy groups, so the linkage of the phosphine might not only be electrostatic in nature, but it could be a combination of electrostatic cation-anion interactions and covalent bonding to the surface-bound ethoxysilyl group. The latter is most likely, as the phosphonium salts are strongly bound to the support surface, and they cannot be washed off the support even by polar organic solvents. It has been demonstrated with quantitative ^{31}P MAS NMR spectroscopy that in the case of tetrahedral tetraphosphine linker scaffolds with tetraphenylelement cores three phosphine groups are transformed into phosphonium groups that are bound to the surface under the right conditions.[16-17] Due to the tetrahedral geometry, one phosphine group cannot react with surface-activated ethoxysilyl groups and remains unchanged, ready to coordinate a metal complex.[16-17] Using this principle, together with the optimized reaction conditions, the tetraphosphines **2-4** have been immobilized successfully to give **2i-4i** as depicted in Scheme 1.7.

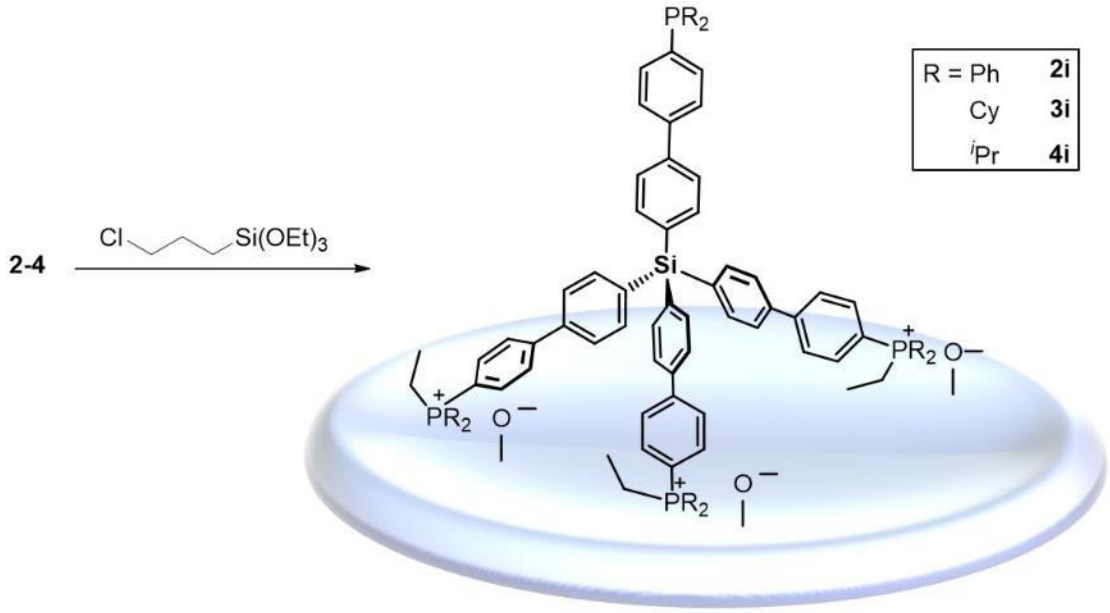

Scheme 1.7. Immobilization of **2-4** on silica to generate **2i**-**4i**.

The number of binding phosphonium groups versus phosphine groups in **2i**-**4i** has been determined by quantitative ^{31}P MAS (Figure 1.4). For this purpose, cross-polarization (CP)[25] cannot be applied, because it would give the phosphonium signals an "unfair" boost in signal intensity due to the many alkyl protons in the ethyl groups that provide optimal magnetization transfer. Therefore, the spectra in Figure 4 have been recorded only with high-power ^{1}H decoupling and MAS without magnetization transfer, combined with a long relaxation delay of 10 s.[16] The chemical shifts of the downfield phosphonium and upfield phosphine resonances lie within the expected ranges.[15-17] The signal intensity ratios are about 3:1 for the phosphonium and the phosphine signals. The exact values are given in Table 1.1. Therefore, it can be concluded that the

tetraphosphines with tetrabiphenylsilane cores match the immobilization behavior of the previously studied tetraphosphines with tetraphenylsilane and -stannan cores.[16-17] The configuration with three "feet" down and one up, as displayed in Scheme 1.7 is confirmed.

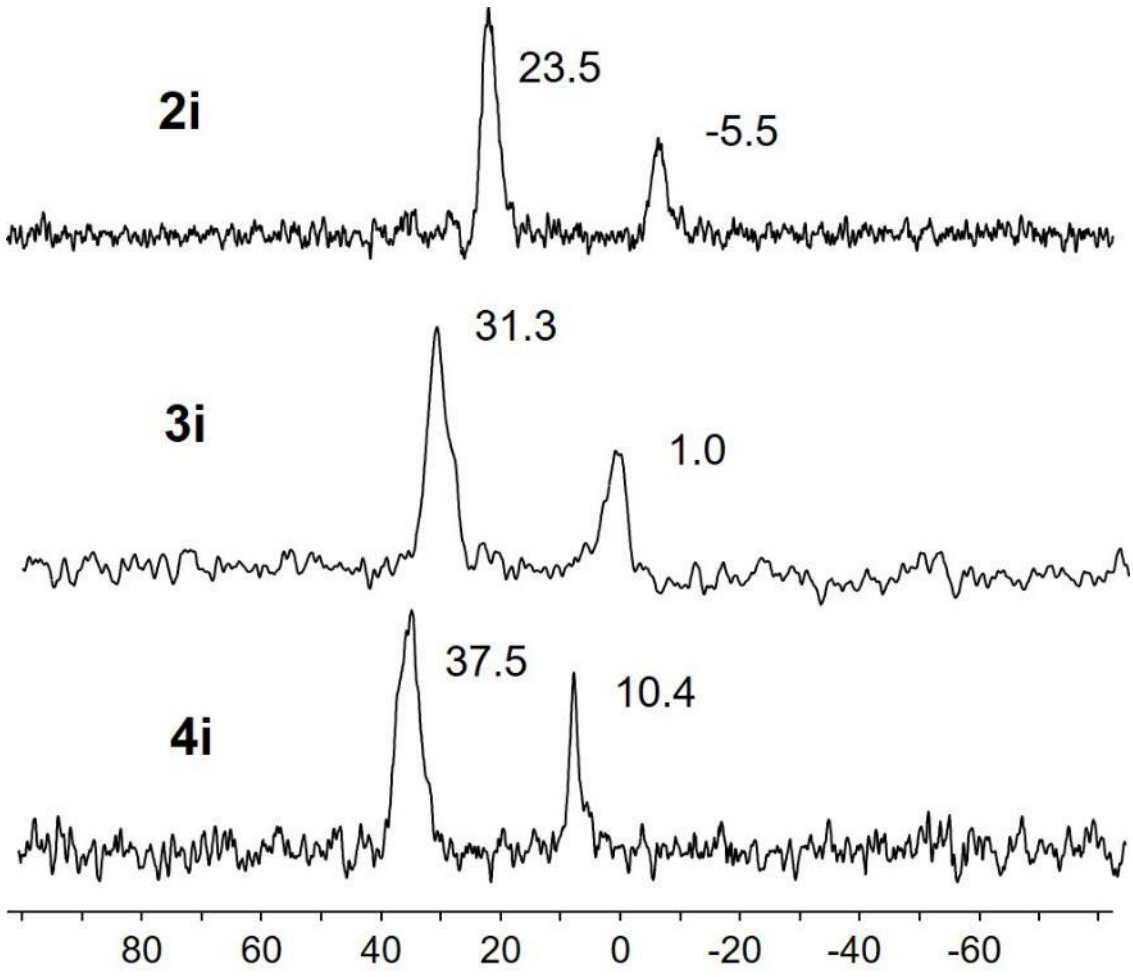

Figure 1.4. ^{31}P MAS NMR spectra of the immobilized linkers **2i-4i**. The chemical shifts are given in ppm.

The surface coverages of **2i**-**4i** have been obtained by reacting the silica with known specific surface area with an amount of tetraphosphine that creates a submonolayer of molecules on the surface, as estimated by the footprint of the tetrahedral molecules, bound by three "feet". After the reaction the supernatants have been checked carefully for residual phosphines by ^{31}P NMR. The surface coverages are given in Table 1.1. They were chosen to lie within the typical range for tetraphosphines with tetraphenylelement cores.[16]

Table 1.1. ^{31}P NMR chemical shifts of resonances from phosphonium (P^+) and phosphine (P) groups, their integral ratios, and surface coverages for **2i**-**4i**.

Immobilized Species	$\delta(^{31}P^+)$	$\delta(^{31}P)$	Ratio P^+:P	Molecules per 100 nm^2
2i	23.5	-5.5	3:1.3	2.9
3i	31.3	1.0	3:1.5	4.7
4i	37.5	10.4	3:1.1	4.0

1.2.4 Generating Immobilized Wilkinson-type Catalysts

The immobilized Rh complexes **2iRh**, **3iRh** and **4iRh** have been generated from the immobilized linker phosphines **2i**, **3i**, and **4i**, respectively. This has been achieved via ligand exchange by stirring the modified silica with a slight excess of Wilkinson's catalyst, $ClRh(PPh_3)_3$, at room temperature (Scheme 1.8). Within a few minutes the originally white silica support turns orange while the color of the supernatant is fading. After decanting the supernatant and washing the silica with toluene to remove PPh_3 and

excess Wilkinson's catalyst, the solid is dried *in vacuo* and subjected to ^{31}P solid-state NMR analysis.

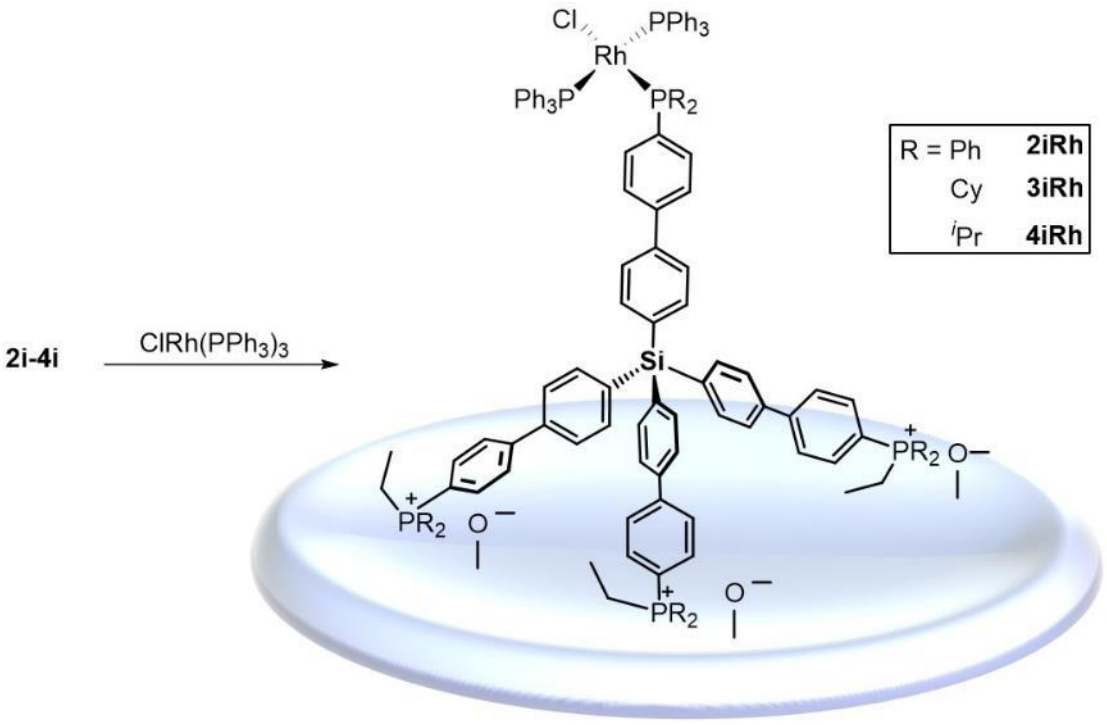

Scheme 1.8. Immobilized catalysts **2iRh**-**4iRh**, generated from **2i**-**4i** by ligand exchange with Wilkinson's catalyst.

The ^{31}P MAS NMR spectra of **2iRh**-**4iRh** show that no surface-adsorbed PPh_3[29] is left in the silica. This can, for example, be seen in Figure 5. Furthermore, the signals of the uncoordinated phosphines vanish when the complexes are bound. This can clearly be seen for **3iRh** versus **3i** (Figure 1.5), where the signal of the PCy_2 group at 1.0 ppm vanishes upon coordination. Unfortunately, the ^{31}P NMR signals of the bound Wilkinson-type catalyst at about 30 ppm[12d] are overlapping with the phosphonium

resonance and are therefore not resolved. However, the presence of unwanted sideproducts, like phosphine oxides, can be excluded, as those resonances[15b,36] would have larger chemical shift anisotropies[25] and their rotational sidebands would show prominently in the spectrum of Figure 1.5.

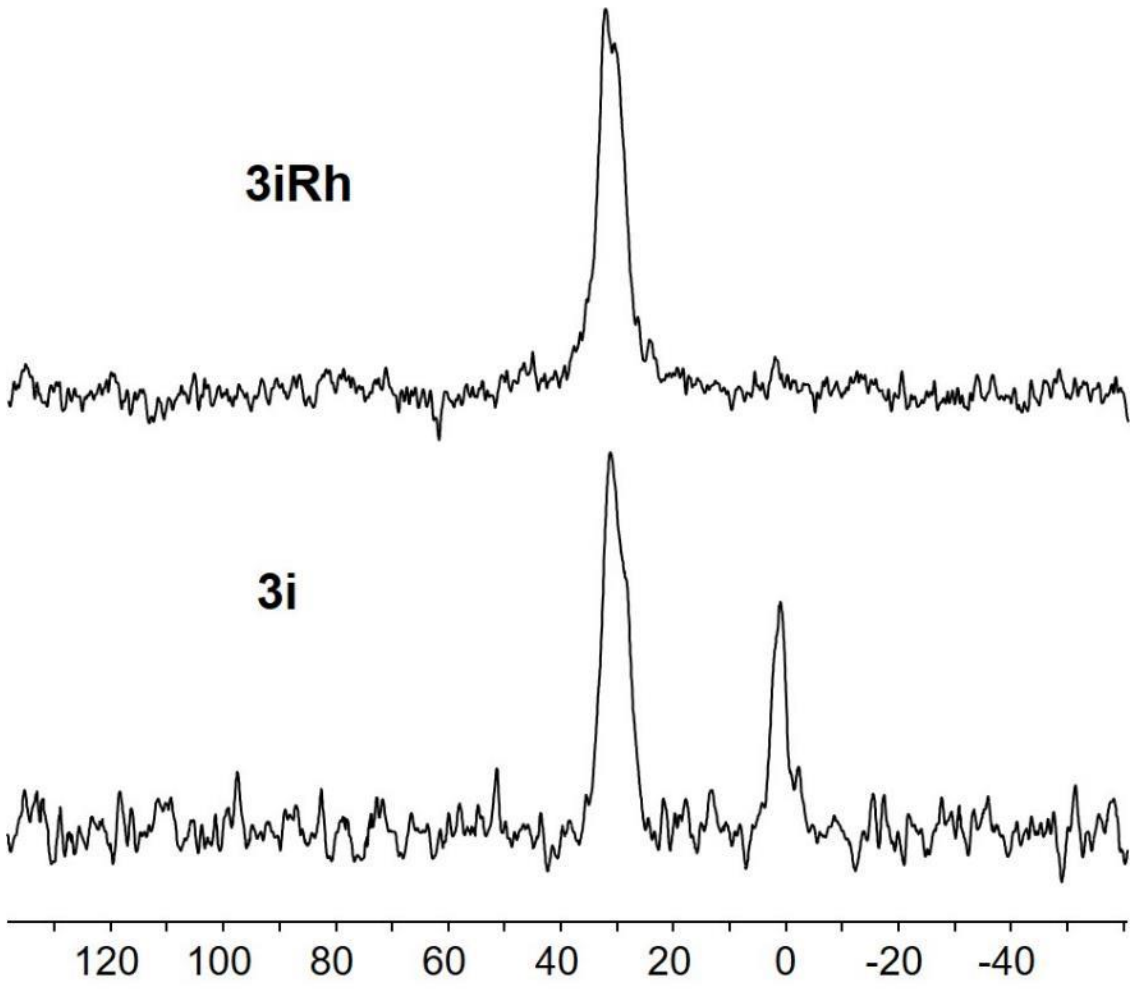

Figure 1.5. ^{31}P MAS spectra of **3i** and **3iRh**.

1.2.5 Catalytic Hydrogenation and Recycling

Rigid scaffold-type linkers are favorable for immobilized catalysts because they hold the catalyst at a safe distance from the reactive support surface. In this way, the premature decomposition of the catalyst by contact with the silica surface is prevented. Furthermore, due to the rigid nature of the linkers, the coordinated metal complexes cannot form dimers[13] with neighboring catalysts that would no longer be catalytically active. It has been demonstrated with Wilkinson-type catalysts immobilized via rigid linkers with tetraphenylstannane cores previously that this is a winning concept.[17] These catalyst could be recycled in a batchwise manner for 30 times, and the olefin conversion remained quantitative within a time window of 60 h.[17]

Regarding, in comparison, the immobilized catalysts **2iRh**-**4iRh**, there are three important aspects. (a) The primary question is whether the catalytic performance and especially the longevity improves when the longer biphenyl units are used in the linkers, since the distances to the support and to neighboring catalysts are increased. (b) Furthermore, it is of interest to check whether the record hydrogenation activity reported for the rigid stannane linker reported previously[17] is due in part to the presence of the tin in the center that could function as an activator for hydrogen. Therefore, linkers with silicon in the center that does not influence catalysis are chosen here. (c) Finally, it will be important to see whether the increased distance between the metal centers prevents nanoparticle formation or at least delays its onset. Nanoparticle formation at an early stage of catalysis, due to reduction of Rh(I) to Rh(0) by hydrogen, has been found primarily when using linker systems with flexible alkyl chains.[5,12a]

In order to allow for optimal comparability with the previous studies, the same substrate, 1-dodecene, reaction conditions, and hydrogenation apparatus were applied for the catalytic runs.[5,12a] The immobilized catalyst **2iRh** was studied first because it provides a silicon atom in the center and the biphenyl "distance holders", but leaves the coordination of the rhodium center by triarylphosphine groups in place for a direct comparison with the results in the literature.[17]

Figure 1.6 shows the results of 1-dodecene hydrogenation with **2iRh**. The data points were collected during each hydrogenation cycle by monitoring the hydrogen gas consumption and recording the volume of H_2 every hour. After each catalytic run, the immobilized catalyst was allowed to settle and the supernatant was removed. The catalyst was subsequently washed with toluene before the next catalytic run was started for checking the batchwise recyclability. Figure 1.6 shows that the catalytic activity decreases gradually with every run. However, even in the eighth run the catalytic reaction is completed within 40 hours. This performance of **2iRh** is comparable to the results obtained previously,[17] but does not exceed expectations. Interestingly, the differences between the completion times are not as pronounced as the ones reported in earlier work using the tetraphenylstannane linker.[17]

Overall, at this point regarding question (a) one can safely conclude that the activity and recyclability of the catalyst is similar when using linkers with phenyl versus biphenyl spacers. Perhaps the advantage that the larger distances between the metal centers and to the surface provides is partly diminished by the linkers filling a large portion of the pore space and thus impeding the diffusion of the substrate. This would

explain why the reaction is slower already in the first run as compared to the characteristics found in earlier work.[17] Experiments with silica with larger pores will be necessary to answer this question.

Furthermore, one can tentatively answer question (b), the catalytic activity and recyclability are not influenced in a major way by the tin[17] versus silicon center of the linker.

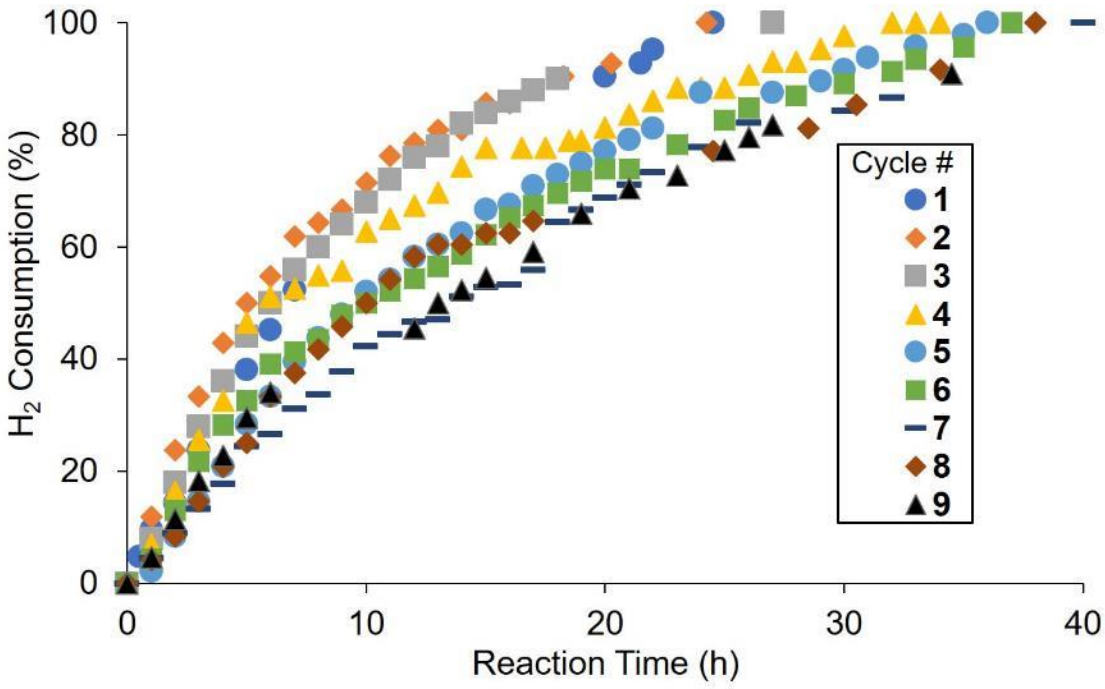

Figure 1.6. Percent consumption of H_2 over time for nine batchwise catalytic runs with **2iRh**. The last catalytic run was performed without inert atmosphere.

One of the factors indicating the presence of rhodium nanoparticles is that catalytic activity persists even when oxygen is allowed into the system. This has been described previously for rhodium nanoparticles formed when Wilkinson-type catalysts were

immobilized via linkers with long alkyl chains.[12a] When **2iRh** was exposed to oxygen for several hours after the eighth run and used for the catalytic cycle 9 without inert gas atmosphere, the catalytic activity deviated only minimally from the one observed in run 8 (Figure 1.6). Therefore, one has to conclude that question (c) can also be answered now. The more extended biphenyl containing linker scaffold does not prevent nanoparticle formation. Taking a close look at the characteristics displayed in Figure 1.6 one might speculate that the onset of nanoparticle formation occurs in the fourth run, when the activity transitions into a slower, then persistent mode. This would mean that the onset of nanoparticle formation is delayed for **2iRh**, as nanoparticles already form within the first hours of the initial run for the catalyst tethered with long alkyl chains.[12a]

In order to test the influence of alkyl versus aryl substituents at the phosphine groups of the biphenyl linker system, the characteristics of the catalyst **4iRh** with P^iPr_2 groups at the ends of the linker scaffold were investigated. Most importantly, this catalyst needs a reaction temperature of 80 °C before it becomes active. When catalyst **4iRh** is then recycled in a batchwise manner, the activity stays about the same in the first three cycles (Figure 1.7). However, in the 4^{th} cycle, the hydrogenation slowed down substantially without obvious reason.

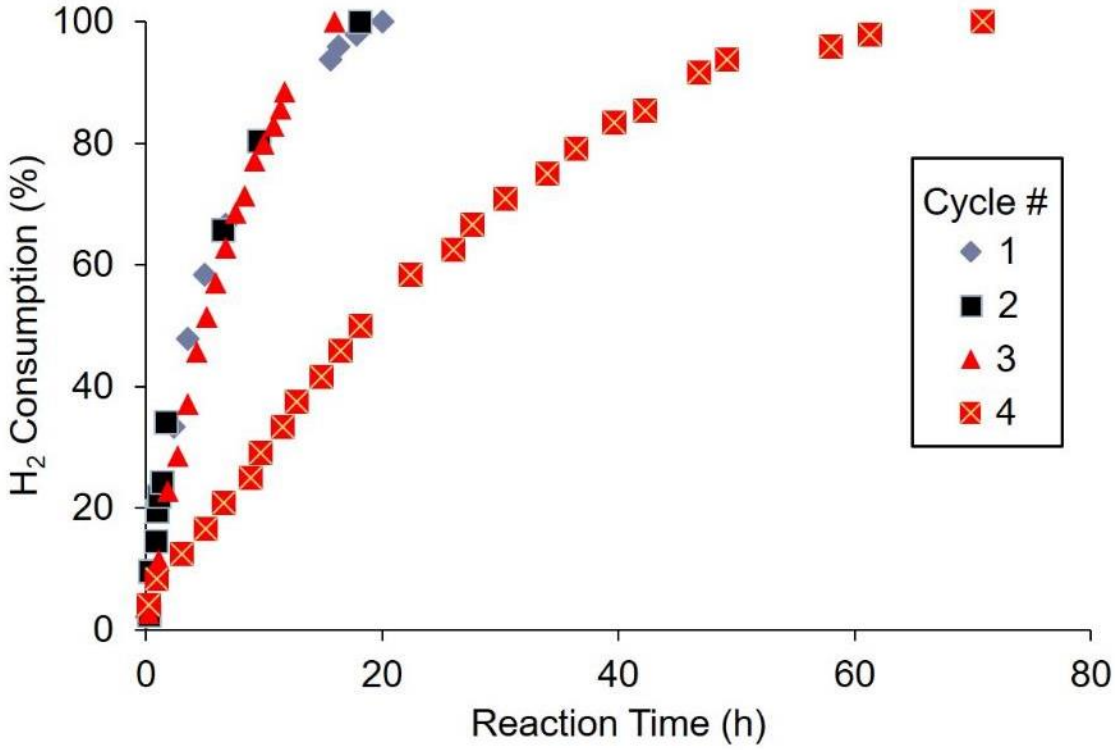

Figure 1.7. Hydrogenation of 1-dodecene using the catalyst **4iRh**.

It is noteworthy with respect to point (c) that the material **4iRh** darkened gradually and turned from originally orange to black at the end of the first run (Figure 1.8). This indicates the eventual formation of nanoparticles which proceeded faster than for **2iRh**. This might be due to the higher temperature applied, or the nature of the phosphine groups. Again, in order to prove the nanoparticle formation during catalysis, the catalyst was exposed to air after the fourth run. The material remained catalytically as active as in run 4, meaning that no molecular rhodium catalyst that would get deactivated under these conditions remained.

Figure 1.8. Images of the catalyst **4iRh** before (left) and after (right) the first hydrogenation cycle. The white spheres are the stirring bar.

1.3 Conclusions

Two tetrabromo compounds (**1**,**6**) and five tetraphosphines (**2-5**,**7**) with tetra(biphenyl)silane and -stannane cores were synthesized and characterized. Three tetraphosphines were immobilized onto silica (**2i-4i**) and investigated by solid-state NMR. Surface-bound Wilkinson-type rhodium catalysts have been generated by ligand exchange with the immobilized linkers (**2iRh-4i-Rh**). Catalytic hydrogenation was performed using the catalysts immobilized with **2iRh** and **4iRh**. The former could be recycled at least 9 times without significant loss of activity and the reactions were completed within 40 hours. Based on the appearance change of the catalyst and previous results with similar linkers with tetraphenylelement cores, the formation of nanoparticles was suggested. Exposing the used catalyst to air and running another catalytic cycle confirmed the presence of catalytically active rhodium nanoparticles that were inert against oxygen. In future work different pore sizes for the support will be explored in combination with **2iRh** to check whether substrate diffusion slows the catalytic runs.

Furthermore, a chelate phosphine group will be attached to the scaffolds which will reduce the detachment of the metal complex as compared to the present monodentate phosphine groups at the linker scaffolds.

1.4 Experimental Section

1.4.1 General Information and Procedures

All reactions were performed by using standard Schlenk techniques or in a glove-box in an oxygen-free argon atmosphere. The solvents were dried by boiling over Na, distilled and kept under nitrogen. Alternatively, they were obtained from a solvent purification system. All the immobilization experiments were carried out with Merck silica 40 (specific surface area 750 m^2/g; average pore size 40 Å; particle size 0.063-0.2 mm) that was dried at 300 °C in *vacuo* (10^{-2} Pa) for at least three days in order to remove adsorbed water and condense surface silanol groups.

The ^{1}H, ^{13}C, and ^{31}P NMR spectra of molecular compounds were recorded at 499.70, 125.66, and 202.28 MHz on a 500 MHz Varian Inova spectrometer. The ^{13}C and ^{31}P NMR spectra were measured with ^{1}H decoupling if not stated otherwise. Neat Ph_2PCl ($\delta(^{31}P)$ = +81.92 ppm) in a capillary centered in the 5 mm NMR tubes was used for referencing the ^{31}P chemical shifts of the compounds. For referencing the ^{1}H and ^{13}C chemical shifts the residual proton signals of the solvent $CDCl_3$ and the carbon signal have been used ($\delta(^{1}H)$ = 7.26 ppm, $\delta(^{13}C)$ = 77.00 ppm). The signal assignments have been obtained by two-dimensional $^{1}H,^{1}H$ COSY, $^{13}C,^{1}H$ HSQC, and $^{13}C,^{1}H$ HMBC NMR measurements, and by comparisons with analogous tetraphosphines with tetraphenylelement cores.[16-17] All ^{31}P solid-state NMR spectra were recorded on a

Bruker Avance 400 spectrometer, equipped with a 2.5 mm broadband MAS probehead and ZrO_2 rotors. The modified silica was loosely filled into the rotors under argon in a glove-box. The relaxation delays were 10 s for all surface-immobilized compounds, and the rotational frequency 4 kHz if not mentioned otherwise. High-power decoupling, but no cross-polarization (CP) [25] was applied. All spectra were recorded at room temperature (298 K). The ^{31}P MAS NMR spectra were referenced with respect to 85% H_3PO_4 (aq) by setting the ^{31}P NMR peak of solid $(NH_4)H_2PO_4$ as the external standard to +0.81 ppm. For the ^{29}Si NMR spectra the external chemical shift standard $Si(SiMe_3)_4$ was used.

1.4.2 Synthesis of Si(*p*-C_6H_4-*p*-$C_6H_4Br)_4$ (**1**):

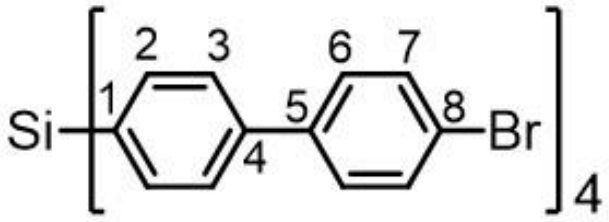

In a 500 ml Schlenk flask, 4,4'-dibromobenzene (2.718 g, 8.71 mmol) is dissolved in 300 ml of ether. The solution is cooled to -78 °C and 4.00 ml of 2.5 M ^{n}BuLi (10.0 mmol) in hexanes is added dropwise. After allowing the mixture to stir at room temperature for 90 min, the solution is separated from the precipitate via cannula and placed in a different 500 ml Schlenk flask. The flask is cooled to -78 °C and 0.20 ml of $SiCl_4$ (0.297 g, 1.75 mmol) is added dropwise. The reaction mixture is warmed to room temperature and stirred overnight. The solvent is then removed in *vacuo* and the crude product is redissolved in 80 ml of chloroform. Flash chromatography is then performed with chloroform as the eluent. The solvent is removed in *vacuo* and the powder is washed 3 times with 20 ml of hexanes. Residual solvent is removed in *vacuo* and the product is obtained as white powder in a yield of 88% (1.470 g, 1.54 mmol). Crystals suitable for single crystal X-ray analysis are grown by taking 10 ml of a saturated solution of **1** in acetone, diluting with another 10 ml, and slowly allowing the solvent to evaporate.

^{1}H NMR ($CDCl_3$, 500.1 MHz): δ = 7.73 (H2, d, ^3J(H-H) = 7.5 Hz), 7.62 (H3, d, ^3J(H-H) = 7.8 Hz), 7.58 (H7, d, ^3J(H-H) = 8.2 Hz), 7.50 (H6, d, ^3J(H-H) = 8.5 Hz) ppm; ^{13}C NMR ($CDCl_3$, 125.8 MHz): δ = 141.28 (C4, s), 139.67 (C5, s), 136.94 (C2, s),

133.07 (C1, s), 131.98 (C6, s), 128.72 (C7, s), 126.50 (C3, s) 121.95 (C8, s) ppm; ^{29}Si NMR ($CDCl_3$, 79.5 MHz): δ = -14.36 ppm; ^{29}Si CP/MAS: δ = -14.7, -15.7 ppm (ν_{rot} = 10 kHz). mp 149 °C.

1.4.3 Synthesis of Si(*p*-C_6H_4-*p*-$C_6H_4PPh_2$)$_4$ (**2**):

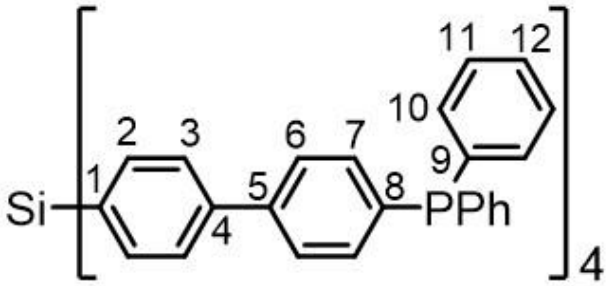

In a 250 ml Schlenk flask, **1** (0.600 g, 0.63 mmol) is dissolved is 75 ml of THF. The solution is cooled to -78 °C and 1.51 ml of 2.5 M ^{n}BuLi (3.8 mmol) in hexanes is added dropwise and the solution is stirred for 90 minutes. Then 0.84 g of $ClPPh_2$ (3.8 mmol) is added dropwise, the reaction mixture is allowed to warm to room temperature and stirred overnight. The solvent is removed in *vacuo* which results in an oil. The product is precipitated with ethanol and filtered onto a frit under N_2. The powder is washed three more times with 25 mL of ethanol and dried in *vacuo*. The product is obtained as 0.695 g of a white powder (0.50 mmol, yield 80%).

^{1}H NMR ($CDCl_3$, 500.1 MHz): δ = 7.72 (H2, d, 3*J*(H-H) = 7.8 Hz), 7.66 (H6, dd, ^{3}*J*(H-H) 7.5 Hz), ^{4}*J*(P-H) = 1.6 Hz), 7.62 (H3, d, ^{3}*J*(H-H) = 7.4 Hz), 7.39 (H7, dd, ^{3}*J*(H-H) = 7.6 Hz, ^{3}*J*(P-H) = 7.6 Hz), 7.37 (H10-H12, m) ppm; ^{13}C NMR ($CDCl_3$, 125.8 MHz): δ 141.70 (C4, s), 141.01 (C5, s), 136.92 (C2, s), 134.18 (C7, d, ^{2}*J*(P-C) = 19.5 Hz), 133.77 (C10, d, ^{2}*J*(P-C) = 19.5 Hz), 133.69 (C1, s), 132.69 (C8, d, ^{1}*J*(P-C) = 18.6 Hz), 130.31 (C9, d, ^{1}*J*(P-C) = 21.4 Hz), 128.79 (C12, s), 128.54 (C11, d, ^{3}*J*(P-C) = 7.0 Hz), 127.15 (C6, d, ^{3}*J*(P-C) = 6.5 Hz), 126.59 (C3, s) ppm; ^{31}P NMR ($CDCl_3$, 162.0 MHz) -6.11 ppm. mp 125 °C. ESI-MS$^+$: [M+1] 1377.37 (96%) and [M+2] 1378.34 (100%) plus decomposition products, calculated 1377.44 (96%), 1378.44 (100%).

1.4.4 Synthesis of Si(*p*-C_6H_4-*p*-$C_6H_4PCy_2)_4$ (**3**):

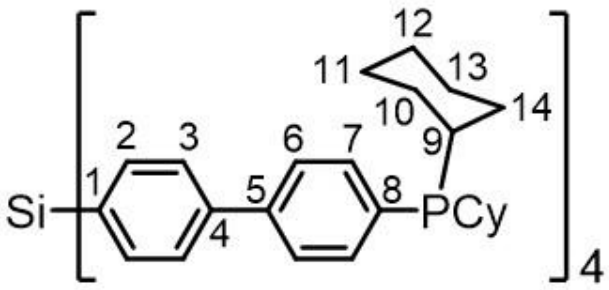

The synthesis of **3** was performed in analogy to the synthesis of **2** described above. Compound **3** was obtained as a white powder in a yield of 93%.

^{1}H NMR ($CDCl_3$, 500.1 MHz): δ = 7.75 (H2, d, ^3J(H-H) = 8.1 Hz), 7.70 (H3, d ^3J(H-H) = 8.3 Hz), 7.64 (H7, d, ^3J(H-H) = 7.8 Hz), 7.56 (H6, dd, ^3J(H-H) = 7.3 Hz, ^3J(P-H) = 7.3 Hz), 1.98-1.66 (9, 10e, 11e, 13e, 12e, 14e, m), 1.43-0.91 (11a, 13a, 10a, 12a, 14a, m) ppm; ^{13}C NMR ($CDCl_3$, 125.8 MHz): δ 141.70 (C4, s), 140.91 (C5, s), 136.91 (C2, s), 135.18 (C7, d, ^2J(P-C) = 19.1 Hz), 134.02 (C8, d, ^1J(P-7C) = 17.7 Hz), 133.05 (C1, s), 126.54 (C6, s), 126.40 (C3, d, ^3J(P-C) = 7.4 Hz), 32.49 (C9, d, ^3J(P-C) = 11.2 Hz), 30.01 (C10, d, (^1J(P-C) = 15.8 Hz), 28.82 (C14, d, ^3J(P-C) = 7.0 Hz), 27.24 (C11, d, ^2J(P-C) = 12.6 Hz), 27.00 (C13, d, ^3J(P-C) = 7.4 Hz), 26.39 (C14, s) ppm; ^{31}P NMR ($CDCl_3$, 162.0 MHz) 1.92 ppm. mp 117 °C. ESI-MS$^+$: [M+1] 1425.78 (96%) and [M+2] 1426.76 (100%) plus decomposition products, calculated 1425.81 (92%), 1426.81 (100%).

1.4.5 Synthesis of Si(*p*-C_6H_4-*p*-$C_6H_4P^iPr_2)_4$ (**4**):

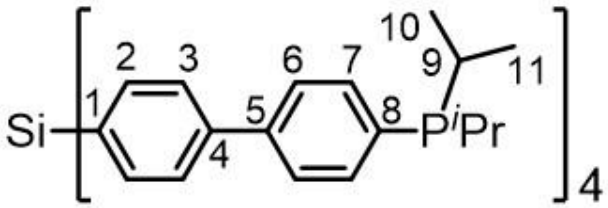

The synthesis of **4** was performed in analogy to the synthesis of **2** described above. Compound **4** was obtained as a white powder in a yield of 64%.

^{1}H NMR ($CDCl_3$, 500.1 MHz): δ = 7.75 (H2, d, ^3J(H-H) = 8.3 Hz), 7.70 (H3, d, ^3J(H-H) = 8.3 Hz), 7.64 (H6, d, ^3J(H-H) = 7.8 Hz), 7.57 (H7, dd, ^3J(H-H) = 8.0 Hz, ^3J(P-H) = 6.6 Hz), 2.16 (H9, m), 1.13 (H10, dd (^3J(H-H) = 7.1 Hz, ^3J(P-H) = 15.1 Hz), 0.98 (H11, dd (^3J(H-H) = 6.9 Hz, ^3J(P-H) = 11.6 Hz) ppm; ^{13}C NMR ($CDCl_3$, 125.8 MHz): δ 141.86 (C4, s), 141.12 (C5, s), 136.93 (C2, s), 135.05 (C7, d, ^2J(P-C) = 18.5 Hz), 134.06 (C8, d, ^1J(P-C) = 16.0 Hz), 133.10 (C1, s), 126.58 (C3, s), 126.46 (C6, d, ^3J(P-C) = 7.6 Hz), 22.79 (C9, d, ^2J(P-C) = 10.9 Hz), 19.86 (C10, d, (^1J(P-C) = 18.5 Hz), 18.79 (C11, d, ^2J(P-C) = 8.4 Hz) ppm; ^{31}P NMR ($CDCl_3$, 162.0 MHz) 10.54 ppm. ^{29}Si NMR ($CDCl_3$, 79.5 MHz): δ = -15.3 ppm. mp 205 °C. ESI-MS$^+$: [M+1] 1105.51 (100%) and [M+2] 1106.49 (78%) plus decomposition products, calculated 1105.56 (100%), 1106.56 (83%).

1.4.6 Synthesis of Si(*p*-C_6H_4-*p*-$C_6H_4P^tBu_2)_4$ (**5**):

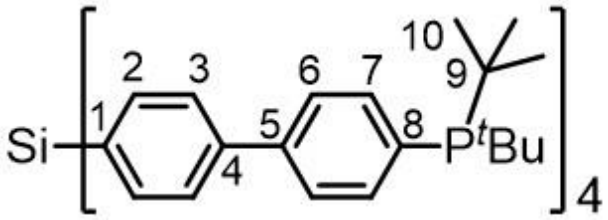

The synthesis of **5** was performed in analogy to the synthesis of **2** described above. Compound **5** was obtained as a white powder in a yield of 75%.

^{1}H NMR ($CDCl_3$, 500.1 MHz): δ = 7.78 (H7, dd, ^3J(H-H) = 7.6 Hz, ^3J(P-H) = 7.6 Hz), 7.75 (H2, d, ^3J(H-H), 7.70 (H3, d, ^3J(H-H) = 7.3 Hz), 7.62 (H6, d, ^3J(H-H) = 7.6 Hz), 1.24 (H10, d, ^3J(P-H) = 11.7 Hz) ppm; ^{13}C NMR ($CDCl_3$, 125.8 MHz): δ 141.80 (C4, s), 141.15 (C5, s), 136.93 (C2, s), 136.90 (C7, d, ^2J(P-C) = 15.2 Hz), 136.15 (C8, d, ^1J(P-C) = 22.0 Hz), 133.10 (C1, s), 126.59 (C3, s), 126.13 (C6, d, ^3J(P-C) = 8.4 Hz), 32.02 (C9, d, ^1J(P-C) = 20.2 Hz), 30.48 (C10, d, (^2J(P-C) = 14.3 Hz); ^{31}P NMR ($CDCl_3$, 162.0 MHz) 38.18 ppm. mp 240 °C (decomp.). ESI-MS$^+$: [M+1] 1217.66 (100%) and [M+2] 1218.66 (100%) plus decomposition products, calculated 1217.69 (100.0%), 1218.69 (92.8%).

1.4.7 Synthesis of Sn(*p*-C_6H_4-*p*-$C_6H_4Br)_4$ (**6**):

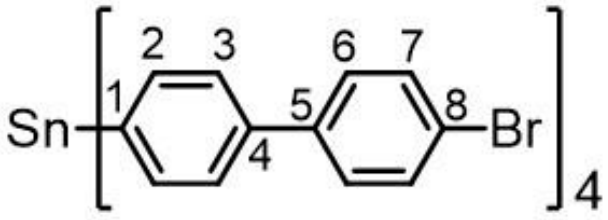

In a 500 ml Schlenk flask, 4,4'-dibromobenzene (2.718 g, 8.71 mmol) is dissolved in 300 ml of ether. The solution is cooled to -78 °C and 6.25 ml of 1.6 M ^{n}BuLi (10.0 mmol) in hexanes is added dropwise. After stirring the mixture at room temperature for 90 min, the supernatant is separated from the precipitate via cannula and placed in a different 500 mL Schlenk flask. The flask is cooled to -78 °C and 0.20 mL of $SnCl_4$ (0.442 g, 1.70 mmol) is added dropwise. The reaction mixture is warmed to room temperature and stirred overnight. The solvent is then removed in *vacuo* and the crude product is redissolved in 80 ml of dichloromethane. Flash chromatography is then performed with dichloromethane as the eluent. The solvent is removed in *vacuo* and the powder is washed 3 times with 20 ml of hexanes. Residual solvent is removed in *vacuo* and the product is obtained as white powder in a yield of 29% (0.660 g, 0.49 mmol).

^{1}H NMR ($CDCl_3$, 500.1 MHz): δ = 7.74 (H2, d, ^3J(H-H) = 8.3 Hz), 7.63 (H3, d, ^3J(H-H) = 8.0 Hz), 7.57 (H7, d, ^3J(H-H) = 8.8 Hz), 7.47 (H6, d, ^3J(H-H) = 8.8 Hz) ppm; ^{13}C NMR ($CDCl_3$, 125.8 MHz): δ = 140.95 (C4, s), 139.75 (C5, s), 137.70 (C2, s), 136.80 (C1, s), 131.98 (C6, s), 128.71 (C7, s), 127.19 (C3, s) 121.88 (C8, s) ppm; ^{119}Sn NMR ($CDCl_3$, 149.2 MHz): δ = -124.3 ppm.

1.4.8 Synthesis of Sn(*p*-C_6H_4-*p*-$C_6H_4PPh_2$)$_4$ (**7**):

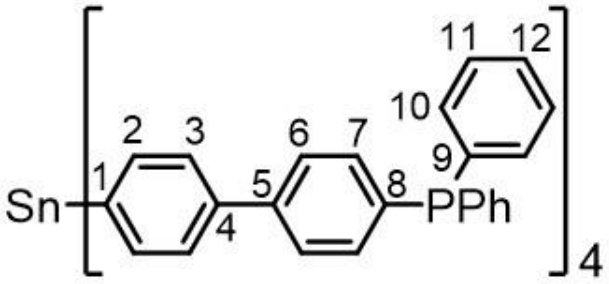

In a 50 ml Schlenk flask, **8** (0.320 g, 0.77 mmol) is dissolved is 10 ml of THF. The solution is cooled to -78 °C and 5 ml of THF, together with ^{n}BuLi (0.77 mmol) and TMEDA (0.97 mmol), is added dropwise while stirring the solution for 5 minutes. Then $SnCl_4$ (0.050 g, 0.19 mmol) is added dropwise, the reaction mixture is allowed to warm to room temperature and stirred overnight. The solution is then passed through SiO_2 and the solvent is removed in *vacuo*. The residue is washed with ethanol and the suspension is filtered through a frit under N_2. The retained powder is washed three more times with 15 ml aliquots of ethanol and dried in *vacuo*. The product is obtained as 0.148 g of a light yellow powder (0.10 mmol, crude yield 52%).

^{1}H NMR ($CDCl_3$, 500.1 MHz): δ = 7.75 (H2, d, 3*J*(H-H) = 7.8 Hz), 7.66 (H6, dd, ^{3}*J*(H-H) 7.5 Hz), ^{4}*J*(P-H) = 1.5 Hz), 7.63 (H3, d, ^{3}*J*(H-H) = 7.8 Hz), 7.40 (H7, dd, ^{3}*J*(H-H) = 8.3 Hz, ^{3}*J*(P-H) = 8.3 Hz), 7.37 (H10-H12, m) ppm; ^{13}C NMR ($CDCl_3$, 125.8 MHz): δ 141.70 (C4, s), 141.01 (C5, s), 136.92 (C2, s), 136.82 (C1, s), 134.20 (C7, d, ^{2}*J*(P-C) = 19.6 Hz), 133.79 (C10, d, ^{2}*J*(P-C) = 19.4 Hz), 132.69 (C8, d, ^{1}*J*(P-C) = 17.4 Hz), 132.31 (C9, d, ^{1}*J*(P-C) = 25.5 Hz), 128.81 (C12, s), 128.57 (C11, d, ^{3}*J*(P-C) = 7.0 Hz), 127.22 (C3, s), 127.16 (C6, d, ^{3}*J*(P-C) = 7.0 Hz) ppm; ^{31}P NMR ($CDCl_3$, 162.0 MHz) -6.12 ppm.

1.4.9 Synthesis of *p*-BrC_6H_4-*p*-$C_6H_4PPh_2$ (**8**):

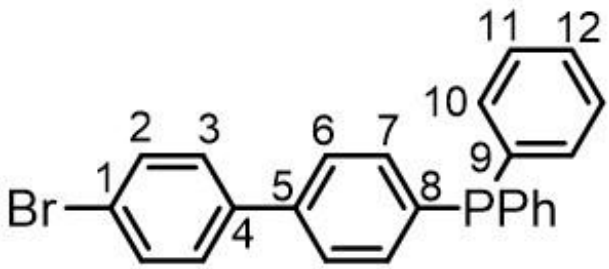

In a 500 mL Schlenk flask, 4,4'-dibromobenzene (1.952 g, 6.26 mmol) is dissolved in 350 ml of ether. The solution is cooled to -78 °C and 4.30 mL of 1.6 M ^{n}BuLi (6.9 mmol) in hexanes is added dropwise. After allowing the mixture to stir at room temperature for 90 min, the solution is separated from the precipitate via cannula and placed in a different 500 ml Schlenk flask. The flask is cooled to -78 °C and 1.12 ml of $ClPPh_2$ (6.9 mmol) is added. The reaction mixture is warmed to room temperature and stirred overnight. The solvent is then removed in *vacuo* and the crude product is filtered through a frit and washed 3 times with 20 ml of ethanol. The residual ethanol is removed in *vacuo* and the product is obtained as a white powder in a yield of 48% (1.230 g, 2.95 mmol).

^{1}H NMR ($CDCl_3$, 500.1 MHz): δ = 7.57 (H2, d, ^{3}J(H-H) = 8.3 Hz), 7.53 (H6, d, ^{3}J(H-H) = 7.8 Hz), 7.47 (H3, d, ^{3}J(H-H) = 8.3 Hz), 7.39 (H7), 7.37 (H10-12) ppm; ^{13}C NMR ($CDCl_3$, 125.8 MHz): δ = 140.17 (C5, s), 139.41 (C4, s), 136.96 (C9, d, ^{1}J(P-C) = 10.2 Hz), 136.75 (C8, d, ^{1}J(P-C) = 10.2 Hz), 134.43 (C7, d, ^{2}J(P-C) = 19.5 Hz), 133.75 (C10, d, ^{2}J(P-C) = 19.5 Hz) 131.93 (C2, s), 128.83 (C3, s), 128.63 (C12, s), 128.56 (C11, d, ^{3}J(P-C) = 7.0 Hz) 126.92 (C6, d, ^{3}J(P-C) = 7.0 Hz), 121.83 (C1, s) ppm; ^{31}P NMR ($CDCl_3$, 162.0 MHz) -6.17 ppm.

1.4.10 Immobilization of Si(*p*-C_6H_4-*p*-$C_6H_4PPh_2$)$_4$ to give **2i**:

Immobilization of **2** on SiO_2 via three phosphonium groups: 2.480 g of rigorously dried SiO_2 is suspended in 10 ml of toluene, and a solution of 0.120 g (0.08 mmol) of **2** in 20 ml of toluene, together with 1.70 g (7.0 mmol) of $Cl(CH_2)_3Si(OEt)_3$ is added. The mixture is heated to 90 °C and stirred for 6 d in a gas storage vessel. After cooling to ambient temperature and allowing the silica to settle, the supernatant is decanted. Then the silica is washed with three 25 ml aliquots of toluene and dried in *vacuo*. Since no traces of phosphorus containing substances are found in the supernatant, the surface coverage can be determined to be about 2.9 linker molecules per 100 nm^2 of silica surface. ^{31}P MAS (quantitative): δ_{iso} = 23.5 (*P*Ph_2Et^+), -5.5 ppm (*P*Ph_2), intensity ratio 3.0:1.3.

1.4.11 Immobilization of Si(*p*-C_6H_4-*p*-$C_6H_4PCy_2$)$_4$ to give **3i**:

The immobilization procedures for **3i** was analogous to the one described above for **2i**. Surface coverage: 4.7 particles/100 nm^2, ^{31}P MAS: 31.3 ppm (PCy_2Et^+), 1.0 ppm (PCy_2), intensity ratio 3.0:1.5.

1.4.12 Immobilization of Si(*p*-C_6H_4-*p*-$C_6H_4P^iPr_2$)$_4$ to give **4i**:

The immobilization procedure for **4i** was analogous to the one described above for **2i**. Surface coverage of 4.0 particles/100 nm^2, ^{31}P MAS: 37.4 ppm ($P^iPr_2Et^+$), 10.4 ppm (P^iPr_2), intensity ratio 3.0:1.1.

1.4.13 Generating Immobilized Catalysts **2iRh**, **3iRh** and **4iRh**:

The linker-modified silica **2i-4i** are suspended in 20 ml of toluene and combined with a solution of $ClRh(PPh_3)_3$ (slight excess, 1.1 mmol per 1 mmol of linker molecule)

in 10 ml of toluene. After stirring for 5 h at ambient temperature, the silica is allowed to settle and the supernatant is decanted. The silica is washed with three 15 ml aliquots of toluene to remove excess $ClRh(PPh_3)_3$ and PPh_3, and dried in *vacuo*. The surface coverages are calculated based on the fact that no signals for uncoordinated PR_2 (R = Ph, Cy, ^{i}Pr) groups are visible in the ^{31}P CP/MAS spectra, and the knowledge of the linker surface coverages. For **2iRh** 2.9 Rh complexes, **3iRh** 4.7 Rh complexes, and for **4iRh** 4.0 Rh complexes are bound on 100 nm^2 of silica surface.

1.4.14 General Hydrogenation Procedure

Immobilized catalyst **2iRh** (240 mg, containing 10 mg of Wilkinson's catalyst, corresponding to 0.010 mmol Rh) is suspended in 5 ml of toluene in a Schlenk flask. The mixture appears opaque and orange/pink in color. The flask is then attached to the hydrogenation apparatus described earlier[12d] and 1 mmol of 1-dodecene, dissolved in toluene (5 ml), is added to the suspension of **2iRh** with a syringe through the stopcock. Subsequently the suspension is stirred vigorously and the hydrogen consumption is monitored. After complete substrate conversion the catalyst is allowed to settle, the supernatant is removed via syringe and the material is washed three times with 5 ml of toluene. To start the second and following cycles, fresh toluene is added and the described procedure is repeated.

CHAPTER II

SYNTHESES AND TREATMENT OF NOVEL PEEK MODEL COMPOUNDS WITH COMPLETION FLUID AND BROMINATION OF PEEK

2.1 Introduction

Polyaryletherketones (PAEK) represent an important group within the family of thermoplastic polymers.[37] PEEK (polyetheretherketone) (Scheme 2.1) constitutes one part of the PAEK polymer family and is the most widely utilized for applications where high temperatures, high differential pressures and corrosive environments are encountered. However, $ZnBr_2$ completion fluids which are often used in the most demanding downhole environments, have been long known in industry to greatly shorten the lifetime of PEEK components. Therefore, in this project the determination of the specific chemical changes to PEEK under HP/HT (high pressure/high temperature) conditions with $ZnBr_2$ fluids was sought after to understand the predominant decomposition pathways and to offer solutions to this costly problem.

PEEK is a semi-crystalline polymer which is essentially insoluble in conventional organic solvents and water and therefore the polymer itself is difficult to work with. Many studies have been completed using solid-state NMR as well as IR. These investigations show chemical as well as crystallinity changes within the PEEK polymer. However, none of these methods provide detailed enough information to define a mechanism of degradation to a satisfactory level. High resolution techniques needed to identify the chemical changes involved, such as NMR of liquids and mass spectrometry (MS), are not accessible without dissolving the material. To mimic the degradation

mechanisms with the capability of solubilizing all of the initial material, two novel model compounds, **1** and **2**, were synthesized and fully characterized (Scheme 2.1). Both model compounds contain the same keto and bisarylether functional groups in the same sequence as the actual PEEK polymer. The only difference are the terminal methyl groups of **1**, which further increase the solubility.

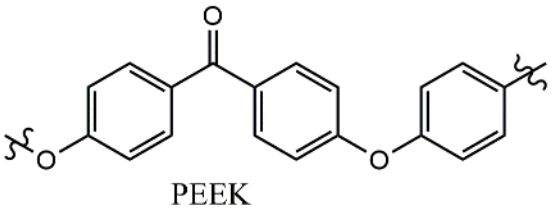

PEEK

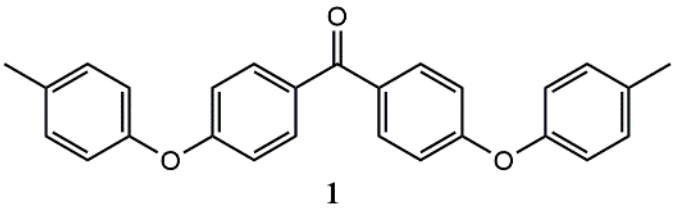

1

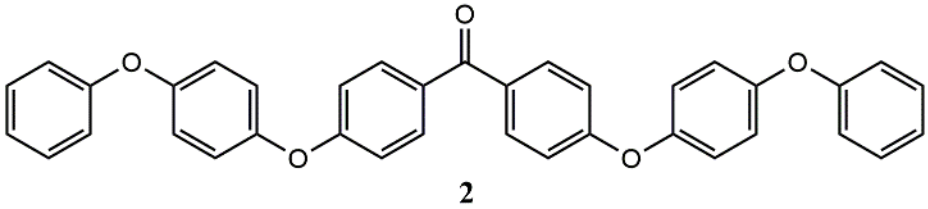

2

Scheme 2.1. Structures of polyetheretherketone (PEEK) and molecular model compounds **1** and **2**.

2.2 Results and Discussion

2.2.1 Syntheses of Model Compounds

To mimic PEEK and facilitate the decomposition studies, the model compounds **1** and **2** (Scheme 2.1) were required to have a minimum number of aryl ether linkages as well as diaryl ketone groups. PEEK contains activated benzene rings that are susceptible to electrophilic aromatic substitution. Under extreme temperatures radical pathways are

also expected as found in other studies.[37] It is important to note that none of these studies were completed in an acidic environment prior to our work.

Both model compounds were synthesized mimicking procedures developed previously for the nucleophilic aromatic substitution of either *p*-difluorobenzophenone or *p*-dichlorobenzophenone.[38] This nucleophilic substitution route is also utilized in most modern PEEK polymer syntheses.[39] This method produces a linear straight chain polymer with only little branching. The targeted compounds **1** and **2** were isolated in very pure form after the nucleophilic substitution and with high yields (Schemes 2.2 and 2.3, respectively).

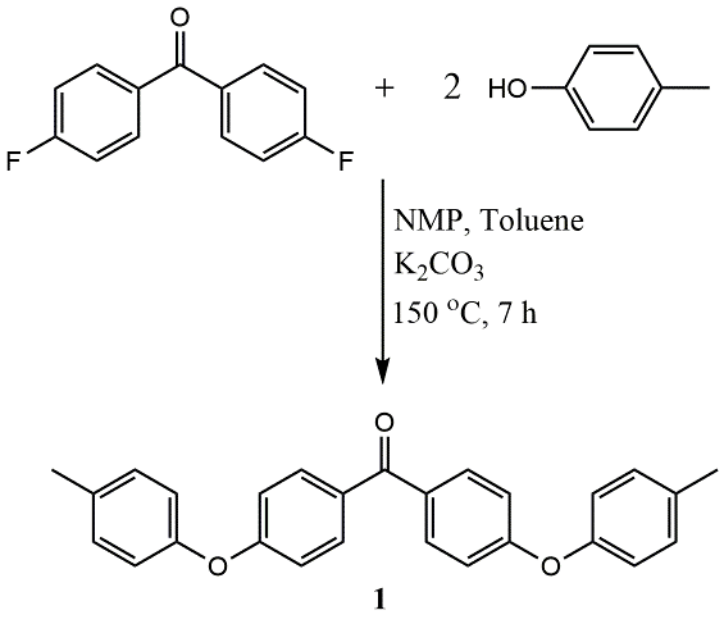

1

Scheme 2.2. Synthesis of model compound **1**.

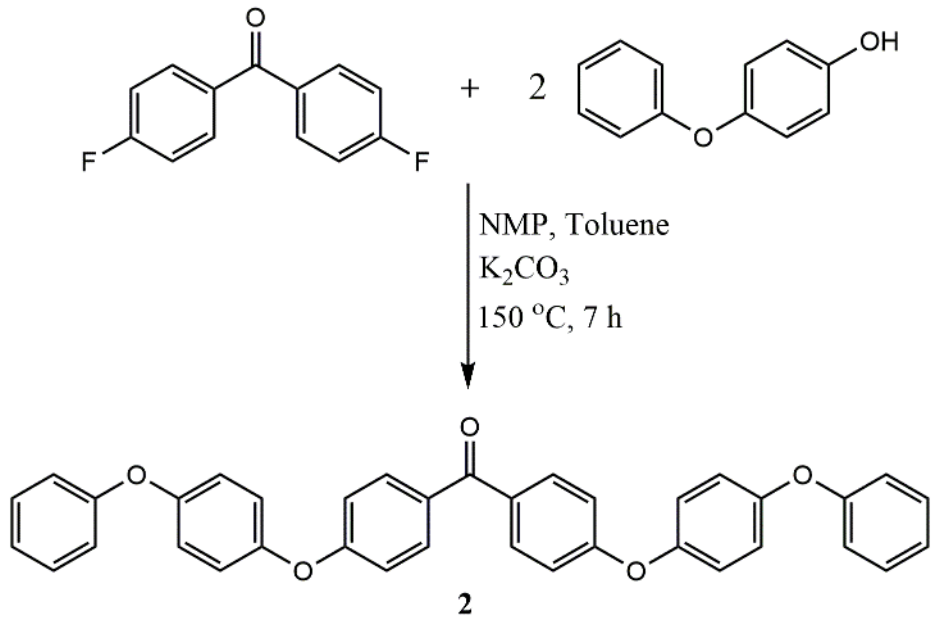

Scheme 2.3. Synthesis of model compound **2**.

2.2.2 Treatment of Model Compounds under HP/HT Conditions with $ZnBr_2$ Completion Fluid

Both model compounds were exposed to the same extreme conditions under which even the PEEK polymer degrades (Figure 2.1). The results were studied via high resolution solution NMR spectroscopy and mass spectrometry. After exposure to a fluid composed of 4.25 M $ZnBr_2$ and 2.65 M $CaBr_2$ at a temperature of 260 °C for 48 hours, both model compounds were found to be brominated at the aryl rings. Model compound **1** was shown via MALDI-MS to also form larger compounds (Figure 2.1). The latter mechanism would mimic cross linking of the polymer strands. Interestingly, none of the ketone signals were detectable in the ^{13}C NMR spectra after the treatment of **1** and **2**. Considerable amounts of material that was insoluble in chloroform had formed in both

cases after the high temperature treatments. This was confirmed by mass measurements after extraction of the filtered solid with chloroform.

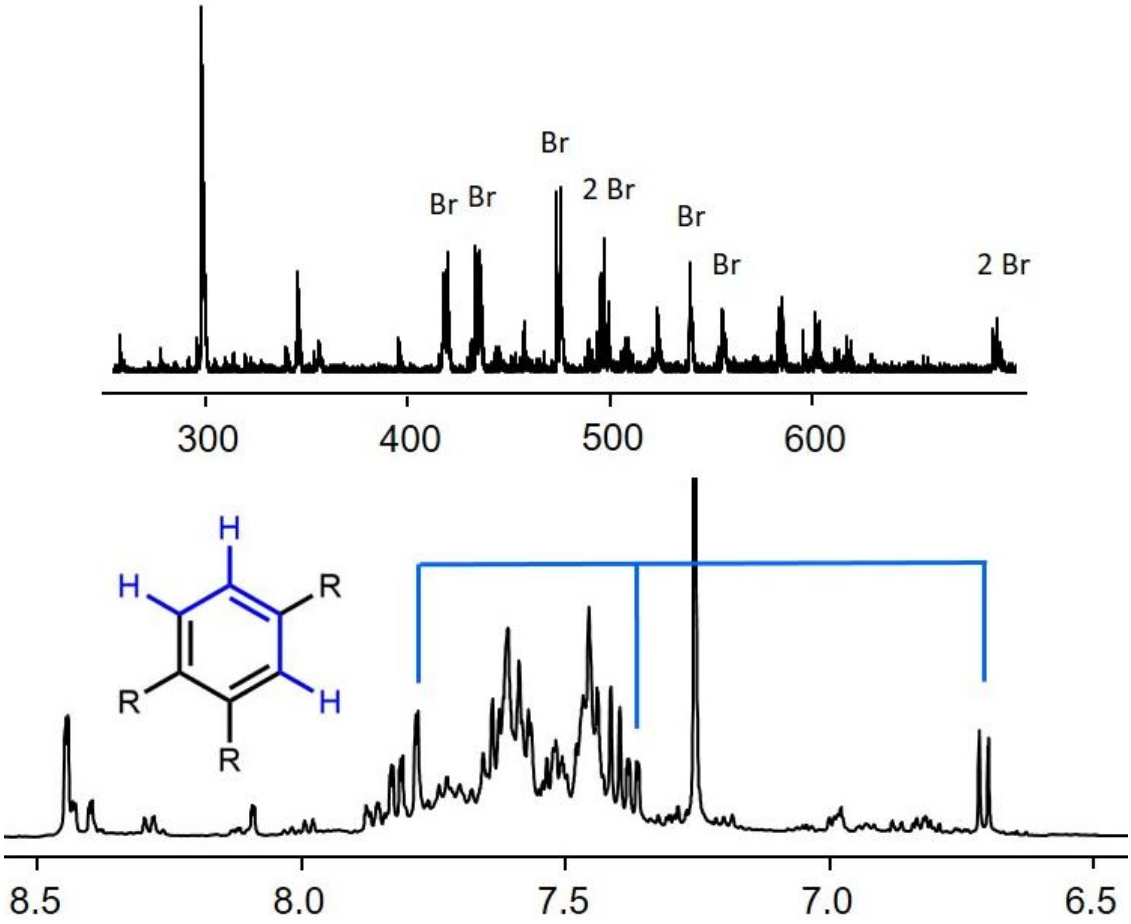

Figure 2.1. MALDI-MS (top) and ^{1}H NMR (bottom) of resulting soluble **1** after treatment with 4.25 M $ZnBr_2$/2.65 M $CaBr_2$ completion fluid for 48 hours at 260 °C.

2.2.3 Low Temperature Exposure of Model Compounds in a Completion Fluid and Individual Components Thereof

Since both model compounds were fully degraded after a short period of exposure at HP/HT in the completion fluid, long term treatments were completed at the lower temperature of 90 °C. This limits the degradation pathways to those chemically, but not

thermally induced. Experiments with pure water were completed and no chemical changes were seen. In the more corrosive fluids, however, substantial chemical changes are seen by ^{1}H NMR. In general, **2** proved more resistant to the treatments. The methyl groups on **1** were oxidized to aldehydes in the concentrated 17.8 M $ZnBr_2$ fluid, as evidenced by the characteristic ^{1}H NMR signals at 9.96 ppm. The major conclusion that can be drawn from the resulting spectra of these low temperature treatments (Figure 2.2) is that increasing the concentration of $ZnBr_2$ does cause faster chemical changes to the model compounds even at this much lower temperature of 90 °C. The spectra were calibrated with respect to the standard $CHDCl_2$ in a centered capillary with a resonance at 5.30 ppm.

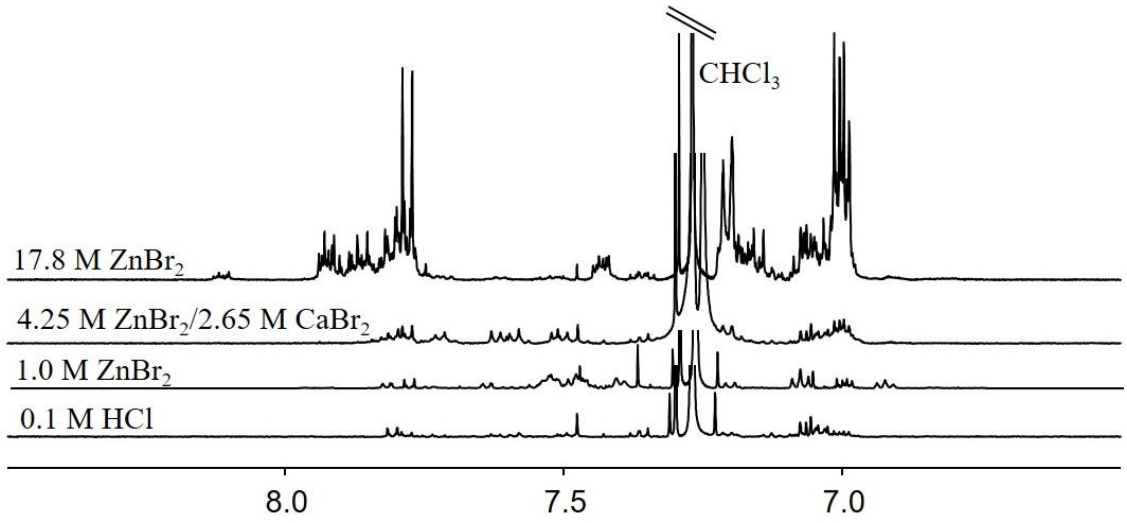

Figure 2.2. Chloroform extracts of **1** after treatment at 90 °C for 17 days in different aqueous solutions.

2.2.4 Bromination of Model Compounds with Liquid Br_2

Since bromination was occurring when the model compounds were treated under HP/HT conditions in the $ZnBr_2$ containing fluid, it was sought to determine the effects of bromination on the PEEK polymer. As the first step, the bromination was explored using the model compounds. The completion fluids are aqueous in nature, so we initially tried to brominate **1** and **2** using H_2O as the solvent (Scheme 2.4). The model compounds are completely insoluble in water. A prefabricated aqueous Br_2 solution added to the suspension of the model compounds did not result in any brominated products. However, at low temperatures bromination occurred readily when neat Br_2 was brought into contact with the model compounds.

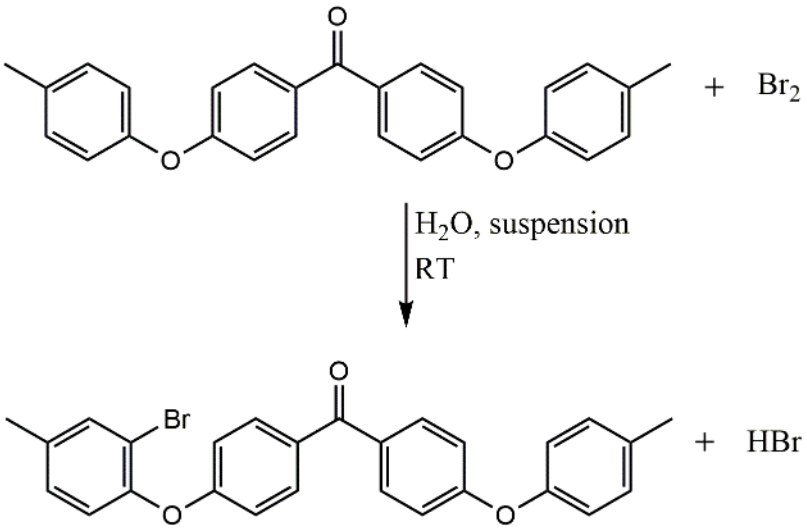

Scheme 2.4. Bromination of model compound **1** with Br_2.

The endeavor to better understand the effects of bromine addition to the PEEK polymer induced numerous attempts to isolate the brominated model compounds.

However, due to the many activated positions in each benzene ring of the model compounds **1** and **2**, only inseparable mixtures of the multiply brominated compounds were typically obtained. In order to determine the NMR signal assignments of the brominated model compounds an experiment with 1/3 equivalents of Br_2 was initially completed. For **1** about 90% of the bromine was added to the outer benzene rings and the rest to the inner rings (Figure 2.3). Other attempts were made in organic solvents to isolate a monobrominated compound, including chloroform and dichloromethane with $FeBr_3$ as a catalyst.

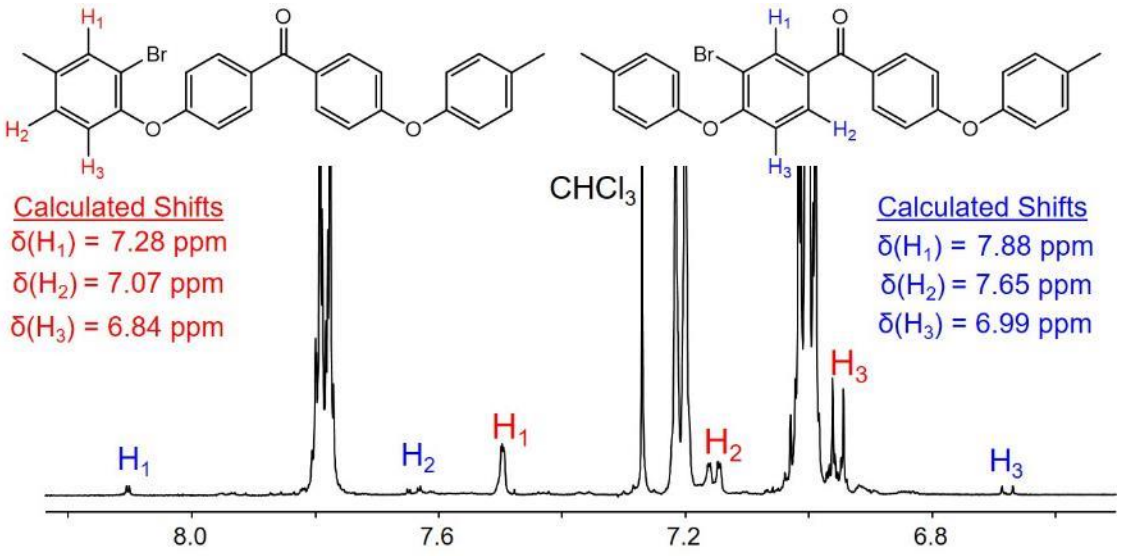

Figure 2.3. ^{1}H NMR of partially brominated **1** in $CDCl_3$ with signal assignments based on $^{3/4}J(^{1}H\text{-}^{1}H)$ couplings and calculated NMR chemical shifts.

2.2.5 Bromination of PEEK with Br_2

Similarly to the model compounds, the bromination of PEEK occurs by simply exposing the polymer directly to neat Br_2 (Scheme 2.5). Bromination takes place rapidly, initially at the surface, which is obvious within a few minutes. With a large excess of

Br_2, relative to the polymer, it dissolves and becomes gel-like (Figure 2.4). The excess bromine can be washed off with a large amount of water. Further purification is achieved by first dissolving the brominated polymer in chloroform and then precipitating it with an excess of ethanol. A fine white powder of the brominated PEEK ("bromo-PEEK") results (Figure 2.4).

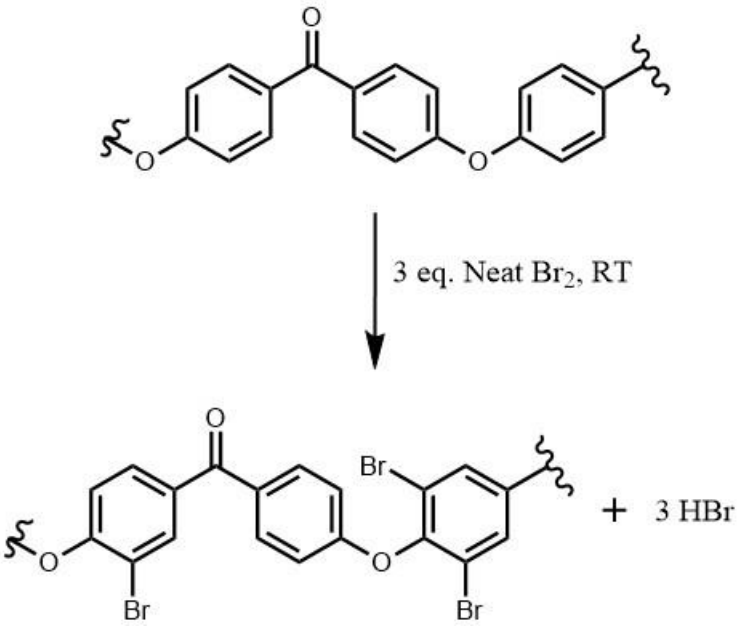

Scheme 2.5. Bromination of PEEK to give bromo-PEEK.

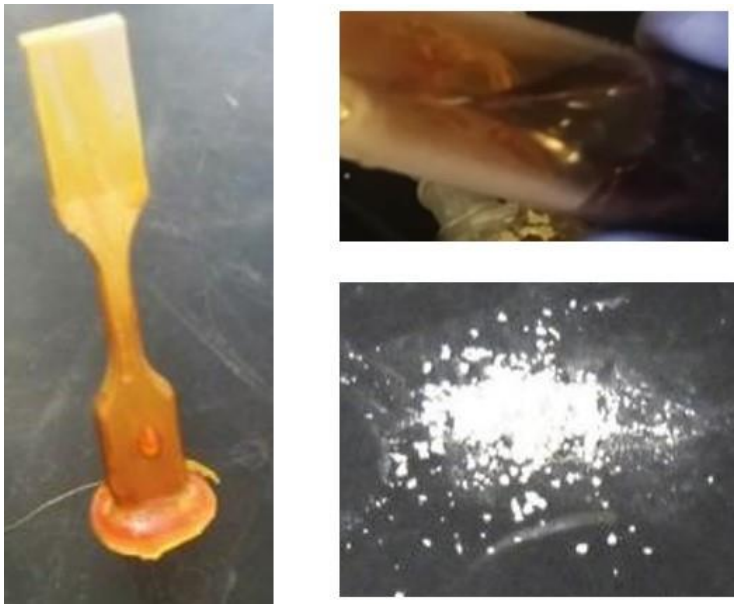

Figure 2.4. PEEK specimen after being completely submerged in liquid Br_2 (top right) and after only the bottom part being submerged and rinsed with water (left). A white powder is obtained after purification (bottom right) of the brominated PEEK.

In contrast to PEEK, the brominated polymer is soluble in common organic solvents such as chloroform, dichloromethane and tetrahydrofuran. Therefore, its solution NMR data can easily be obtained (Figure 2.5). The ^{1}H NMR signals are assigned in a straightforward manner based on the chemical shifts of the model compounds. For example, the signal at 8.15 ppm corresponds to the proton adjacent to the carbonyl group. The ^{13}C NMR spectrum (Figure 2.5) shows that there are three different chemical environments for the carbonyl group. From the model compound results we know that these stem from the starting compound with no bromine, and then one and two Br substituents on the inner rings (Scheme 2.6). Mass spectrometry and microprobe results confirm that the polymer contains more than three bromine atoms per repeat unit. As there are multiple possible scenarios for the bromination of the ring

between the ether linkages, however, these cannot be easily distinguished even using 2D NMR experiments.

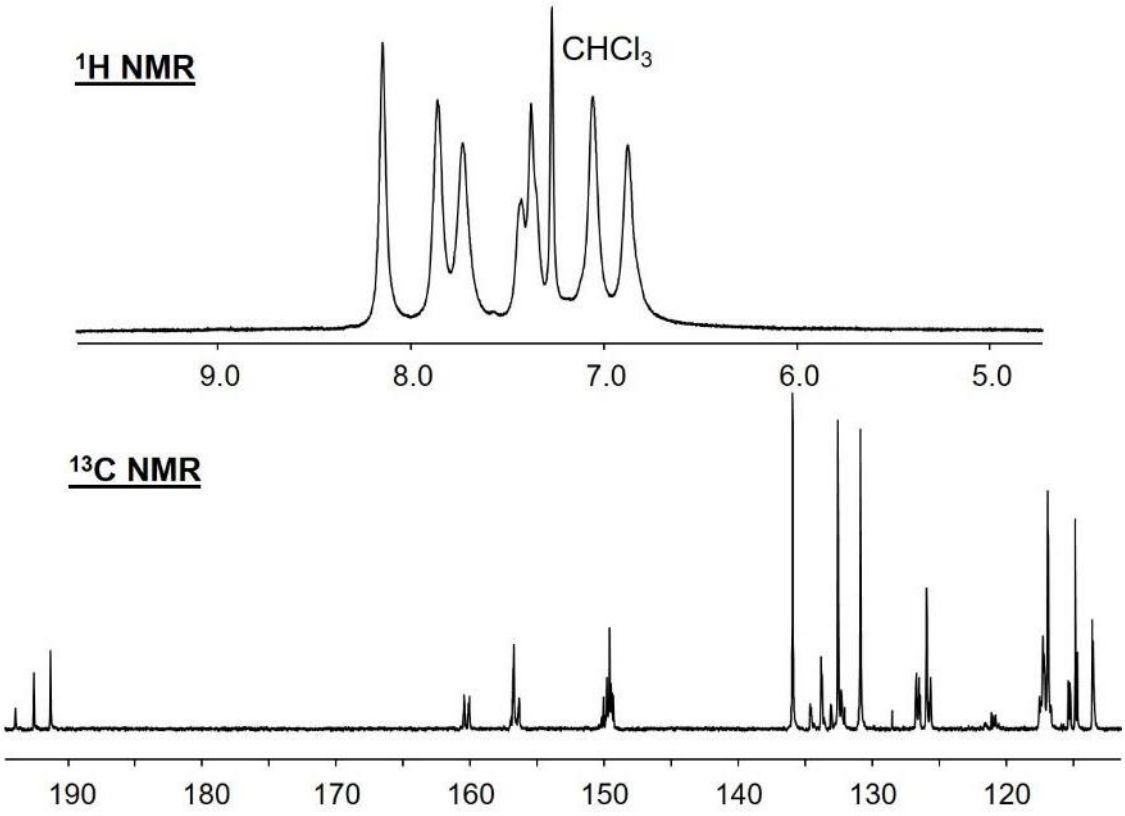

Figure 2.5. Solution ^{1}H (top) and ^{13}C (bottom) NMR spectra ($CDCl_3$) of PEEK brominated by submersion in liquid Br_2.

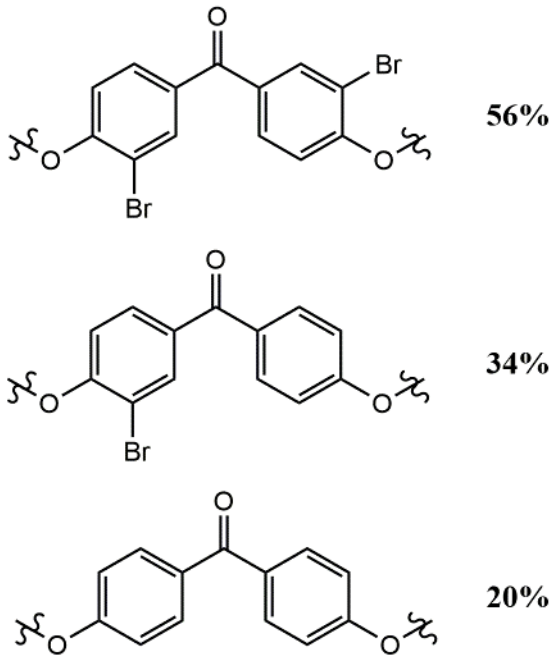

Scheme 2.6. Positions of bromination of internal rings next to the ketone group.

In contrast to the original specimen, the brominated PEEK is amorphous, as determined by DSC. Surprisingly, the DSC does have a very small change in slope at 210 °C, which is reversible upon cooling. Investigating the polymer visually by heating it in a melting point apparatus does not clarify what is causing the change in slope at this point. No gas evolution or color change took place.

The ^{13}C CP/MAS spectrum of brominated PEEK shows subtle changes as compared to the spectrum of pristine PEEK (Figure 2.6). The generally increased signal linewidth in the spectrum of bromo-PEEK implies that there is lower crystallinity and this result correlates well with the DSC measurements.

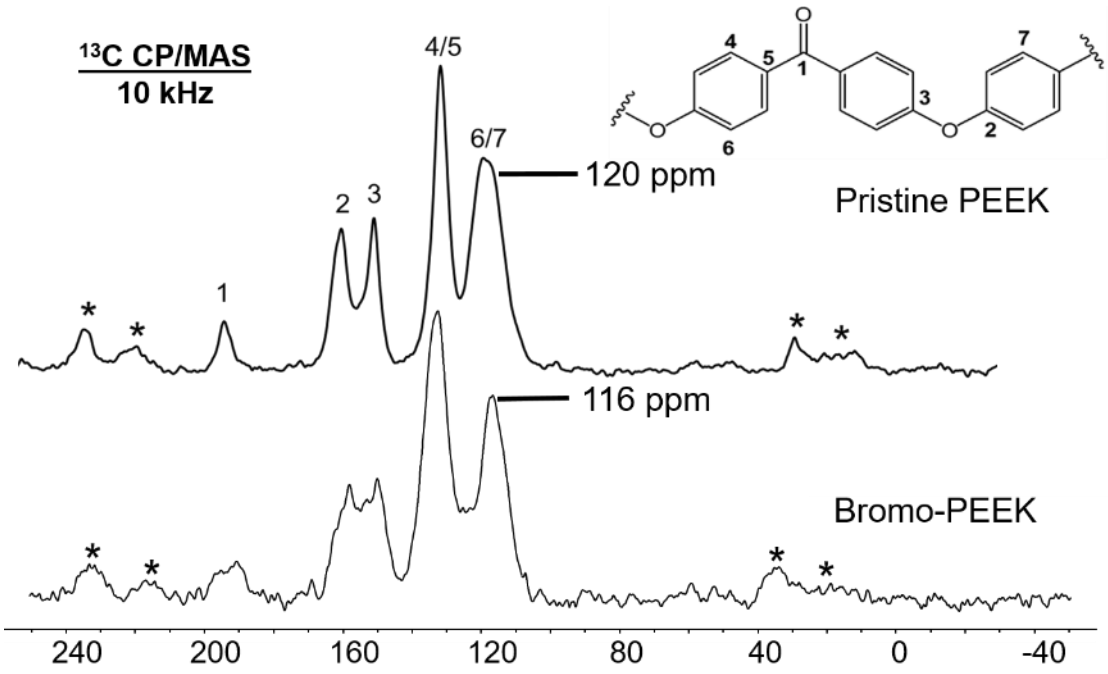

Figure 2.6. ^{13}C CP/MAS spectra of PEEK as received (pristine PEEK, top) and PEEK after bromination (bromo-PEEK, bottom).

The TGA results of bromo-PEEK (Figure 2.7) show similar oxygen tolerance to that of PEEK. Using air as the flow gas, the onset point shifts from that of the original PEEK by 50 °C. With N_2 as flow gas, the onset point of the bromo-PEEK did not deviate from the air gas measurement, similarly to PEEK.[37b] The decomposition profile of bromo-PEEK is very comparable to that of the original PEEK. The chemical processes occurring during TGA degradation seem to be similar, only taking place at lower temperatures. Results from parallel work comparing untreated PEEK to PEEK treated with completion fluids containing $ZnBr_2$ also feature this lower onset temperature.

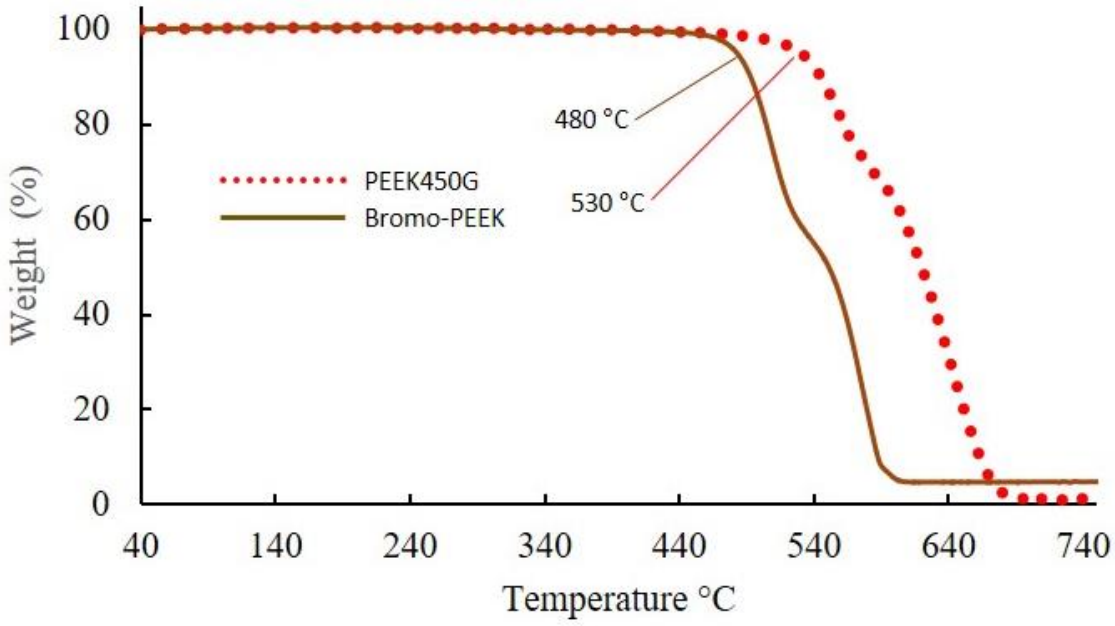

Figure 2.7. TGA results of bromo-PEEK and PEEK in air.

2.3 Conclusions

Two molecular model compounds with the functional groups arranged like in PEEK were synthesized and completely characterized. Then they were exposed to extreme heat and pressure (HT/HP) in completion fluids under controlled conditions. Hereby, both model compounds fully degraded in the completion fluid and bromination occurred on the aryl rings. PEEK was brominated in liquid Br_2 at ambient temperature and the material was obtained as a fine white powder after purification. Brominated PEEK is soluble in organic solvents and is easily analyzed with solution NMR methods. Bromo-PEEK is amorphous and has a significantly decreased onset temperature as compared to that of the unmodified PEEK.

2.4 Experimental Section

All solution NMR spectra were measured in $CDCl_3$ on either a 500 MHz INOVA spectrometer or a Bruker 500 MHz instrument equipped with a cryo probehead. Signal assignments for model compounds **1** and **2** and for bromo-PEEK were completed with 2D measurements which included $^{1}H,^{1}H$ COSY, $^{1}H,^{13}C$ HSQC, and $^{1}H,^{13}C$ HMBC techniques. All calculated chemical shifts were obtained using the program ChemBioDraw Ultra, version 13.0, with $CDCl_3$ set as the solvent.

The solid-state NMR spectra were measured on a Bruker AVANCE 400 spectrometer operating at 100.6 MHz for ^{13}C. All experiments were carried out using densely packed powders of the polymers in 2.5 mm ZrO_2 rotors. The ^{13}C CP/MAS (Cross Polarization with Magic Angle Spinning) spectra were recorded at MAS rates of 10 kHz. The ^{1}H $\pi/2$ pulse was 2.5 μs and TPPM (two pulse phase modulation) decoupling was used during the acquisition. The Hartmann-Hahn matching condition was optimized using the polymer Victrex 450P at a rotational speed of 10 kHz. Adamantane served as the external ^{13}C chemical shift standard (δ = 37.95 and 28.76 ppm). All spectra were measured with a contact time of 1.5 ms and a relaxation delay of 3.0 s.

The IR spectra were recorded on a Shimadzu IRAffinity-1 FTIR spectrometer by placing the powdered polymers on top of a Pike Technologies MIRacle ATR diamond plate. Typically 100 scans were accumulated for optimal spectrum quality.

TGA presented here was recorded with air or N_2 as flow gas. The temperature was equilibrated at 40 °C and then ramped at 10 °C/min until 700 °C after which the ramp was increased to 40 °C/min until 900 °C.

2.4.1 Synthesis of 1

1.99 g (9.1 mmol) of 4,4′-difluorobenzophenone, 2.55 g (2.5 mmol) of cresol and 3.25 g (2.2 mmol) of potassium carbonate are placed in a Schlenk flask and 90 mL of a 5:1 NMP/toluene (NMP: N-methylpyrrolidone) solution are added. The reaction mixture is heated to 140 °C and stirred at this temperature for 7 h. Then the crude mixture is exposed to oxygen and the temperature is increased to 150 °C. The mixture is stirred overnight. After cooling, 100 mL of H_2O is added to precipitate the product. The precipitate is filtered and washed thoroughly with a 5% KOH solution (3x 100 mL), with H_2O (3x 100 mL), and with cold ethanol (3x 50 mL), and subsequently dried to give a white crystalline powder (3.19 g, 8.1 mmol) 89.0%. mp. 155-158 °C. IR stretching band (cm^{-1}): 1641 (C=O).

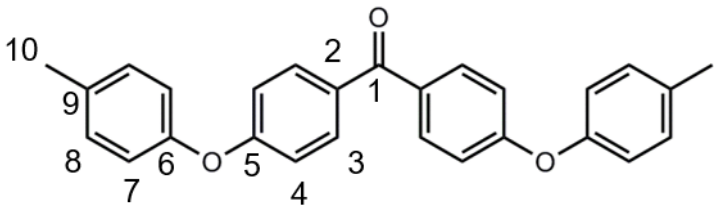

^{1}H NMR (500 MHz, $CDCl_3$): δ (ppm) 7.79 (d, 9.1 Hz, 4H, H3); 7.21 (d, 7.8 Hz, 4H, H8); 7.01 (d, 8.8 Hz, 4H, H7); 7.00 (d, 8.6 Hz, 4H, H4); 2.38 (s, 6H, H10). ^{13}C NMR (125 MHz, $CDCl_3$): δ (ppm) 194.20 (C1); 161.77 (C5); 153.13 (C6); 134.20 (C9); 132.13 (C3); 131.95 (C2); 130.48 (C8); 120.10 (C7); 116.71 (C4); 20.75 (C10). ESI-MS (positive mode): m/z 395 [M+H].

2.4.2 Synthesis of 2

In a Schlenk flask 2.584 g (12.0 mmol) of 4,4′-difluorobenzophenone, 5.586 g (30.0 mmol) of *p*-hydroxydiphenylether and 4.110 g (30.0 mmol) of potassium carbonate are suspended in 90 mL of a 5:1 NMP/toluene solution. The reaction mixture is heated at 140 °C for 7 h and after being exposed to oxygen the temperature is increased to 150 °C. The mixture is then stirred overnight. After cooling, the desired compound is precipitated by the addition of 100 mL of H_2O. The precipitate is filtered and washed thoroughly with a 5% KOH solution (3x 100 mL), with H_2O (3x 150 mL) and with cold ethanol (2x 50 mL). The white crystalline powder weighs 6.202 g corresponding to a yield of 93.9%. mp. 197-199 °C. IR stretching band (cm^{-1}): 1641 (C=O).

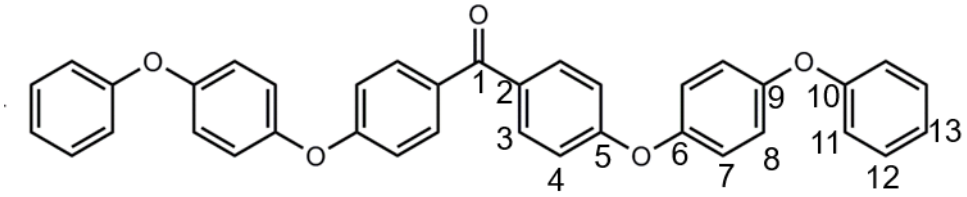

^{1}H NMR (500 MHz, $CDCl_3$): δ (ppm) 7.81 (d, 8.7 Hz, 4H, H3); 7.37 (t, 7.6 Hz, 4H, H12); 7.13 (t, 7.4 Hz, 2H, H13); 7.07 (d, 5.2 Hz, 4H, H7); 7.07 (d, 5.2 Hz, 4H, H8); 7.04 (d, 7.9 Hz, 4H, H11); 7.04 (d, 8.8 Hz, 4H, H4). ^{13}C NMR (125 MHz, $CDCl_3$): δ (ppm) 194.20 (C1); 161.77 (C5); 157.36 (C10); 153.87 (C6); 150.88 (C9); 132.24 (C3); 132.12 (C2); 129.82 (C12); 123.34 (C13); 121.60 (C7); 120.39 (C8); 118.62 (C11); 116.71 (C4). $^{1}J(^{13}C\text{-}^{13}C)$ Coupling constants for non-quaternary carbon nuclei with intensive signals: 132.23 (d, 58.1 Hz); 129.80 (d, 57.2 Hz); 123.31 (d, 56.4 Hz); 121.60

(d, 58.1 Hz, d, 69.0 Hz); 120.39 (d, 57.2 Hz, d, 68.2 Hz); 118.62 (d, 57.2 Hz, d, 67.3 Hz); 116.71 (d, 58.1 Hz, d, 67.3 Hz). MALDI (positive mode): m/z 551.2 [M+H].

2.4.3 Treatment of 1 and 2 at 260 °C for 48 hours

100 mg of **1** or **2** were suspended in 100 mL of 4.25 M $ZnBr_2$/2.65 M $CaBr_2$ and heated to 260 °C for 48 hours in a hastelloy pressure vessel. The resulting suspension was removed from the vessel and extracted two times with 50 mL of chloroform. The chloroform was removed in vacuo and the resulting solid was weighed. Subsequently, the solid was dissolved in $CDCl_3$ for NMR and MALDI-MS experiments.

2.4.4 Treatment of 1 and 2 at 90 °C for 17 days

30 mg of **1** or **2** were suspended in 10 mL of the fluids described in Figure 2.2 (17.8 M $ZnBr_2$, 4.25 M $ZnBr_2$/2.65 M $CaBr_2$, 1.0 M $ZnBr_2$, 0.1 M HCl) in a glass vial. The vial was heated to 90 °C and then sealed with a glass stopper. After 17 days the solution was filtered through weighed filter paper. The filtrate was extracted two times with 10 mL of chloroform. The chloroform was then removed in *vacuo*. 1.0 mL of $CDCl_3$ was added to the resulting film and a ^1H NMR spectrum was recorded. The remaining solid that had been filtered off was also dissolved in chloroform and measured by ^1H NMR in $CDCl_3$.

2.4.5 Representative Bromination via Suspension in H_2O

100 mg of **1**, **2**, or PEEK450PF was suspended in 10 mL of H_2O in a round bottom flask. While stirring vigorously between 0.3 and 10 equivalents of liquid Br_2 was slowly added. The suspended material quickly cocooned around the stir bar. The reaction is complete immediately after the addition of Br_2. The solid material was then removed

from the stir bar and washed thoroughly with H_2O. 2D NMR techniques were utilized to determine signal patterns and assignments of specific brominated positions.

2.4.6 Bromination with Br_2 Vapor

A vial with 0.875 g of PEEK450G was inserted into a Schlenk flask with 0.1 mL liquid Br_2 at the bottom. Care was taken that the specimen did not get into contact with the liquid Br_2. After sitting overnight the liquid was entirely gone and the polymer had swelled to fit the glass vial. The resulting material was thoroughly washed with H_2O and its weight was determined to be 1.017 g. The material was orange on the outside, however, after removing the exposed outer surface, the color went away and the main body of the material was still unaltered PEEK.

2.4.7 Bromination of PEEK450G by Submersion in Liquid Br_2

A small piece of a PEEK tensile specimen (0.520 g) was inserted into a vial containing liquid Br_2. The polymer was completely submerged. Within minutes most of the liquid had soaked into the polymer and it stuck to the glass. After allowing it to sit overnight, the cap was unscrewed and HBr was released. The resulting material was pulled from the vial, washed with water and ethanol and weighed. The material now weighed 0.940 g, corresponding to a degree of bromination of 3 Br atoms per repetitive unit of the polymer. The bromine content of the bromo-PEEK was also measured by microprobe and the result was 52.16 weight%. This value also matches 3 bromine atoms on average per repetitive unit of the polymer. Furthermore, purification was performed by dissolving the brominated PEEK in chlorofrom and reprecipitating it with ethanol.

CHAPTER III

PEEK AND PEKK TREATMENT UNDER HP/HT CONDITIONS IN ZINK BROMIDE COMPLETION FLUIDS WITH IDENTIFICATION AND QUANTIFICATION OF DECOMPOSITION PRODUCTS

3.1 Introduction

PEEK (polyetheretherketone) has a wide variety of applications including medical implants, 3D printing, and as fittings for analytical instruments such as HPLC equipment. PEEK is also utilized in the form of lightweight parts in the oil and gas industry. These PEEK parts are exposed to the harsh downhole conditions and completion fluids. Currently, PEEK performs well under most of these extreme conditions. Unfortunately, when $ZnBr_2$ fluids are used the parts must be replaced frequently which stops the drilling process. There is considerable value in obtaining accurate lifetime predictions of the components based on the downhole conditions and the exact completion fluids used. This task is extremely difficult as PEEK itself is insoluble in common organic solvents, even at elevated temperatures, limiting the analytical methods available to study the polymer. New methods to analyze the PEEK polymer, as well as the mechanisms and causes of the degradation, need to be further explored. This will provide vital feedback to enable more accurate lifetime predictions and ultimately help prevent degradation and eventually extend the lifetime of the parts.

Long-term high temperature treatment of PEEK has been reported under both aqueous and dry conditions previously.[37a,40] However, these studies have not been performed under low pH conditions as, for example, with highly concentrated $ZnBr_2$

fluids. Four different completion fluids were used to study the degradation of PEEK between 27 and 63 days of treatment. The four fluids used vary in the concentration of $ZnBr_2$ to allow one the see the effect that the concentration of this salt has on the polymer degradation (Table 3.1). One fluid contained no $ZnBr_2$ and was used as a control.

Table 3.1. Fluids used for long term exposure experiments with PEEK.

	Fluid **1** (M)	Fluid **2** (M)	Fluid **3** (M)	Fluid **4** (M)
$ZnBr_2$	4.25	4.09	3.63	0.00
$CaBr_2$	2.65	2.69	2.80	4.30

Besides any more sophisticated analytical analyses, it was visually evident that there was extensive polymer degradation, caused by $ZnBr_2$ in the solution (Figure 3.1). $ZnBr_2$ has already for a long time been known in the oil and gas industry lore to be detrimental to PEEK. However, there has been no understanding as to how or why this is the case.

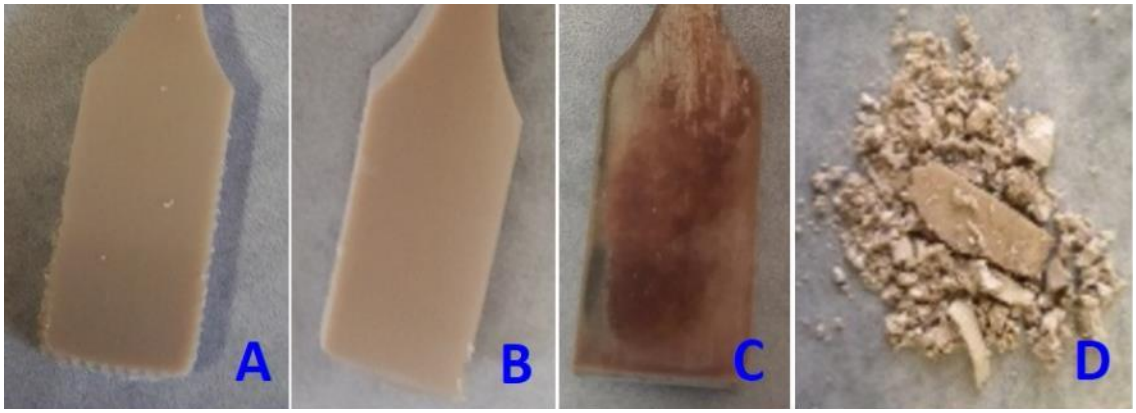

Figure 3.1. A) PEEK450G as received, **B**) PEEK after treatment for 63 days in fluid **4**, **C**) PEEK after treatment for 28 days in fluid **3**, and 35 days in fluid **4**, and **D**) PEEK after treatment for 27 days in fluid **1**. All experiments were performed at 260 °C.

Traditional methods to analyze insoluble polymers, including TGA, DSC, IR and solid-state NMR, were applied. DSC, IR, and solid-state NMR data all corroborate the assumption that initially there is a significant increase in crystallinity in the polymer after the treatments, especially with $ZnBr_2$ fluids. TGA also shows a significant drop in onset temperature and that new events are occurring in these fluids as well. Unfortunately, these methods were not detailed enough to provide insight into any chemical mechanisms occurring within the polymer or even sufficient evidence to say whether there were any chemical reactions at all.

Limited work has been devoted to studying the small molecules that result from the decomposition process.[37c,40] Our novel and major method of analysis has been high resolution solution NMR. Extraction of the small molecules that are formed during the PEEK treatment can be completed with chloroform. The small molecules could then be

identified and quantified to provide mechanistic details that otherwise would never have been understood.

3.2 Results and Discussion

3.2.1 Identification and Quantification of Eluents

As a first step to identify the major degradation products from PEEK, simple extractions with $CDCl_3$ from both the completion fluid and the treated specimens were carried out. ^{1}H, ^{13}C, HSQC, HMBC and COSY NMR experiments were then performed for identification based on a concentrated sample (Figure 3.2, Figure 3.3). A capillary standard was used for quantification of the samples over long periods of time by ^{1}H NMR. For the capillary standard to be at a concentration in the realm of the sub-millimolar concentrations of eluents being measured, the residual ^{1}H NMR signal of deuterated dichloromethane was used. The capillary was calibrated to benzophenone because it has a relaxation time similar to those of the small molecules eluted from PEEK.

3.2.2 Completion Fluid Extractions from Long Term Exposures of PEEK

Each of the long term experiments started with 25 ASTM D638 type 5 tensile specimens and 600 mL of completion fluid in a hastelloy pressure vessel. After each data point, 5 tensiles were removed along with 30 mL of completion fluid. With fluid **3** there were initially 28 days of exposure, then the PEEK was removed and treated an additional 35 days with fluid **4**. The fluid change allowed us to study any potential further degradation in a fluid that does not cause degradation to pristine PEEK samples.

The identified compounds extracted from the completion fluid include the processing solvent, diphenylsulfone, phenol, and 1,4-diphenoxybenzene (dpb). Only diphenylsulfone does not degrade at any significant rate. In each set of measurements a small amount of the processing solvent is eluted and maintains concentration for the rest of treatment time.

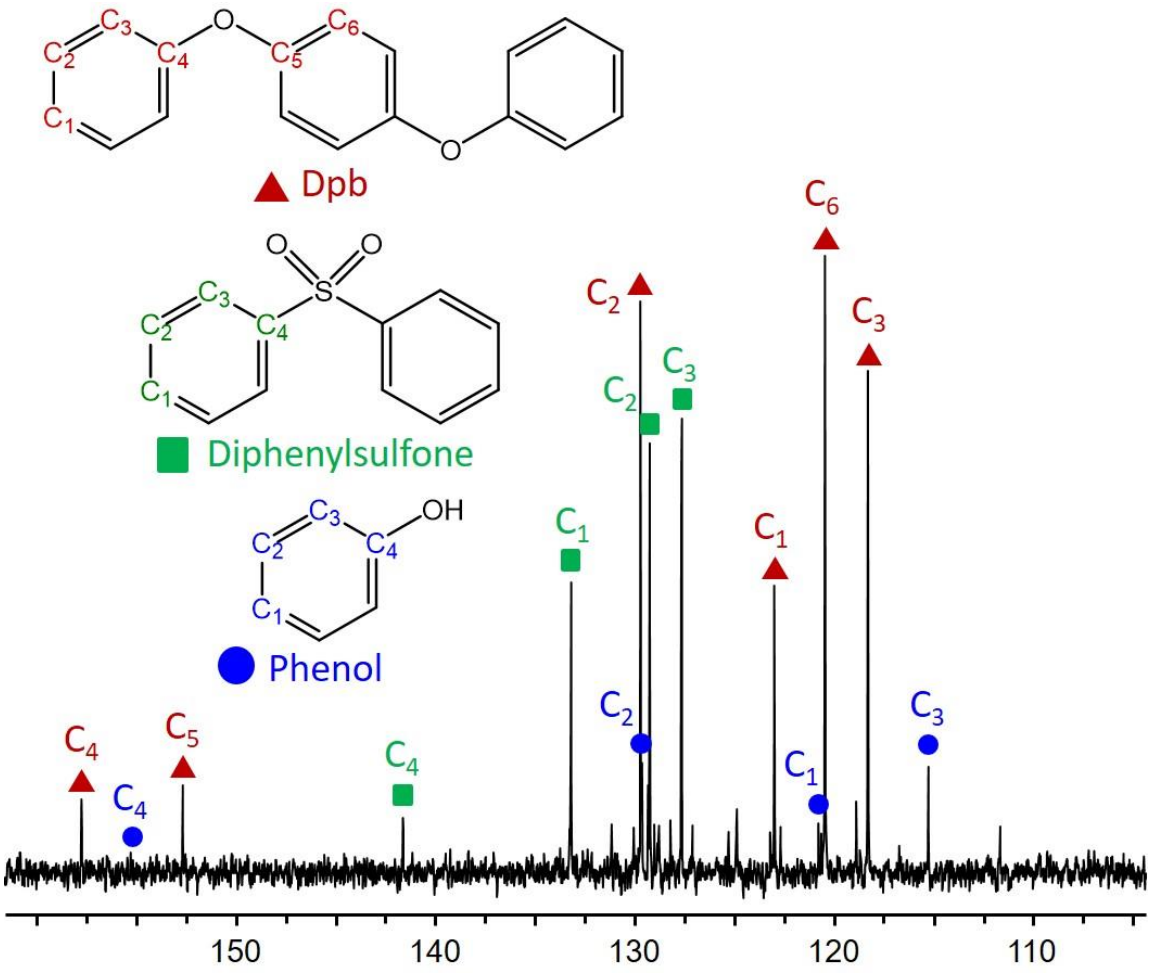

Figure 3.2. ^{13}C NMR in $CDCl_3$ after extraction from completion fluid **1**, which was treated for 89 hours with PEEK.

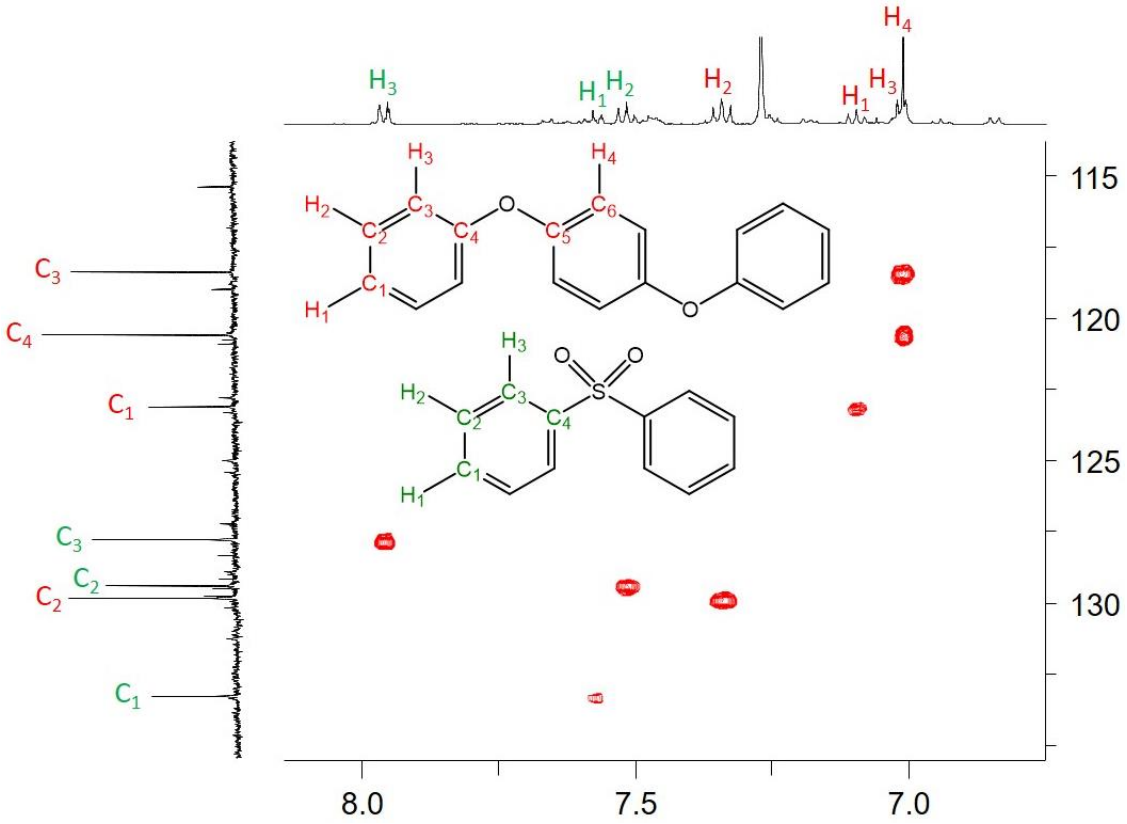

Figure 3.3. HSQC in $CDCl_3$ after extraction from completion fluid **1**, which was treated for 89 hours with PEEK.

The rate of phenol correlates with the concentration of dpb at most data points for each fluid set (Figure 3.4, Figure 3.5). There is a nearly linear rate in two of the four experiments. These are the two treatments with constant concentrations of dpb in solution. The constant concentration of dpb results from an initial saturation of the fluid. It can continue to decompose in the fluid and still maintain a constant concentration in this way, producing a constant source for the secondary production of phenol. In an additional experiment, after the PEEK was treated in the completion fluid for 28 days, it was removed. The remaining fluid still containing the eluents was kept under the same

conditions. Measurements showed that dpb and phenol are both degrading in the fluid. This result also means that as we are monitoring concentrations and one must keep in mind that these are rates of formation minus rates of degradation.

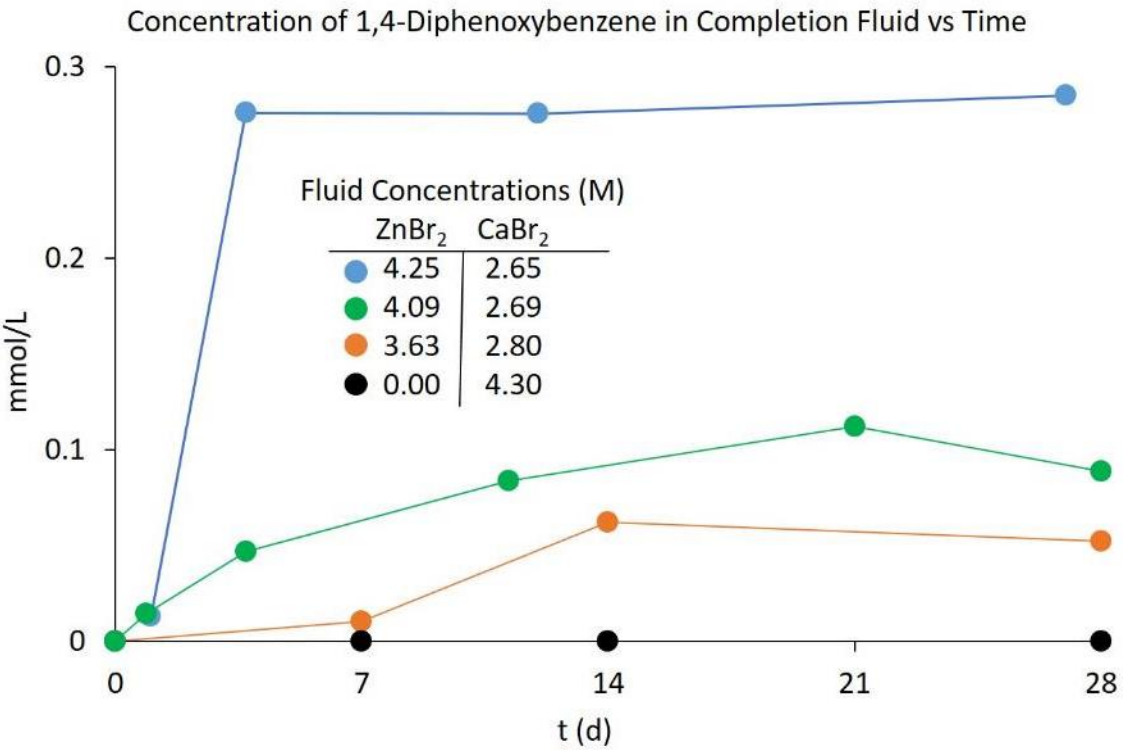

Figure 3.4. Concentrations of 1,4-diphenoxybenzene after extractions from completion fluid with exposed PEEK specimens.

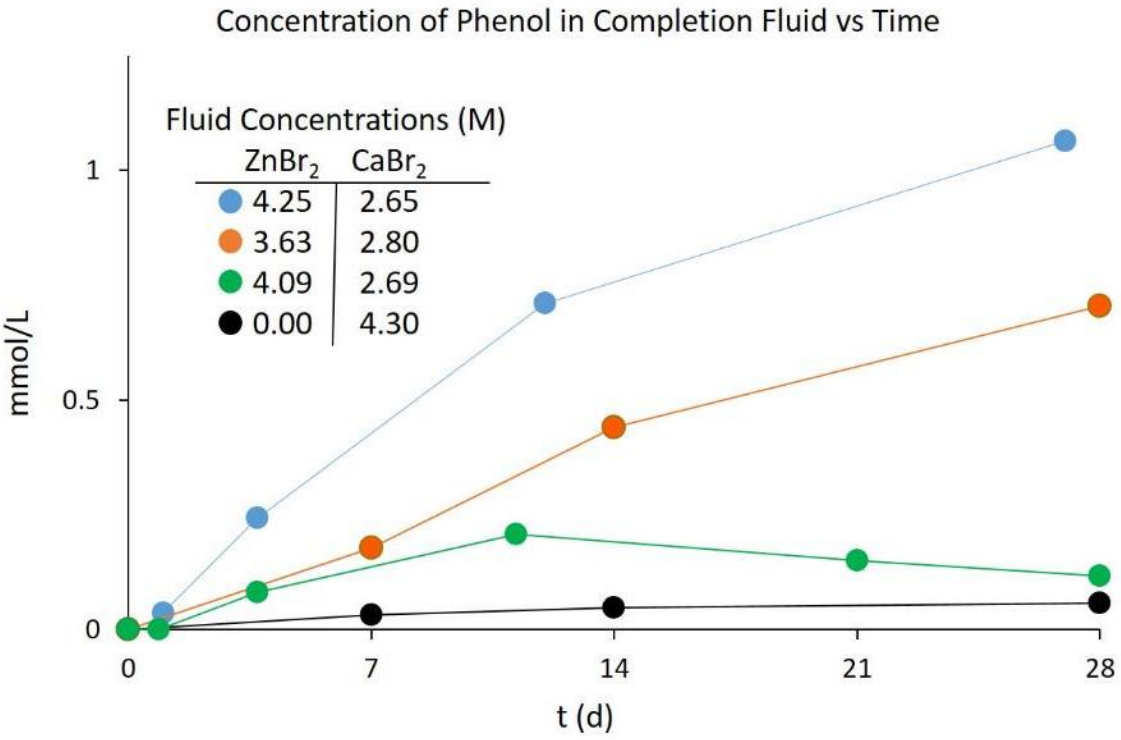

Figure 3.5. Concentrations of phenol after extractions from completion fluid with treated PEEK specimens.

The extractions from the PEEK specimens further verify that the $ZnBr_2$ completion fluids used are being saturated with dpb. Although in each of the fluid extractions an eventual concentration limit is reached, the specimen extractions show that the formation of dpb is continuing to occur and in fact at a faster rate with longer exposure. The NMR results of the extractions from the treated specimens of PEEK are surprisingly simple (Figure 3.6). Much higher concentrations of dpb are found inside the PEEK specimens. Furthermore, bis((4-phenoxy-4-phenoxy)phenyl)ketone, a model compound that we previously synthesized (model **2**), was found as a degradation product. The identities of these products were also confirmed with MS experiments.

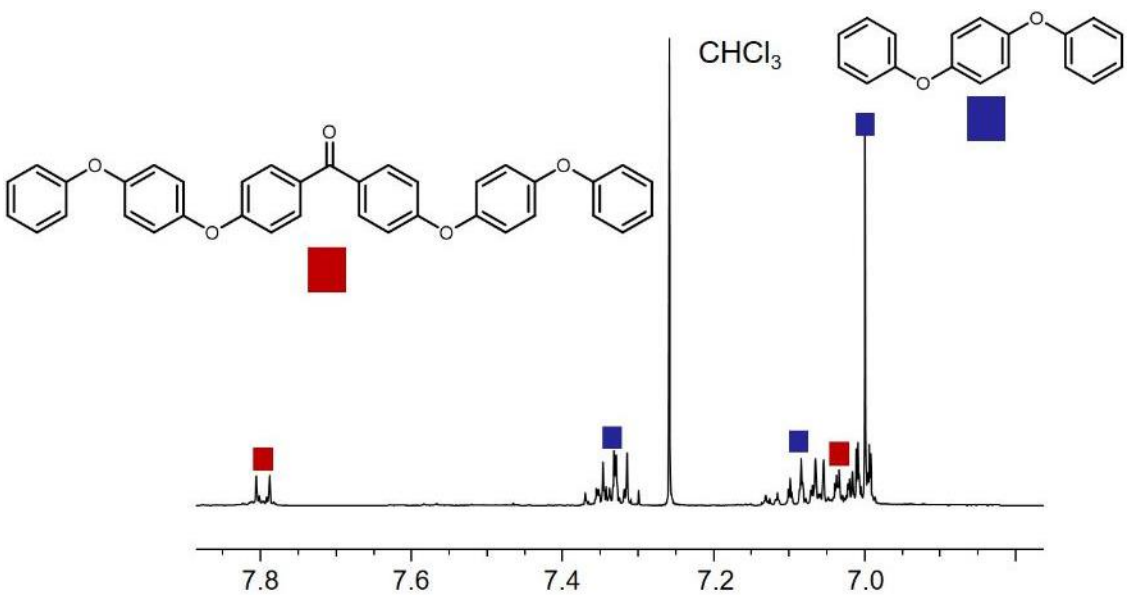

Figure 3.6. ^{1}H NMR of PEEK specimen extraction after treatment in 3.63 M $ZnBr_2$ and 2.80 M $CaBr_2$ fluid.

Table 3.2 shows the amount of 1,4-diphenoxybenzene extracted from the PEEK material before and after it was cryomilled. It turns out that chloroform does not penetrate the PEEK material far enough to extract all of the small molecules produced. Even at elevated temperatures there was a limited amount of extracted dpb without prior cryomilling.

Table 3.2. Extraction of dpb with and without prior cryomilling of the PEEK specimen. These PEEK specimens were treated in fluid **2**. The weight% is based on the amount of dpb after extraction from 200 mg of sample as measured by ^{1}H NMR with a capillary standard.

Treatment Time (d)	**Cryomilled** (wt%)	**Solid Piece** (wt%)
0.88	0.0	0.0
3.71	0.5	0.003
11	1.5	0.27
21	2.7	0.13
28	6.7	-

After determining there was such a high amount of dpb produced, we thought that this could potentially be quantified by TGA. TGA is a simple tool and an easy method to analyze many PEEK samples in a short period of time. As we had already measured TGA on the PEEK specimens, we measured pure dpb to see if it matched any of the TGA mass loss events (Figure 3.7). Indeed, dpb does match a mass loss event between 150 and 350 °C with degraded PEEK samples from the $ZnBr_2$ fluids. The pure dpb is lost in a much shorter period of time than it is released from the PEEK matrix. However, this is expected as even water in the polymer takes a longer period of time when measuring PEEK with TGA. This thermal event occurs with both N_2 and air as the flow gas. The TGA mass results show that the NMR experiments correlate well with the amount of dpb, especially after longer treatment times (Figure 3.8). The difference in the amount of dpb as measured by TGA and NMR with shorter treatment times is most probably due to incomplete extraction with chloroform. As PEEK is exposed for longer times to $ZnBr_2$ fluids, the crystallinity increases. Coupled with this increase in

crystallinity is increasing brittleness, so although the amount of time spent in the cryomill was the same for all samples, the particle size was likely smaller for the samples treated for longer times than for samples with shorter exposure periods.

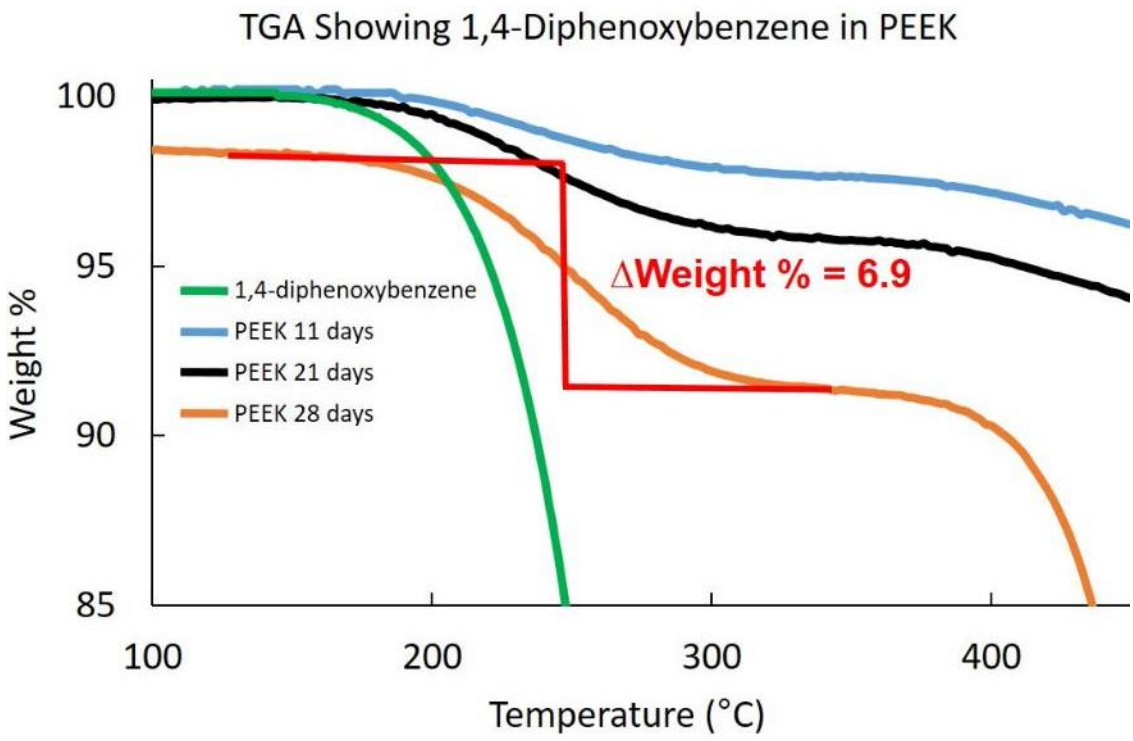

Figure 3.7. TGA of PEEK specimens that were treated in a 4.09 M $ZnBr_2$/2.69 M $CaBr_2$ fluid, compared to the TGA of pure dpb.

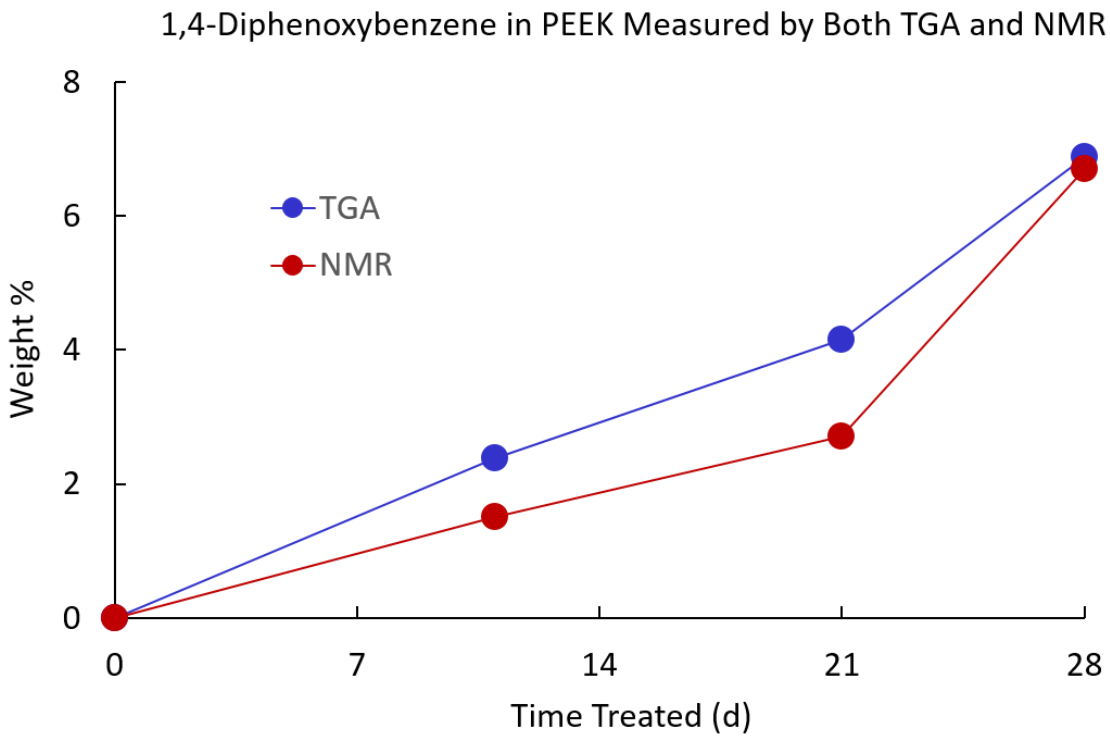

Figure 3.8. Comparison of dpb quantified by TGA with dpb quantified by ^{1}H NMR after cryomilling the samples.

An important note at this point is that the concentration of dpb in the PEEK samples sharply increases between 21 days and 28 days of treatment in fluid **2** (Figure 3.8). This also corresponds to the time when the treated specimens are breaking apart while being exposed in the vessel (Figure 3.9). This breaking of the specimens increases the specific surface area and exposes the polymer to faster degradation by the corrosive $ZnBr_2$ fluid.

Figure 3.9. Images of the PEEK specimens in the vessel, treated with fluid **3** for 21 days (left) and 28 days (right).

3.2.3 Chemical Mechanisms: C-C Bond Cleavage and Subsequent Hydrolysis

The major degradation pathway for PEEK under the conditions applied here is clearly C-C bond cleavage at the ketone group (Scheme 3.1). Others have measured CO and CO_2 gas via GC/MS upon pyrolytic decomposition of PEEK.[37c] $ZnBr_2$ is a Lewis acid causing a pH lower than 1.5 in aqueous fluids. It can be compared to other known Lewis acid catalysts for ketone activation and hydrolysis that lower the pH of aqueous solutions.

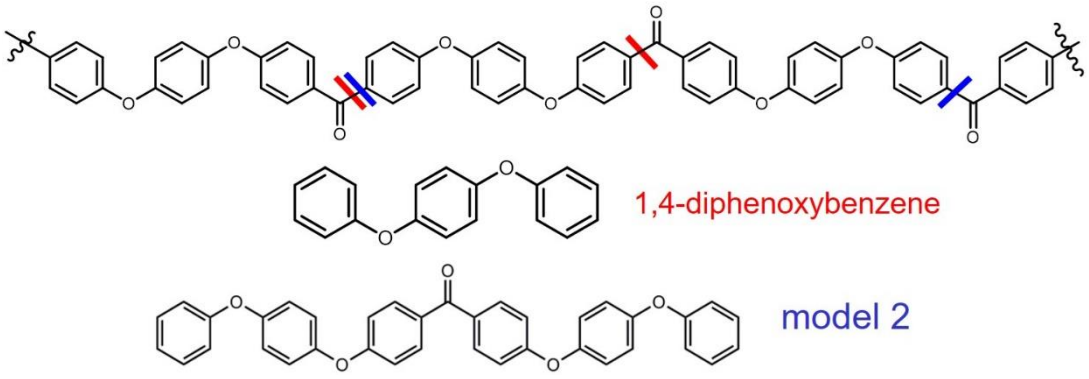

Scheme 3.1. C-C bond cleavage at the ketone position of PEEK to produce major identified degradation products.

With phenol being a major degradation product it was initially expected to stem from a hydrolysis mechanism, although the formation of phenol has been seen previously in thermal degradation pathways.[37b,37c] Diaryl ether linkages are very stable and much more difficult to hydrolyze. However, $In(OTf)_3$ has been shown to be very active for the hydrolysis of diphenylether under similar conditions.[41] To determine if dpb could be the source of phenol, we treated pure dpb similarly to PEEK in fluid **1** (Figure 3.10). The results are unequivocal and confirm that phenol is primarily produced from dpb. This also explains why the concentration of phenol and dpb are correlated well together over long periods of time (Figure 3.4, Figure 3.5). There is a short initiation period to producing significant quantities of phenol from PEEK treatments. When dpb is added to the system initially, within 24 hours the quantity of phenol is much larger than the one obtained after PEEK treatments, even with a much smaller starting amount (200 mg/150 mL vs 50 g PEEK/600 mL). The initiation period corresponds to the formation of dpb from PEEK and its release into the system.

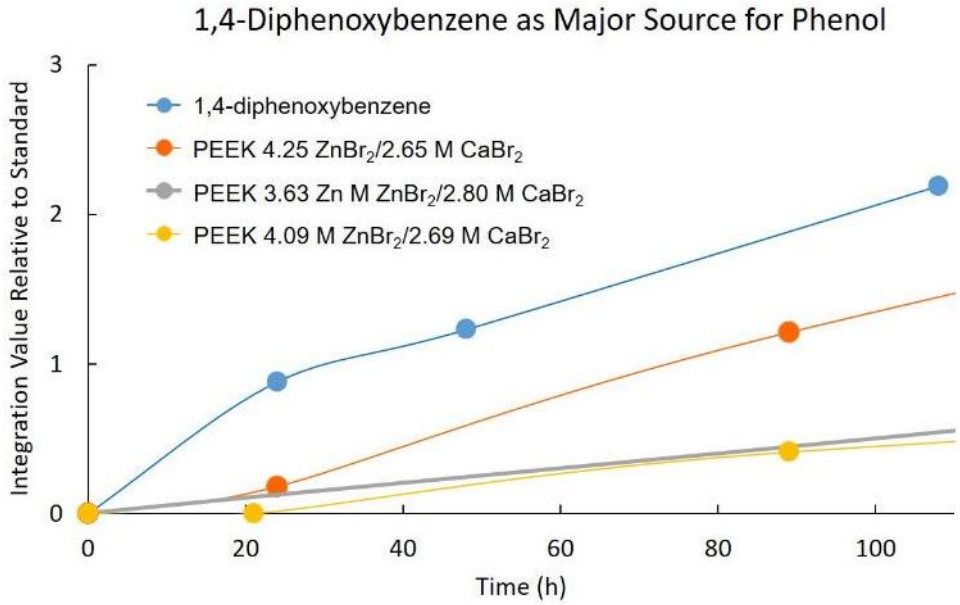

Figure 3.10. Showing relative amounts of phenol when treating dpb compared to treating PEEK.

Hydroquinone and/or p-hydroxybenzophenone should also be produced with the hydrolysis of dpb (Scheme 3.2). A ^{13}C NMR experiment in the completion fluid after extraction with a 5% D_2O addition for shimming did identify hydroquinone but not quantitatively. It was confirmed to be hydroquinone by an NMR spiking experiment with the completion fluid using purchased hydroquinone. When p-phenoxyphenol was treated in the same way as dpb, it rapidly turns into dibenzofuran among other minor unidentified products. The same ^{1}H NMR signals as for dibenzofuran were also found in the dpb treatment (Figure 3.11). Therefore, it can be assumed that hydrolysis of dpb occurs in the $ZnBr_2$ completion fluids. We were able to measure phenol but also found other byproducts from the hydrolysis of dpb in the system.

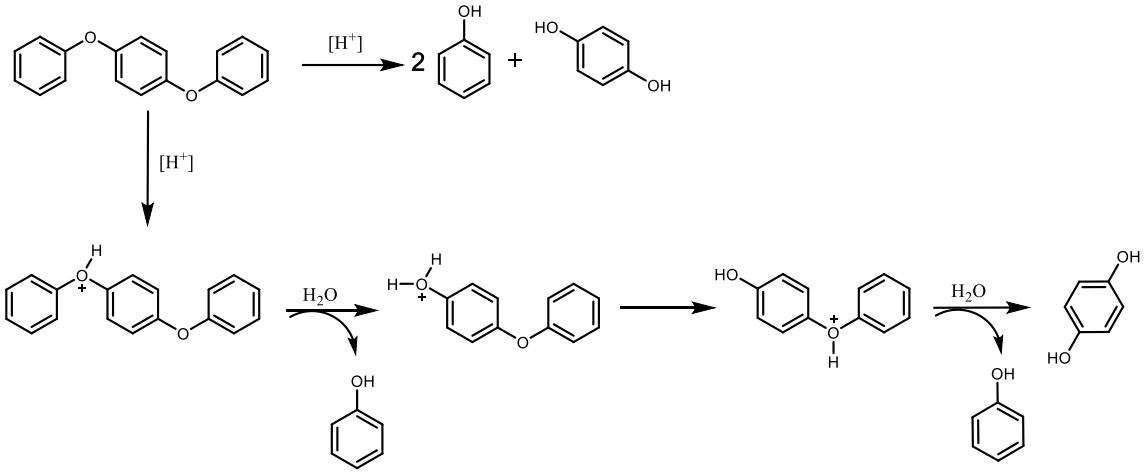

Scheme 3.2. Hydrolysis mechanism of dpb to produce phenol, *p*-phenoxyphenol and hydroquinone.

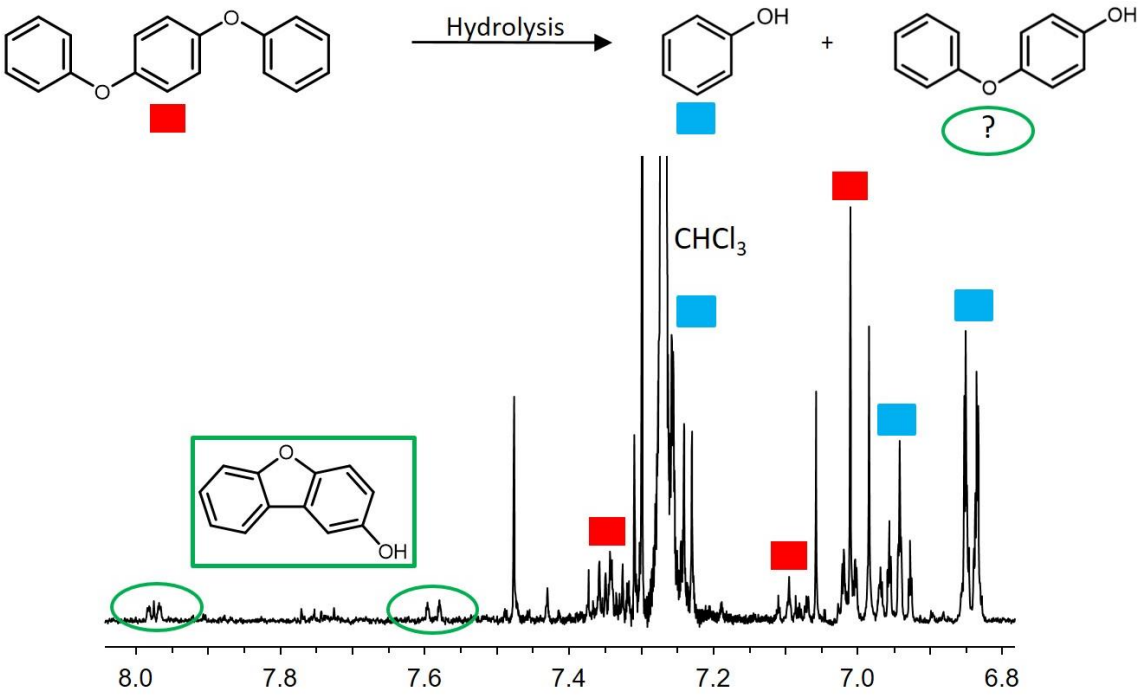

Figure 3.11. ^{1}H NMR of the extracted fluid after treatment of 1,4-diphenoxybenzene in fluid **1**.

3.2.4 Bromination and Radical Chemistry

Previously, two model compounds were synthesized and exposed to fluid **1** at the elevated temperature of 260 °C (chapter 2). After extraction from the fluids both compounds were subjected to ^{1}H NMR and MS analyses with other 2D NMR techniques and were found to have 1,2,4-trisubstituted aryl couplings and bromine substituents. After finding bromination of the model compounds it was expected that the PEEK polymer would be brominated, too. Elemental analyses were performed with Microprobe (Figure 13.12). The results confirm some very important facts. The first is that the concentrations of the elements Zn, Br, and Ca all correlate with the degradation of the PEEK specimens. The longer the exposure and the more concentrated the fluid, the higher is the concentration of the elements. Next, the question arises whether these elements are just adsorbed on the surface of the polymer specimen, or whether they are bound covalently as in the case of an aryl bromide. The long term study where PEEK specimens were treated in fluid **3** for 28 days, then removed and treated an additional 35 days with fluid **4**, shows that even after 35 days in fluid **4** at 260 °C bromine and zinc remain with the polymer. This is an astonishing result considering that the specimens, after treatment only with fluid **4**, hardly contain any Ca or Br elements. A third, very important insight comes from an additional experiment in which the outer surface of one treated PEEK specimen was sanded off. About 0.1 mg was removed from the specimen treated for 12 days in fluid **1**, and the sample's elements were measured with Microprobe. The sample showed no Zn, Ca, or Br after sanding. This means that the bromination initially takes place at the surface of the polymer. Furthermore, this

corroborates the earlier result that the surface area also plays a role in the formation of dpb (Figure 3.8, Figure 3.9).

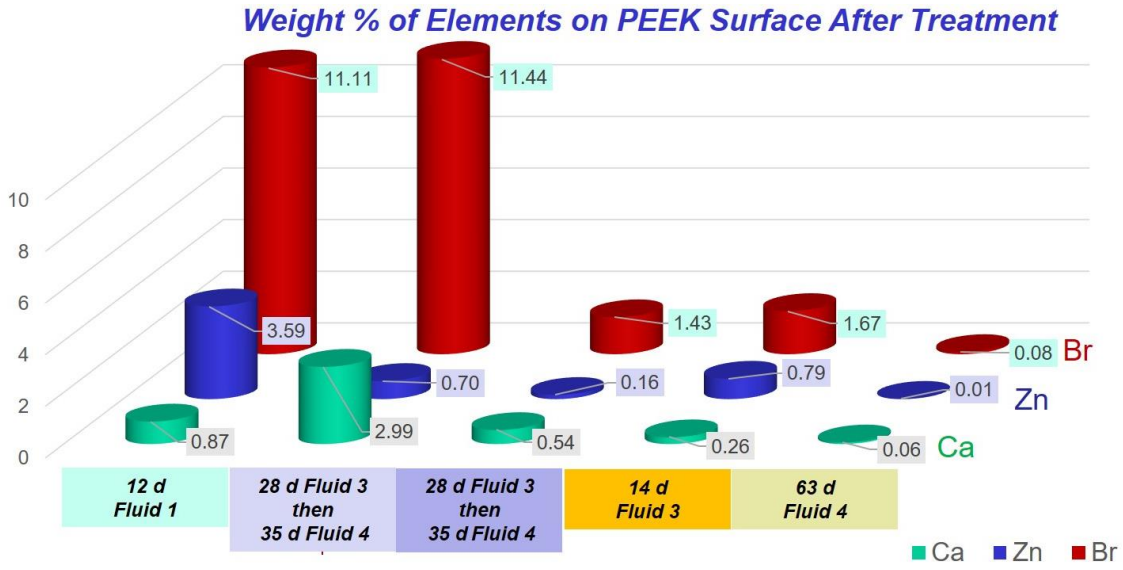

Figure 3.12. Microprobe analyses of PEEK specimens after different exposure times and fluids.

It has already been established that Br_2 brominates the aryl rings of PEEK upon contact of the neat reagents at room temperature (chapter 2). However, bromination did not occur at low temperature when bromine was diluted in aqueous solution. However, at the high temperature of 260 °C, bromination should take place at any offered aryl ring. The formation of bromine is expected to occur during PEEK treatments. The PEEK degradation itself starts from C-C bond cleavage. The degradation products formed directly from PEEK are dpb and model 2. There are likely other, larger polymer fragments also from ketone cleavage, however, at some point these would be insoluble in chloroform. The C-C bond breakage is a radical process that will be accelerated by a

strong Lewis acid like $ZnBr_2$. Dpb and model 2 both have hydrogen atoms where the ketone groups were located in PEEK. These hydrogen atoms are likely from the acid or water. The extraction of the hydrogen atom from water with a C radical comes with an electron and generates a short lived hydroxyl radical (Scheme 3.3). Bromide is known to be an excellent hydroxyl radical scavenger and would result in a Br radical.[42] A Br radical could generate Br_2 if it came into contact with a second Br radical.

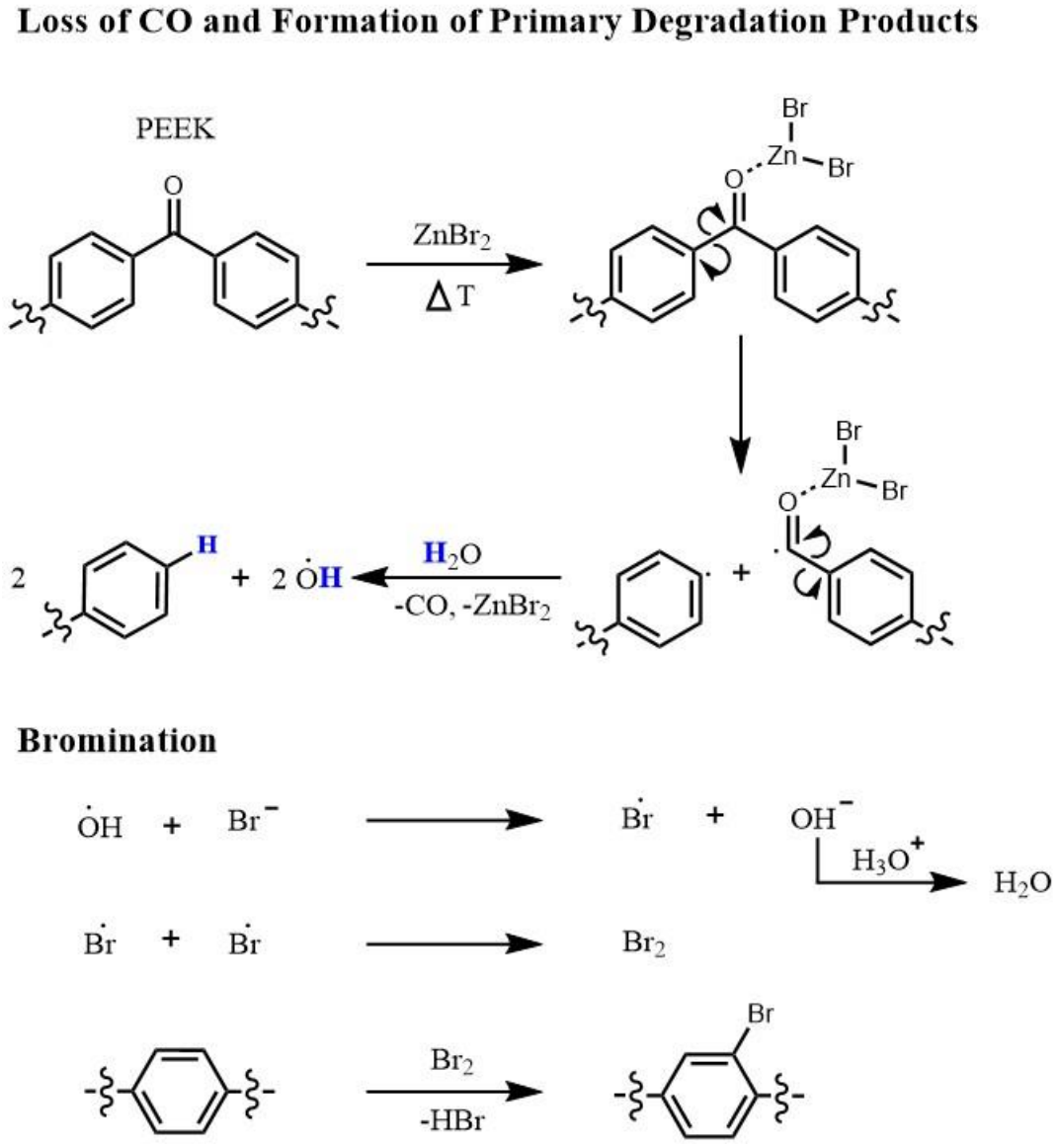

Scheme 3.3. Proposed mechanism for the formation of the primary degradation products during the PEEK treatment and bromination of the polymer.

3.2.5 PEKK Treatments in Completion Fluids and PAEK Degradation Mechanisms

Polyetherketoneketone (PEKK) was exposed to completion fluids under HP/HT conditions to help validate our mechanisms and to show that we can now predict

products formed during PAEK polymer treatment under downhole conditions with completion fluids containing $ZnBr_2$. PEKK was treated with fluid **1** at 260 °C in the same way as the PEEK samples previously. The PEKK specimens studied were not as thermally stable as the PEEK studied, however, for our purposes of comparing the chemical mechanisms it did not affect the results in any meaningful way. In fact, causing degradation at a faster rate is even beneficial with respect to the timeline of the performed studies.

PEKK has more ketone groups in its molecular structure and produces more small molecules that are soluble in chloroform. Fortunately, the products identified by NMR in the fluid and after specimen extractions appear exactly how we expected to see them based on the PEEK studies (Figure 13.13, Scheme 3.4). The compounds eluted into the completion fluid stem from cleavage at the ketone groups and subsequent hydrolysis of the primary degradation product, diphenyl ether, to give the secondary degradation product phenol. The fluid extractions after exposure of PEKK to fluid **1** produce surprisingly clean NMR spectra (Figure 13.13).

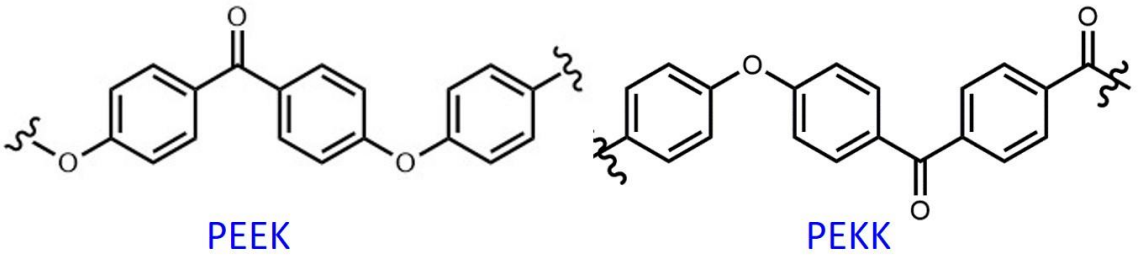

Scheme 3.4. PEEK and PEKK units. The primary degradation products of each polymer result from cleavage at the ketone groups.

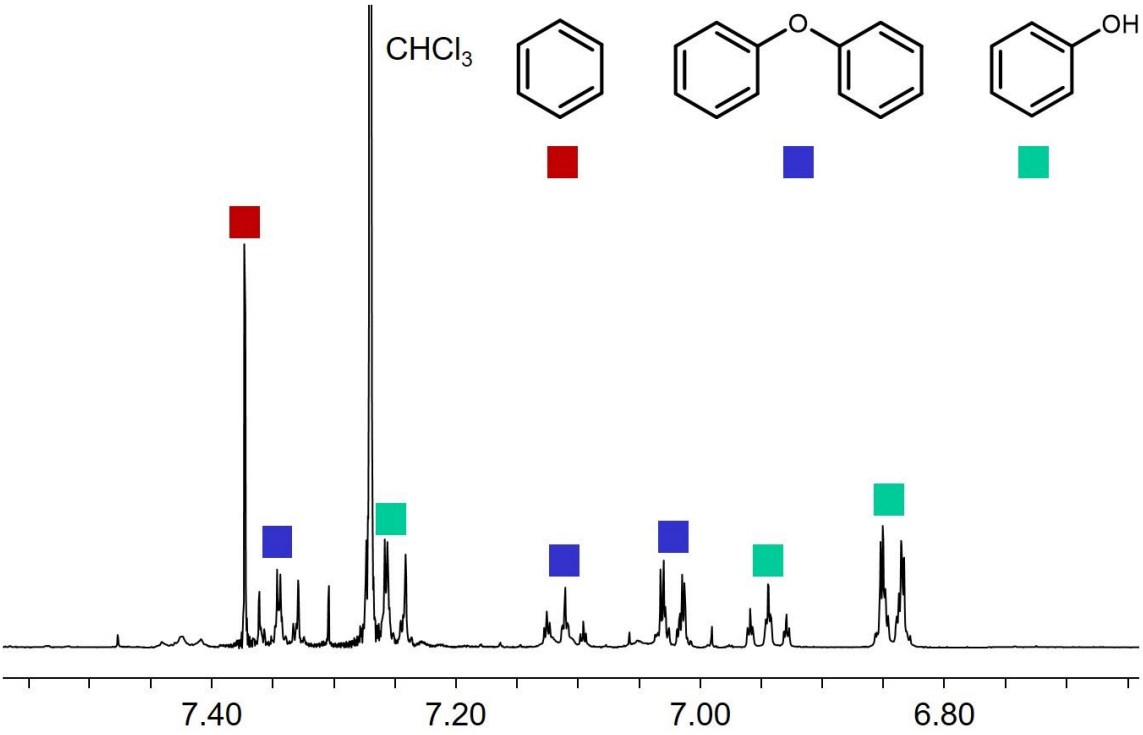

Figure 3.13. ^{1}H NMR of $CDCl_3$ extract of fluid **1** after PEKK was exposed for 4 days.

Unlike PEEK, PEKK forms many small molecules incorporating ketone groups that are soluble in chloroform. Extraction from a specimen treated for four days shows at least eight different ketone signals in the ^{13}C NMR spectrum (Figure 13.15). Many of these compounds were identified by NMR in combination with mass spectrometry (Figure 13.14). Interestingly, there were also some unidentified brominated compounds in this PEKK study, in contrast to the PEEK studies, where none were found by MS. This is likely due to the low concentrations and lack of solubility of many of these products from PEEK. It is also worth noting that a hydrolyzed larger product was

identified with MS. This shows that phenol does not only stem from diphenyl ether in PEKK or from dpb in PEEK, but also from larger polymer fragments.

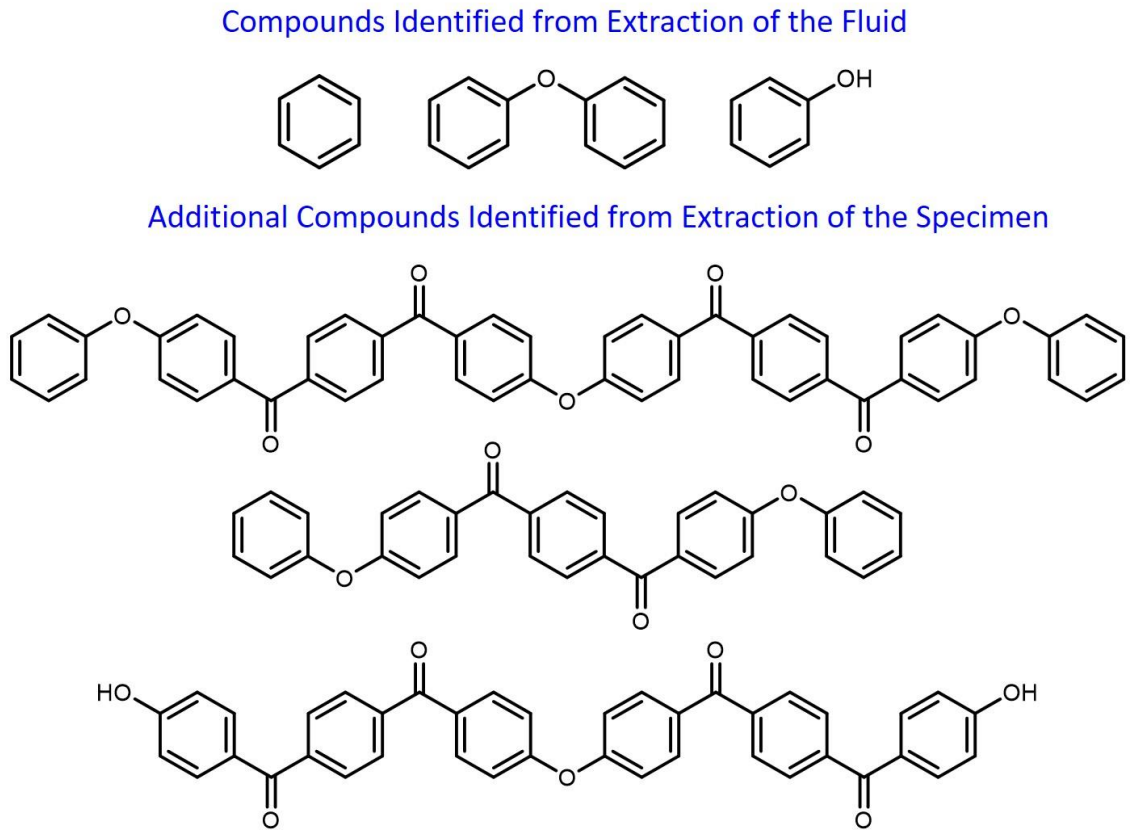

Figure 3.14. Compounds identified in PEKK extracts of the fluids and the specimens.

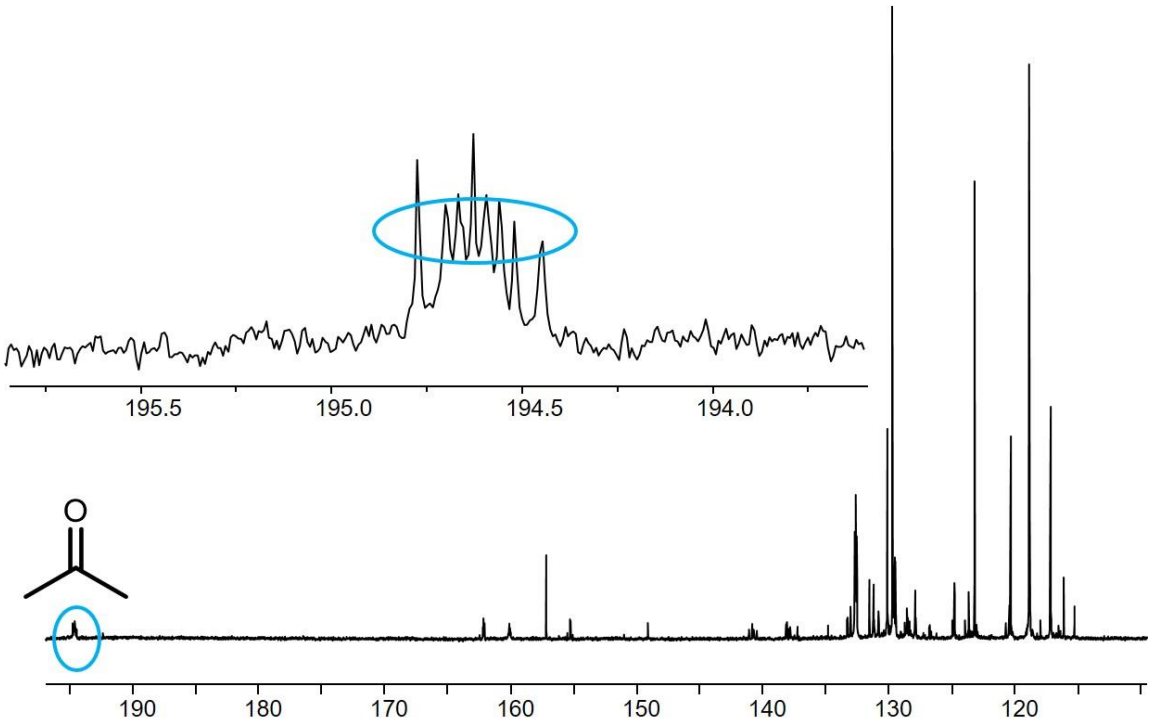

Figure 3.15. ^{13}C NMR of PEKK specimen extract after exposure for 4 days to fluid **1**.

3.3 Conclusions

Using chloroform extraction and quantitative NMR in combination with other analytical techniques, different degradation mechanisms for PEEK as well as PEKK were identified.

1. Radical cleavage at the ketone with subsequent protonation.
2. Hydrolysis
3. Bromination
4. Ring closure to form benzofurans

Especially completion fluids containing $ZnBr_2$ are very detrimental to PAEK polymers, and the $ZnBr_2$ concentration of the fluids plays a large role. In summary, in

order to prevent polymer degradation under extreme HP/HT conditions, $ZnBr_2$ should be avoided as an ingredient of completion fluids.

3.4 Experimental

3.4.1 Materials and Instrumentation

PEEK450G compression molded specimens (6378 tensiles) were provided by the company Hoerbiger and experiments were performed at Texas A&M and at Baker Hughes in Parr Hastelloy Pressure Vessels. The molecular compounds were characterized after extraction by NMR spectroscopy. The liquids NMR spectra were recorded on a Varian Inova-500. The signal assignments have been obtained by $^{1}H,^{1}H$ COSY, $^{13}C,^{1}H$ HSQC, and $^{13}C,^{1}H$ HMBC NMR measurements. Samples were quantified by a separate capillary standard calibrated to the concentration $CHDCl_2$ from CD_2Cl_2. All solid-state NMR spectra of the PEEK specimens were recorded on a Bruker Avance 400 spectrometer, equipped with a 2.5 mm broadband MAS probehead and ZrO_2 rotors. All spectra were recorded at room temperature (298 K). DSC measurements were completed in air with a ramp of 10 °C/min both forward and reverse. TGA measurements were measured at a 10 °C/min in air unless noted.

3.4.2 Extractions from Fluids

In all experiments, 5 mL of completion fluid was extracted with 2.5 mL of $CDCl_3$. After the $CDCl_3$ was added the mixture was stirred for at least 2 hours. Subsequently, 0.78 mL of the $CDCl_3$ was removed and placed in an NMR tube with the centered, calibrated capillary standard. The remaining fluid was checked multiple times to ensure

complete extraction of the small molecules. There were no cases where additional small molecules were extracted after the first procedure.

3.4.3 Extractions from Specimens

Unless noted otherwise, the specimens were first broken into smaller pieces and cryomilled for 5 minutes. This resulted in a fine powder. For the extraction 200 mg of the polymer was weighed and placed in a vial. Then 1.5 mL of $CDCl_3$ was added. This was allowed to sit for at least two hours. Subsequently, the solution was filtered with a micron frit and 0.78 mL of the $CDCl_3$ was measured.

3.4.4 Data of Compounds Identified from PEEK Degradation

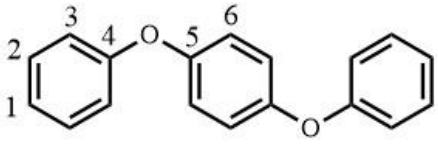

^{1}H NMR ($CDCl_3$, 500.1 MHz): δ = 7.33 (H2, t, ^{3}J(H-H) = 7.5 Hz), 7.09 (H1, t, ^{3}J(H-H) = 7.3 Hz), 7.00 (H3, d, ^{3}J(H-H) = 7.5 Hz), 7.00 (H6, s) ppm; ^{13}C NMR ($CDCl_3$, 125.8 MHz): δ = 157.75 (C4, s), 152.66 (C5, s), 129.72 (C2, s), 122.98 (C1, s), 120.45 (C6, s), 118.26 (C3, s) ppm. GC-MS (retention time 17.85 m), Electron Ionization: 262.09 m/z.

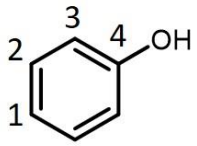

^{1}H NMR ($CDCl_3$, 500.1 MHz): δ = 7.24 (H2, t, ^{3}J(H-H) = 7.3 Hz), 6.93 (H1, d ^{3}J(H-H) = 7.5 Hz), 6.83 (H3, d, ^{3}J(H-H) = 7.7 Hz) ppm; ^{13}C NMR ($CDCl_3$, 125.8 MHz): δ 155.72 (C4, s), 129.65 (C2, s), 120.77 (C1, s), 115.25 (C3, s) ppm. The chemical shifts and coupling constants match those of a pure phenol sample.

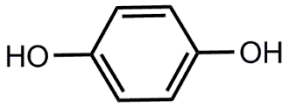

Identified from the ^{13}C NMR signal of the non-quaternary carbon at 117.19 ppm in the completion fluid **1** after 12 days of PEEK treatment and being extracted with $CDCl_3$. To confirm that this signal stems from hydroquinone, both hydroquinone spiked D_2O and completion fluid were compared.

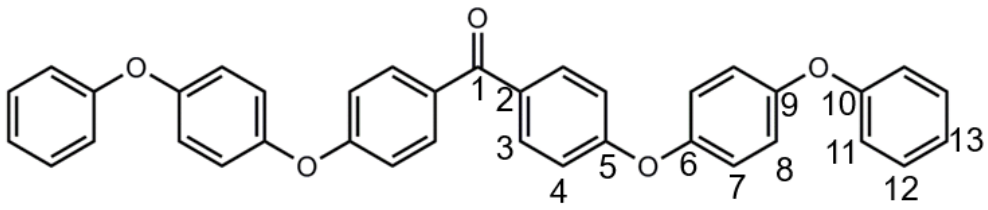

^{1}H NMR (500 MHz, $CDCl_3$): δ(ppm) 7.81 (d, 8.7 Hz, 4H, H3); 7.37 (t, 7.6 Hz, 4H, H12); 7.13 (t, 7.4 Hz, 2H, H13); 7.07 (d, 5.2 Hz, 4H, H7); 7.07 (d, 5.2 Hz, 4H, H8); 7.04 (d, 7.9 Hz, 4H, H11); 7.04 (d, 8.8 Hz, 4H, H4). ^{13}C NMR (125 MHz, $CDCl_3$): δ (ppm) 194.20 (C1); 161.77 (C5); 157.36 (C10); 153.87 (C6); 150.88 (C9); 132.24 (C3); 132.12

(C2); 129.82 (C12); 123.34 (C13); 121.60 (C7); 120.39 (C8); 118.62 (C11); 116.71 (C4). MALDI (positive mode): m/z 551.2 [M+H].

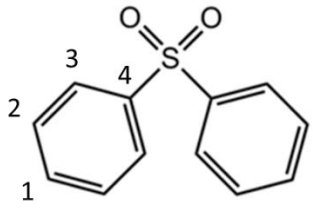

^{1}H NMR ($CDCl_3$, 500.1 MHz): δ = 7.95 (H2, t, ^{3}J(H-H) = 7.3 Hz), 7.57 (H1, d ^{3}J(H-H) = 7.5 Hz), 7.51 (H3, d, ^{3}J(H-H) = 7.7 Hz) ppm; ^{13}C NMR ($CDCl_3$, 125.8 MHz): δ 145.52 (C4, s), 131.00 (C1, s), 129.26 (C2, s), 124.72 (C3, s) ppm. The NMR data from the extractions matches ^{1}H and ^{13}C NMR literature values[43] as well as the NMR data of a compound synthesized by oxidation of diphenylsulfide.

3.4.5 Data of Compounds Identified from PEKK Degradation

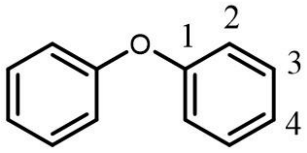

^{1}H NMR ($CDCl_3$, 500.1 MHz): δ = 7.33 (H3, t, ^{3}J(H-H) = 7.8 Hz), 7.10 (H4, d ^{3}J(H-H) = 7.0 Hz), 7.01 (H2, d, ^{3}J(H-H) = 7.8 Hz) ppm; ^{13}C NMR ($CDCl_3$, 125.8 MHz): δ 157.25 (C1, s), 129.75 (C3, s), 120.33 (C4, s), 118.80 (C2, s) ppm.

^{1}H NMR ($CDCl_3$, 500.1 MHz): δ = 7.36 ppm; ^{13}C NMR ($CDCl_3$, 125.8 MHz): δ 128.37 ppm.[44]

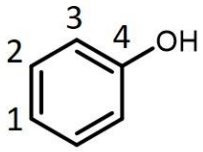

^{1}H NMR ($CDCl_3$, 500.1 MHz): δ = 7.24 (H2, t, ^{3}J(H-H) = 7.3 Hz), 6.93 (H1, d ^{3}J(H-H) = 7.5 Hz), 6.83 (H3, d, ^{3}J(H-H) = 7.7 Hz) ppm; ^{13}C NMR ($CDCl_3$, 125.8 MHz): δ 155.72 (C4, s), 129.65 (C2, s), 120.77 (C1, s), 115.25 (C3, s) ppm.

CHAPTER IV

SUMMARY

Various tetraphosphine linkers with rigid scaffolds have been synthesized to determine whether increasing the distance between the catalyst and the support surface would increase the lifetime of the catalysts and prevent nanoparticle formation. This hypothesis was proven to be correct. It has been determined that the biphenyl spacers incorporated in the linker scaffolds led to highly active and recyclable immobilized catalysts. The reaction time for complete olefin hydrogenation and the recyclability of these catalysts were similar to the results obtained for catalysts immobilized by linkers with tetraphenylelement cores. Catalysts coordinated by alkylphosphine linkers required higher temperatures for the hydrogenation and could not be recycled as many times as those with arylphosphine linkers. Future work will focus on rigid scaffold linkers incorporating chelating alkyldiarylphosphine ligands that do not dissociate readily from the metal center while still allowing for fast catalytic reactions.

PEEK degradation mechanisms in $ZnBr_2$ completion fluids were shown to follow complicated pathways that are still under investigation. A novel standardized method of studying small molecules being eluted during the degradation process with quantitative solution NMR has been developed. This method allowed the determination of three main chemical mechanisms and to distinguish primary degradation products from secondary products. The three mechanisms found are radical C-C bond cleavage, hydrolysis of diaryl ether linkages, and bromination. New molecular model compounds were synthesized that were crucial for determining that bromination occurred at the polymer

backbone during exposure of specimens to high temperatures under high pressures. Higher concentrations of $ZnBr_2$ accelerated the PEEK degradation processes. Future work is focused on other variables during the treatment of the specimens, such as the influence of the surface area of the polymer.

REFERENCES

1. Gladysz, J. A. *Pure Appl. Chem.* **2001**, *73*, 1319-1324.

2. (a) Gladysz, J. A.; Curran, D. P.; Horvath, I. T.; Editors, *Handbook of Flurorous Chemistry*. Wiley-VCH Verlag GmbH & Co. KGaA: 2004; p 594 pp; (b) Juliette, J. J. J.; Rutherford, D.; Horváth, I. T.; Gladysz, J. A. *J. Am. Chem. Soc.* **1999**, *121*, 2696-2704; (c) Guillevic, M. A.; Rocaboy, C.; Arif, A. M.; Horváth, I. T.; Gladysz, J. A. *Organometallics* **1998**, *17*, 707-717; (d) Juliette, J. J. J.; Gladysz, J. A.; Horváth, I. T. *Angew. Chem. Int. Ed.* **1997**, *36*, 1610-1612.

3. Dinh, L. V.; Gladysz, J. A. *Angew. Chem. Int. Ed.* **2005**, *44*, 4095-4097.

4. Selected books and reviews: (a)Barbaro, P.; Liguori, F., Eds., *Heterogenized Homogeneous Catalysts for Fine Chemicals Production*, Springer: Heidelberg, 2010; (b) Blümel, J. *Coord. Chem. Rev.* **2008**, 252, 2410-2423; (c) Hartley, F. R., *Supported Metal Complexes*; Reidel, D. Publ. Co.: Dordrecht, The Netherlands, 1985; (d) DeVos, D.; Vankelecom J.; Jacobs P. A., Eds., *Chiral Catalyst Immobilization and Recycling*: Wiley-VCH: Weinheim, 2000; (e) Rothenberg G., *Catalysis: Concepts and Green Applications*; Wiley-VCH, Weinheim, 2008.

5. Silbernagel, R.; Díaz, A.; Steffensmeier, E.; Clearfield, A.; Blümel, J. *J. Mol. Catal. A: Chem.* **2014**, *394*, 217-223.

6. Merckle, C.; Blümel, J. *Chem. Mater.* **2001**, *13*, 3617-3623.

7. Merck silica 40, average particle size 0.063-0.2 mm, specific surface area 750 m^2/g, average pore diameter 40 Å.

8. (a) Behringer, K. D.; Blümel, J. *Inorg. Chem.* **1996**, *35*, 1814-1819; (b) Blümel, J. *J. Am. Chem. Soc.* **1995**, *117*, 2112-2113.

9. (a) Vansant, E. F.; VanDer Voort, P.; Vrancken, K. C., *Characterization and Chemical Modification of the Silica Surface; Elsevier*: Amsterdam, 1995; (b) Scott R. P. W., *Silica Gel and Bonded Phases*; John Wiley and Sons: New York, 1993.

10. (a) Behringer, K. D.; Blümel, J. *Inorg. Chem.* **1996**, 35, 1814-1819; (b) Reinhard, S.; Soba, P.; Rominger, F.; Blümel, J. *Adv. Synth. Catal.* **2003**, 345, 589-602; (c) Piestert, F.; Fetouaki, R.; Bogza, M.; Oeser, T.; Blümel, J. *Chem. Commun.* **2005**, 11, 1481-1483.

11. (a) Pope, J. C.; Posset, T.; Bhuvanesh, N.; Blümel, J. *Organometallics* **2014**, *33*, 6750-6753; (b) Posset T.; Guenther, J.; Pope, J. C.; Oeser, T.; Blümel, J. *Chem. Commun.* **2011**, *47*, 2059-2061; (c) Posset, T.; Blümel, J. *J. Am. Chem. Soc.* **2006**, *128*, 8394-8395.

12. (a) Guenther, J.; Reibenspies, J.; Blümel, J. *Adv. Synth. Catal.* **2011**, *353*, 443-460; (b) Merckle, C.; Blümel, J. *Top. Catal.* **2005**, *34*, 5-15; (c) Merckle, C.; Blümel, J. *Adv. Synth. Catal.* **2003**, *345*, 584-588; (d) Merckle, C.; Haubrich, S.; Blümel, J. *J. Organomet. Chem.* **2001**, *627*, 44-54.

13. Osborn, J. A.; Jardine, F. H.; Young, J. F.; Wilkinson, G. *J. Chem. Soc. A: Inorganic, Physical, Theoretical* **1966**, 1711-1732.

14. Posset, T.; Rominger, F.; Blümel, J. *Chem. Mater.* **2005**, *17*, 586-595.

15. (a) Sommer, J.; Yang, Y.; Rambow, D.; Blümel, J. *Inorg. Chem.* **2004**, *43*, 7561-7563; (b) Bluemel, J. *Inorg. Chem.* **1994**, *33*, 5050-5056.

16. Yang, Y.; Beele, B.; Blümel, J. *J. Am. Chem. Soc.* **2008**, *130*, 3771-3773.

17. Beele, B.; Guenther, J.; Perera, M.; Stach, M.; Oeser, T.; Blümel, J. *New J. Chem.* **2010**, *34*, 2729-2731.

18. (a) *The Handbook of Homogeneous Hydrogenation*, 1st ed., Vols 1-3 (Eds.: de Vries, J. G.; Elsevier, C. J.), Wiley-VCH, Weinheim, 2007; (b) *Handbook of Heterogeneous Catalysis*, 2nd ed., (Eds.: Ertl, G.; Knözinger, H.; Schüth, F.; Weitkamp, J.), Wiley-VCH, Weinheim, 2008; (c) Wende, M.; Meier, R.; Gladysz, J. A. *J. Am. Chem. Soc.* **2001**, 123, 11490, and lit. cited therein; (d) *Adv. Synth. Catal.* **2003**, 345, vols. 1+2, Special Issue on Hydrogenation, including, e.g.: Knowles, W. S. *Adv. Synth. Catal.* **2003,** 345, 3; Noyori, R. *Adv. Synth. Catal.* **2003**, 345, 15; Imamoto, T. *Adv. Synth. Catal.* **2003**, 345, 79; (e) Heinekey, D. M.; Lledós, A.; Lluch, J. M. *Chem. Soc. Rev.* **2004,** 33, 175-182.

19. (a) Kromm, K.; Osburn, P. L.; Gladysz, J. A. *Organometallics* **2002**, *21*, 4275-4280; (b) Soós, T.; Bennett, B. L.; Rutherford, D.; Barthel-Rosa, L. P.; Gladysz, J. A. *Organometallics* **2001**, *20*, 3079-3086; (c) Kromm, K.; Zwick, B. D.; Meyer, O.; Hampel, F.; Gladysz, J. A. *Chemistry* **2001**, *7*, 2015-27; (d) Rutherford, D.; Juliette, J. J. J.; Rocaboy, C.; Horváth, I. T.; Gladysz, J. A. *Catal. Today* **1998**, *42*, 381-388.

20. (a) Zhang, M.; Chen, Y.-P.; Bosch, M.; Gentle, T.; Wang, K.; Feng, D.; Wang, Z. U.; Zhou, H.-C. *Angew. Chem. Int. Ed.* **2014**, *53*, 815-818; (b) Feng, D.; Wang, K.; Wei, Z.; Chen, Y.-P.; Simon, C. M.; Arvapally, R. K.; Martin, R. L.; Bosch, M.; Liu, T.-F.; Fordham, S.; Yuan, D.; Omary, M. A.; Haranczyk, M.; Smit, B.; Zhou, H.-C. *Nat. Commun.* **2014**, *5*; (c) Wen, L.; Cheng, P.; Lin, W. *Chemical Science* **2012**, *3*, 2288-2292; (d) Ma, L.; Jin, A.; Xie, Z.; Lin, W. *Angew. Chem. Int. Ed.* **2009**, *48*, 9905-9908.

21. (a) Fraccarollo, A.; Canti, L.; Marchese, L.; Cossi, M. *Langmuir* **2014**, *30*, 4147-4156; (b) Yu, H.; Shen, C.; Tian, M.; Qu, J.; Wang, Z. *Macromolecules* **2012**, *45*, 5140-5150; (c) Cossi, M.; Gatti, G.; Canti, L.; Tei, L.; Errahali, M.; Marchese, L.

Langmuir **2012**, *28*, 14405-14414; (d) Lu, W.; Yuan, D.; Zhao, D.; Schilling, C. I.; Plietzsch, O.; Muller, T.; Bräse, S.; Guenther, J.; Blümel, J.; Krishna, R.; Li, Z.; Zhou, H.-C. *Chem. Mater.* **2010**, *22*, 5964-5972.

22. (a) You, J.; Li, G.; Wang, Z. *RSC Advances* **2012**, *2*, 9488-9494; (b) Kim, S. O.; Zhao, Q.; Thangaraju, K.; Kim, J. J.; Kim, Y. H.; Kwon, S. K. *Dyes and Pigments* **2011**, *90*, 139-145.

23. (a) Wang, L.; Wang, D.; Wang, H.; Feng, S. *J. Organomet. Chem.* **2014**, *767*, 40-45; (b) Eryazici, I.; Farha, O. K.; Compton, O. C.; Stern, C.; Hupp, J. T.; Nguyen, S. T. *Dalton Trans.* **2011**, *40*, 9189-9193; (c) Shen, Q.; Ye, S.; Yu, G.; Lu, P.; Liu, Y. *Synth. Met.* **2008**, *158*, 1054-1058; (d) Iyer, P. K.; Wang, S. *Tetrahedron Lett.* **2006**, *47*, 437-439; (e) Bai, D. R.; Wang, S. *Organometallics* **2004**, *23*, 5958-5966; (f) Wang, S.; Oldham, W. J.; Hudack, R. A.; Bazan, G. C. *J. Am. Chem. Soc.* **2000**, *122*, 5695-5709.

24. (a) Yang, C. Y.; Wang, S.; Robinson, M. R.; Bazan, G. C.; Heeger, A. J. *Chem. Mater.* **2001**, *13*, 2342-2348; (b) Pegenau, A.; Hegmann, T.; Tschierske, C.; Diele, S. *Chem. Eur. J.* **1999**, *5*, 1643-1660; (c) Murphy, S.; Yang, X.; Schuster, G. B. *J. Org. Chem.* **1995**, *60*, 2411-22; (d) Lequan, M.; Branger, C.; Simon, J.; Thami, T.; Chauchard, E.; Persoons, A. *Adv. Mater.* **1994**, *6*, 851-853; (e) Blake, E. S.; Hammann, W. C.; Edwards, J. W.; Reichard, T. E.; Ort, M. R. *J. Chem. Eng. Data* **1961**, *6*, 87-98.

25. (a) Fyfe, C. A., *Solid-State NMR for Chemists*; C.F.C. Press, Guelph, Canada, 1983; (b) Duncan, T. M., *A Compilation of Chemical Shift Anisotropies*; Farragut Press: Chicago, IL, 1990; (c) Reinhard, S.; Blümel, J. *Magn. Reson. Chem.* **2003**, *41*, 406.

26. (a) Cluff, K. J.; Blümel, J. *Chem. Eur. J.* **2016**, *22*, 16562-16575; (b) Cluff, K. J.; Blümel, J. *Organometallics* **2016**, *35*, 3939-3948; (c) Cluff, K. J.; Bhuvanesh, N.; Blümel, J. *Organometallics* **2014**, *33*, 2671-2680; (d) Cluff, K. J.; Schnellbach, M.; Hilliard, C. R.; Blümel, J. *J. Organomet. Chem.* **2013**, *744*, 119-124.

27. (a) Kotha, S.; Shah, V. R. *Amino Acids* **2008**, *35*, 83-88; (b) Liu, B.; Dan, T. T.; Bazan, G. C. *Adv. Funct. Mater.* **2007**, *17*, 2432-2438; (c) Takeuchi, Y.; Nishikawa, M.; Hachiya, H.; Yamamoto, H. *Magn. Reson. Chem.* **2005**, *43*, 662-664; (d) Alaviuhkola, T.; Bobacka, J.; Nissinen, M.; Rissanen, K.; Ivaska, A.; Pursiainen, J. *Chem. Eur. J.* **2005**, *11*, 2071-2080.

28. (a) Nagaki, A.; Takabayashi, N.; Tomida, Y.; Yoshida, J. I. *Beilstein Journal of Organic Chemistry* **2009**, *5*, 16; (b) Nagaki, A.; Takabayashi, N.; Tomida, Y.; Yoshida, J. I. *Org. Lett.* **2008**, *10*, 3937-3940; (c) Dolman, S. J.; Gosselin, F.; O'Shea, P. D.; Davies, I. W. *Tetrahedron* **2006**, *62*, 5092-5098.

29. Yang, Y. Doctoral thesis, Universität Heidelberg, 2007.

30. Nising, C. F.; Schmid, U. K.; Nieger, M.; Bräse, S. *J. Org. Chem.* **2004**, *69*, 6830-6833.

31. CCDC 1527673 contains the supplementary crystallographic data for this compound. This data can be obtained free of charge from The Cambridge Crystallographic Data Centre. The unit cell parameters are - a = 16.7257(9), b = 16.7257(9), c = 7.1979(4). The space group is P4.

32. Stahl, J.; Bohling, J. C.; Bauer, E. B.; Peters, T. B.; Mohr, W.; Martin-Alvarez, J. M.; Hampel, F.; Gladysz, J. A. *Angew. Chem. Int. Ed.* **2002**, *41*, 1871-1876.

33. Hinch, R. J.; Krc, J. *Anal. Chem.* **1957**, *29*, 1550-1551.

34. Schraml, J.; Čapka, M.; Blechta, V. *Magn. Reson. Chem.* **1992**, *30*, 544-547.

35. Köhler, F. H.; Hertkorn, N.; Blümel, J. *Chem. Ber.* **1987**, *120*, 2081-2082.

36. Hilliard, C. R.; Kharel, S.; Cluff, K. J.; Bhuvanesh, N.; Gladysz, J. A.; Blümel, J. *Chem. Eur. J.* **2014**, *20*, 17292-17295.

37. (a) Mylläri, V.; Ruoko, T. P.; Vuorinen, J.; Lemmetyinen, H. *Polymer Degradation and Stability* **2015**, *120*, 419-426; (b) Patel, P.; Hull, T. R.; McCabe, R. W.; Flath, D.; Grasmeder, J.; Percy, M. *Polymer Degradation and Stability* **2010**, *95*, 709-718; (c) Tsai, C. J.; Perng, L. H.; Ling, Y. C. *Rapid Commun. Mass Spectrom.* **1997**, *11*, 1987-1995; (d) Day, M.; Sally, D.; Wiles, D. M. *J. Appl. Polym. Sci.* **1990**, *40*, 1615-1625.

38. (a) Zhou, Y.; Wang, N.; Li, M.; Wu, L.; Wu, T.; Xu, J.; Liu, P. *J. Appl. Polym. Sci.* **2013**, *129*, 2393-2398; (b) Akbarian-Feizi, L.; Mehdipour-Ataei, S.; Yeganeh, H. *J. Appl. Polym. Sci.* **2012**, *124*, 1981-1992; (c) Thiruvasagam, P.; Venkatesan, D. *High Perform. Polym.* **2010**, *22*, 682-693; (d) Hayakawa, T.; Goseki, R.; Kakimoto, M. A.; Tokita, M.; Watanabe, J.; Liao, Y.; Horiuchi, S. *Org. Lett.* **2006**, *8*, 5453-5456.

39. Shukla, D.; Negi, Y. S.; Uppadhyaya, J. S.; Kumar, V. *Polymer Reviews* **2012**, *52*, 189-228.

40. Dandy, L. O.; Oliveux, G.; Wood, J.; Jenkins, M. J.; Leeke, G. A. *Polymer Degradation and Stability* **2015**, *112*, 52-62.

41. Yang, L.; Li, Y.; Savage, P. E. *Industrial & Engineering Chemistry Research* **2014**, *53*, 2633-2639.

42. Qian, J.; Mopper, K.; Kieber, D. J. *Deep Sea Research Part I: Oceanographic Research Papers* **2001**, *48*, 741-759.

43. Yang, H.; Li, Y.; Jiang, M.; Wang, J.; Fu, H. *Chem. Eur. J.* **2011**, *17*, 5652-5660.

44. Gottlieb, H. E.; Kotlyar, V.; Nudelman, A. *J. Org. Chem.* **1997**, *62*, 7512-7515.

APPENDIX A

SUPPLEMENTARY CHAPTER 1

Molecular Compounds

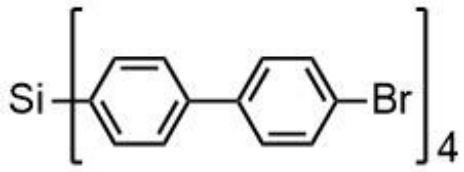

1

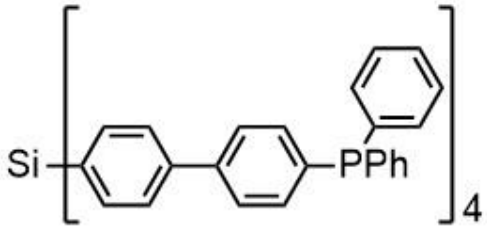

2

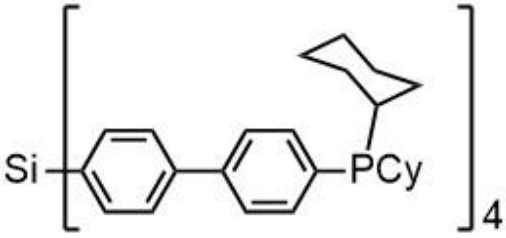

3

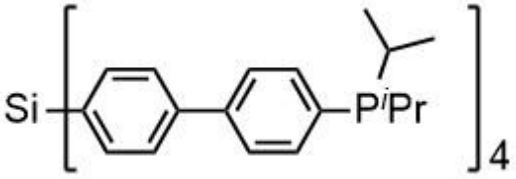

4

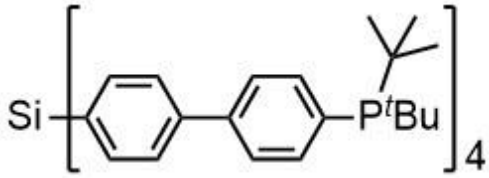

5

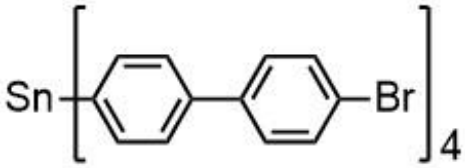

6

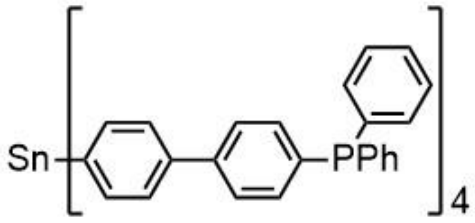

7

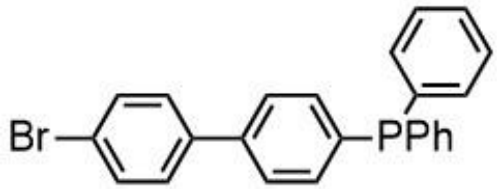

8

Immobilized Species

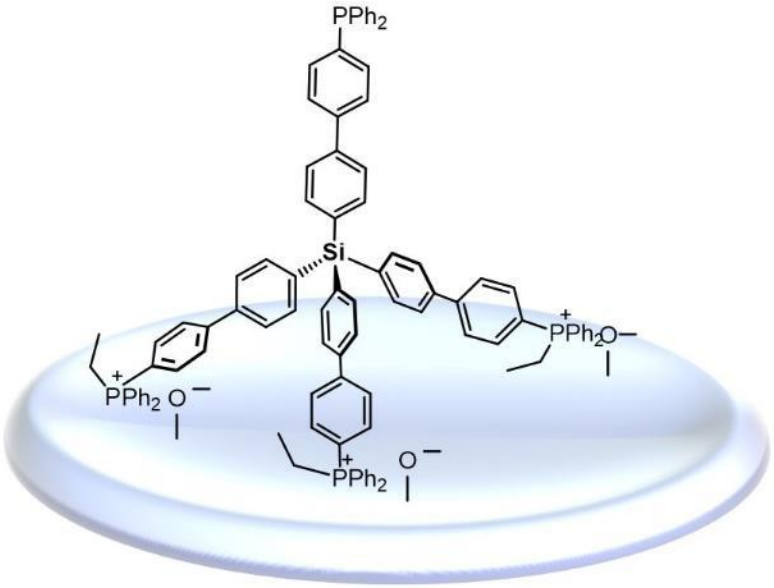

2i

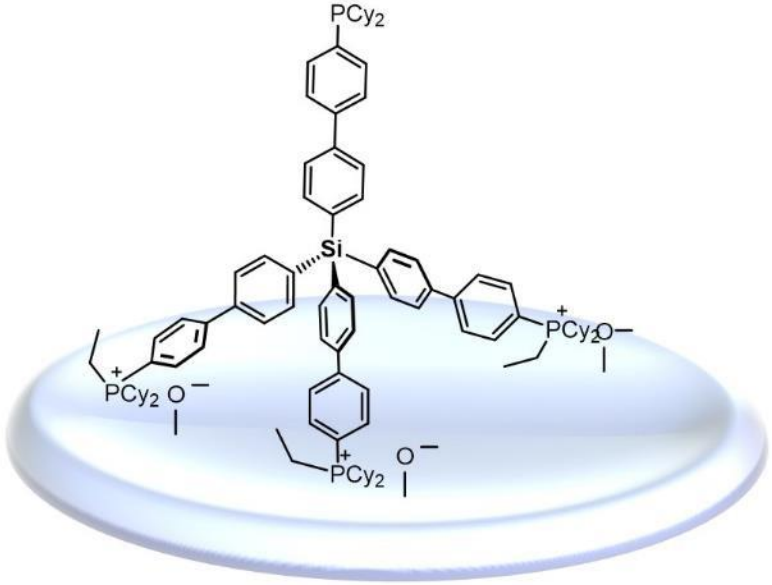

3i

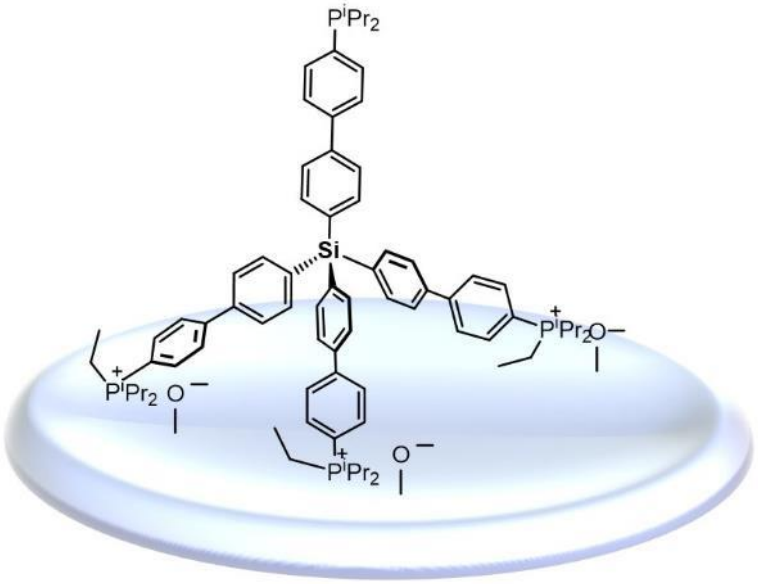

4i

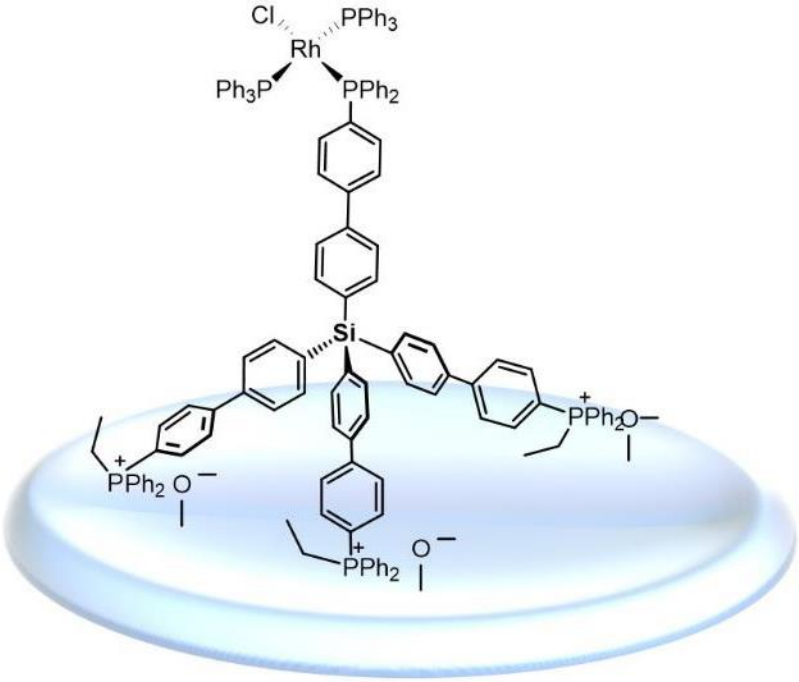

2iRh

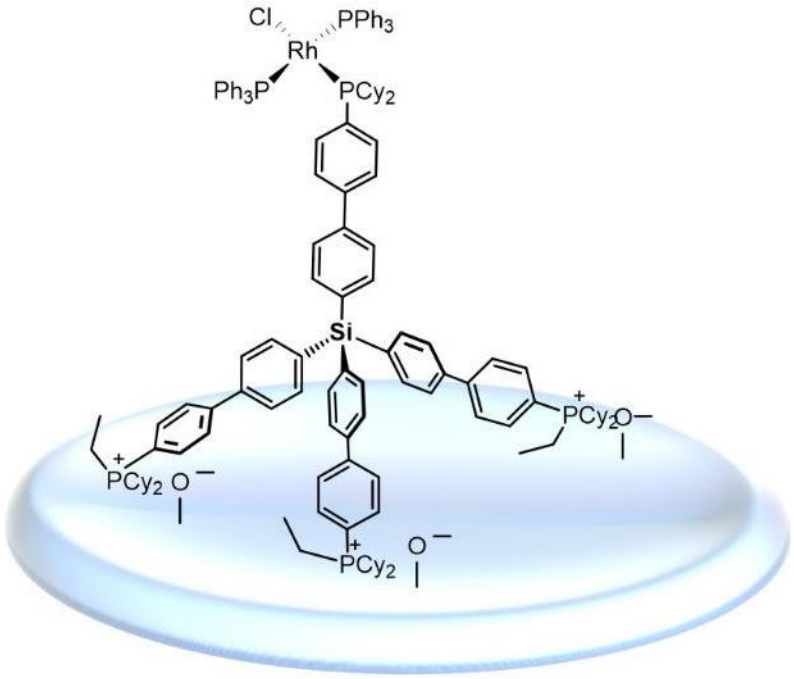
Cl
PPh3
Rh
Ph3P
PCy2
Si
PCy2
O
PCy2
O
PCy2
O

3iRh

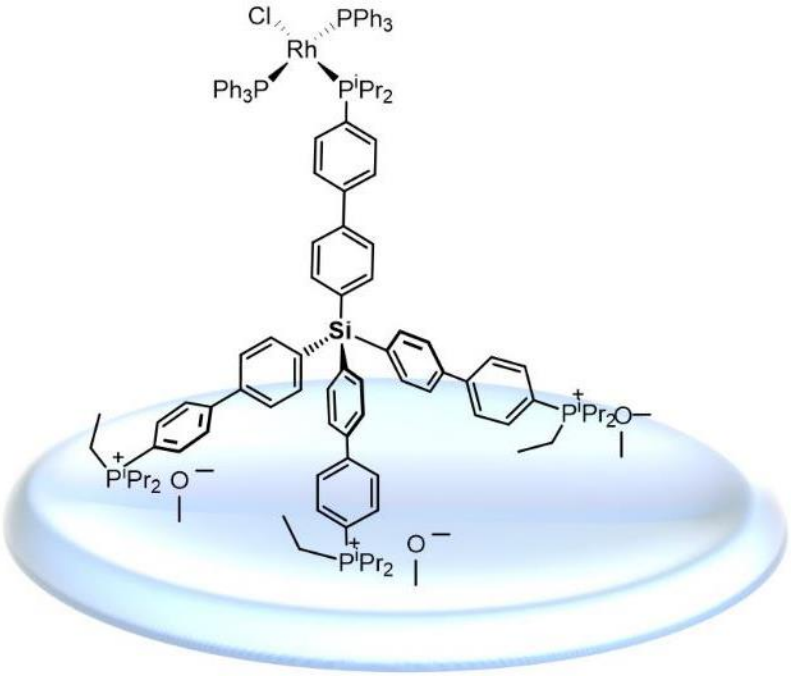
Cl
PPh3
Rh
Ph3P
PiPr2
Si
PiPr2
O
PiPr2
O
PiPr2
O

4iRh

NMR Spectra

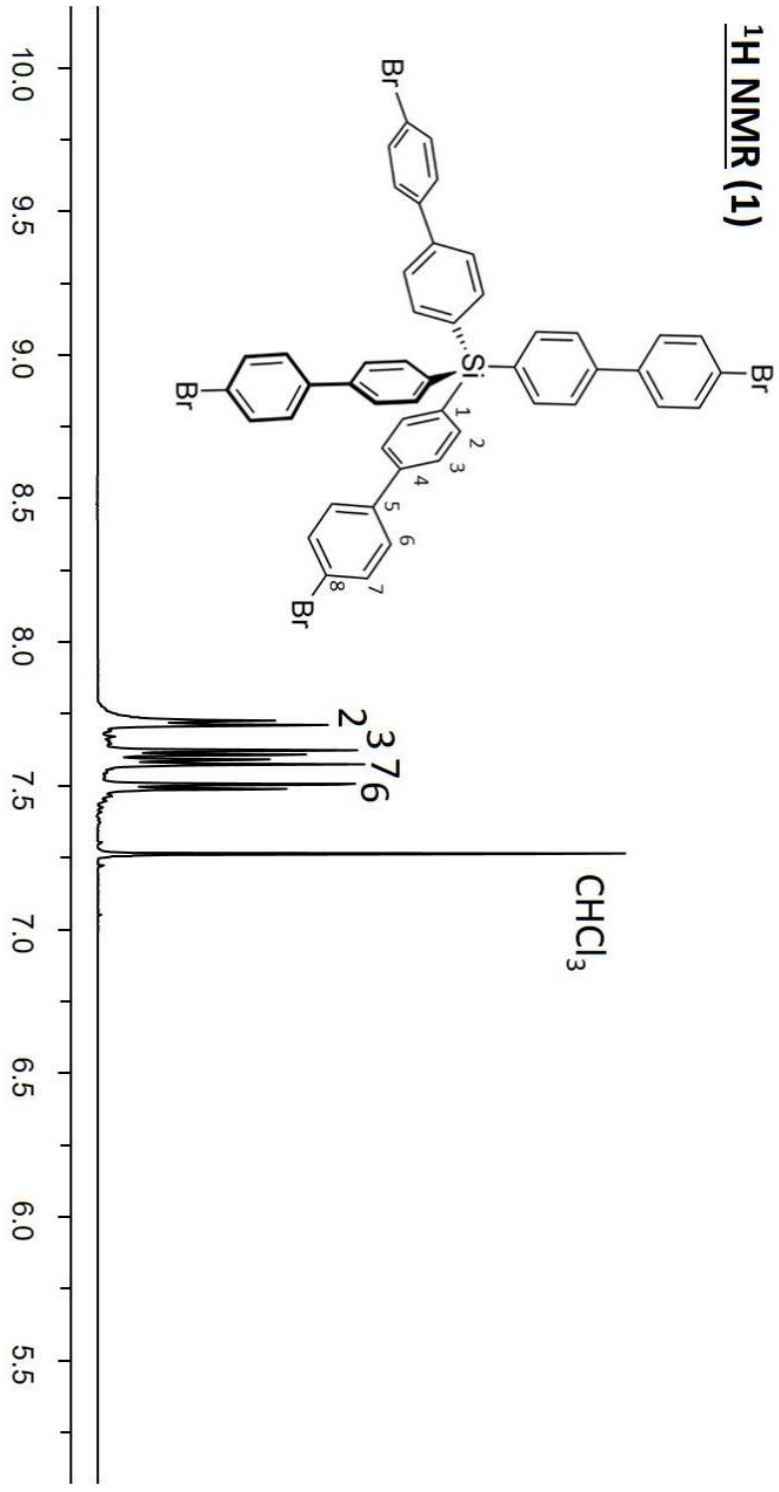
¹H NMR (1)
Br
Br
Br
Br
Si
1
2
3
4
5
6
7
8
2
3
7
6
CHCl3
10.0
9.5
9.0
8.5
8.0
7.5
7.0
6.5
6.0
5.5

^{13}C NMR (1)

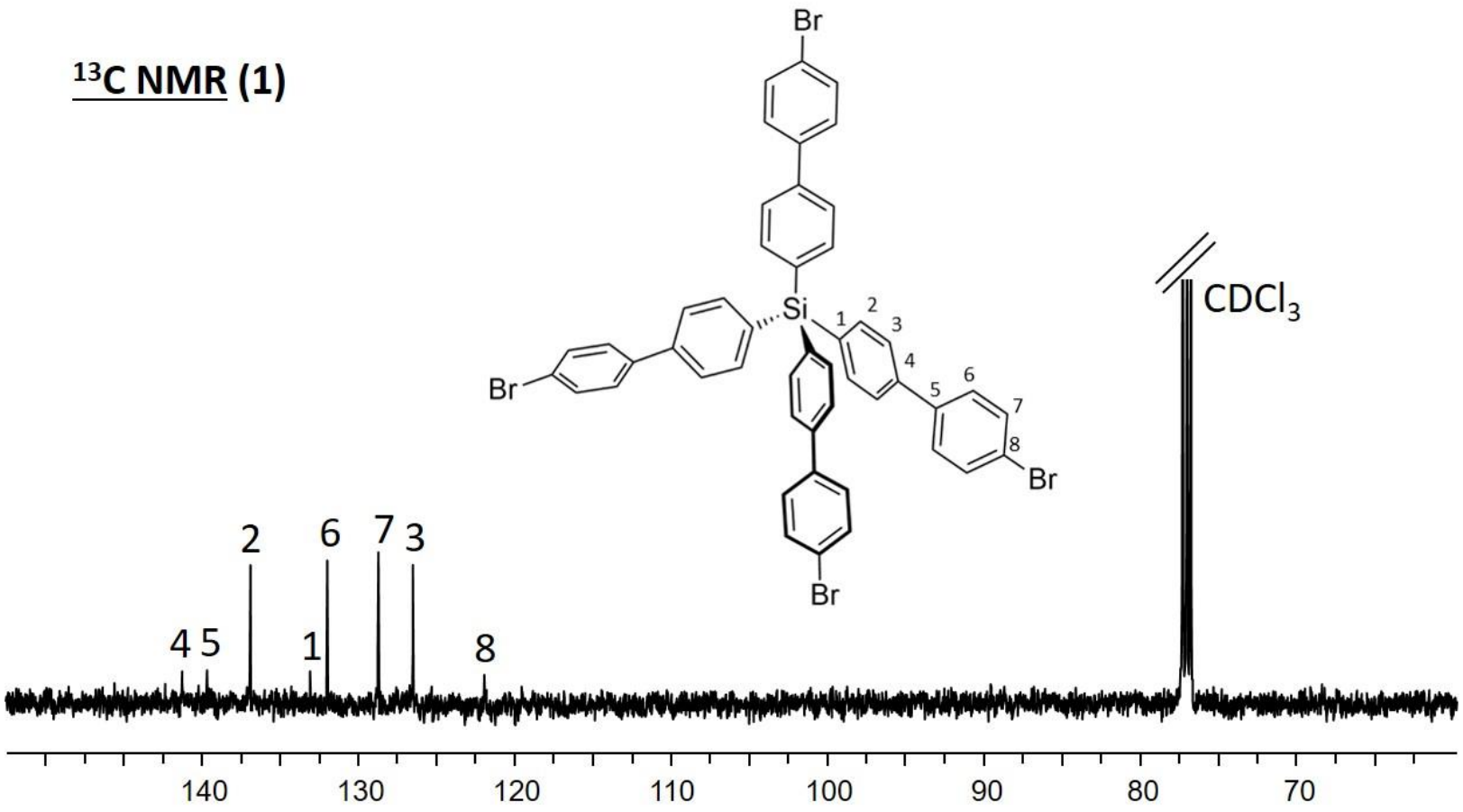
Br
Br
Br
Br
Si
1
2
3
4
5
6
7
8
CDCl3
2
6
7
3
4
5
1
8
140
130
120
110
100
90
80
70

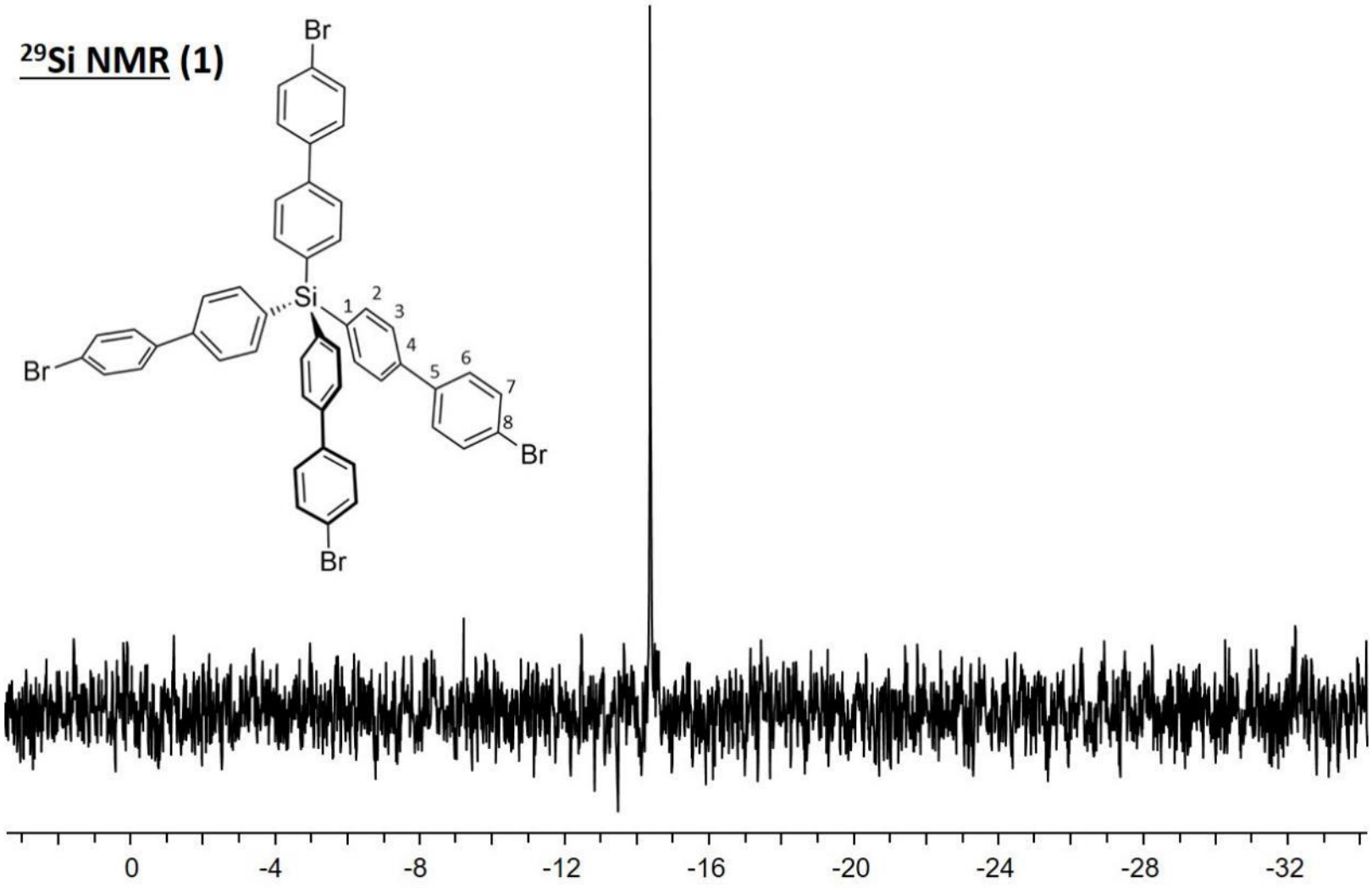
29Si NMR (1)
Br
Br
Br
Br
Si
1
2
3
4
5
6
7
8
0
-4
-8
-12
-16
-20
-24
-28
-32

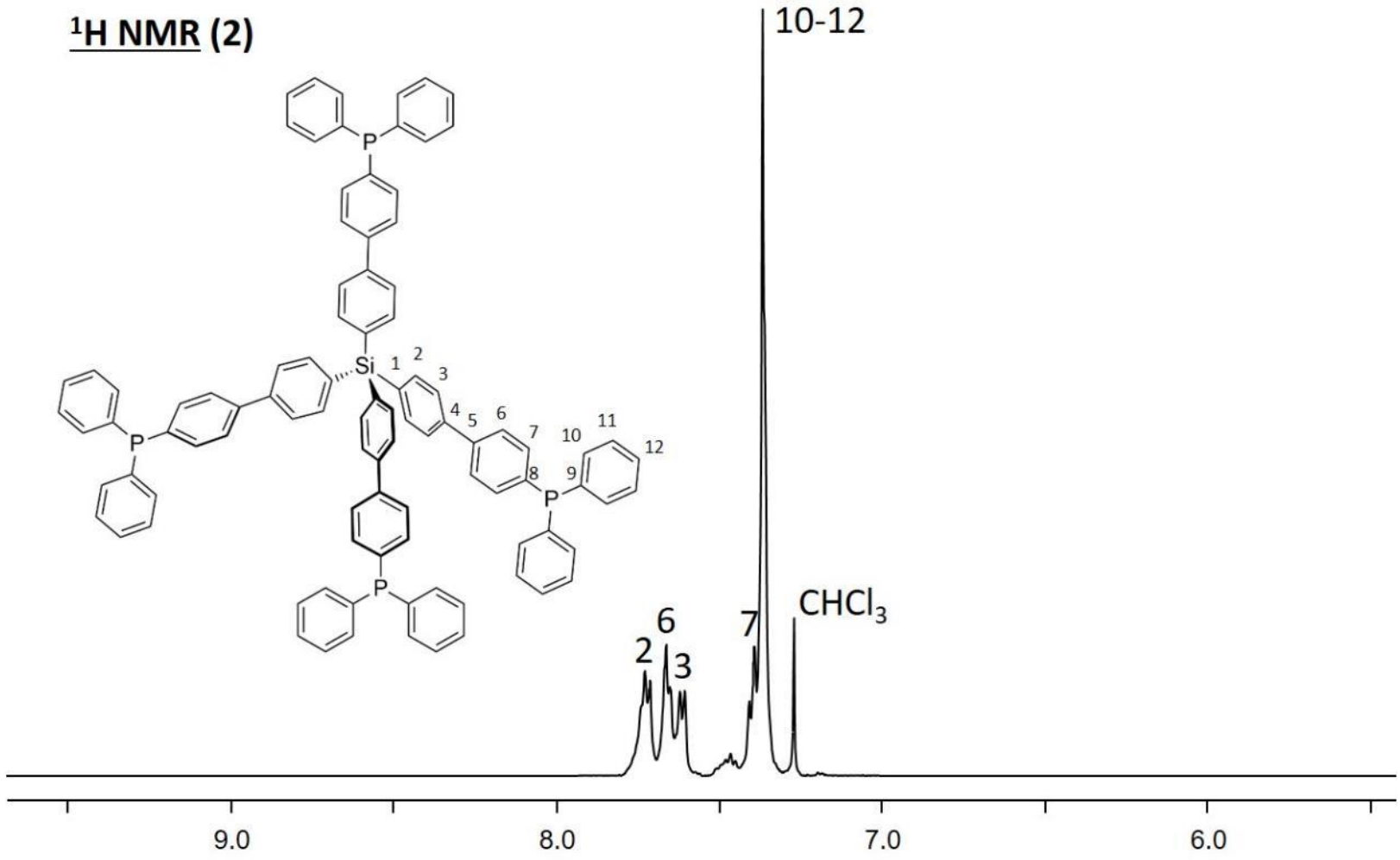
¹H NMR (2)
10-12
Si
P
1
2
3
4
5
6
7
8
9
10
11
12
2
6
3
7
CHCl3
9.0
8.0
7.0
6.0

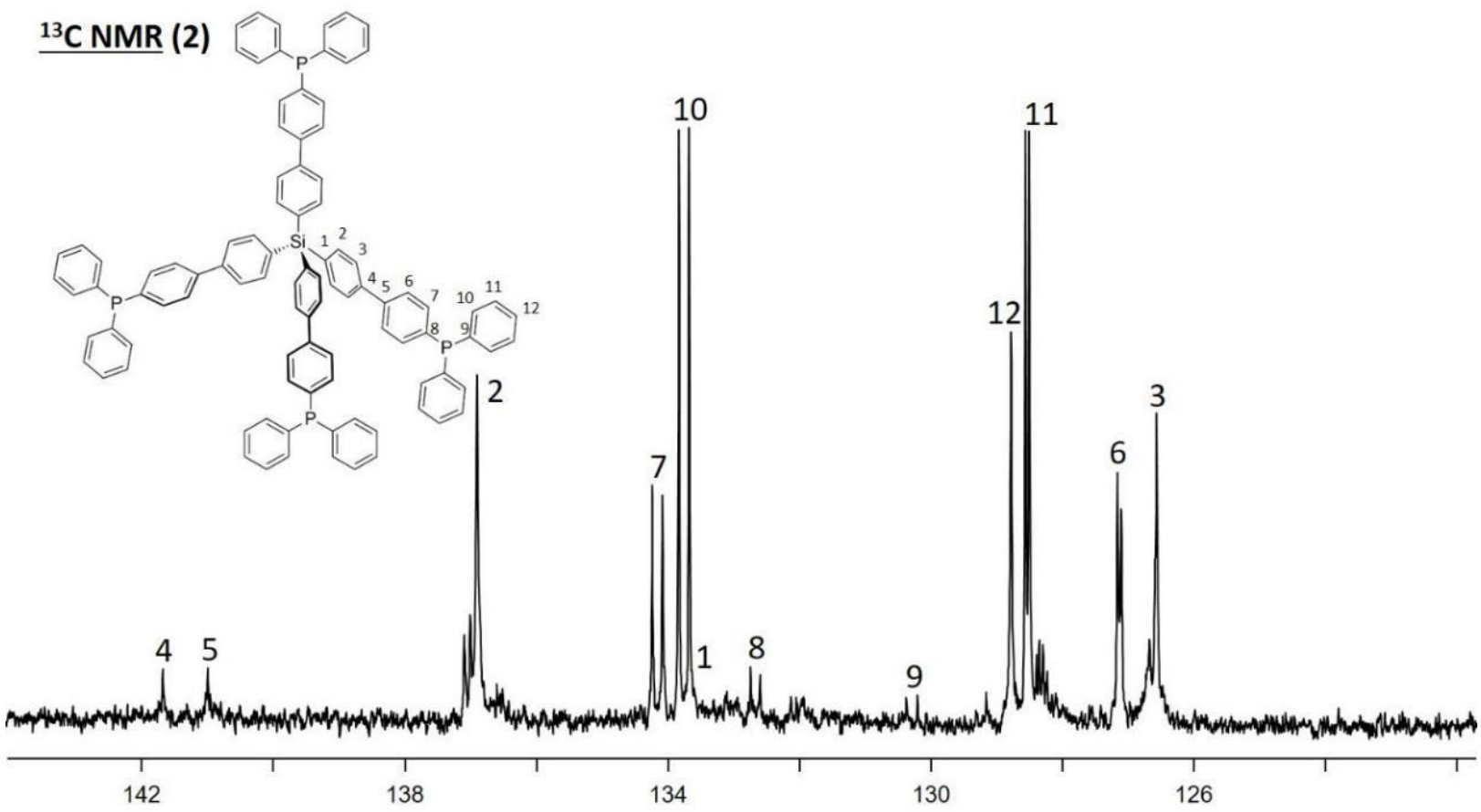
13C NMR (2)
Si
P
P
P
P
1
2
3
4
5
6
7
8
9
10
11
12
10
11
12
7
2
6
3
4
5
1
8
9
142
138
134
130
126

^{1}H, ^{1}H COSY NMR (2)

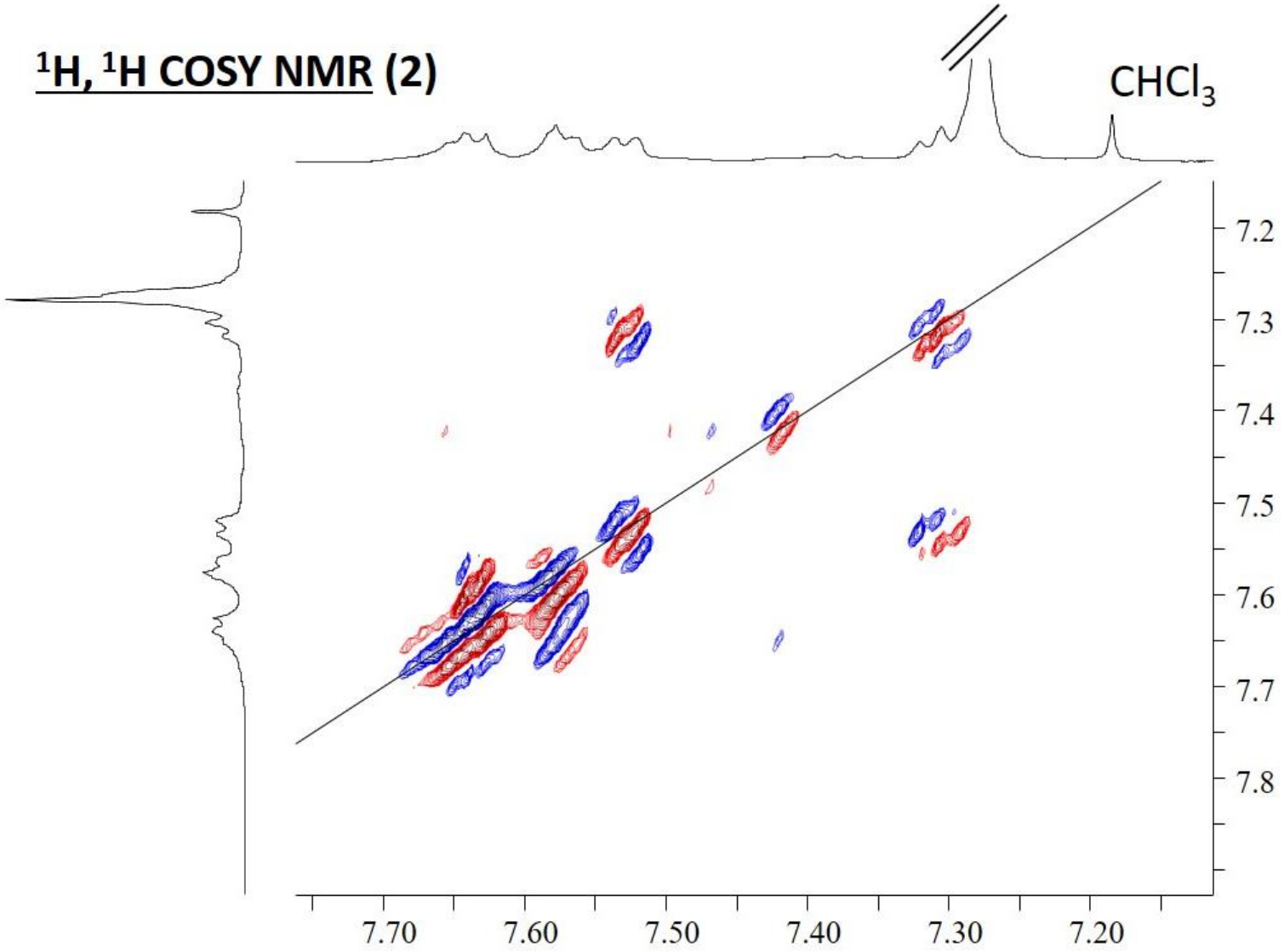

^{13}C, ^{1}H HSQC NMR (2)

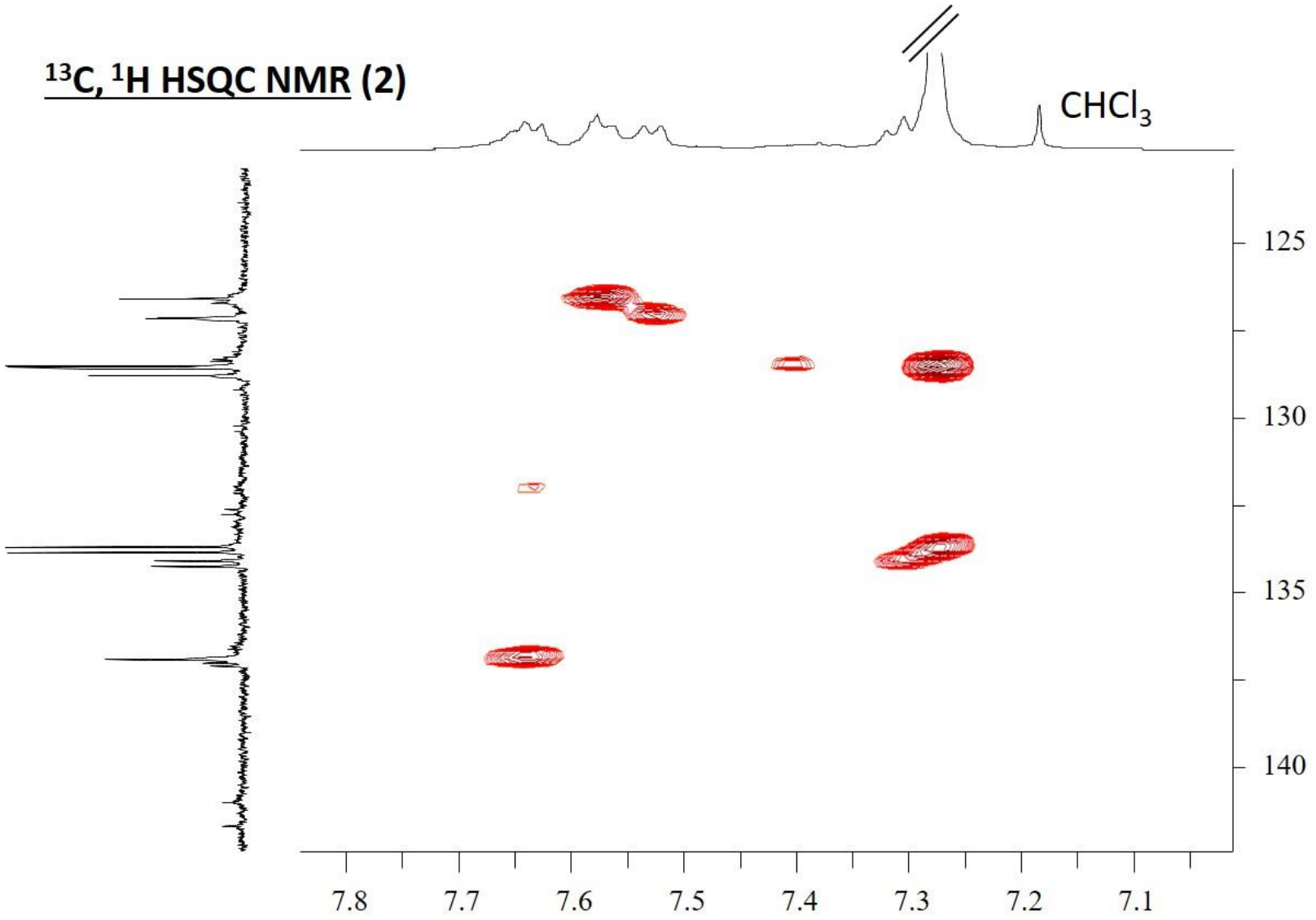

^{13}C, ^{1}H HMBC NMR (2)

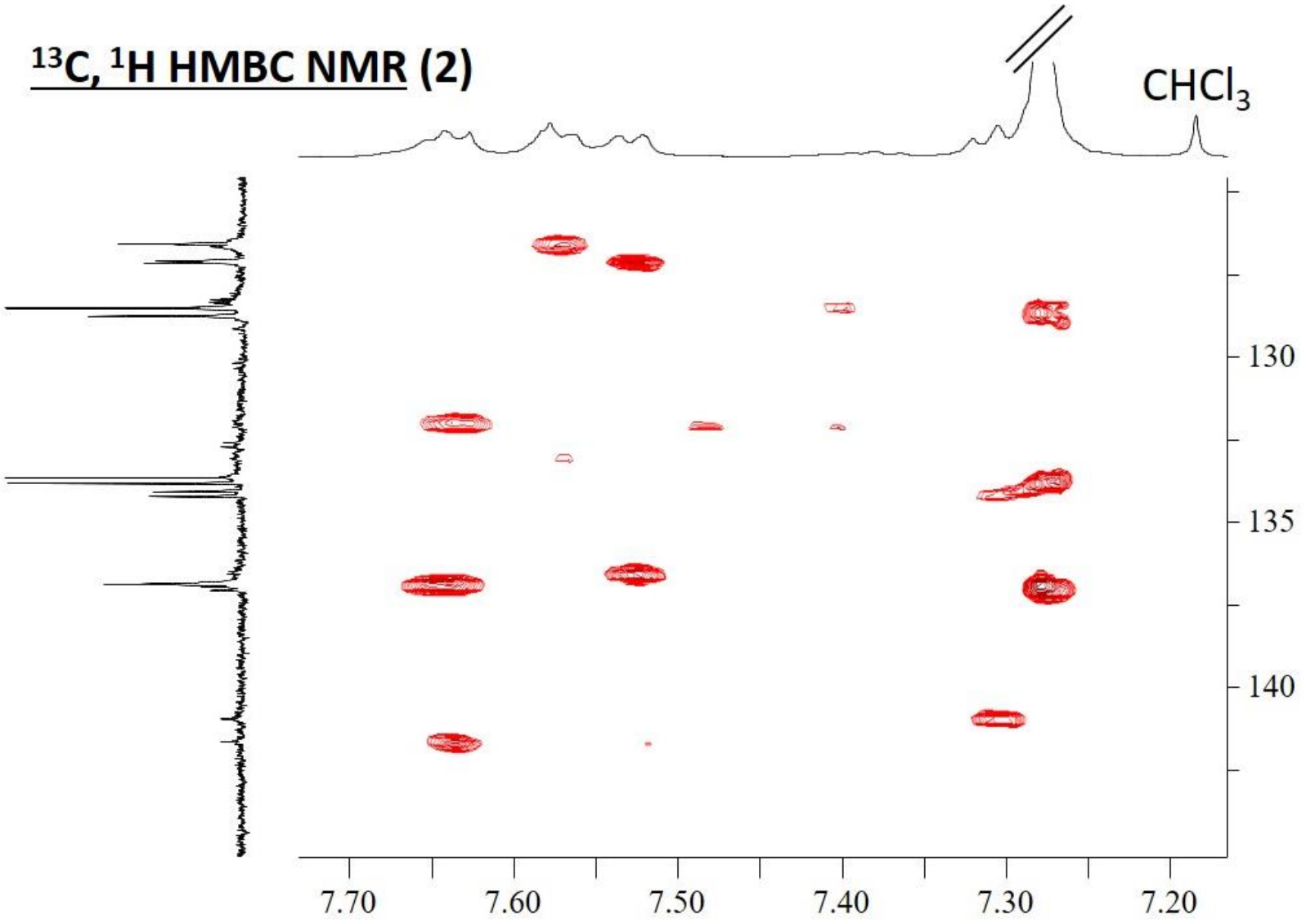

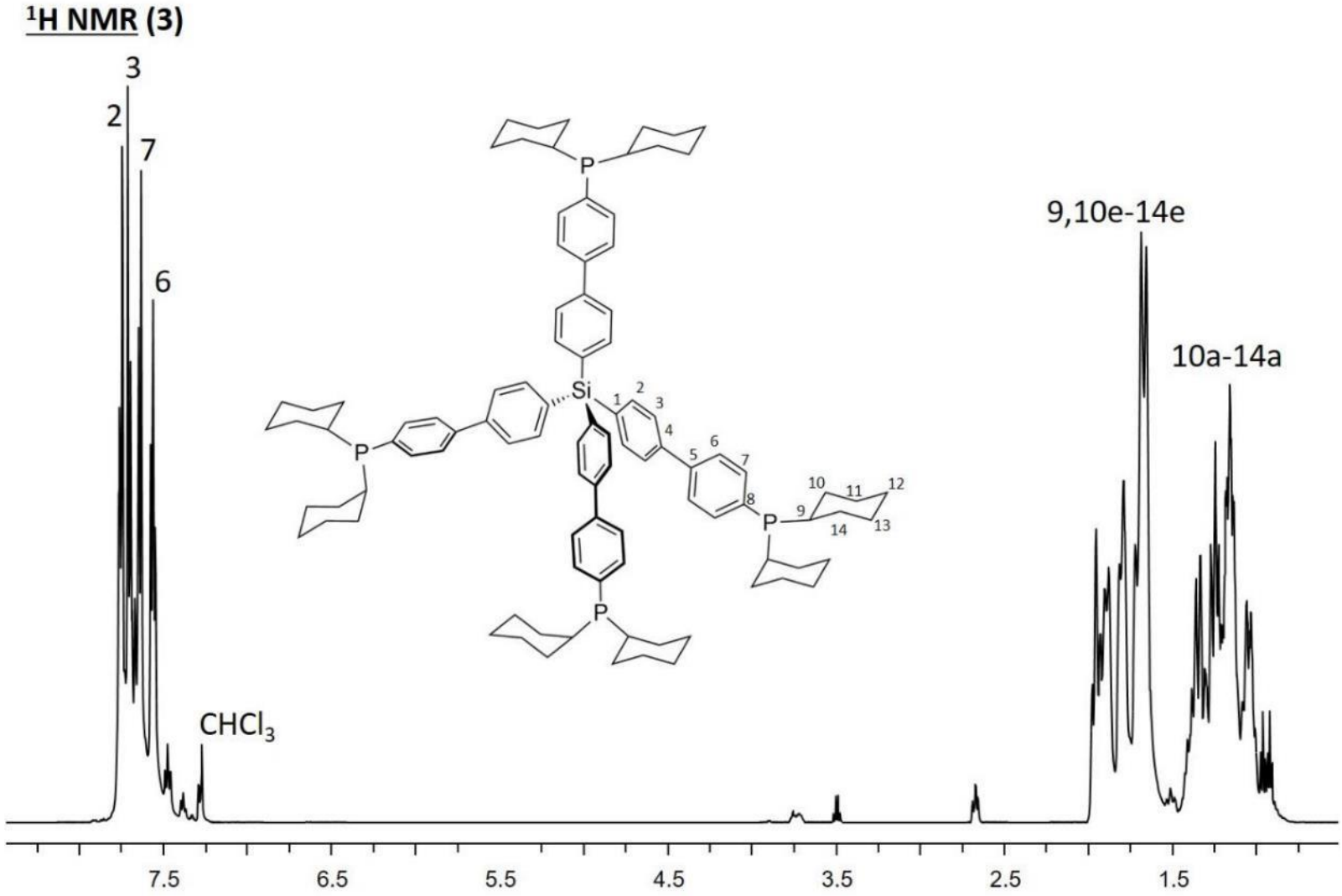
¹H NMR (3)
3
2
7
6
CHCl3
9,10e-14e
10a-14a
Si
P
1
2
3
4
5
6
7
8
9
10
11
12
13
14
7.5
6.5
5.5
4.5
3.5
2.5
1.5

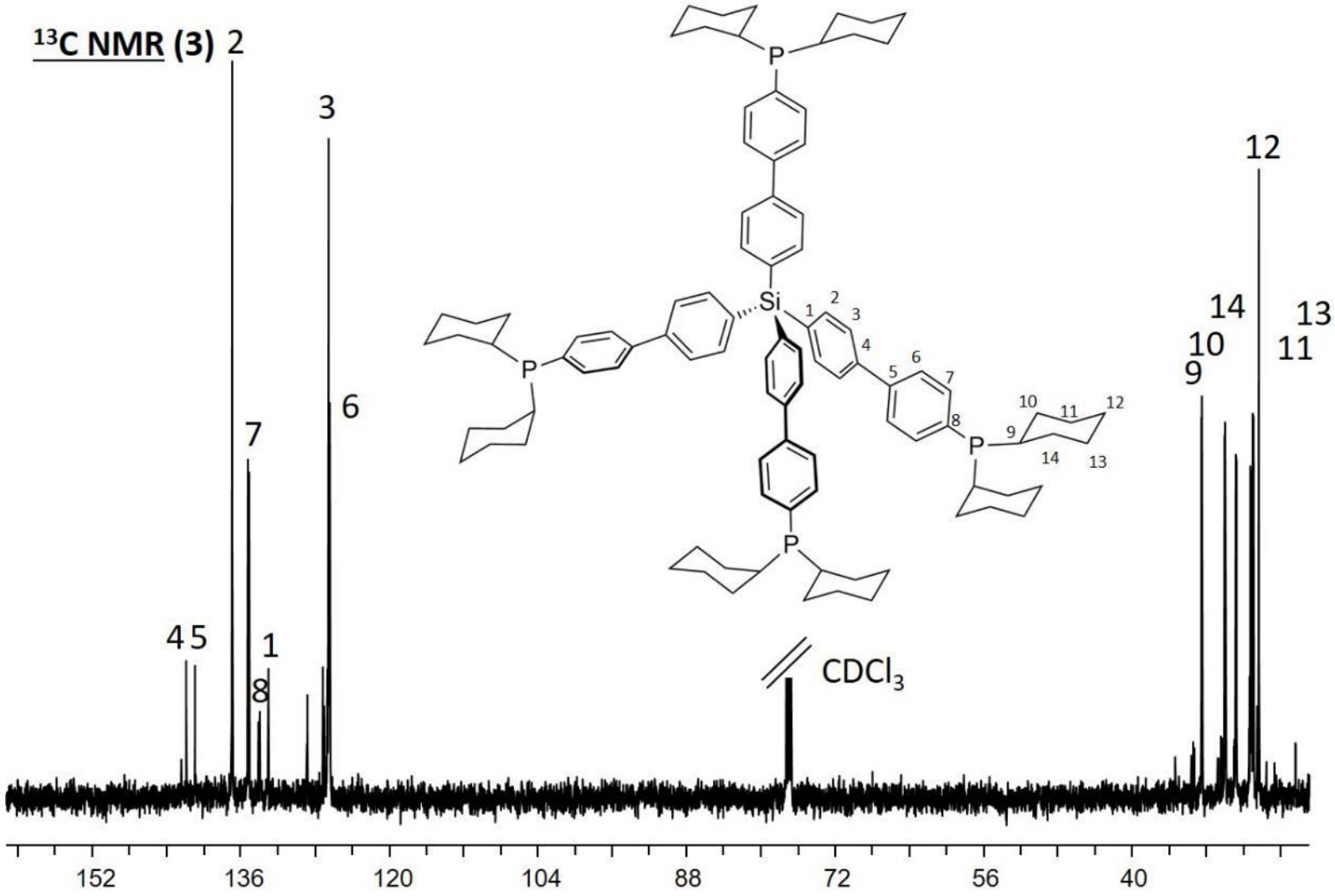
13C NMR (3)
2
3
12
14
13
10
11
9
7
6
4 5
1
8
CDCl3
152
136
120
104
88
72
56
40
Si
P

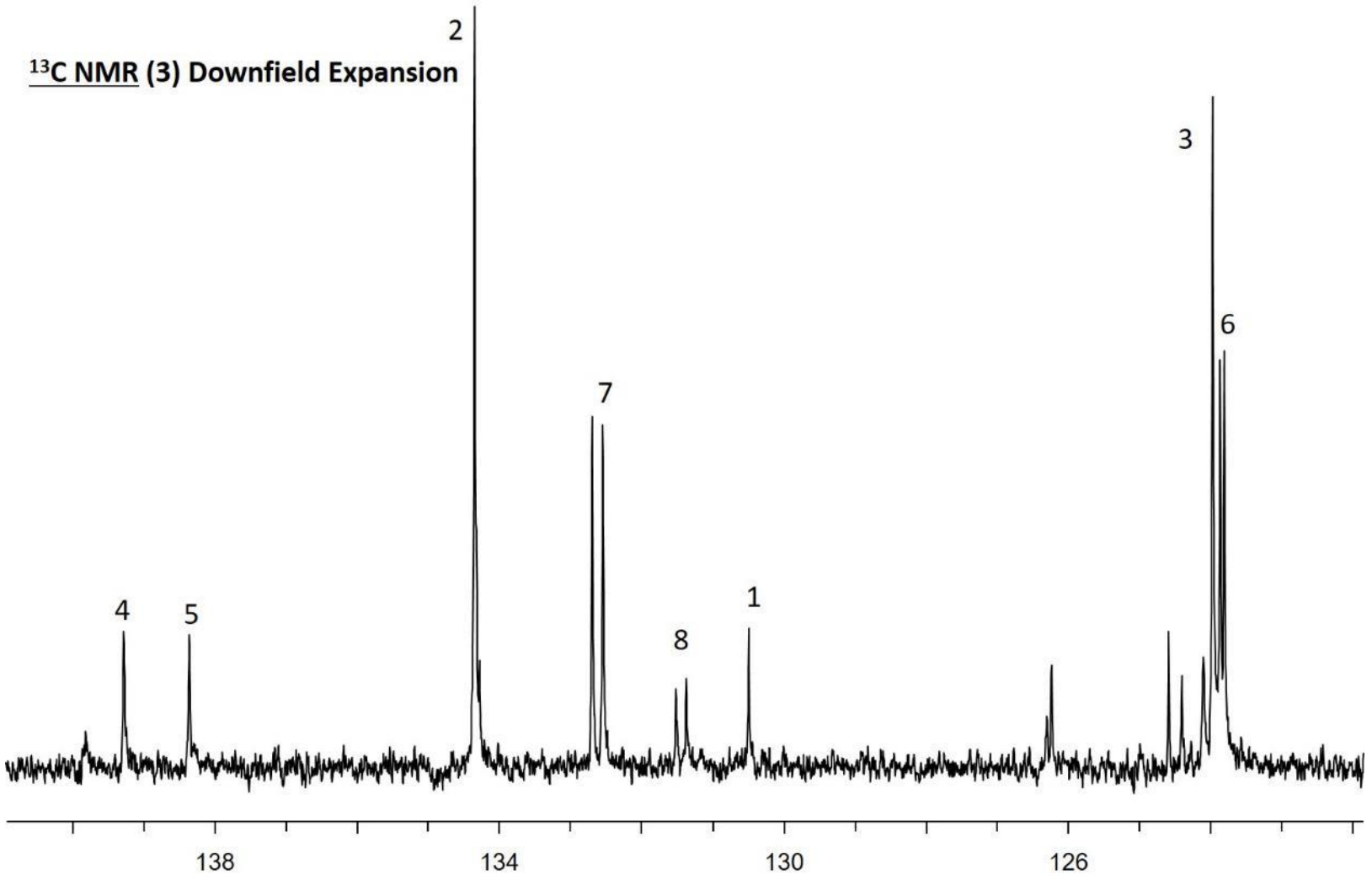
13C NMR (3) Downfield Expansion
2
3
6
7
4
5
8
1
138
134
130
126

^{1}H, ^{1}H COSY NMR (3) – Downfield Expansion

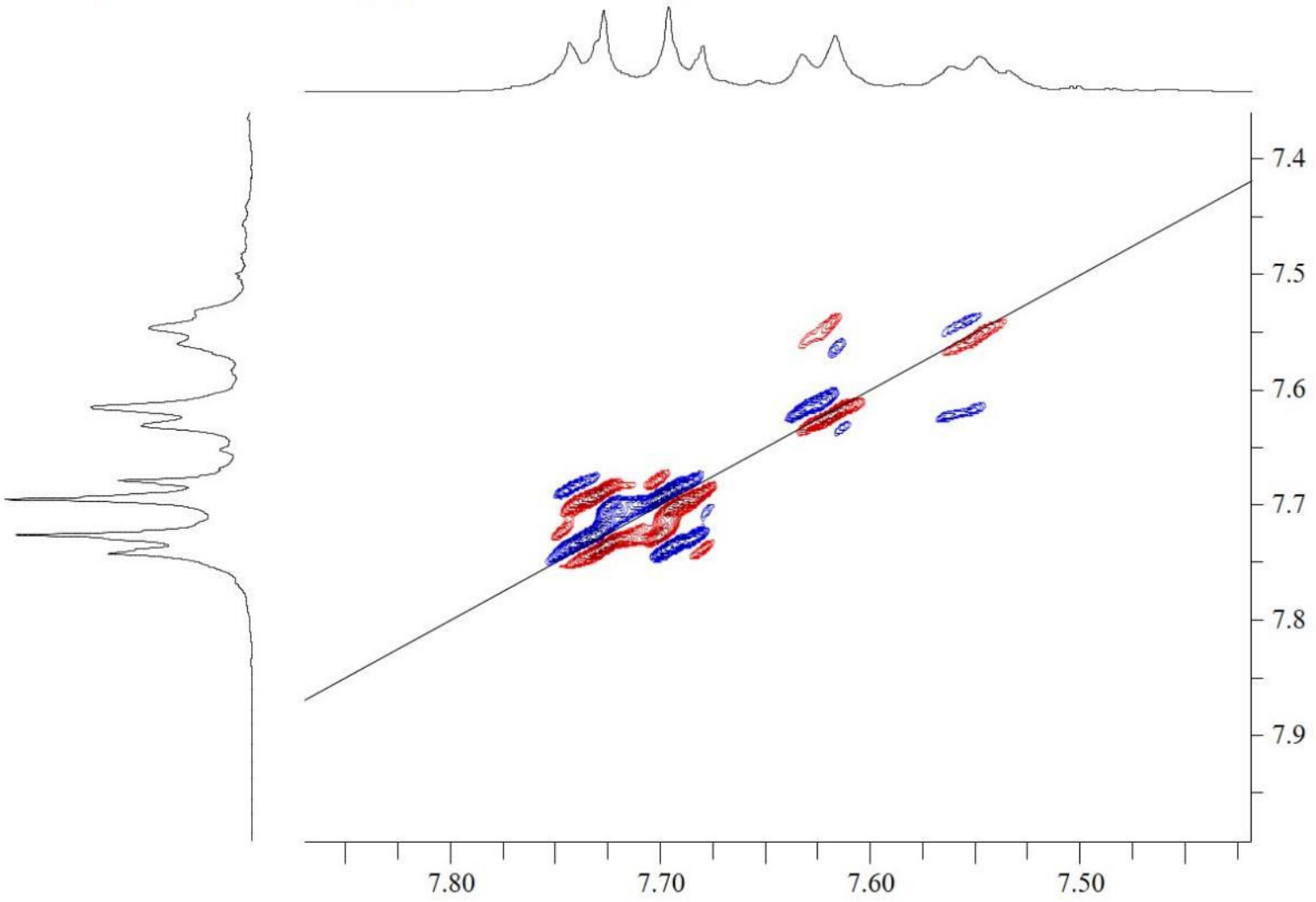

^{1}H, ^{1}H COSY NMR (3) – Upfield Expansion

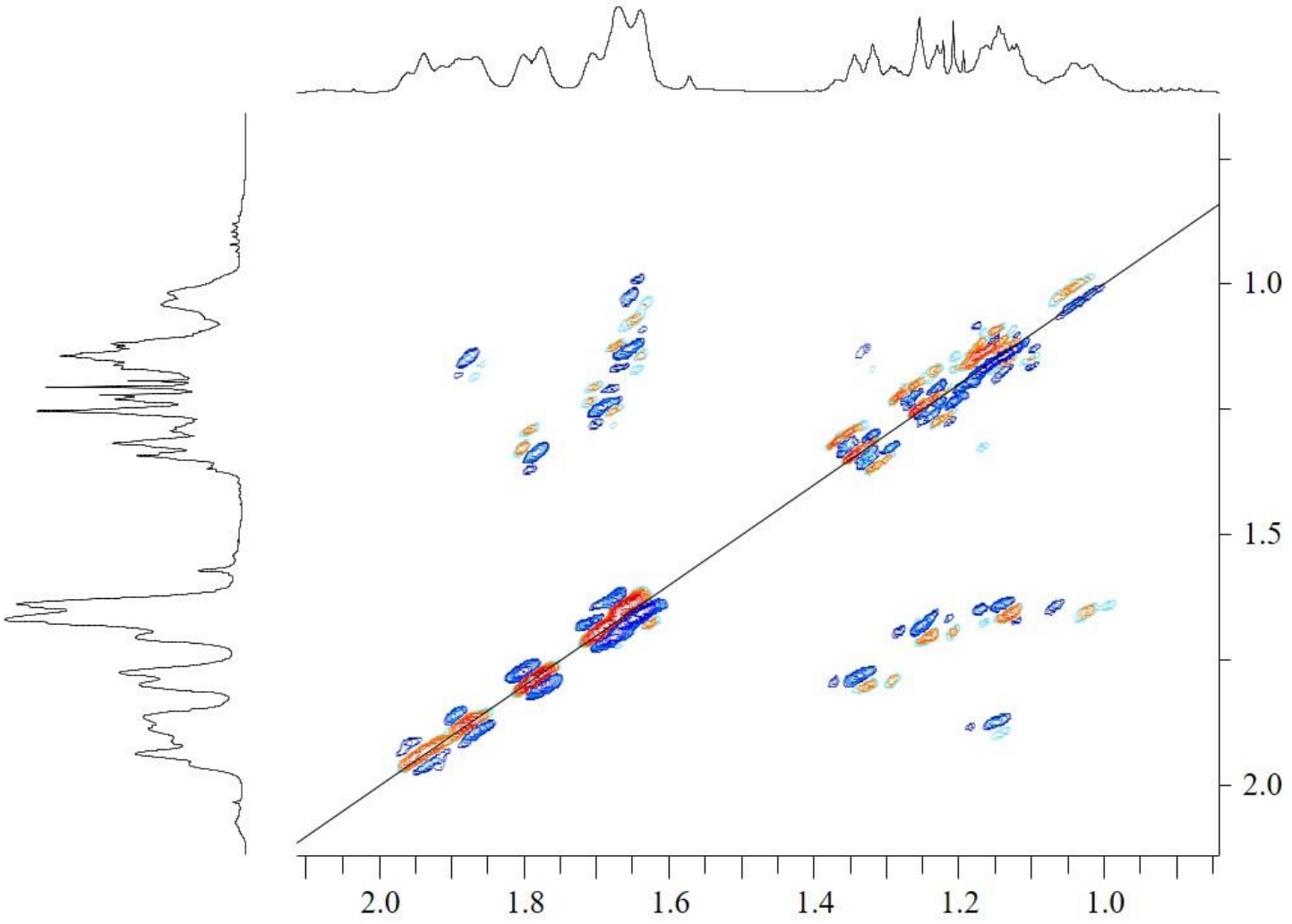

^{13}C, ^{1}H HSQC NMR (3) – Downfield Expansion

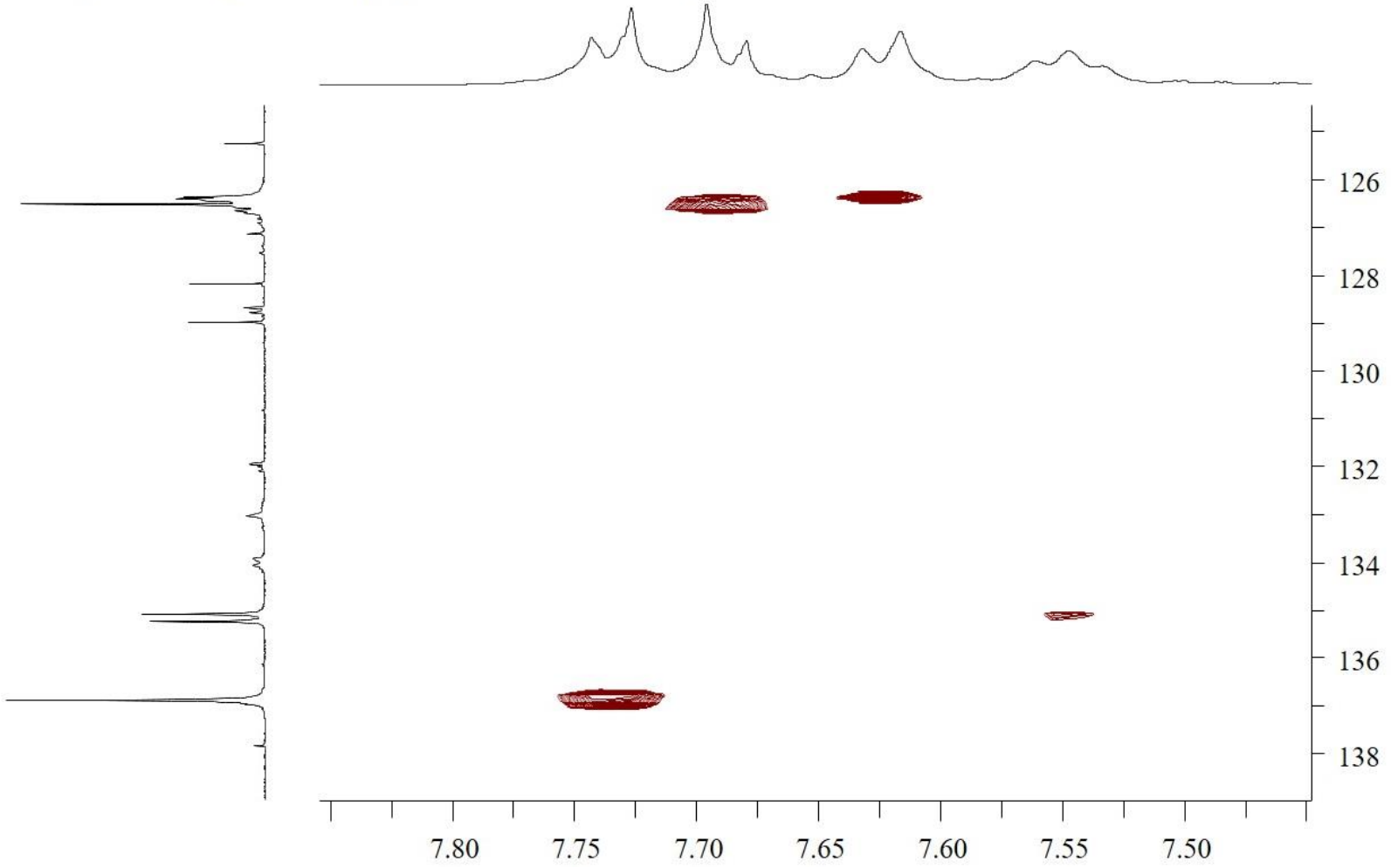

^{13}C, ^{1}H HMBC NMR (3) – Upfield Expansion

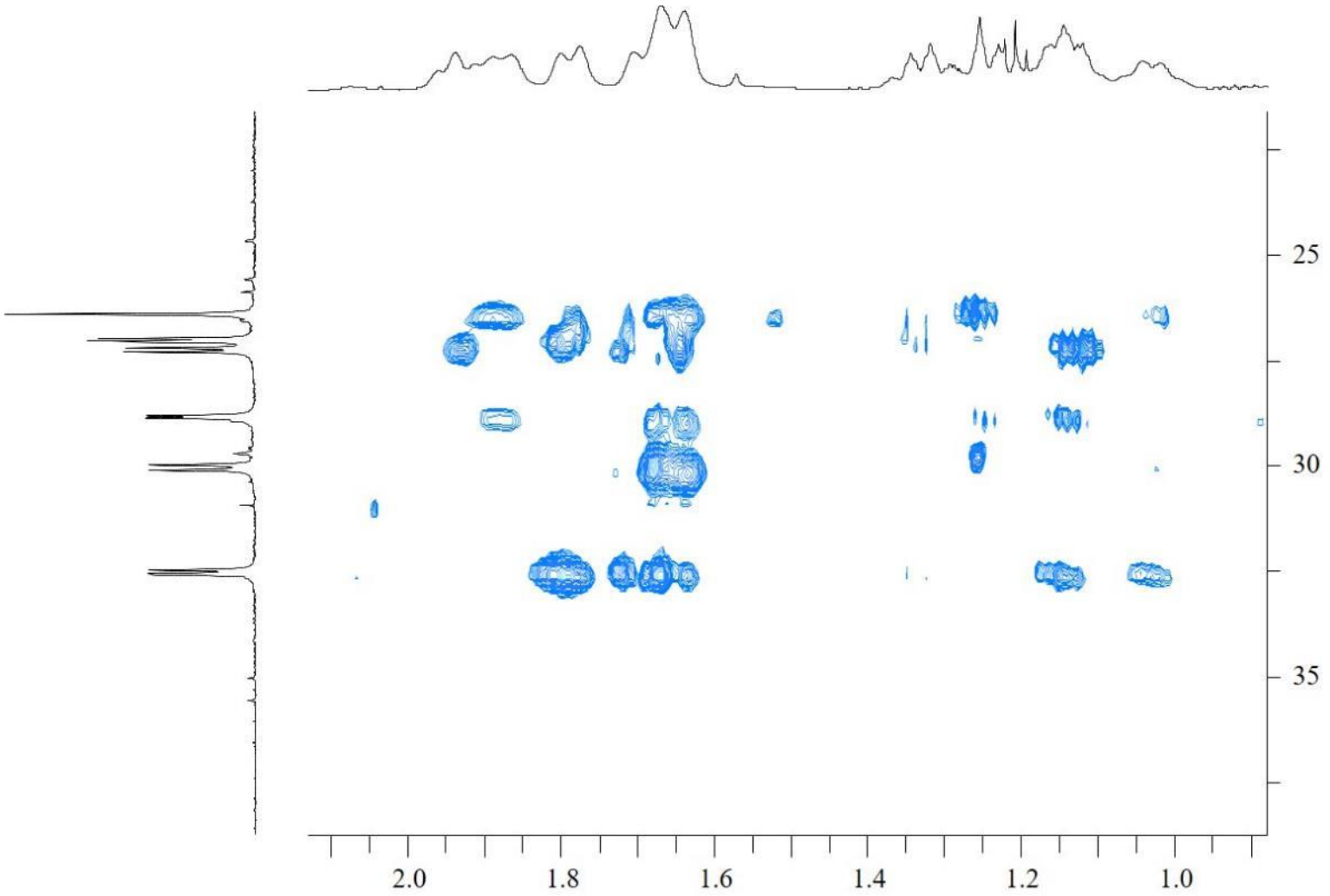

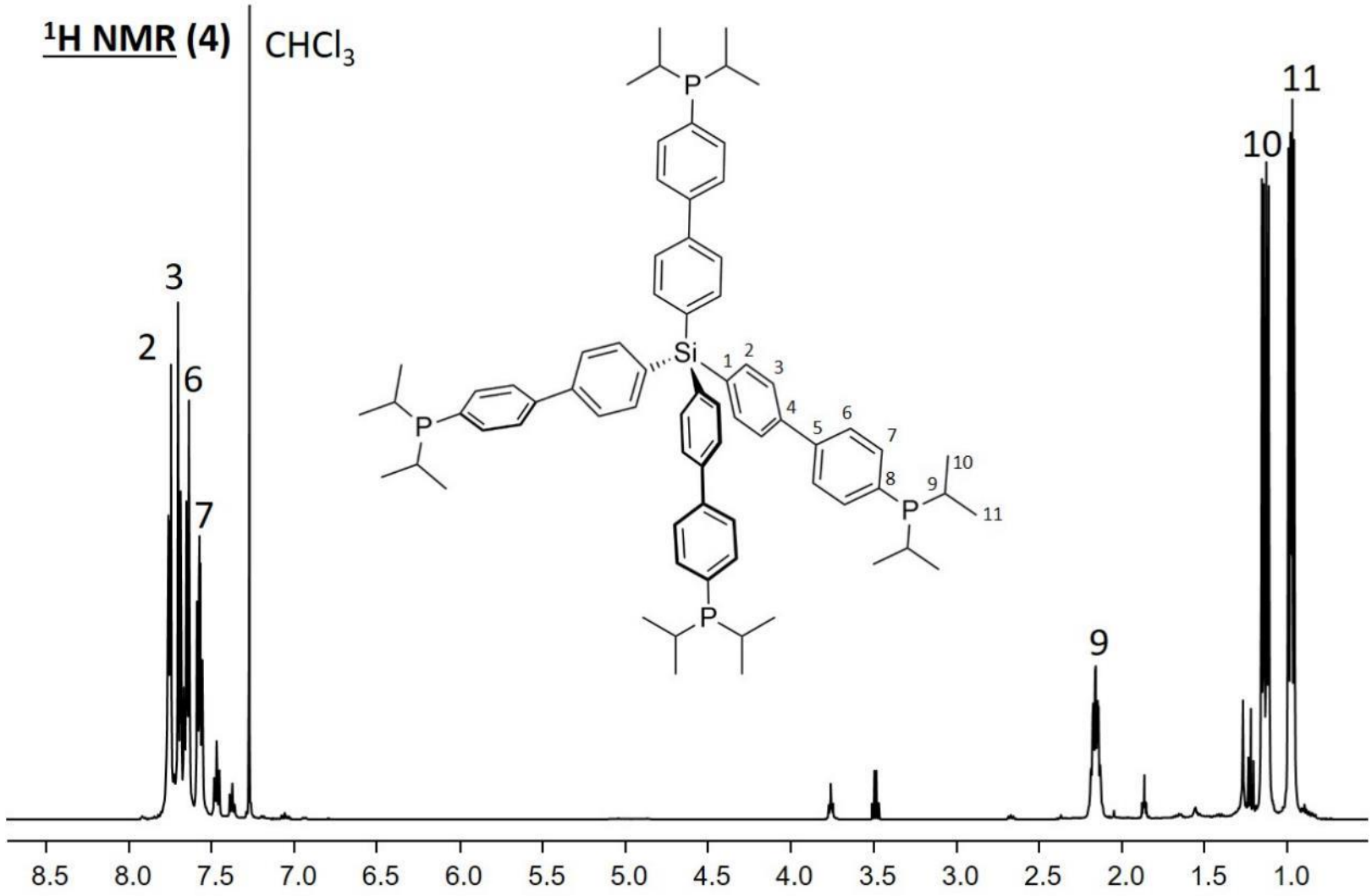
¹H NMR (4)
CHCl3
2
3
6
7
9
10
11
Si
P
1
2
3
4
5
6
7
8
9
10
11
8.5
8.0
7.5
7.0
6.5
6.0
5.5
5.0
4.5
4.0
3.5
3.0
2.5
2.0
1.5
1.0

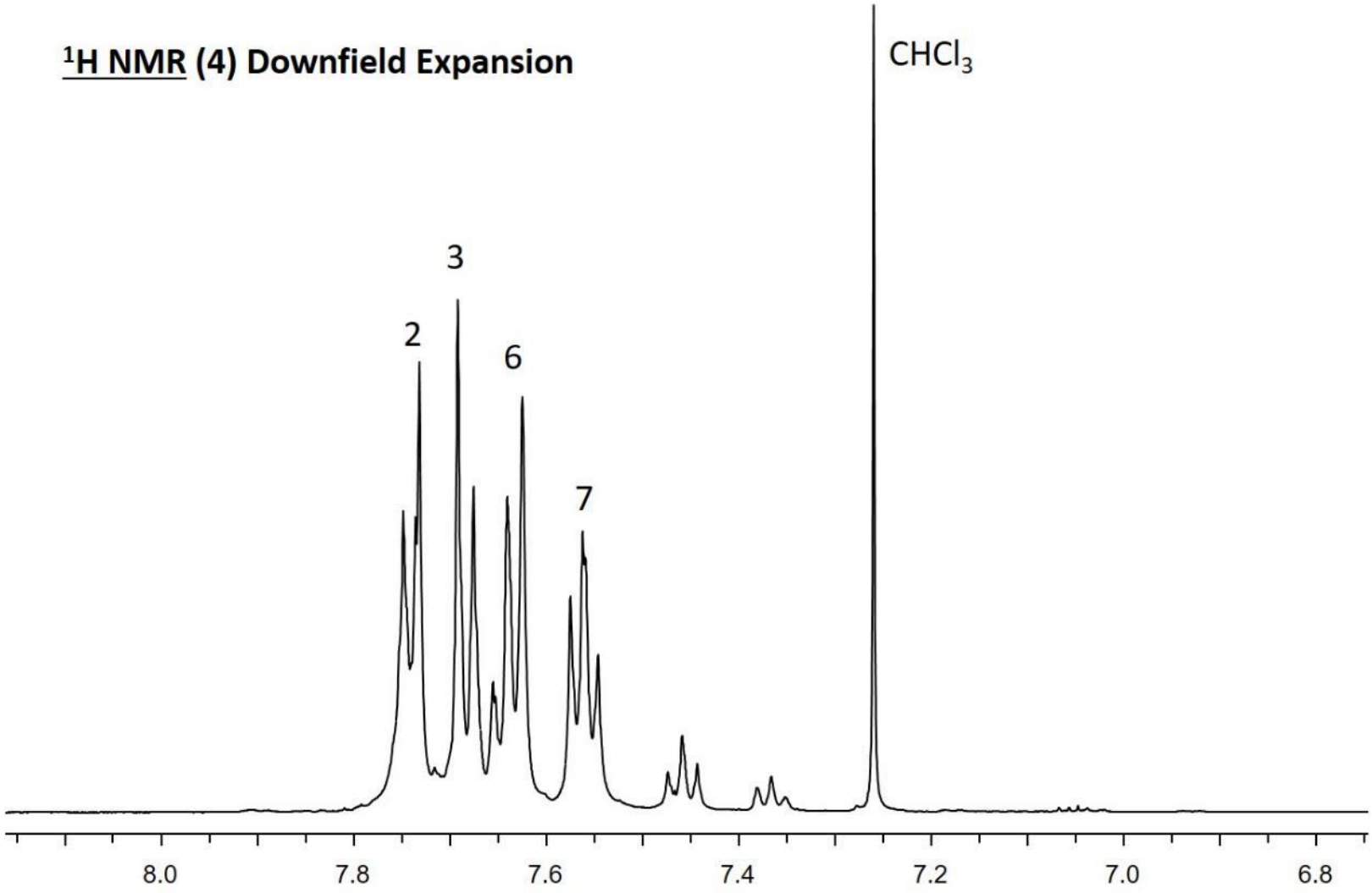
¹H NMR (4) Downfield Expansion
CHCl3
2
3
6
7
8.0
7.8
7.6
7.4
7.2
7.0
6.8

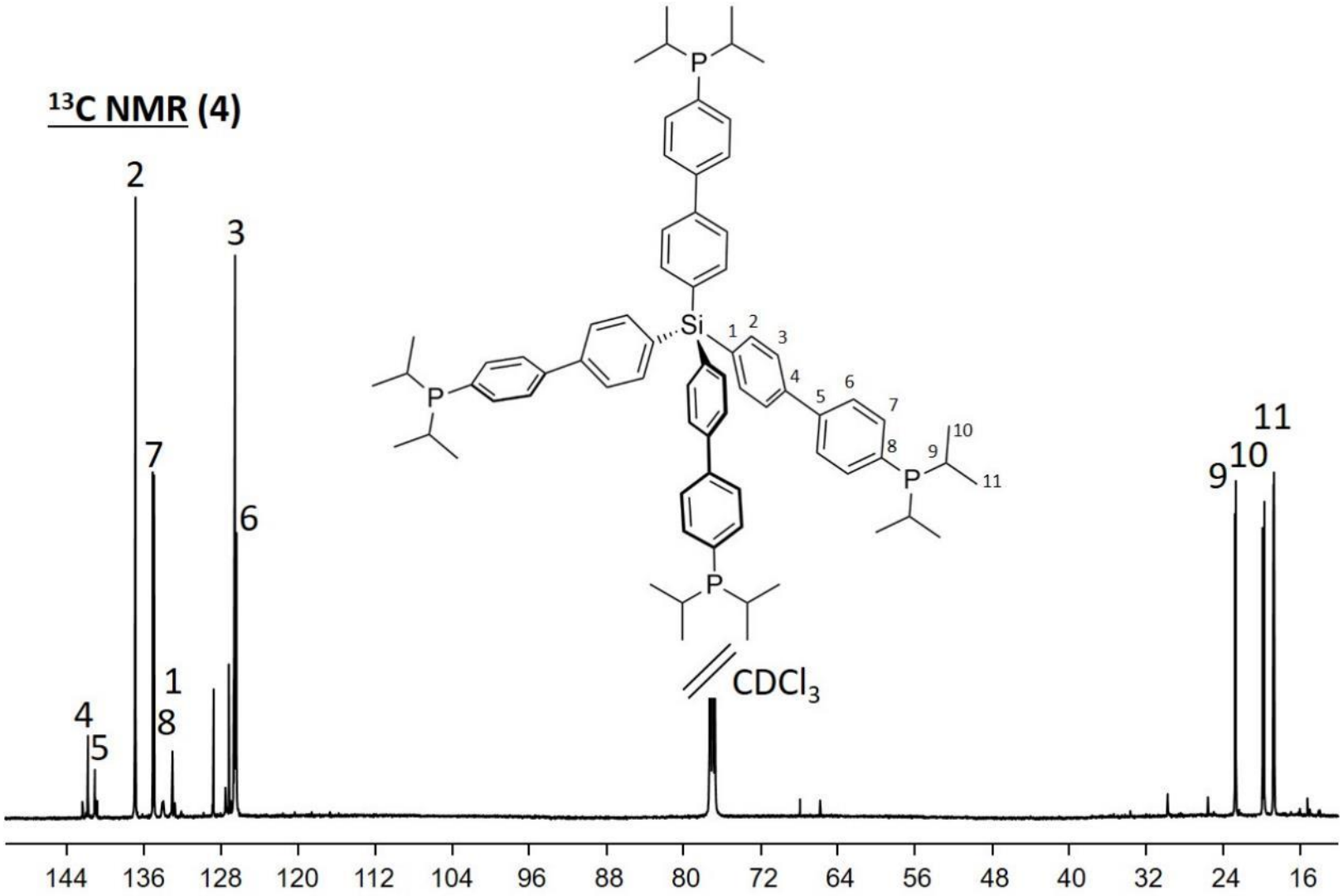
13C NMR (4)
2
3
7
6
1
8
4
5
9
10
11
CDCl3
144
136
128
120
112
104
96
88
80
72
64
56
48
40
32
24
16

^{13}C NMR (4) Downfield Expansion

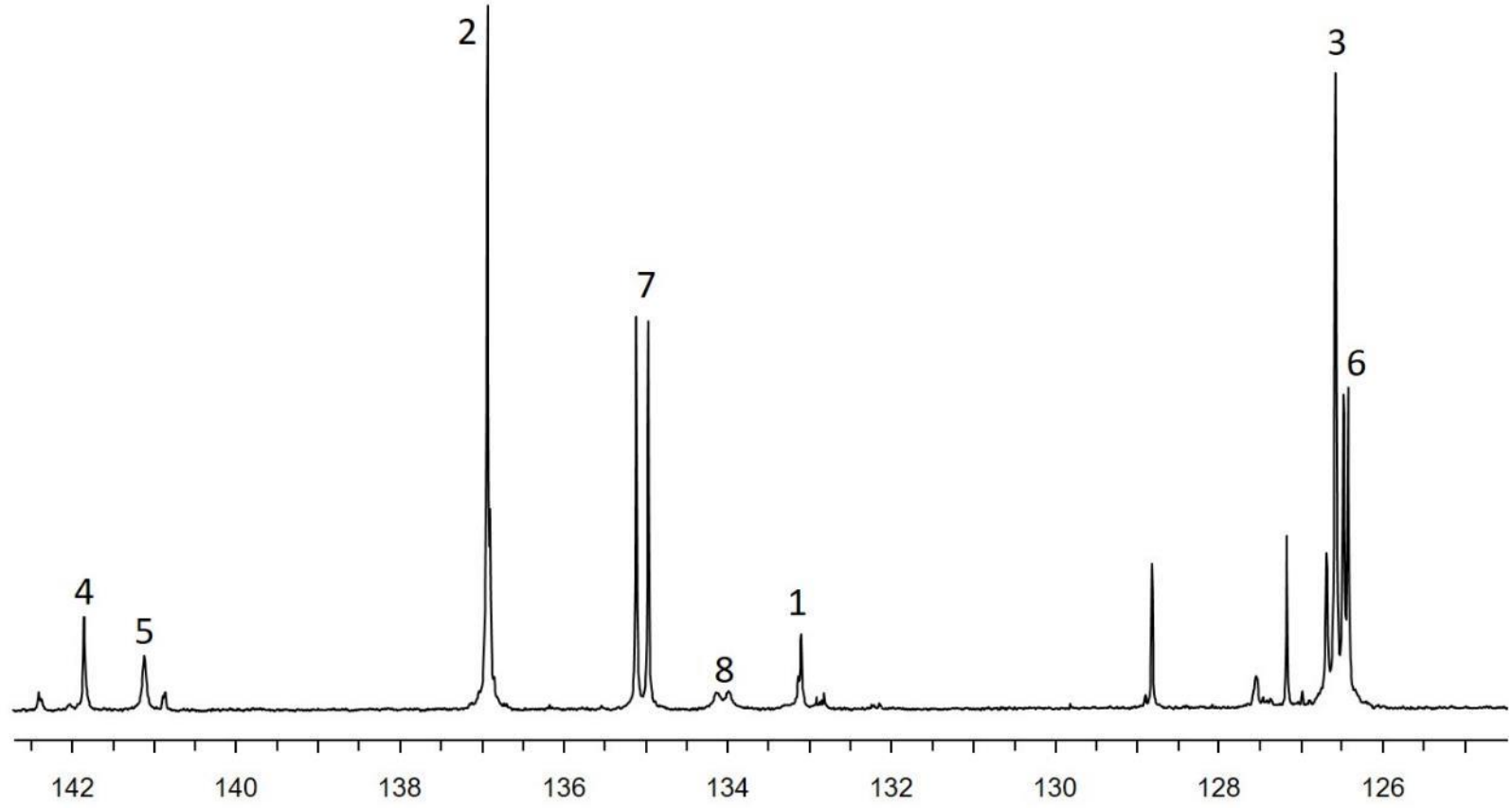

^{1}H, ^{1}H COSY NMR (4) – Downfield Expansion

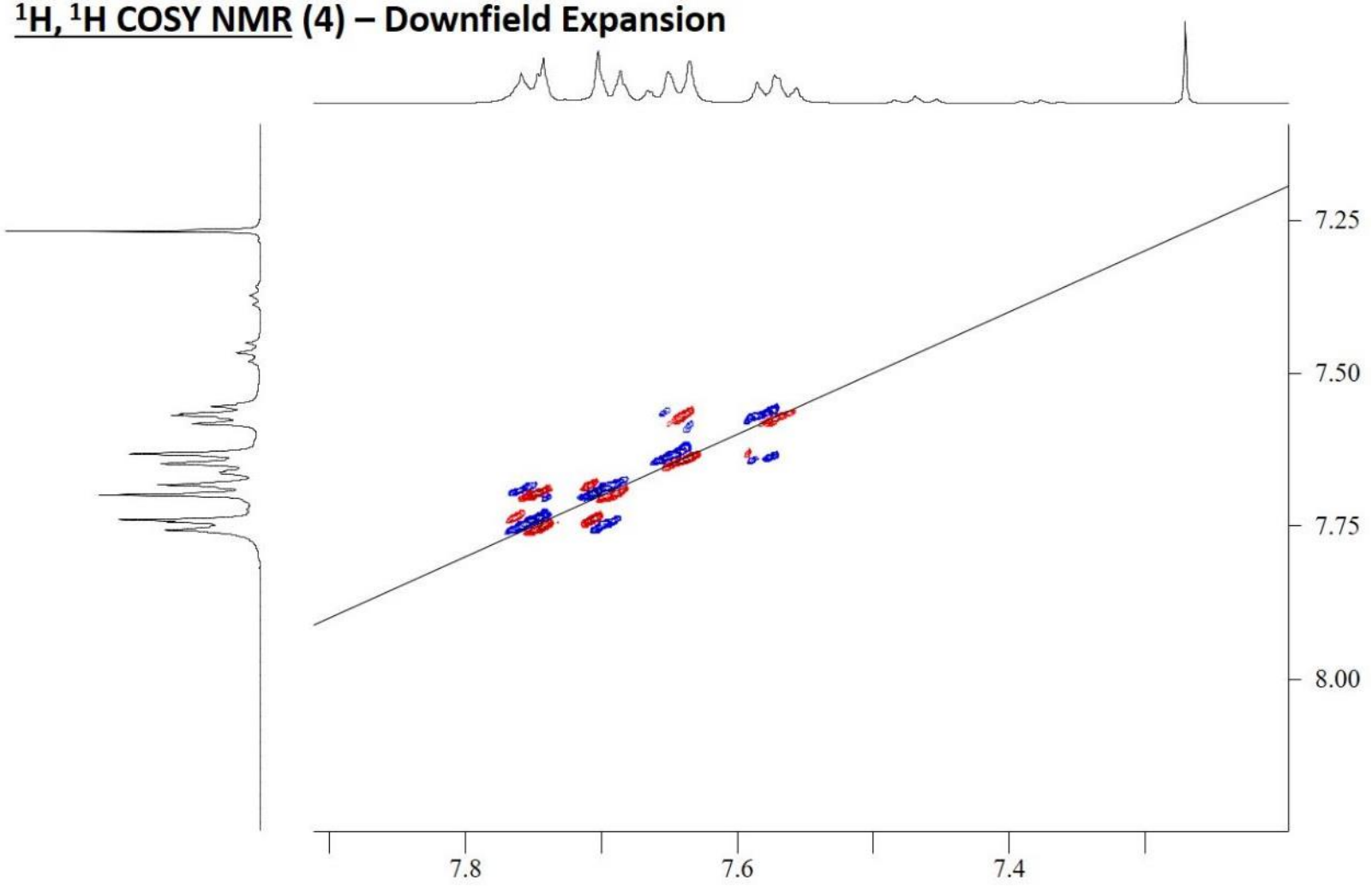

^{1}H, ^{1}H COSY NMR (4) – Upfield Expansion

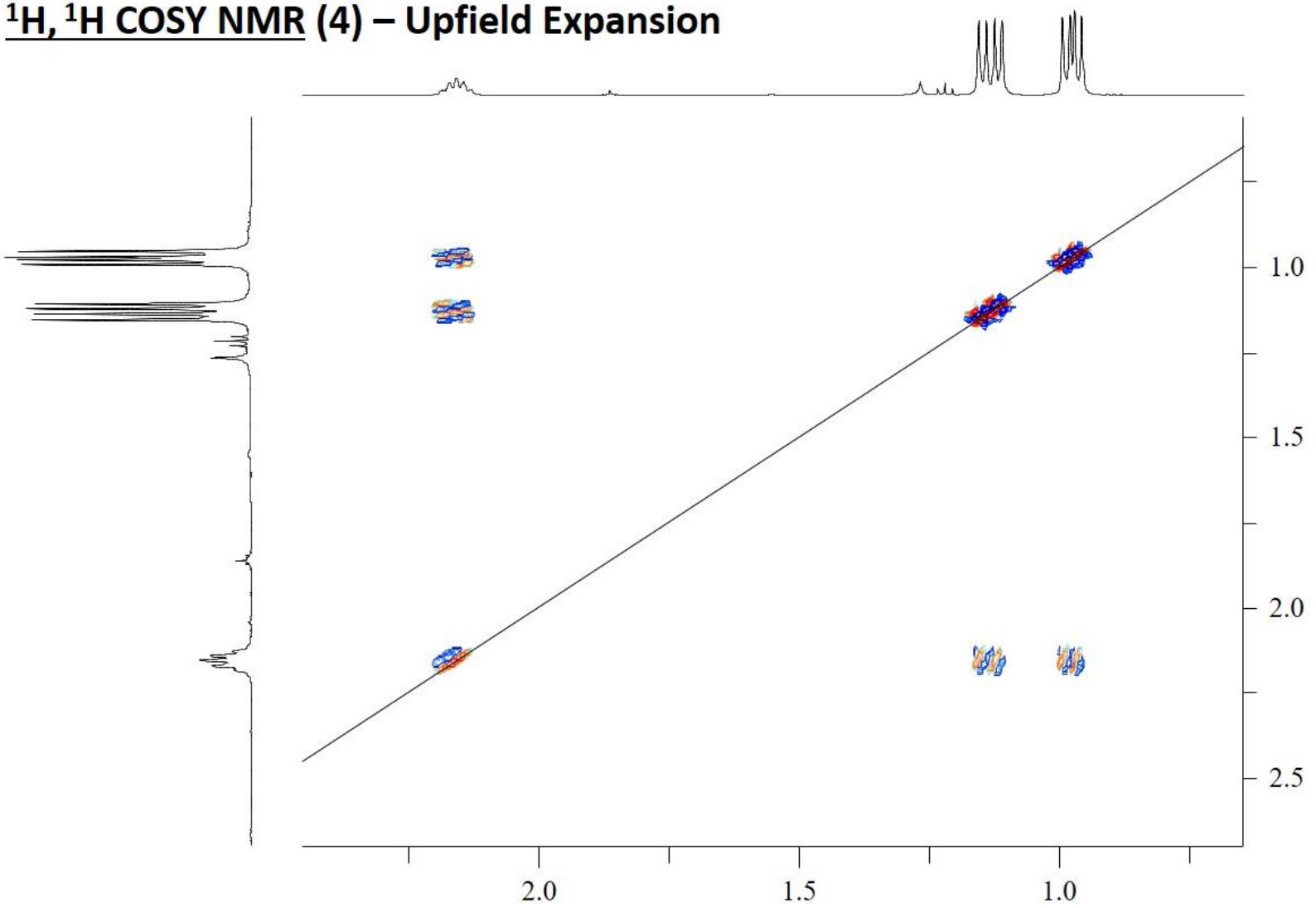

^{13}C, ^{1}H HSQC NMR (4) – Downfield Expansion

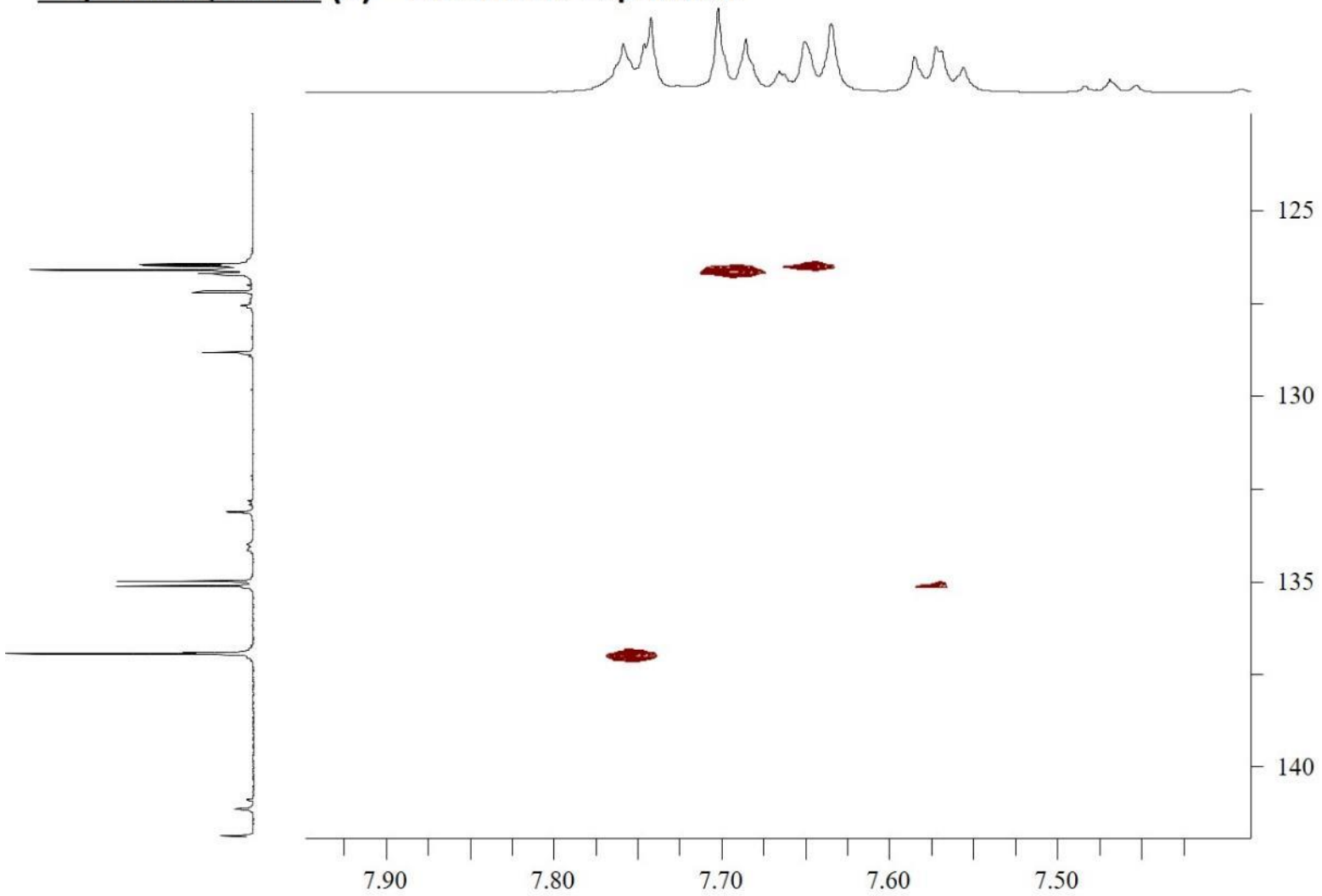

^{13}C, ^{1}H HSQC NMR (4) –Upfield Expansion

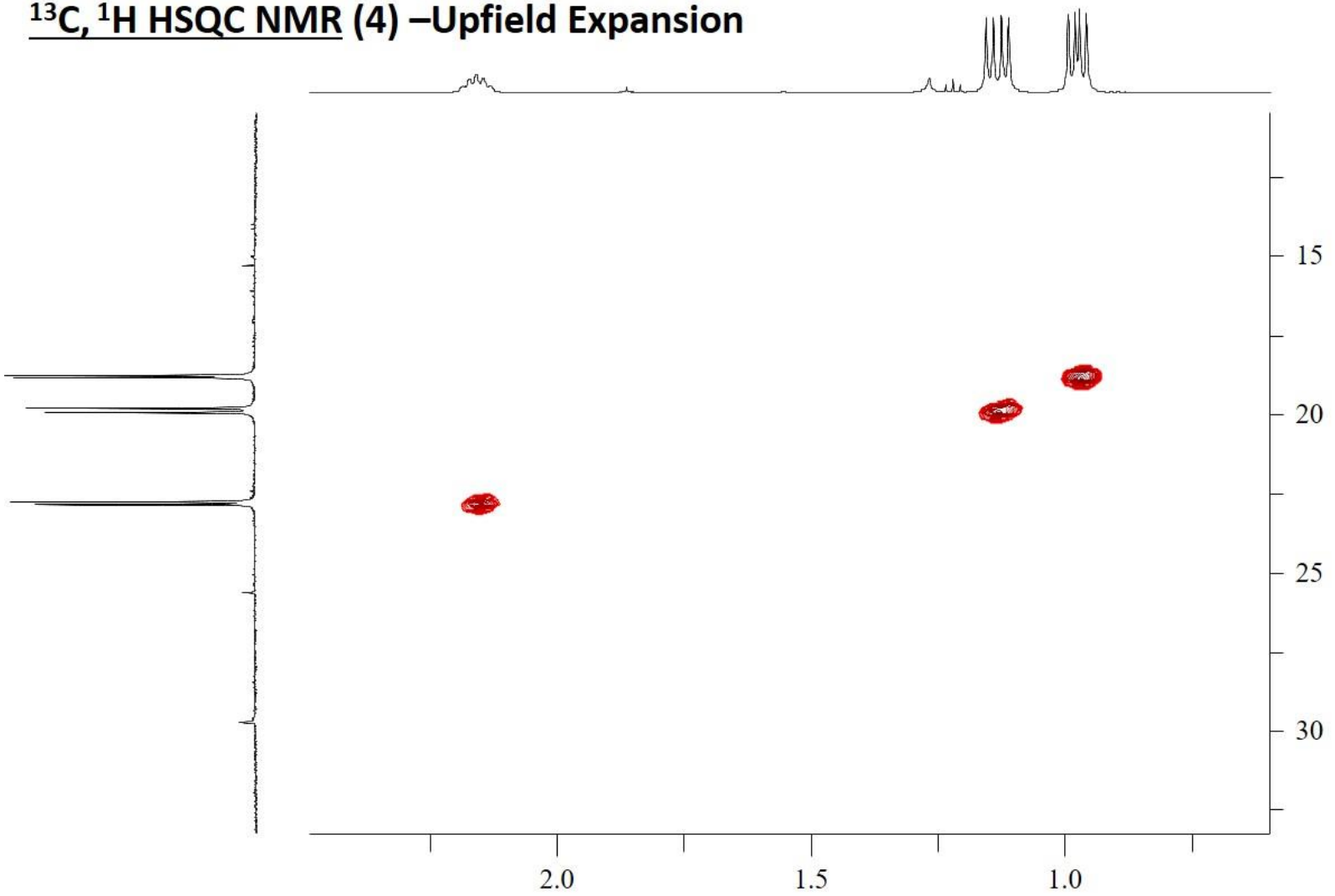

^{13}C, ^{1}H HMBC NMR (4) –Downfield Expansion

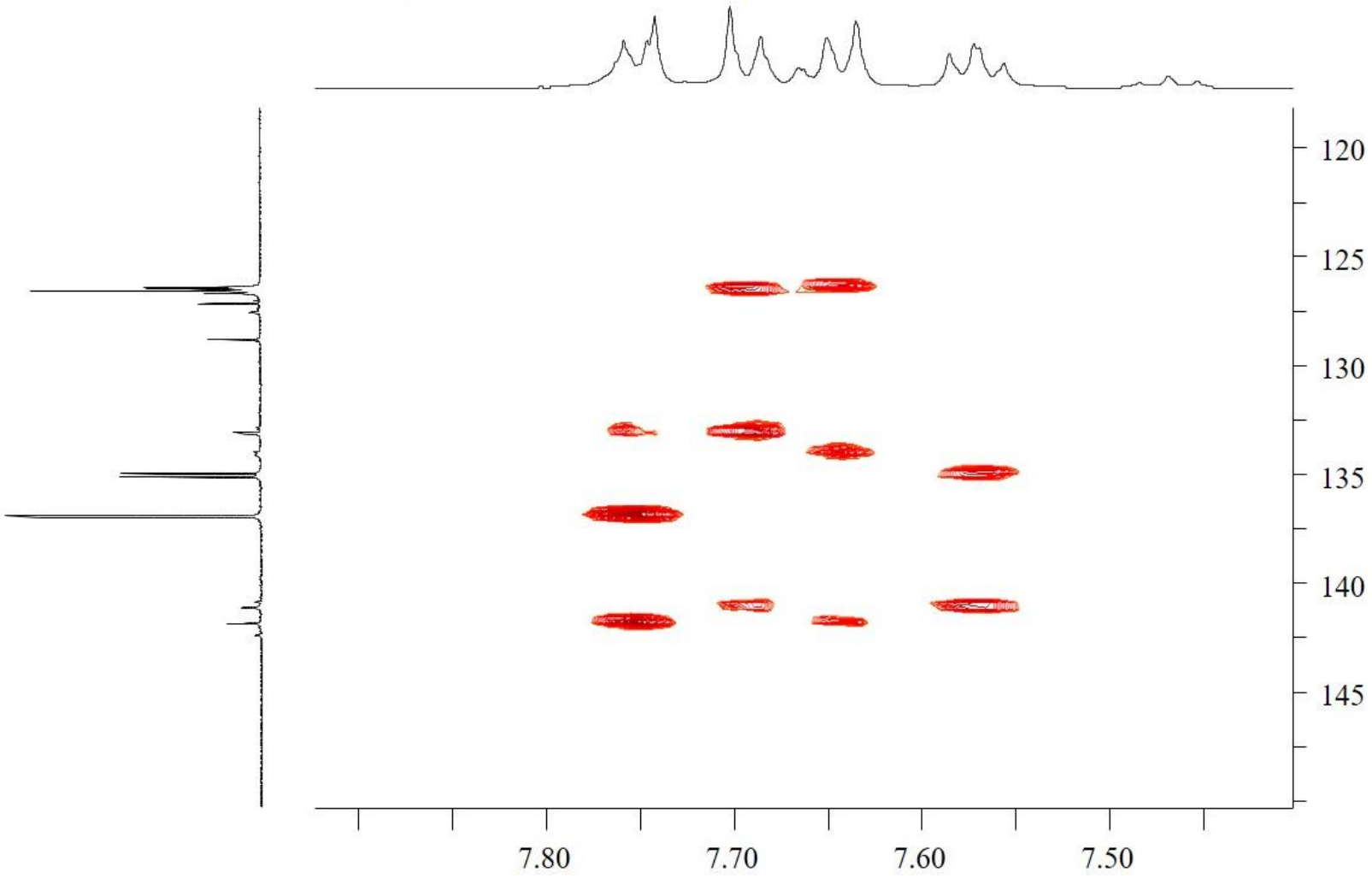

125

^{13}C, ^{1}H HMBC NMR (4) – Upfield Expansion

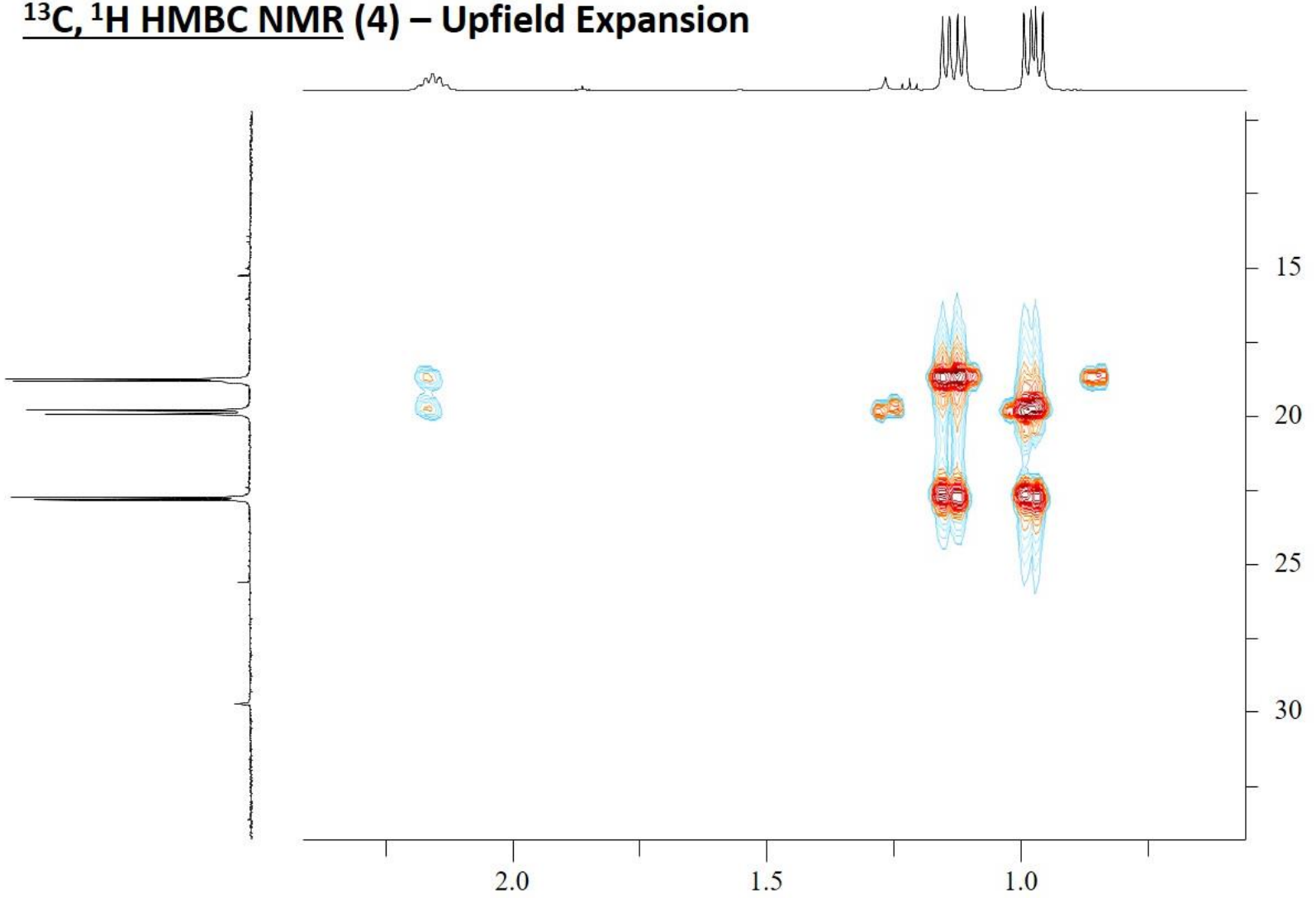

^{1}H NMR (5)

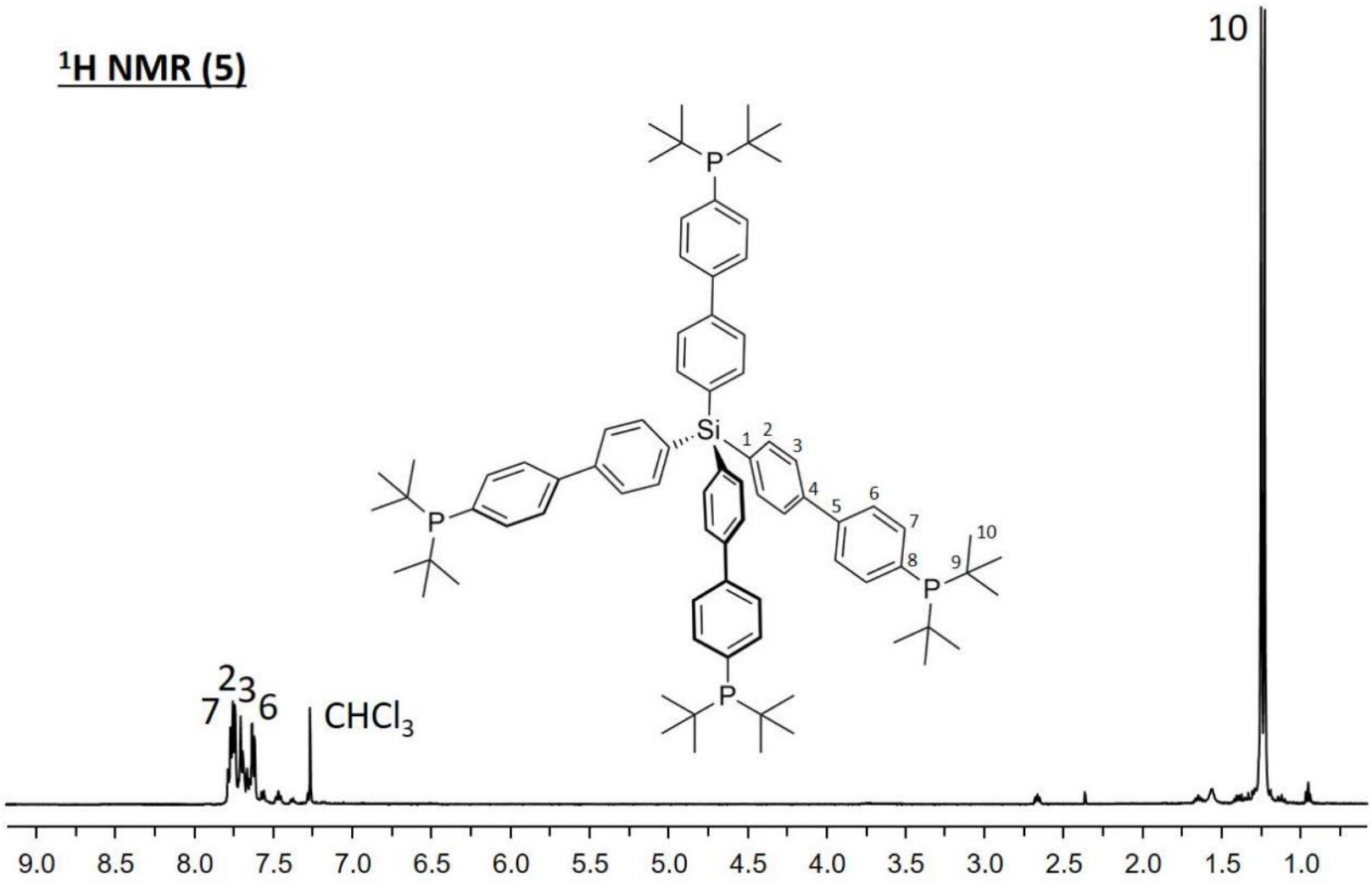

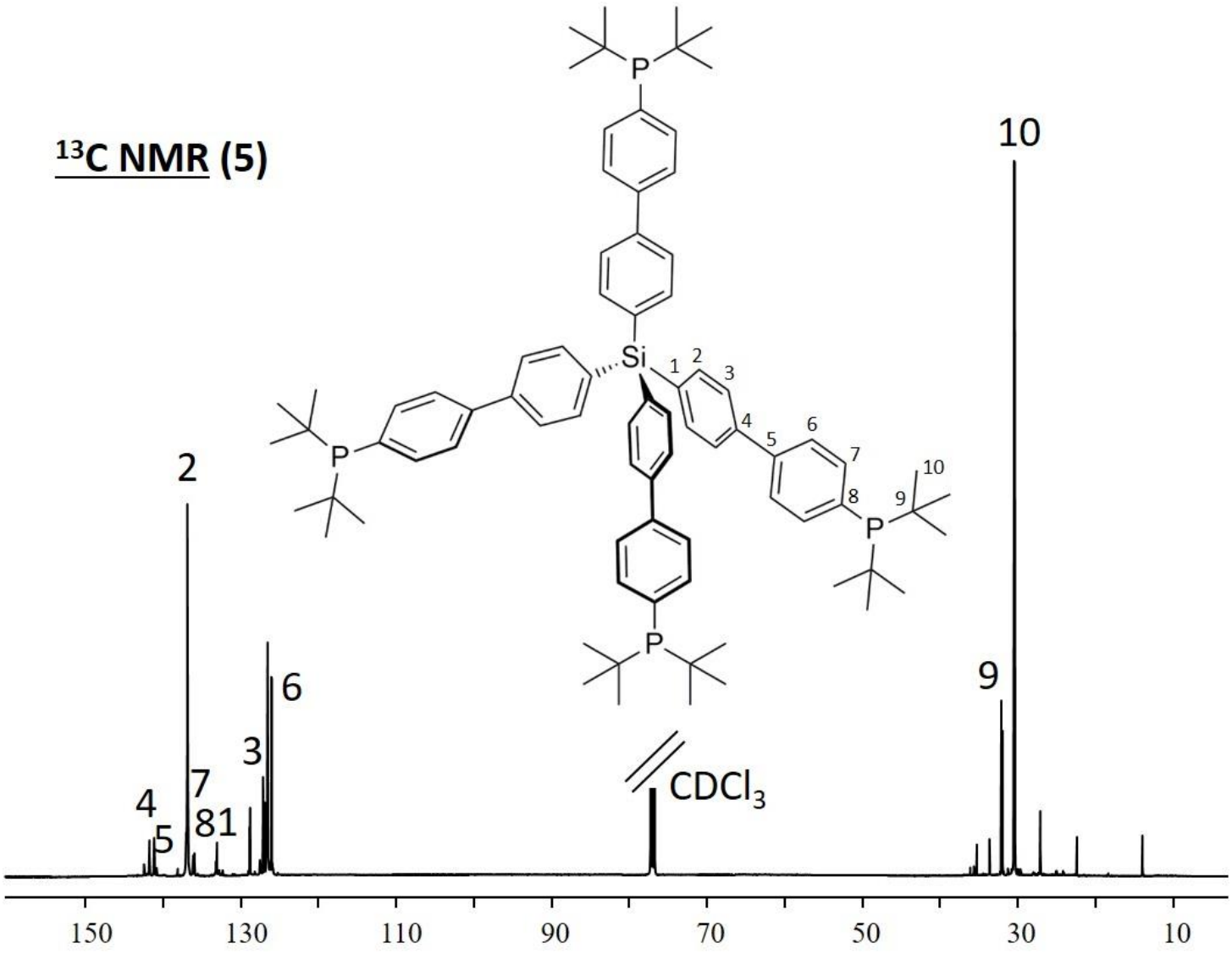
13C NMR (5)
P
Si
1
2
3
4
5
6
7
8
9
10
2
6
3
7
4
8
1
5
9
10
CDCl3
150
130
110
90
70
50
30
10

^{1}H, ^{1}H COSY NMR (5) – Downfield Expansion

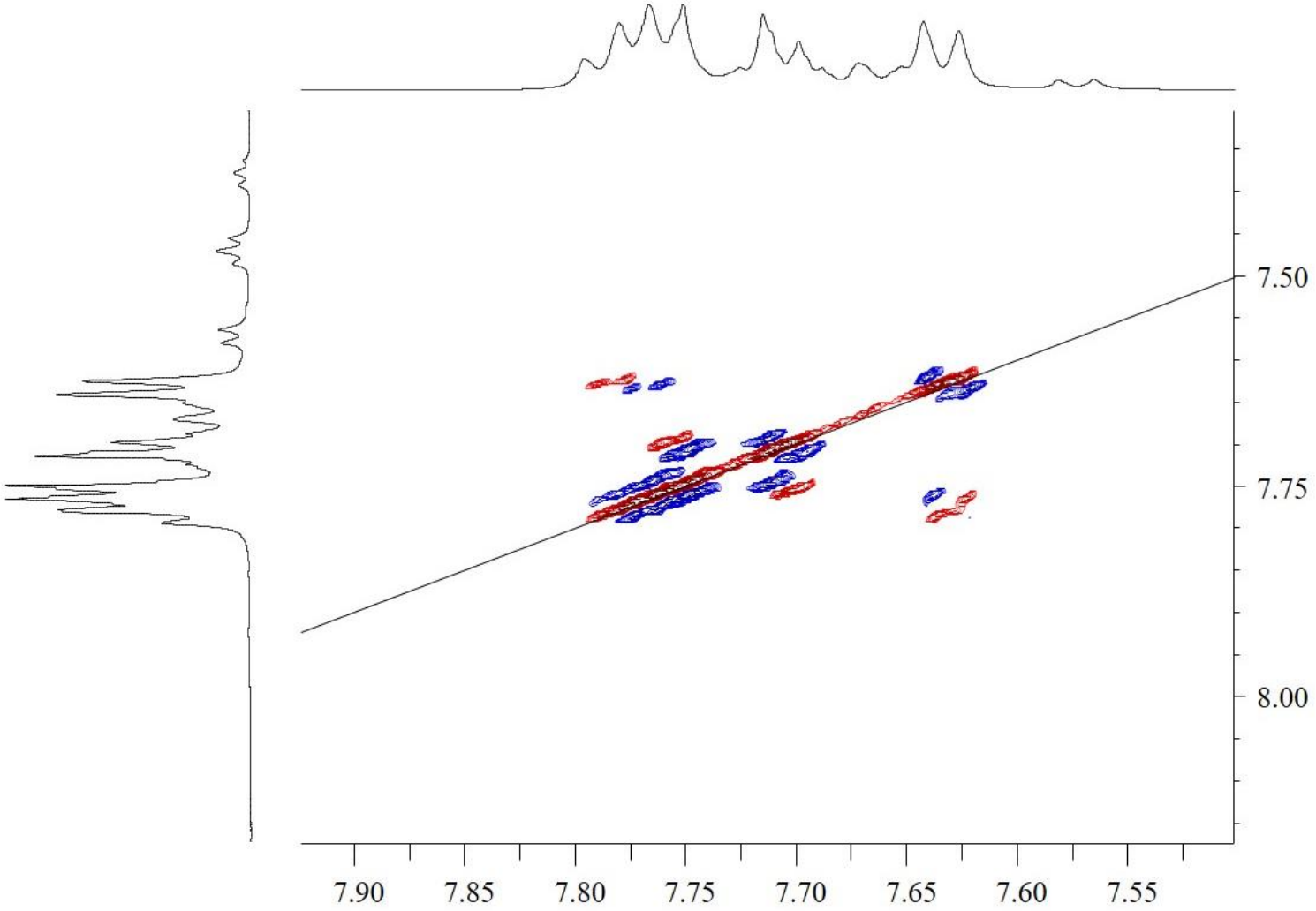

^{13}C, ^{1}H HSQC NMR (5) – Downfield Expansion

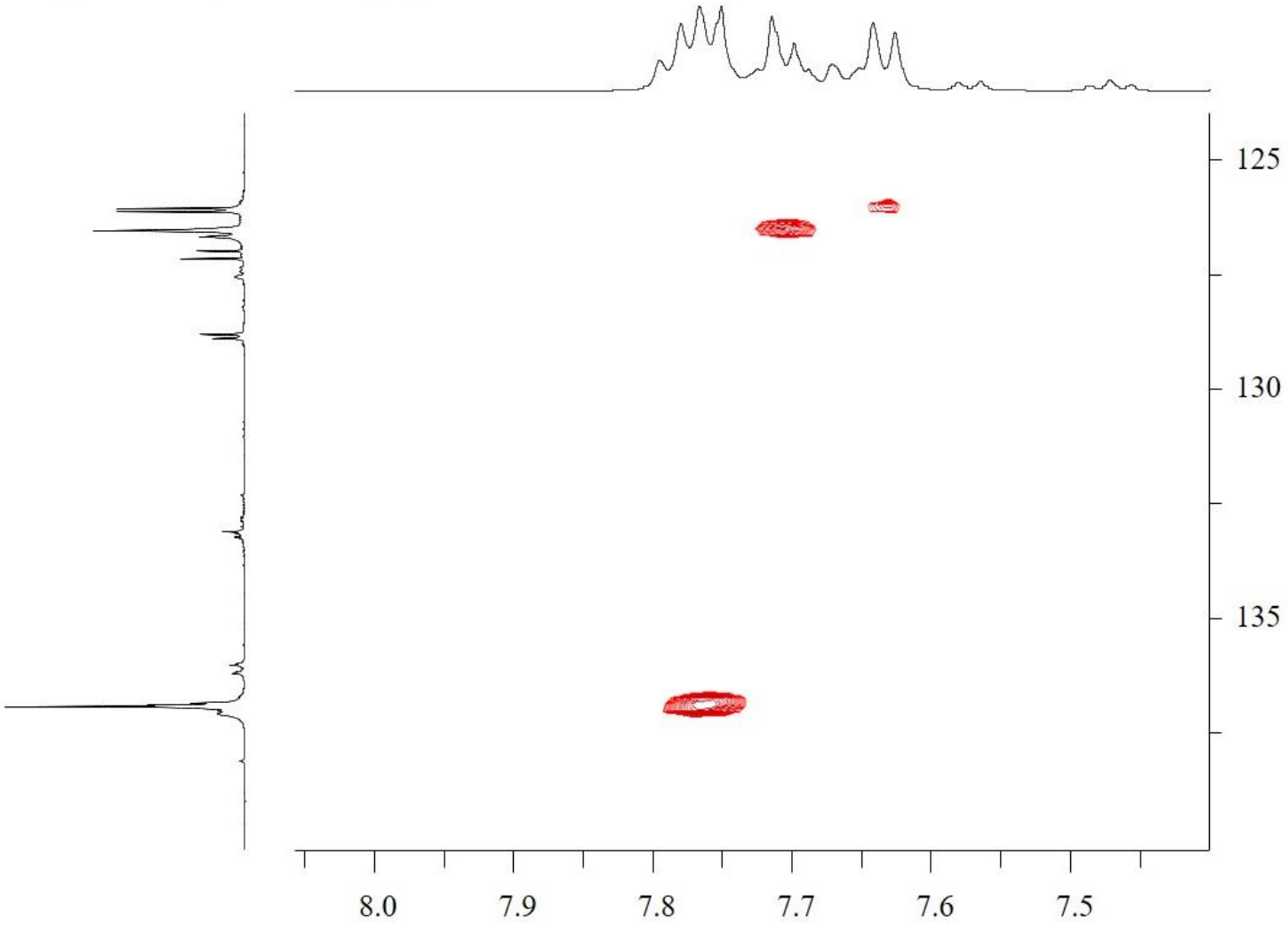

^{13}C, ^{1}H HSQC NMR (5) – Upfield Expansion

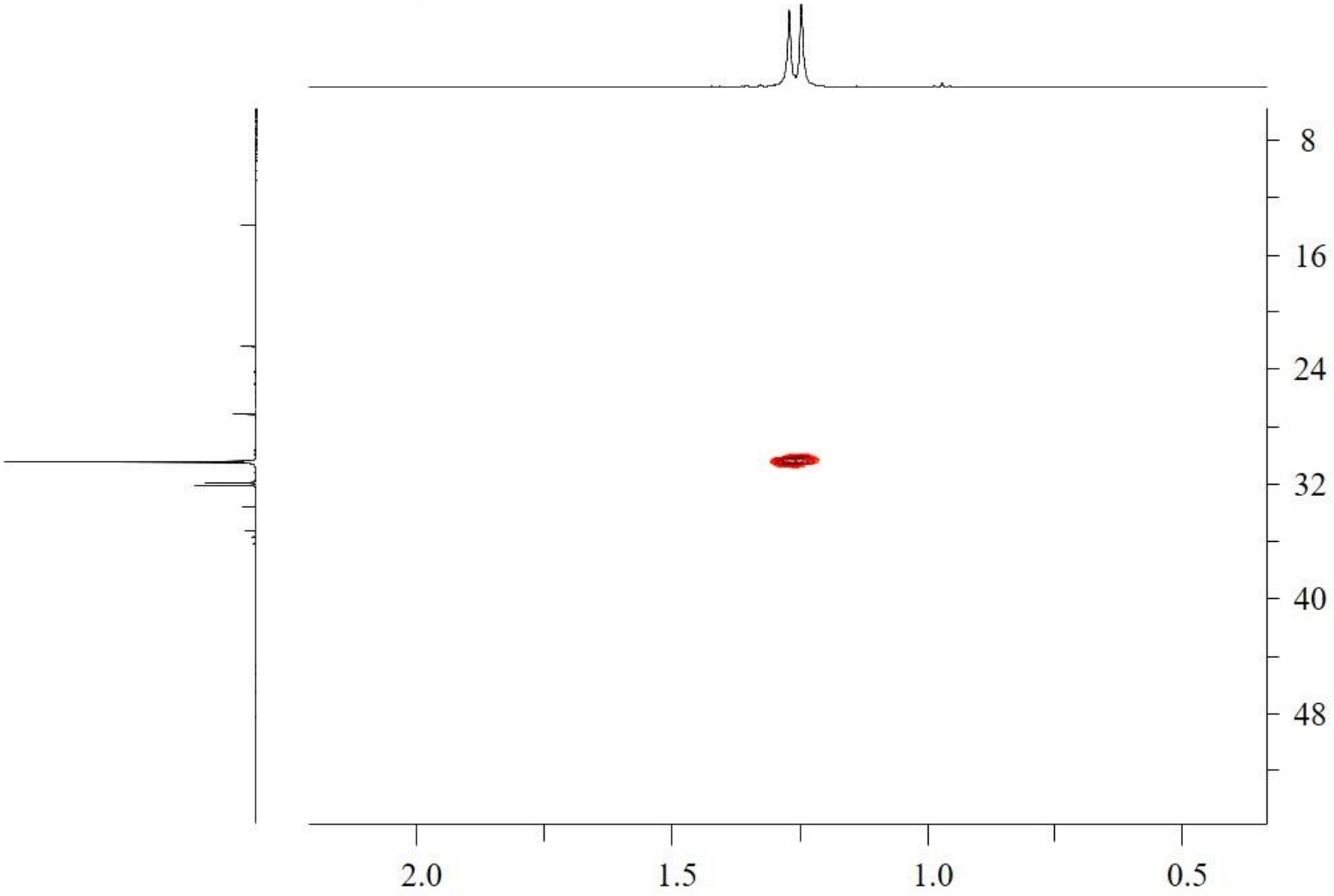

^{13}C, ^{1}H HMBC NMR (5) –Downfield Expansion

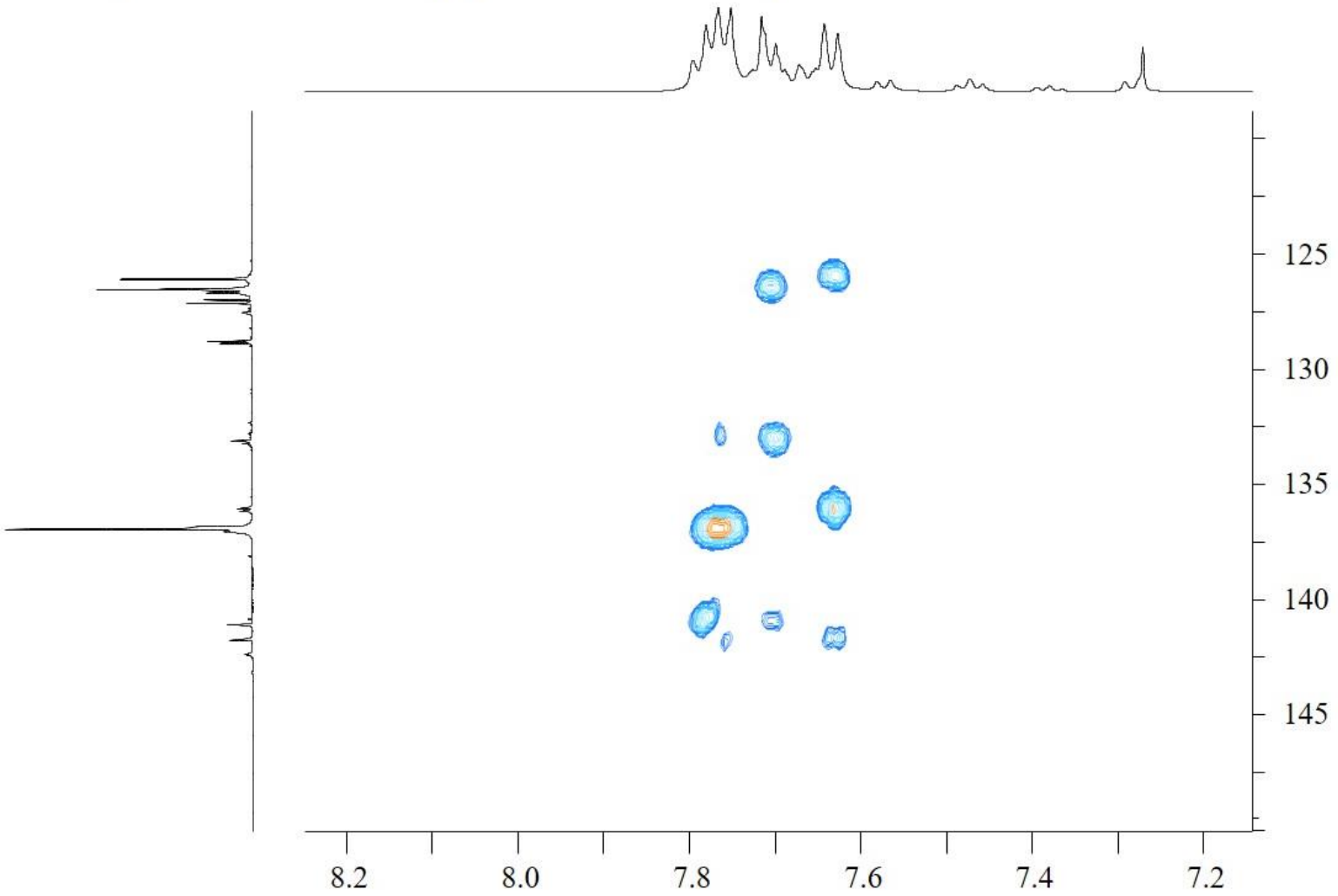

^{13}C, ^{1}H HMBC NMR (5) – Upfield Expansion

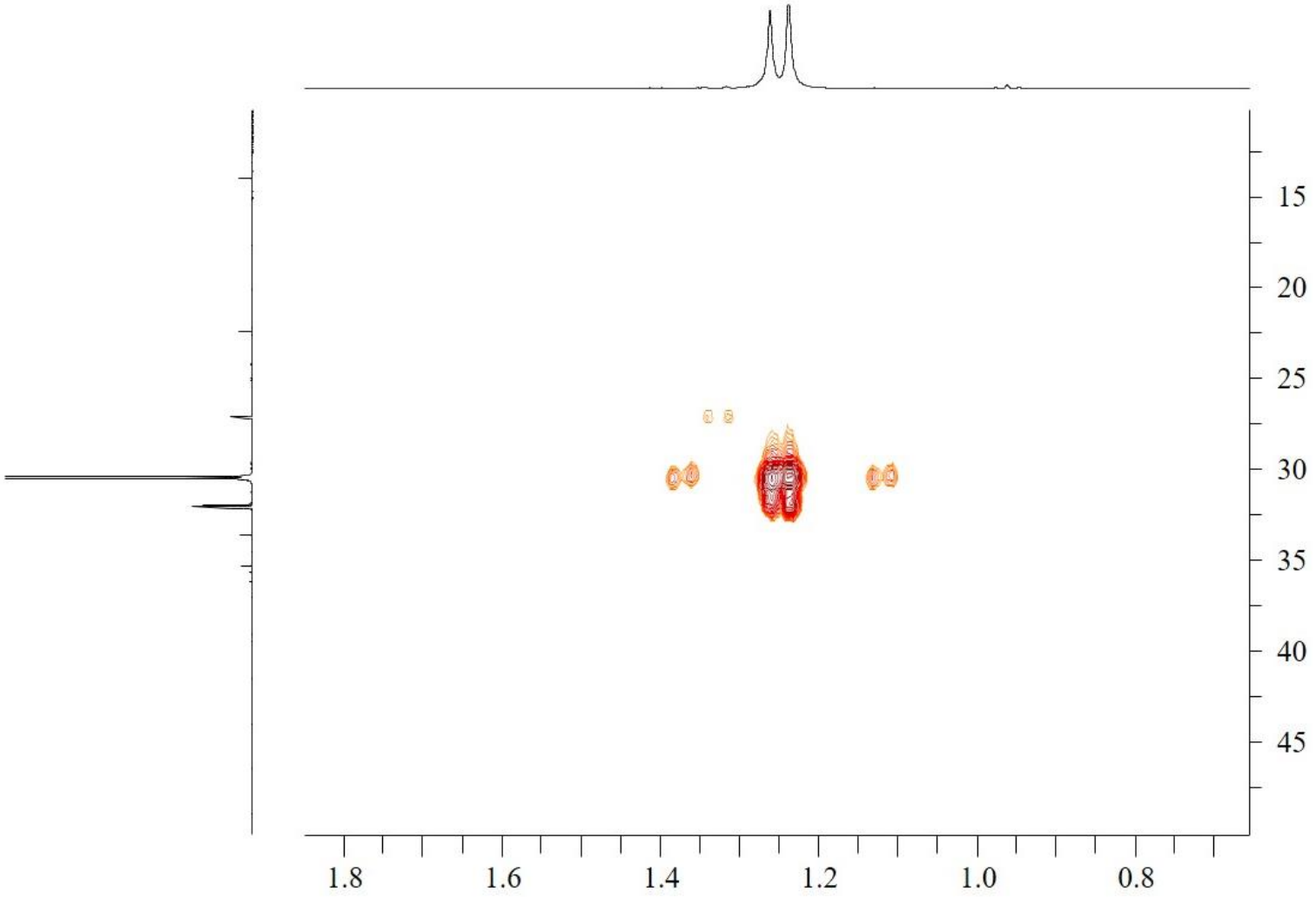

^{1}H NMR (6)

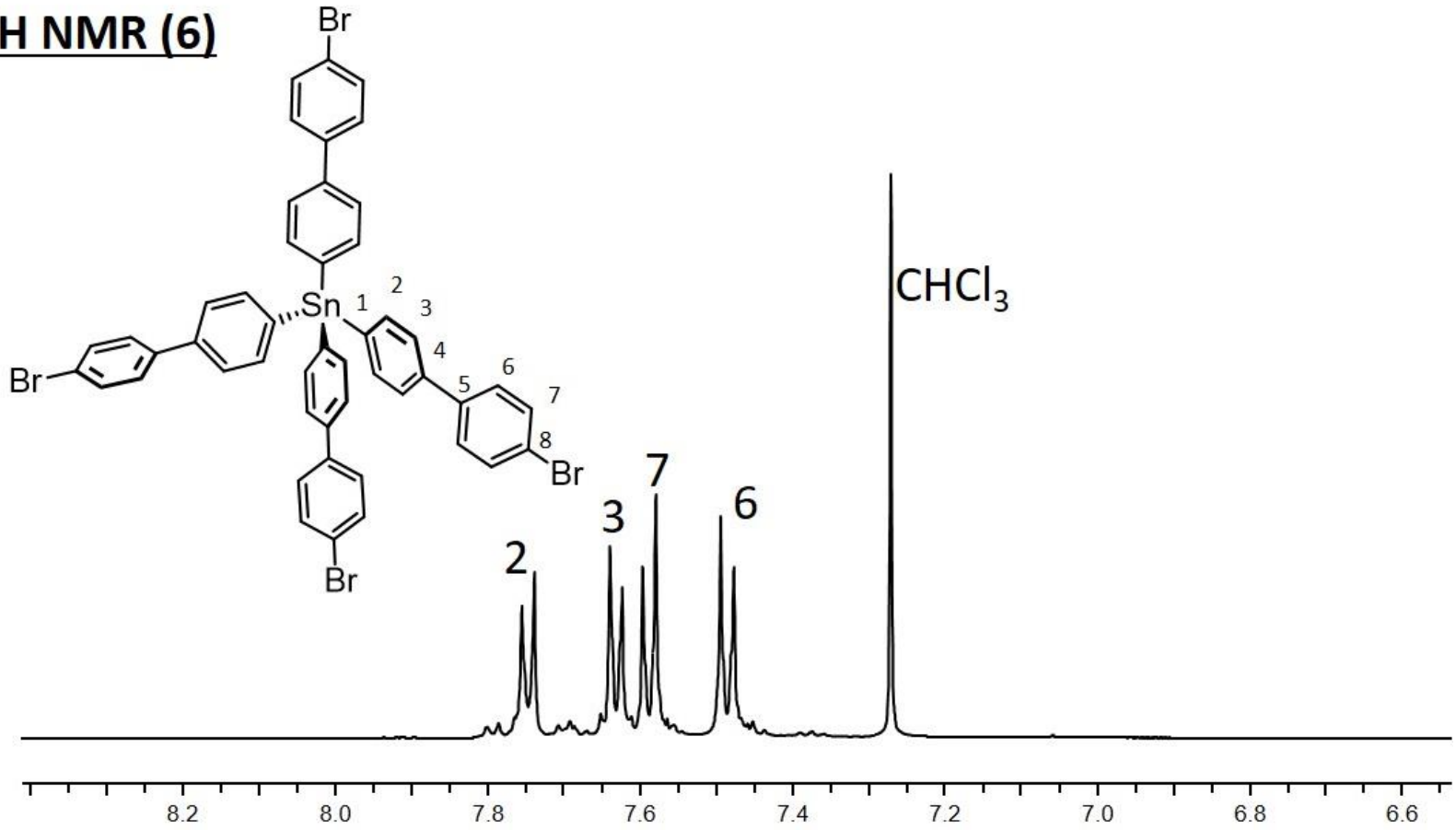

^{13}C NMR (6)

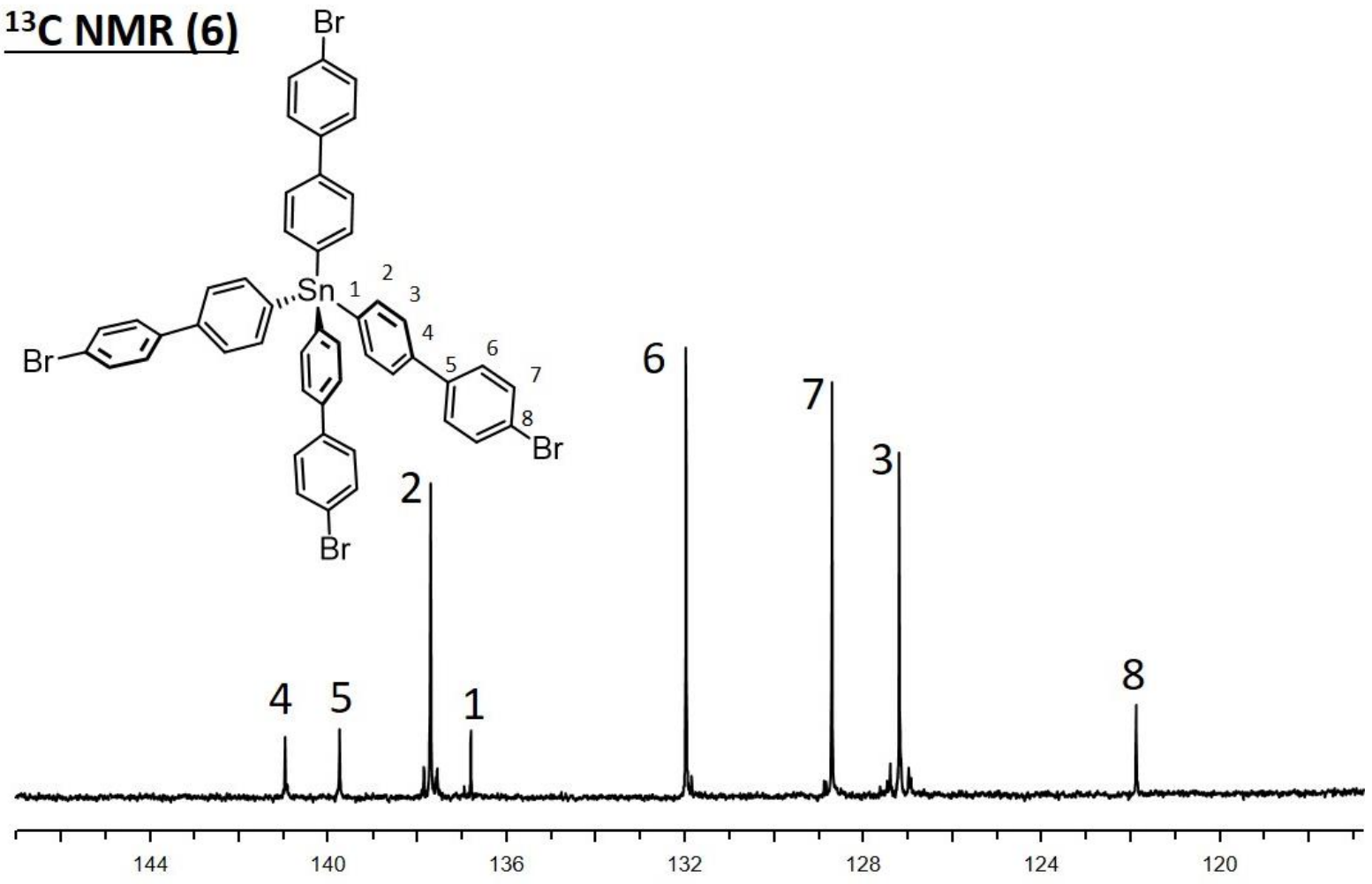

^{1}H, ^{1}H COSY NMR (6)

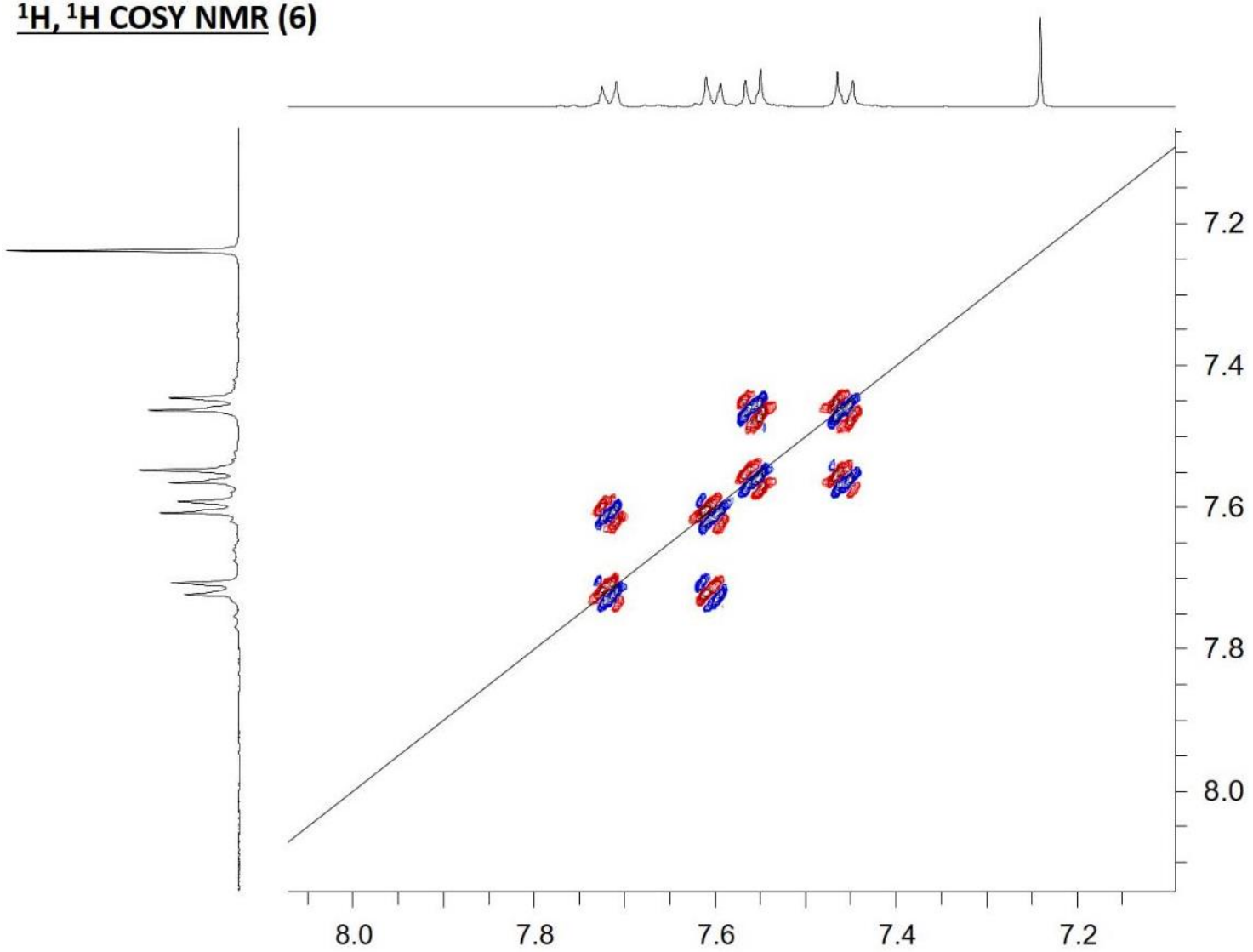

^{13}C, ^{1}H HSQC NMR (6) – Downfield Expansion

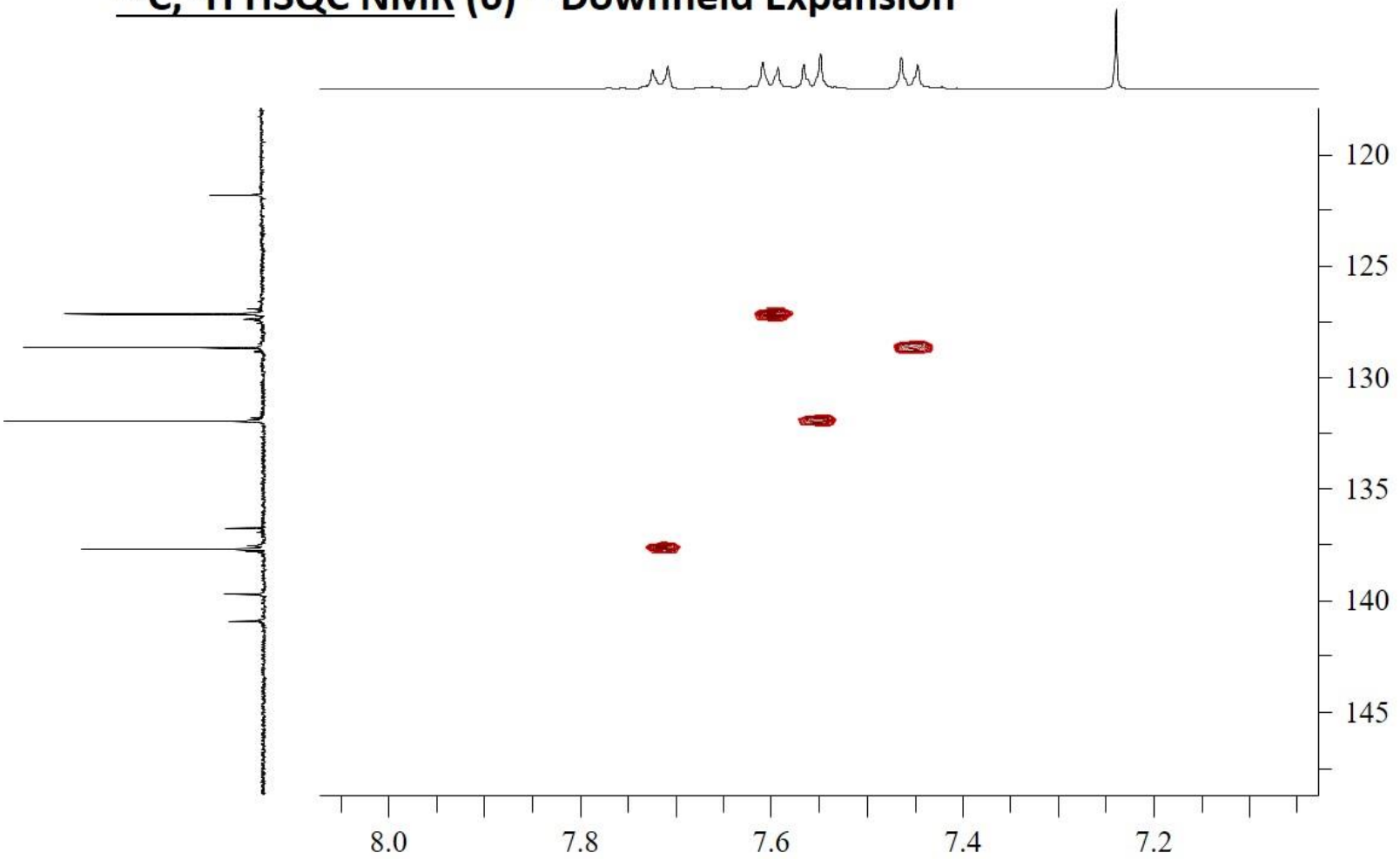

^{13}C, ^{1}H HMBC NMR (6)

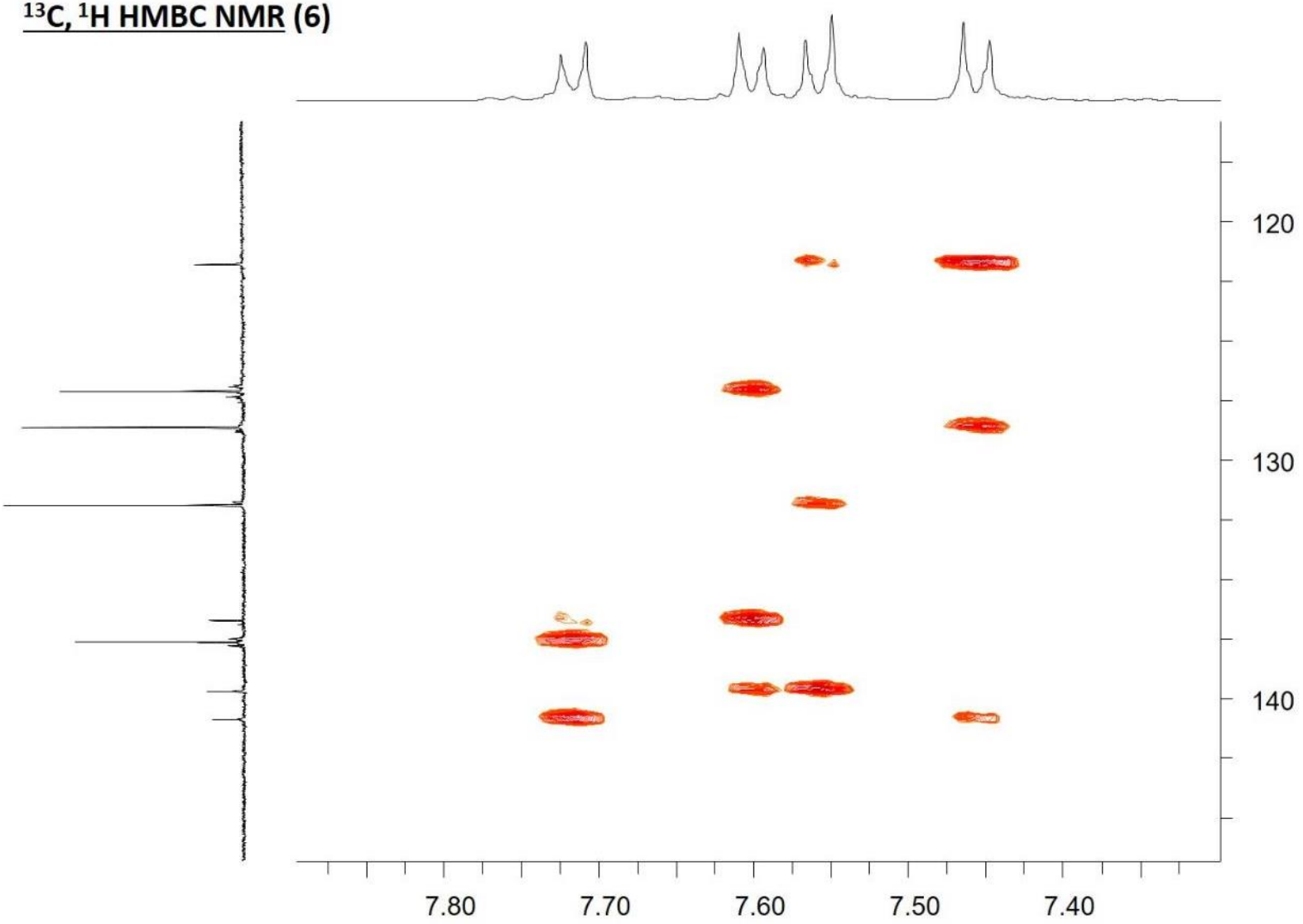

^{1}H NMR (7)

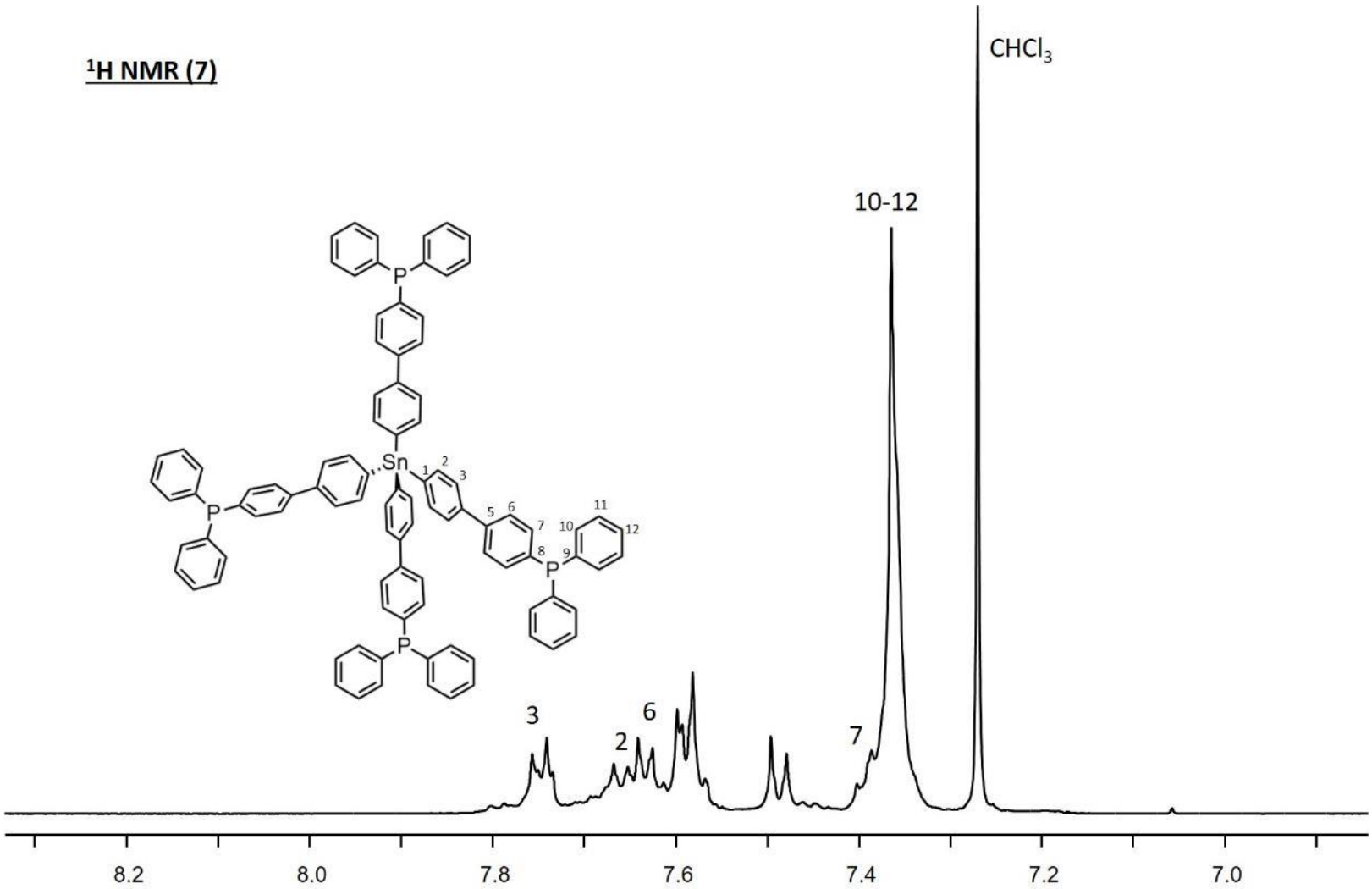

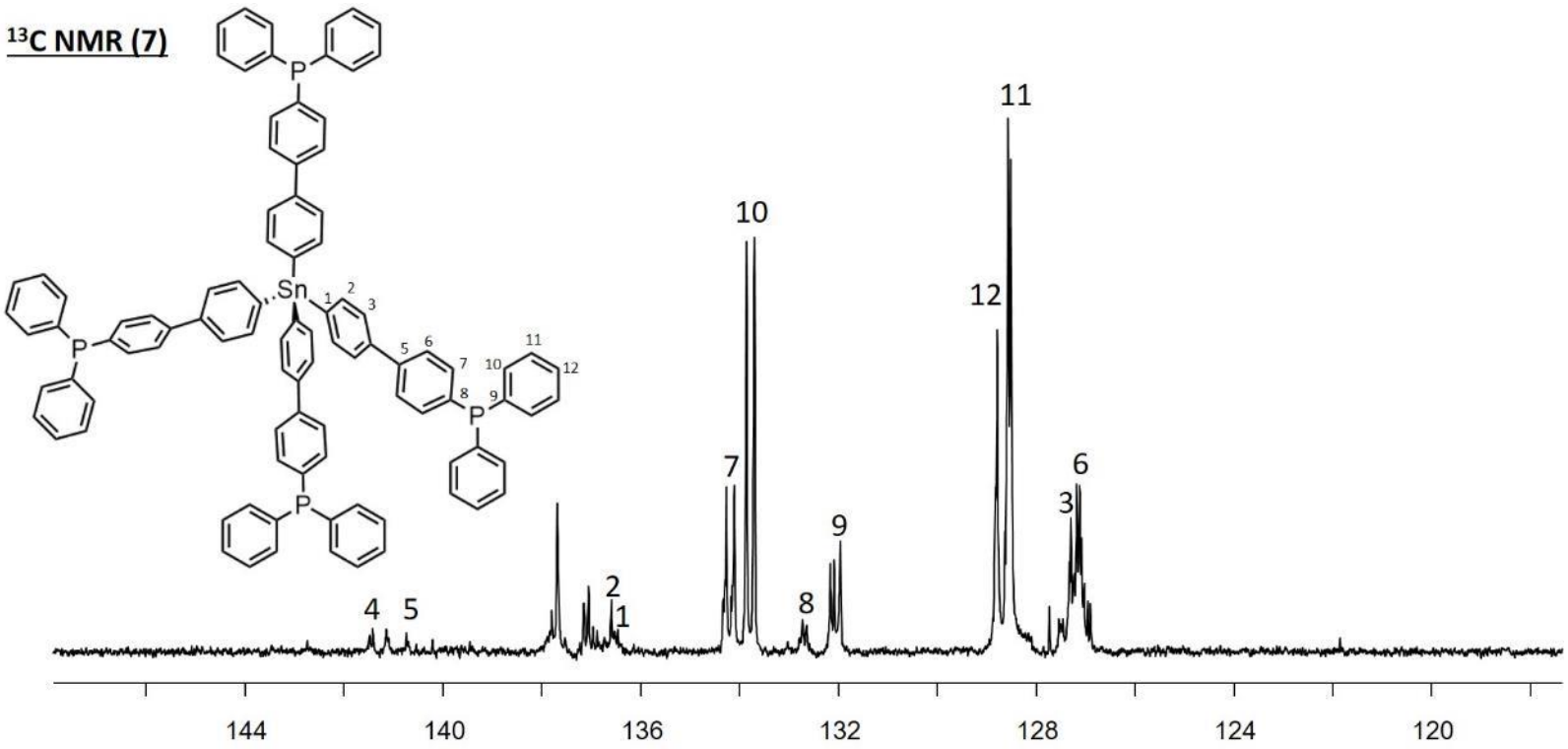
13C NMR (7)
Sn
P
P
P
P
1
2
3
4
5
6
7
8
9
10
11
12
144
140
136
132
128
124
120

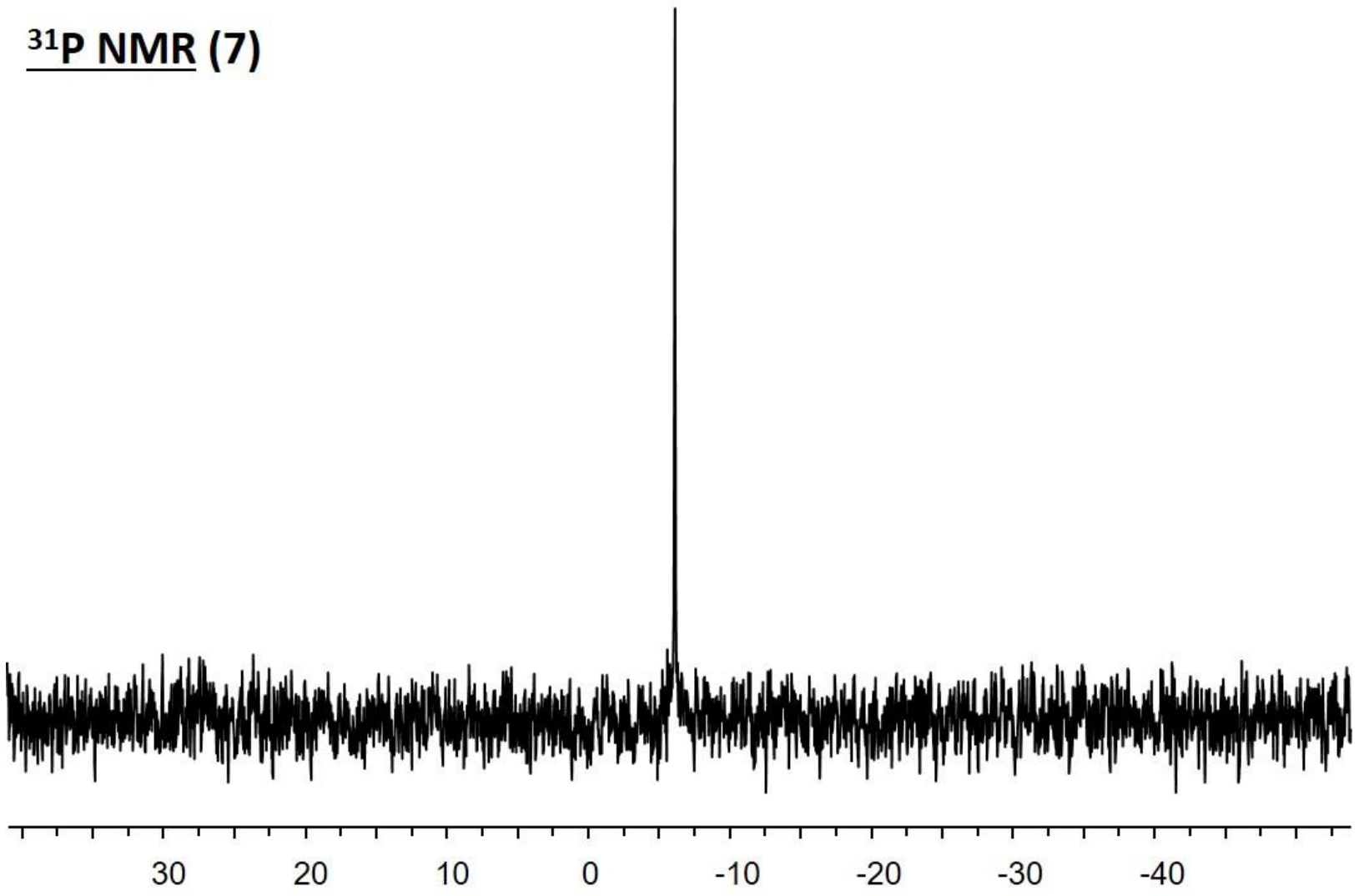
31P NMR (7)
30
20
10
0
-10
-20
-30
-40

^{1}H NMR (8)

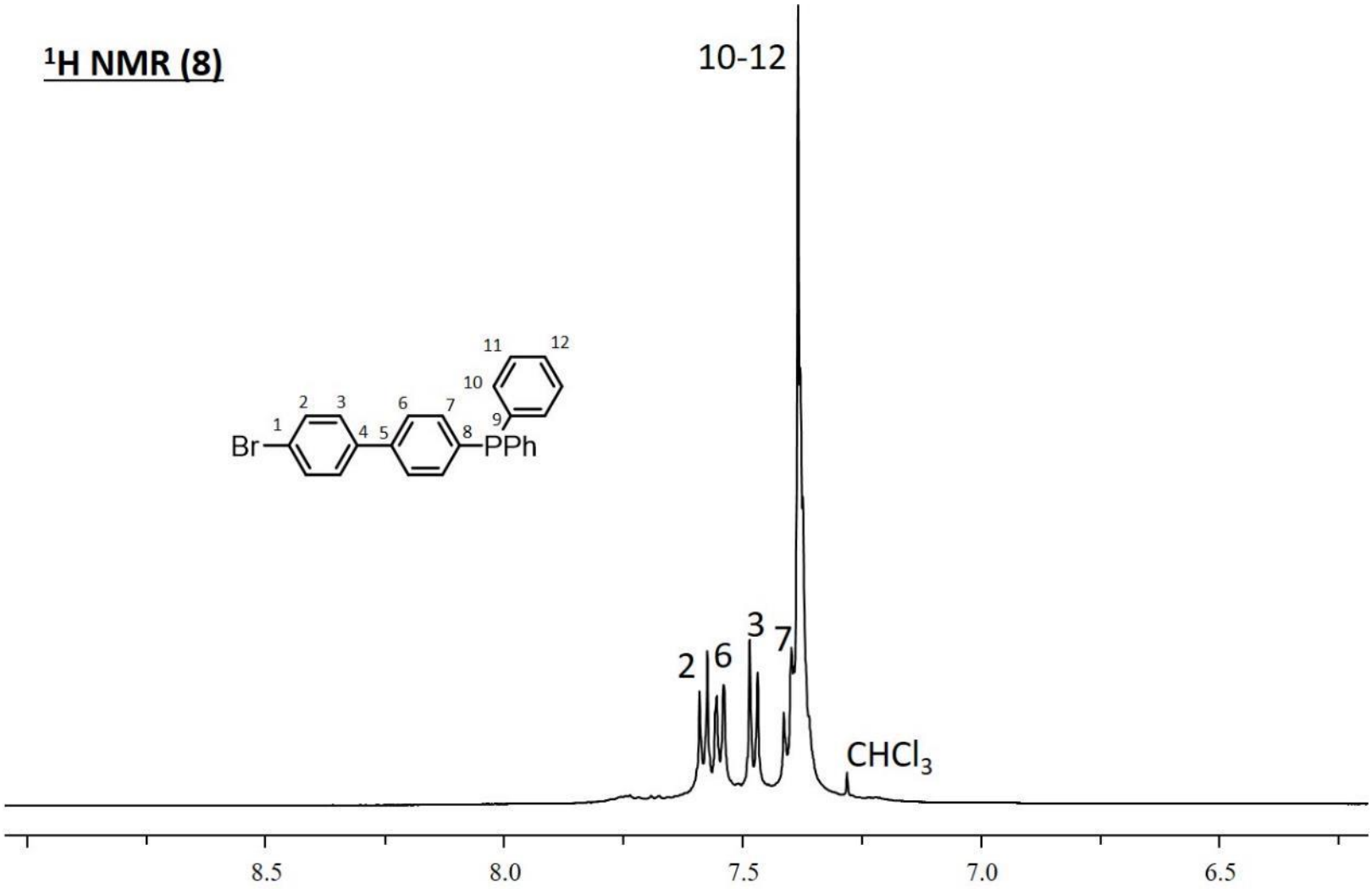

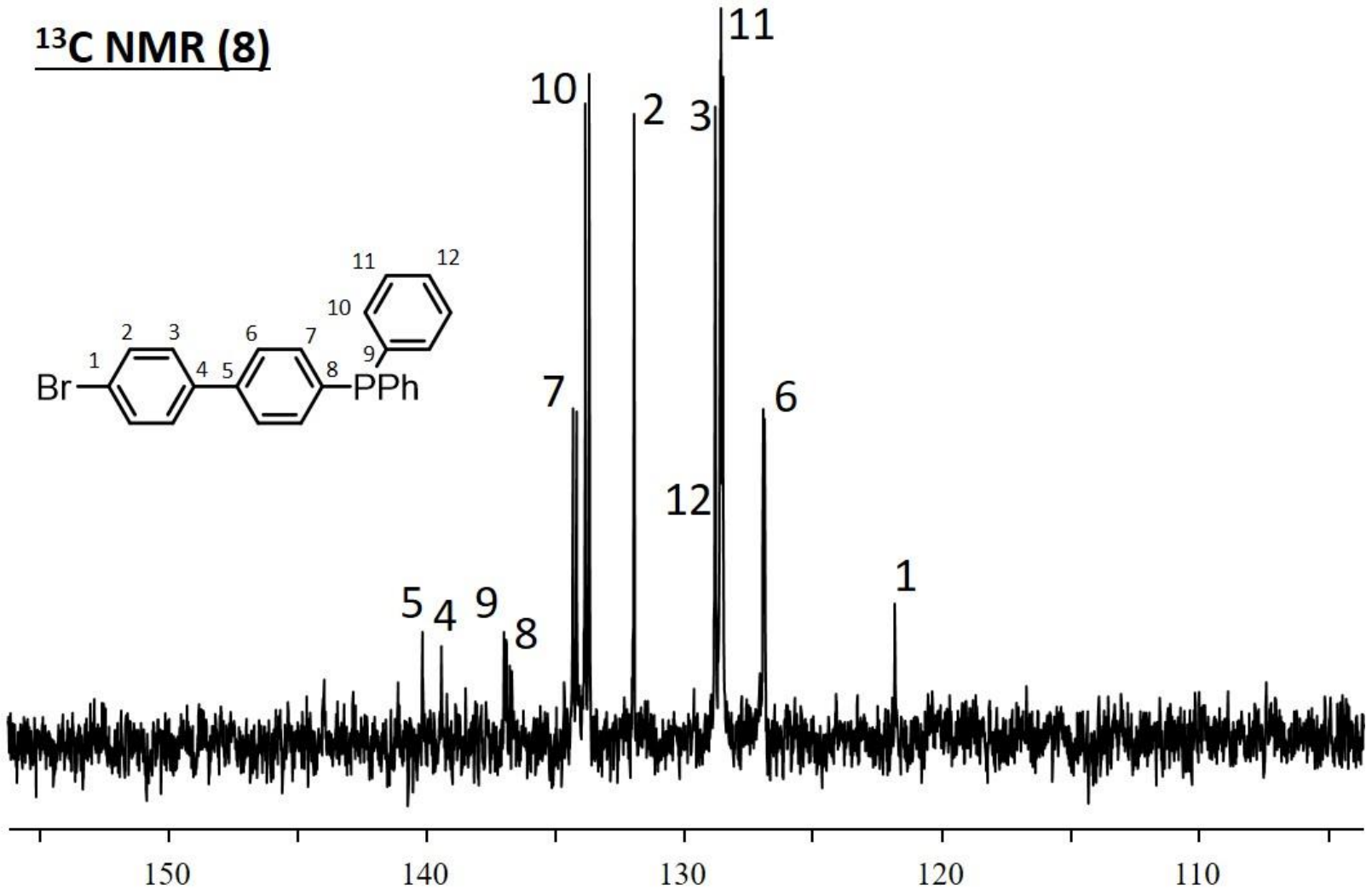
13C NMR (8)
Br
PPh
1
2
3
4
5
6
7
8
9
10
11
12
10
2
3
11
7
6
12
1
5
4
9
8
150
140
130
120
110

^{31}P NMR (8)

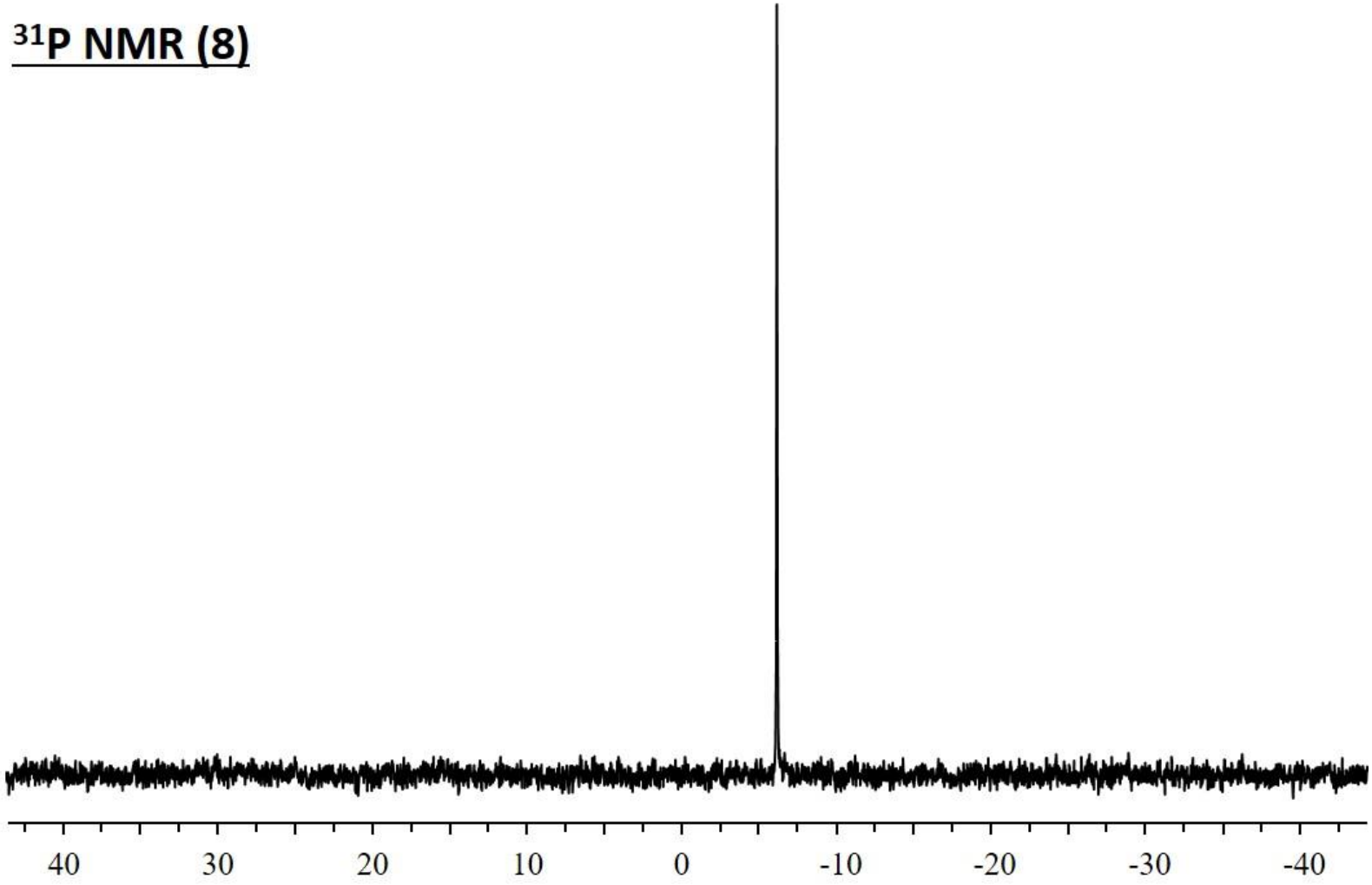

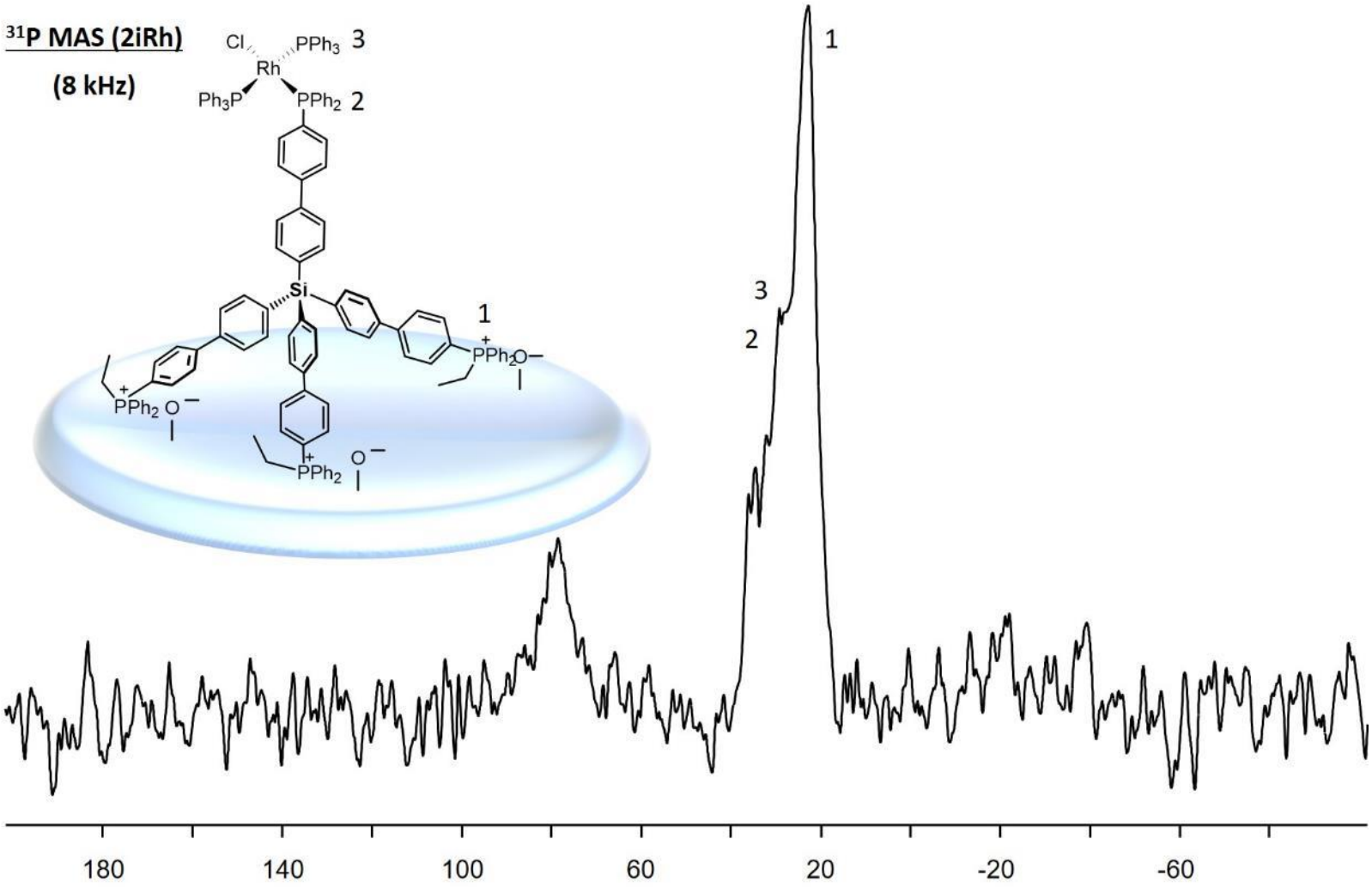
31P MAS (2iRh)
(8 kHz)
Cl
Rh
PPh3
Ph3P
PPh2
3
2
Si
1
PPh2
O
3
2
1
180
140
100
60
20
-20
-60

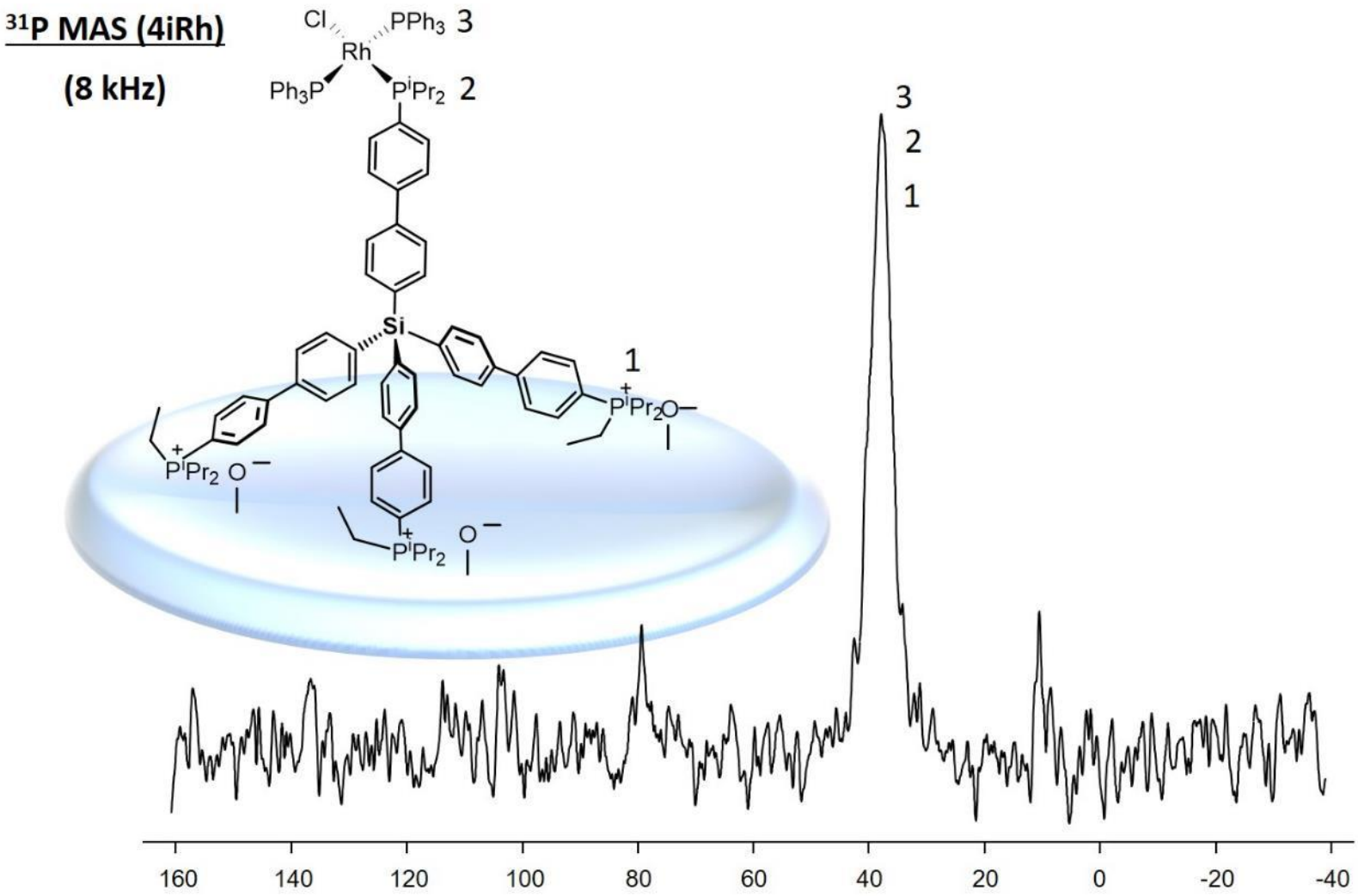
31P MAS (4iRh)
(8 kHz)
Cl
PPh3
3
Rh
Ph3P
PiPr2
2
Si
1
PiPr2O
PiPr2
O
PiPr2
O
3
2
1
160
140
120
100
80
60
40
20
0
-20
-40

APPENDIX B

SUPPLEMENTARY CHAPTER II

DSC of Bromo-PEEK

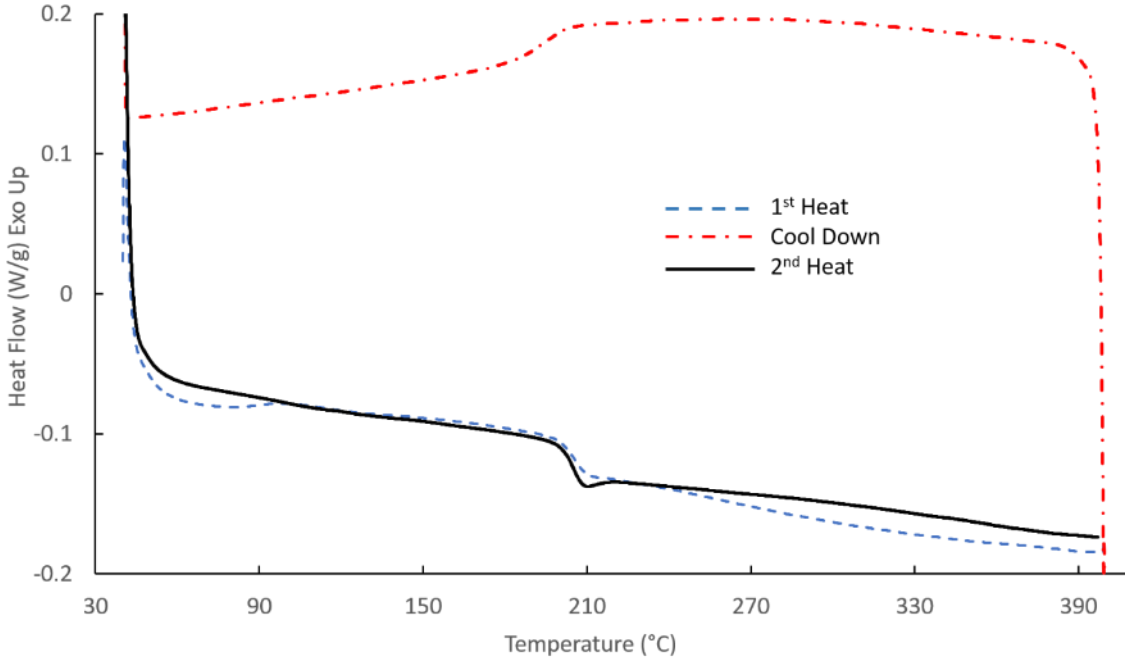

IR Spectra of Model Compounds

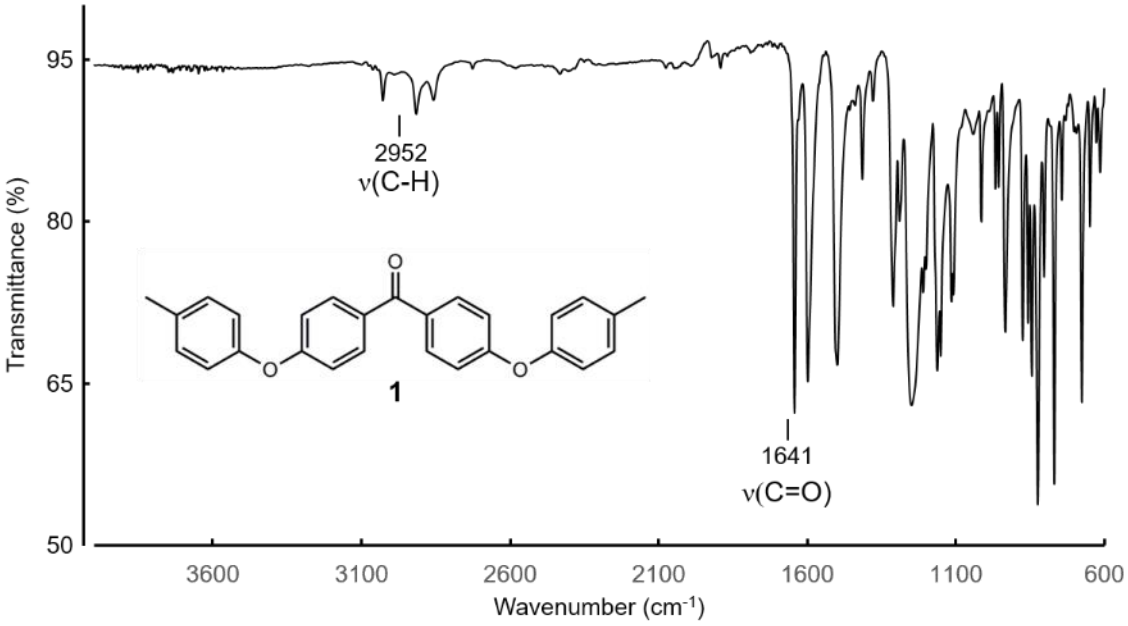

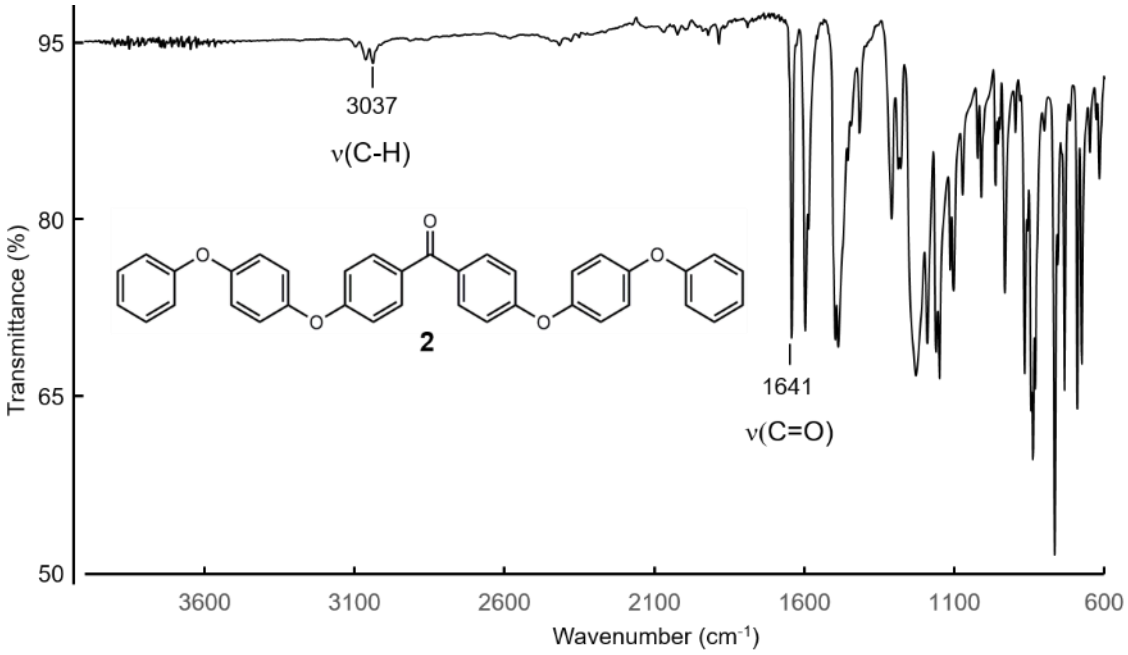

TGA of Model Compounds (Air)

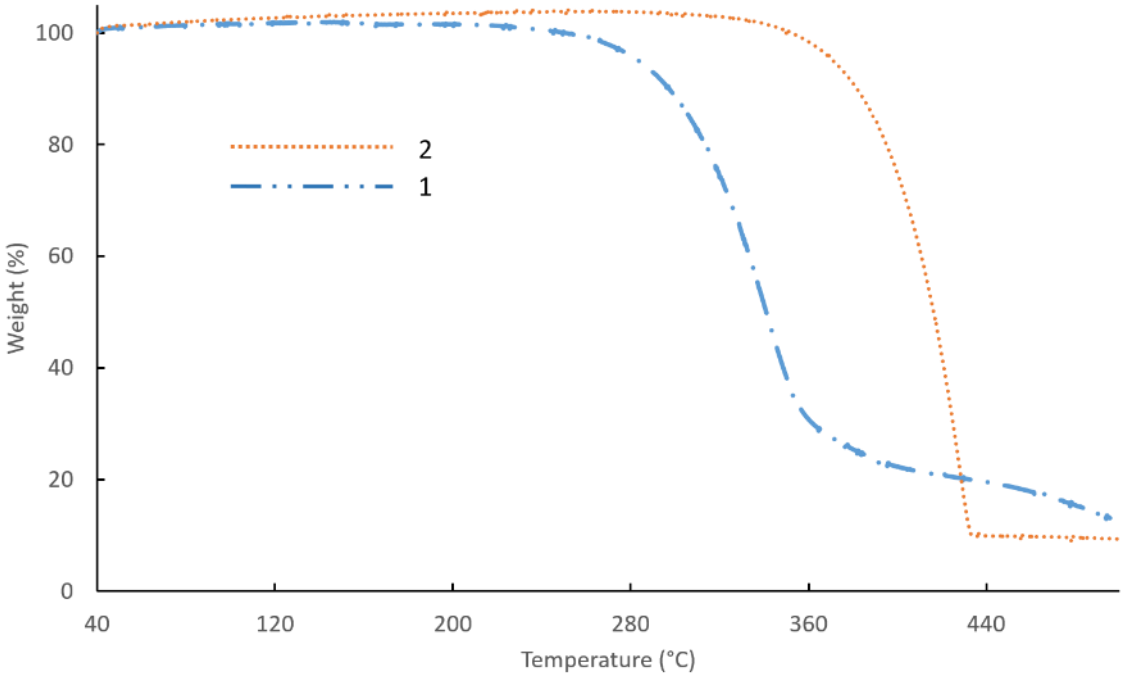

TGA of Model Compounds (N_2)

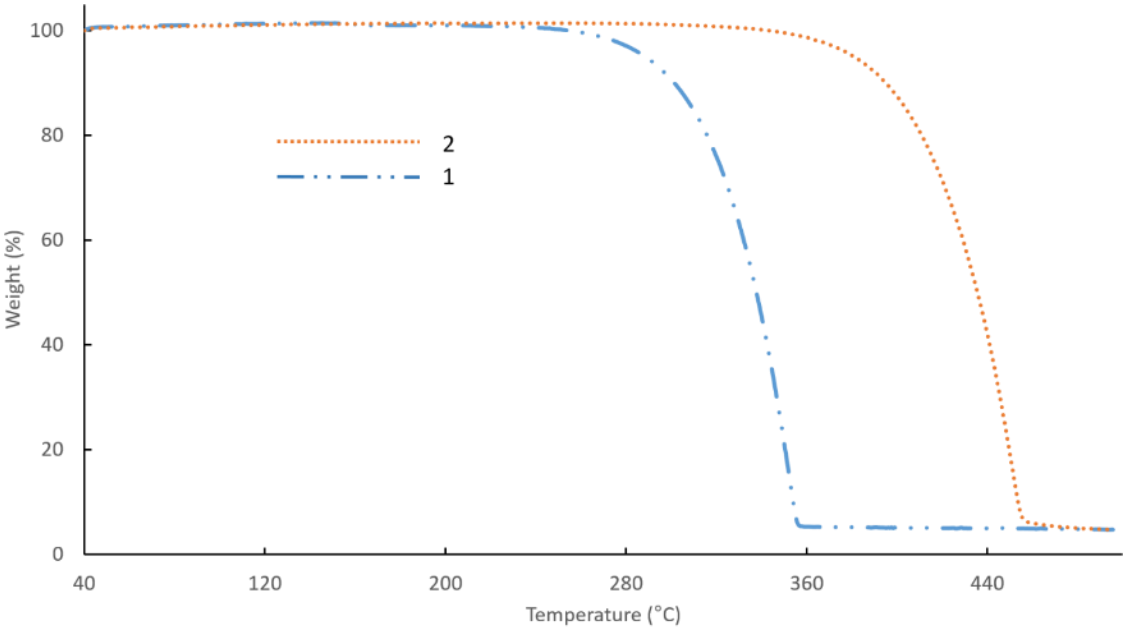

TGA Bromo-PEEK both Air and N_2

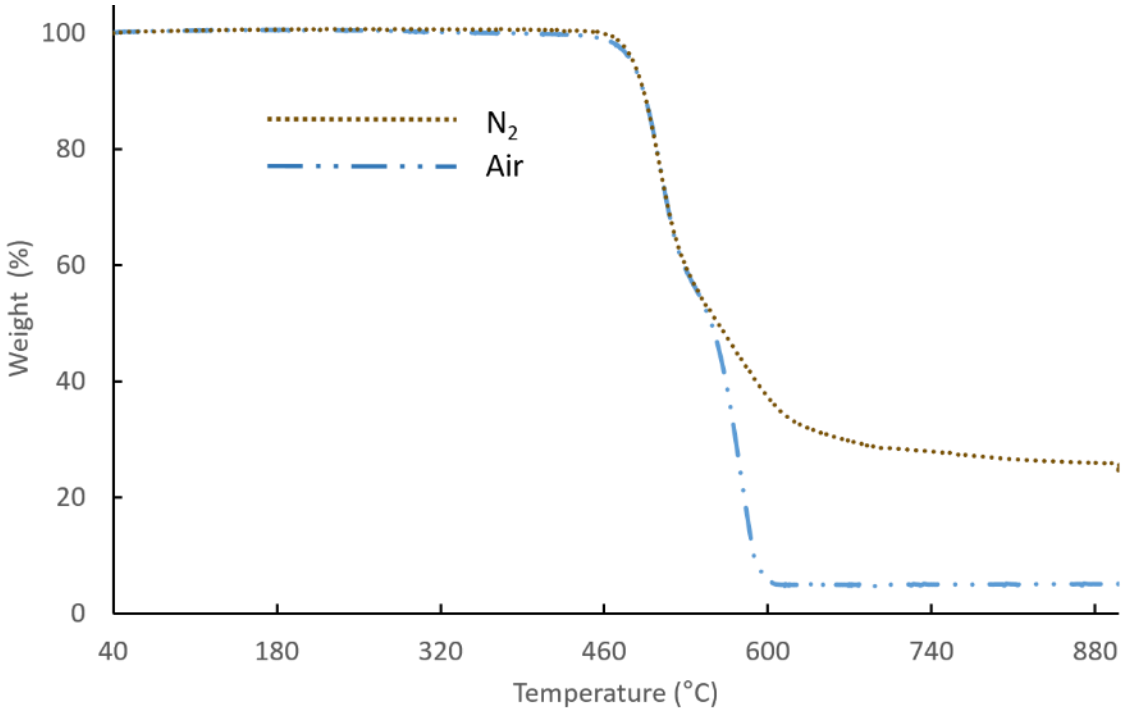

NMR Spectra of Model Compounds

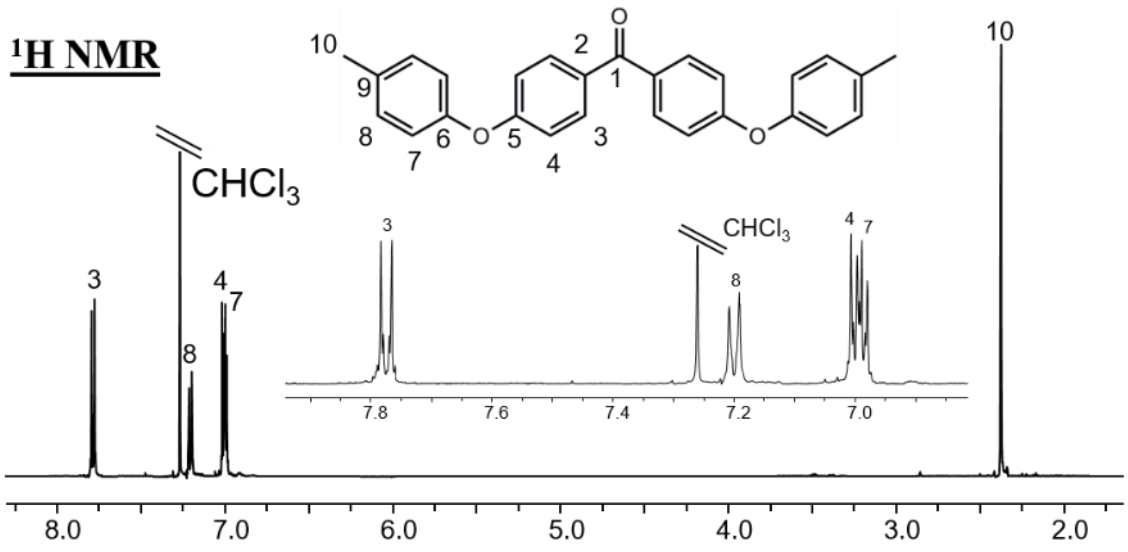

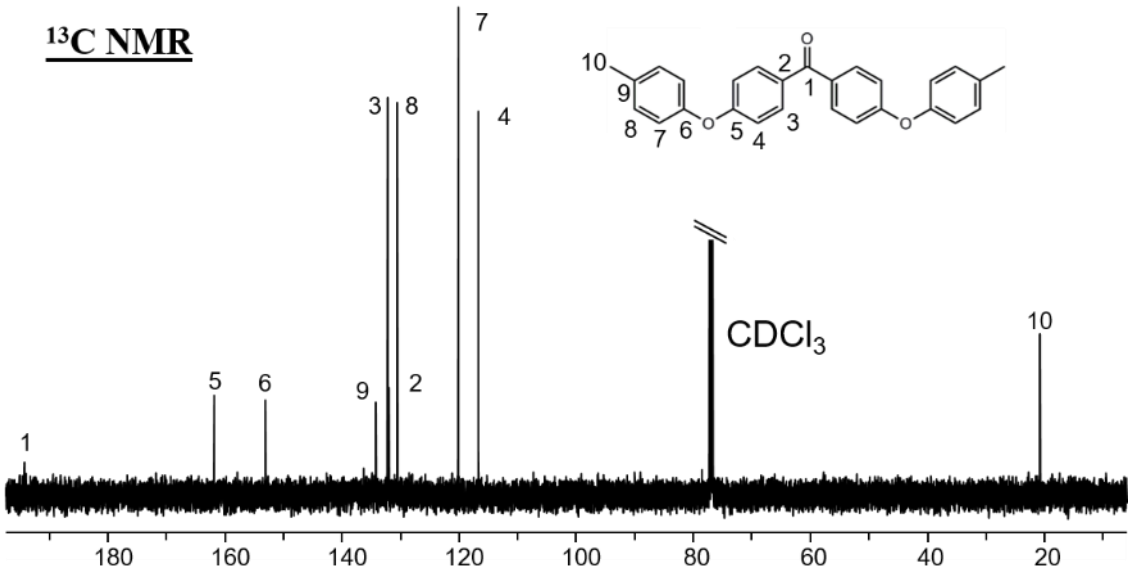
13C NMR
7
3
8
4
10
9
8
7
6
5
4
3
2
1
O
O
O
CDCl3
10
5
6
9
2
1
180
160
140
120
100
80
60
40
20

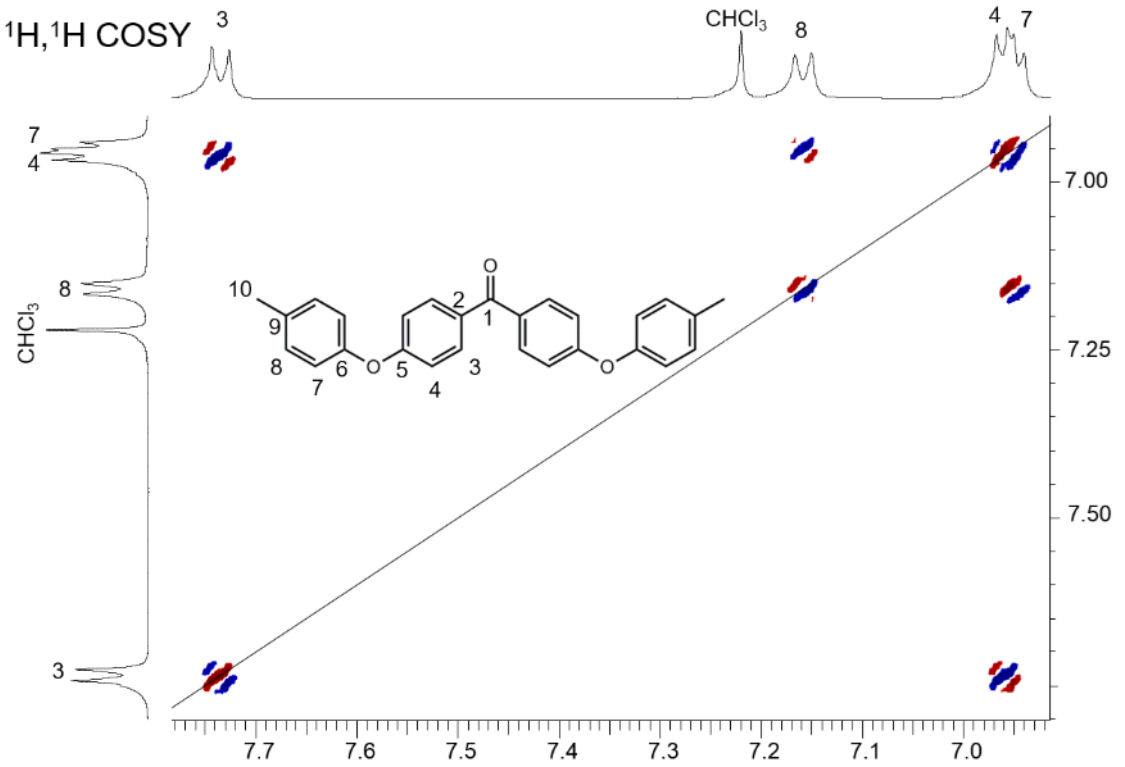
^{1}H,^{1}H COSY
3
CHCl$_3$
8
4
7
7
4
8
CHCl$_3$
3
10
9
8
7
6
O
5
4
3
2
O
1
O
7.00
7.25
7.50
7.7
7.6
7.5
7.4
7.3
7.2
7.1
7.0

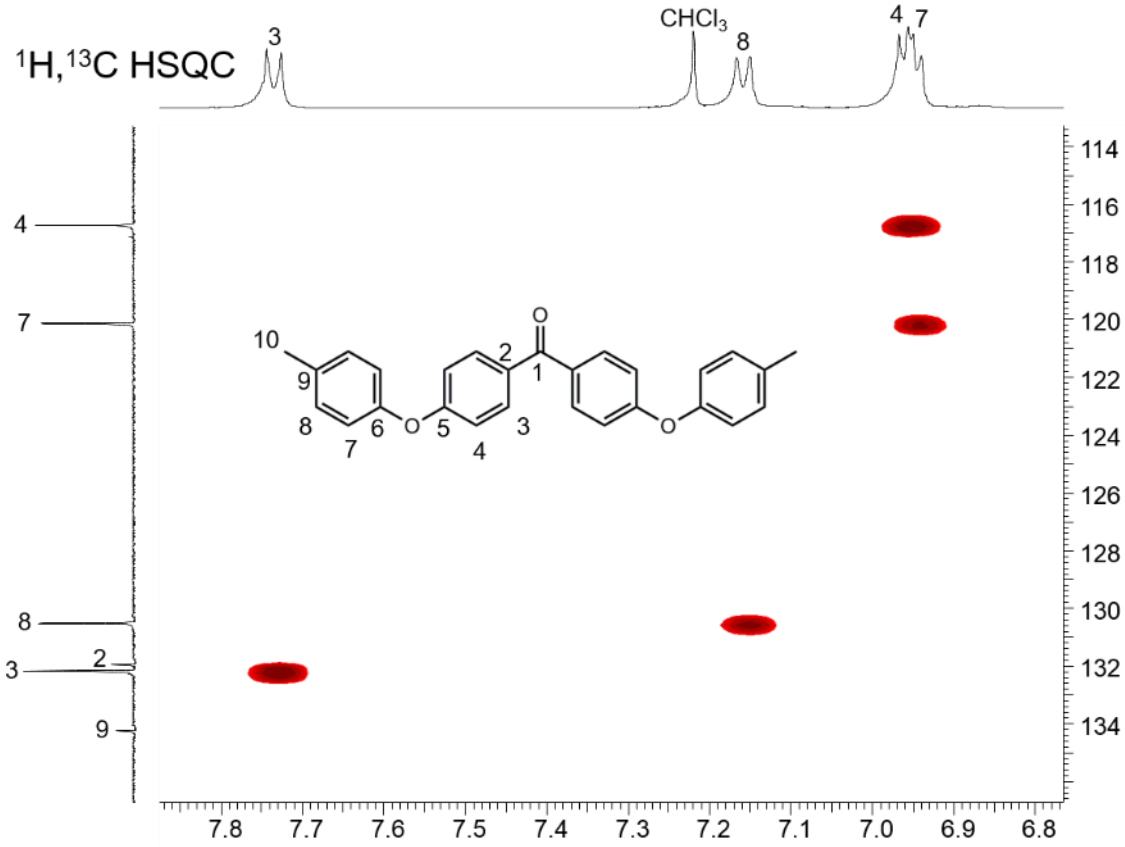
^{1}H,^{13}C HSQC
3
CHCl$_3$
8
4
7
4
7
8
3
2
9
10
9
8
7
6
O
5
4
3
2
O
1
O
114
116
118
120
122
124
126
128
130
132
134
7.8
7.7
7.6
7.5
7.4
7.3
7.2
7.1
7.0
6.9
6.8

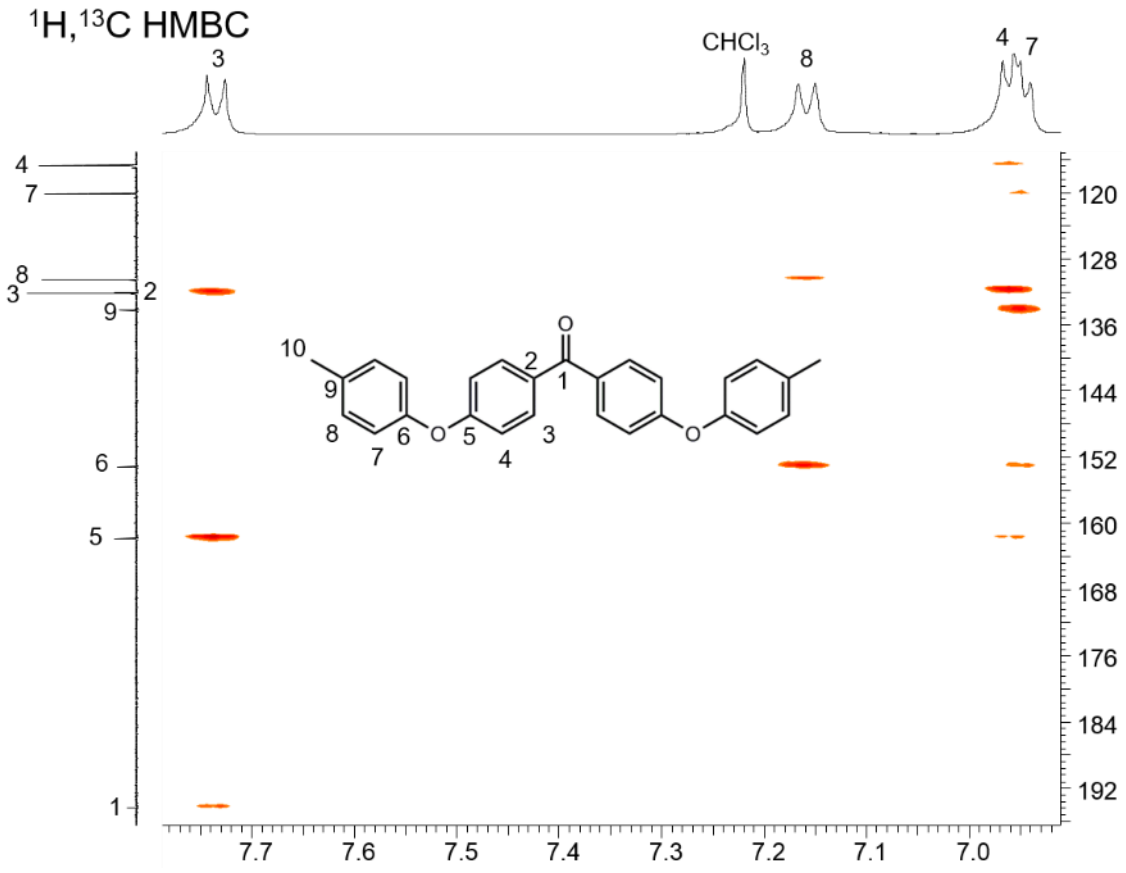
^{1}H,^{13}C HMBC
3
CHCl$_3$
8
4
7
4
7
8
3
2
9
6
5
1
120
128
136
144
152
160
168
176
184
192
7.7
7.6
7.5
7.4
7.3
7.2
7.1
7.0
O
10
9
8
7
6
O
5
4
2
1
3
O

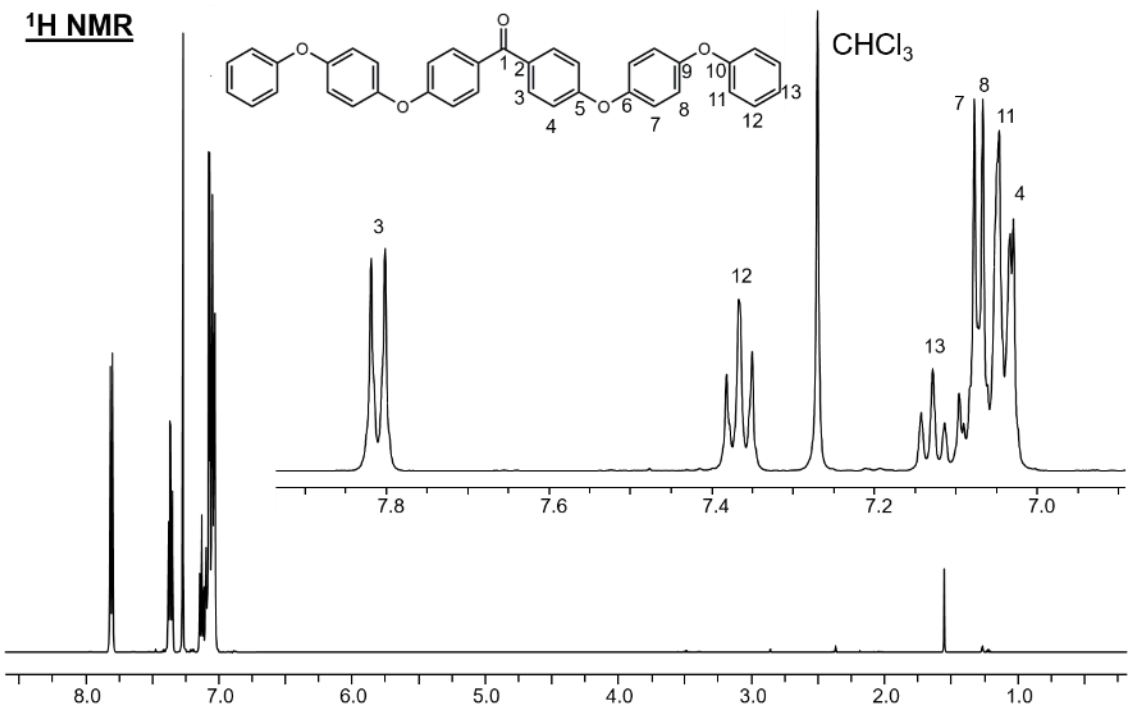
1H NMR
CHCl3
3
12
13
7
8
11
4
7.8
7.6
7.4
7.2
7.0
8.0
7.0
6.0
5.0
4.0
3.0
2.0
1.0

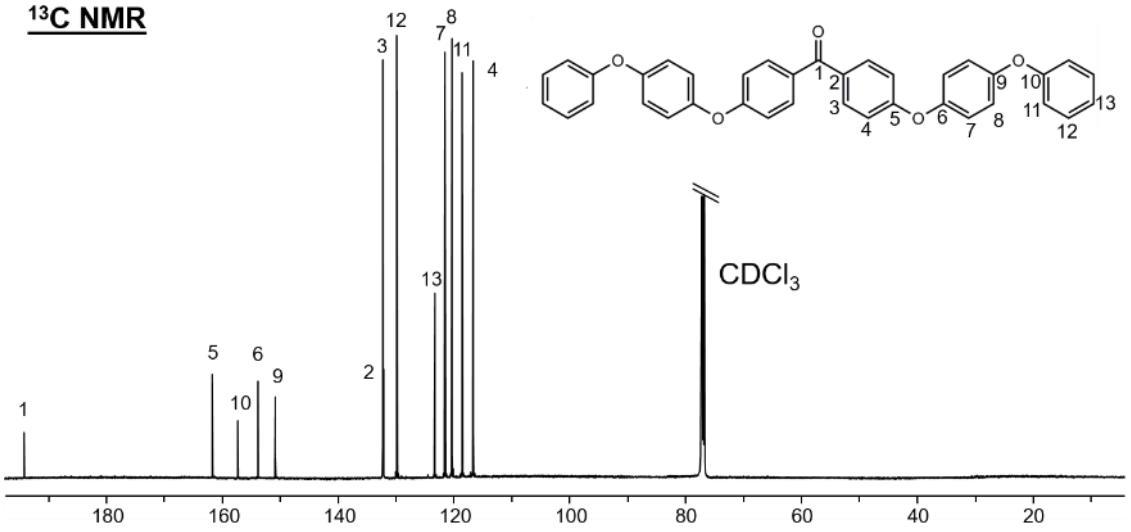
13C NMR
CDCl3
1
5
6
9
10
2
13
3
12
7
8
11
4
180
160
140
120
100
80
60
40
20

^{13}C NMR

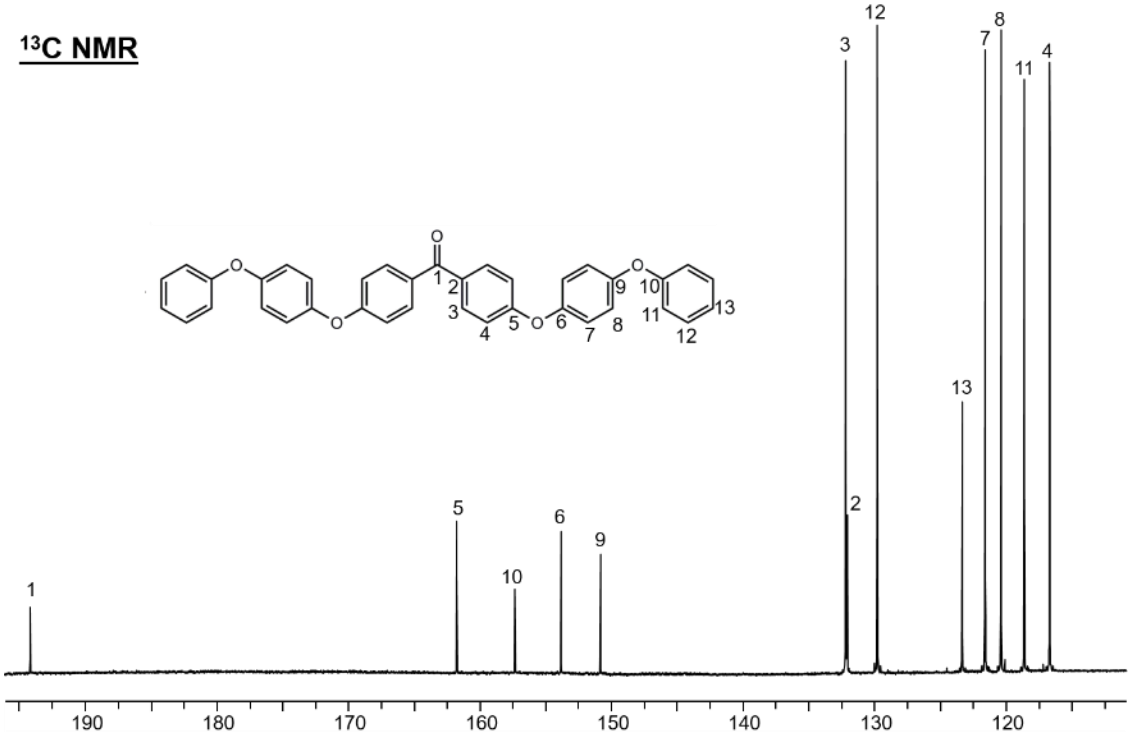

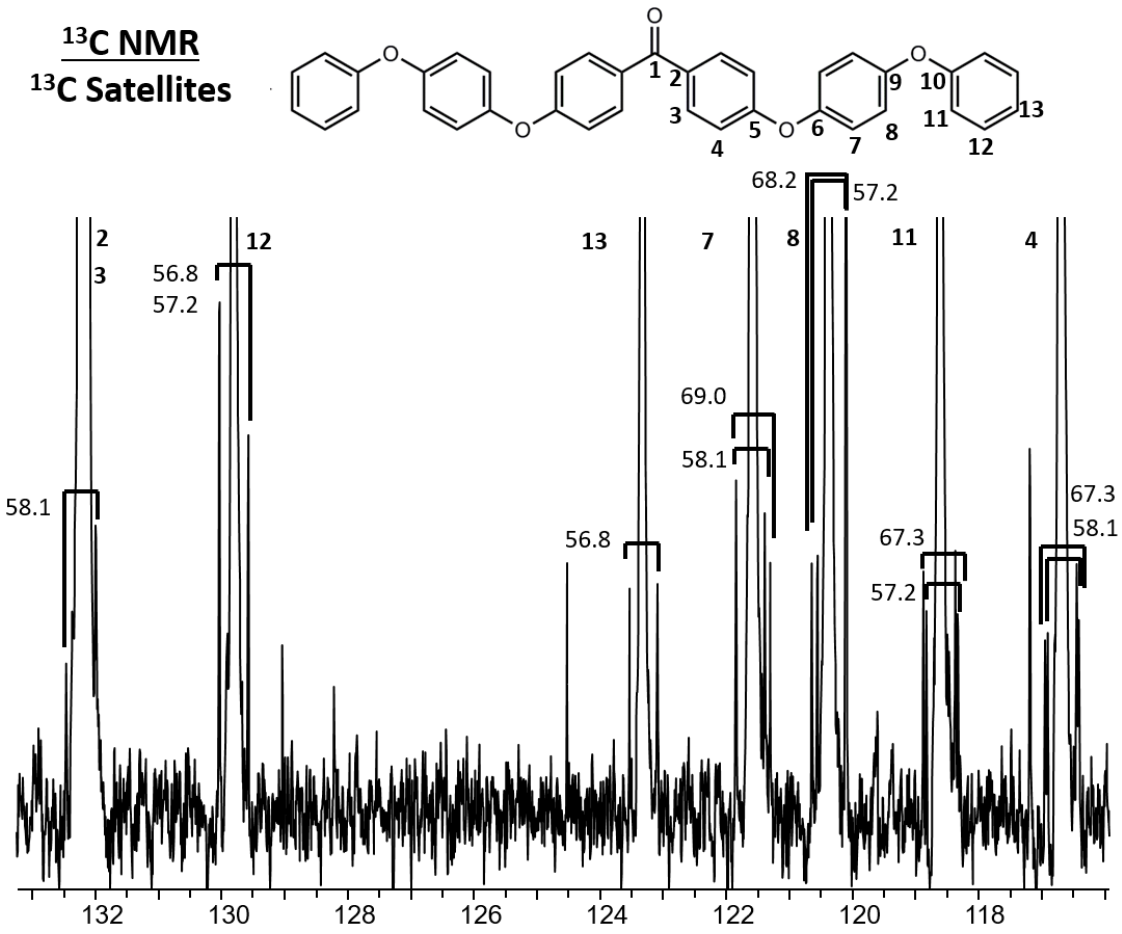
13C NMR
13C Satellites
O
1
2
3
4
5
6
7
8
9
10
11
12
13
68.2
57.2
2
3
56.8
57.2
12
13
7
8
11
4
69.0
58.1
58.1
56.8
67.3
57.2
67.3
58.1
132
130
128
126
124
122
120
118

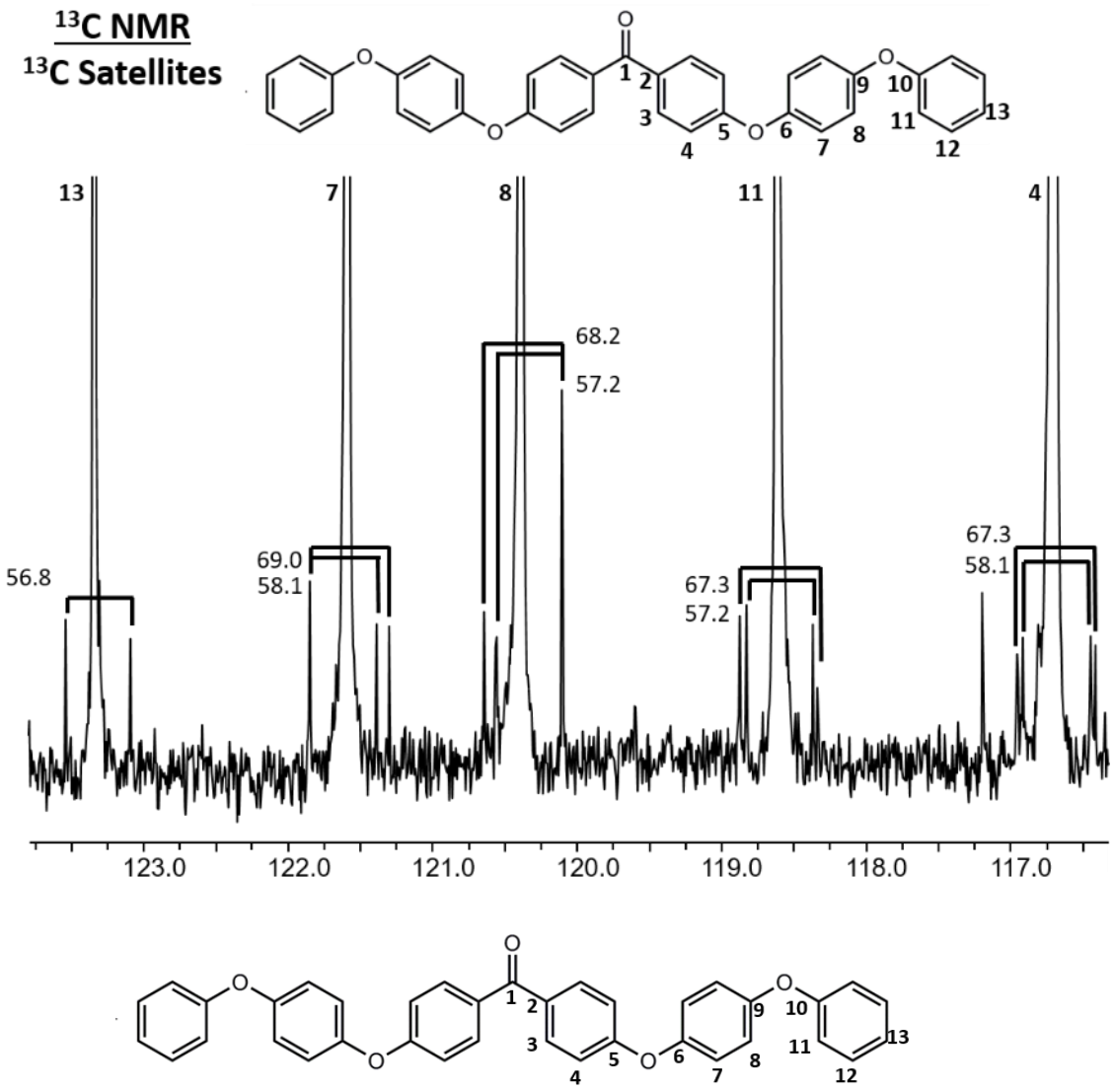

^{13}C	3	4	7	8	11	12	13
δ (ppm) of ^{13}C	132.24	116.71	121.60	120.39	118.62	129.82	123.34
δ (ppm) $^{1}J(^{13}C\text{-}^{13}C)$ C	132.22 (**^{13}C4**)	116.69 (**^{13}C3**) 116.70 (**^{13}C5**)	121.58 (**^{13}C8**) 121.60 (**^{13}C6**)	120.33 (**^{13}C7**) 120.38 (**^{13}C9**)	118.60 (**^{13}C12**) 118.61 (**^{13}C10**)	129.82 (**^{13}C11**) 129.82 (**^{13}C13**)	123.32(**^{13}C12**)
$^{1}J(^{13}C\text{-}^{13}C)$ (Hz)	58.1 (**^{13}C4**)	58.1 (**^{13}C3**) 67.3 (**^{13}C5**)	57.7 (**^{13}C8**) 69.0 (**^{13}C6**)	57.7 (**^{13}C7**) 68.2 (**^{13}C9**)	57.2 (**^{13}C12**) 67.3 (**^{13}C10**)	57.2 (**^{13}C11**) 56.8 (**^{13}C13**)	56.8 (**^{13}C12**)

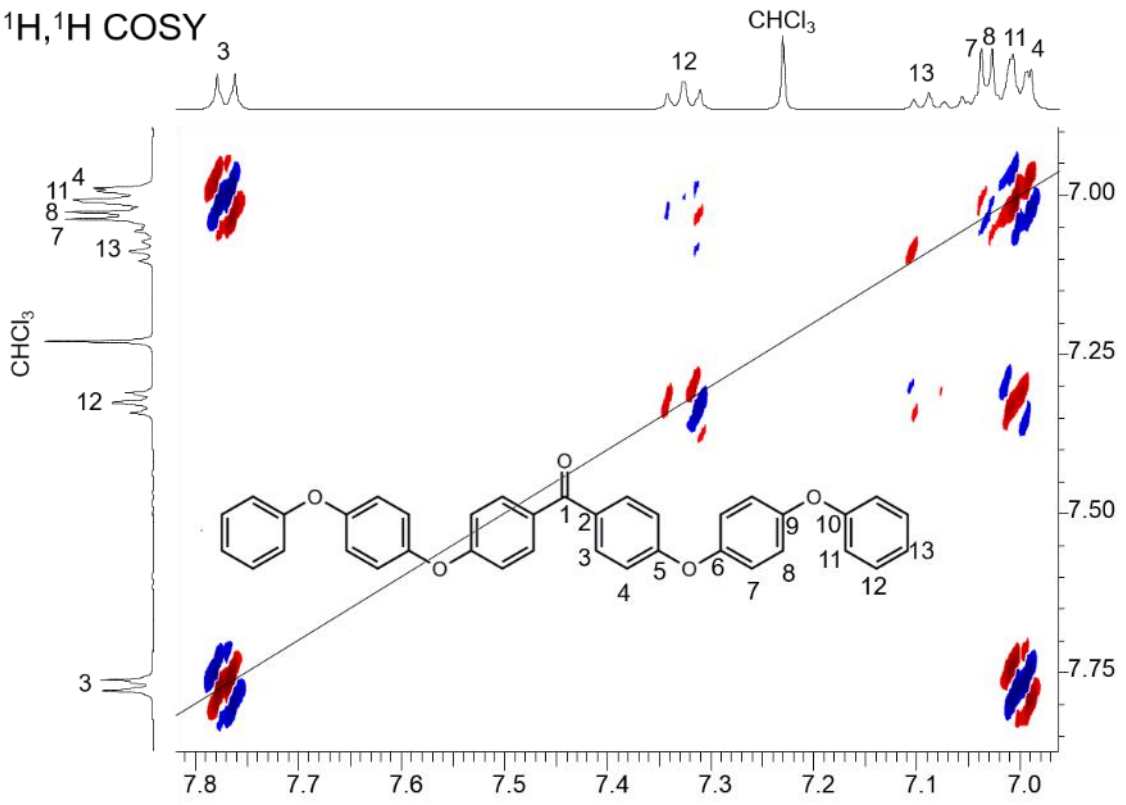
^{1}H,^{1}H COSY
CHCl$_3$
3
12
13
7
8
11
4
CHCl$_3$
7.00
7.25
7.50
7.75
7.8
7.7
7.6
7.5
7.4
7.3
7.2
7.1
7.0

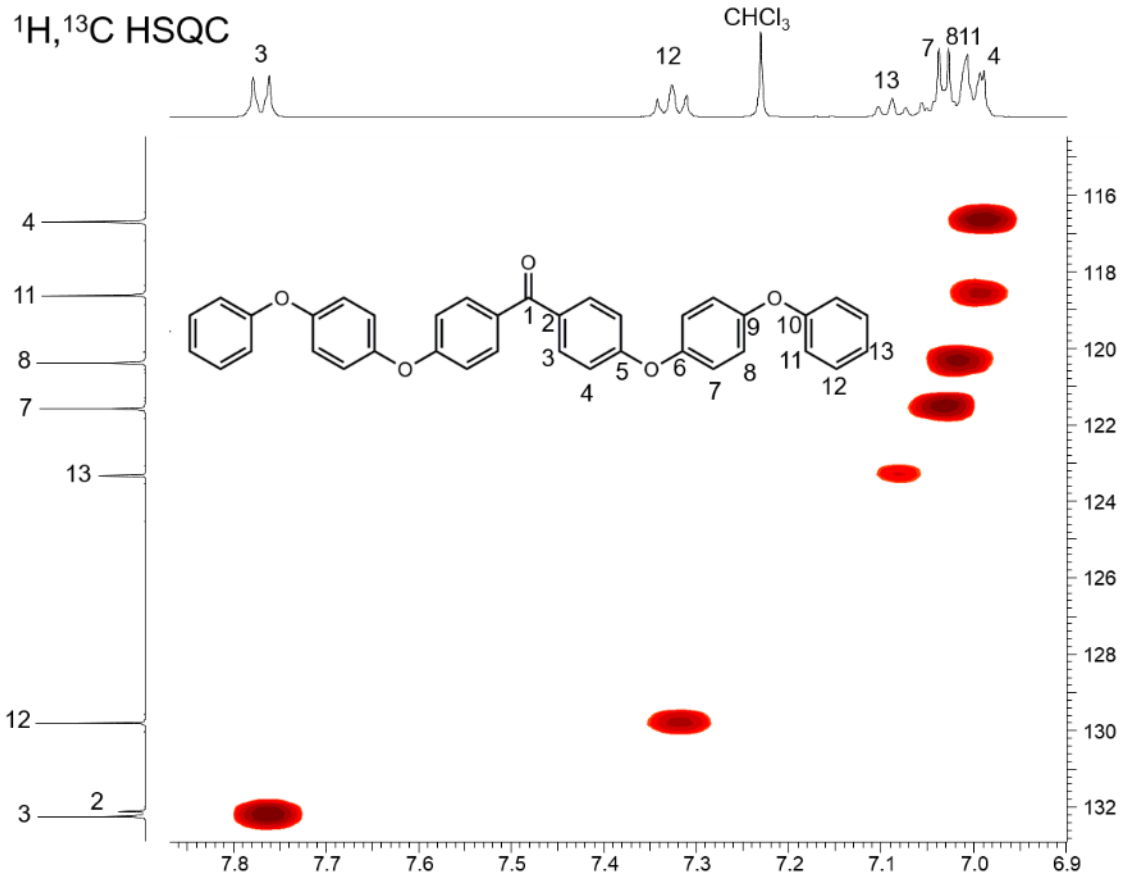
$^{1}H,^{13}C$ HSQC
CHCl3
3
12
13
7
8
11
4
4
11
8
7
13
12
3
2
116
118
120
122
124
126
128
130
132
7.8
7.7
7.6
7.5
7.4
7.3
7.2
7.1
7.0
6.9

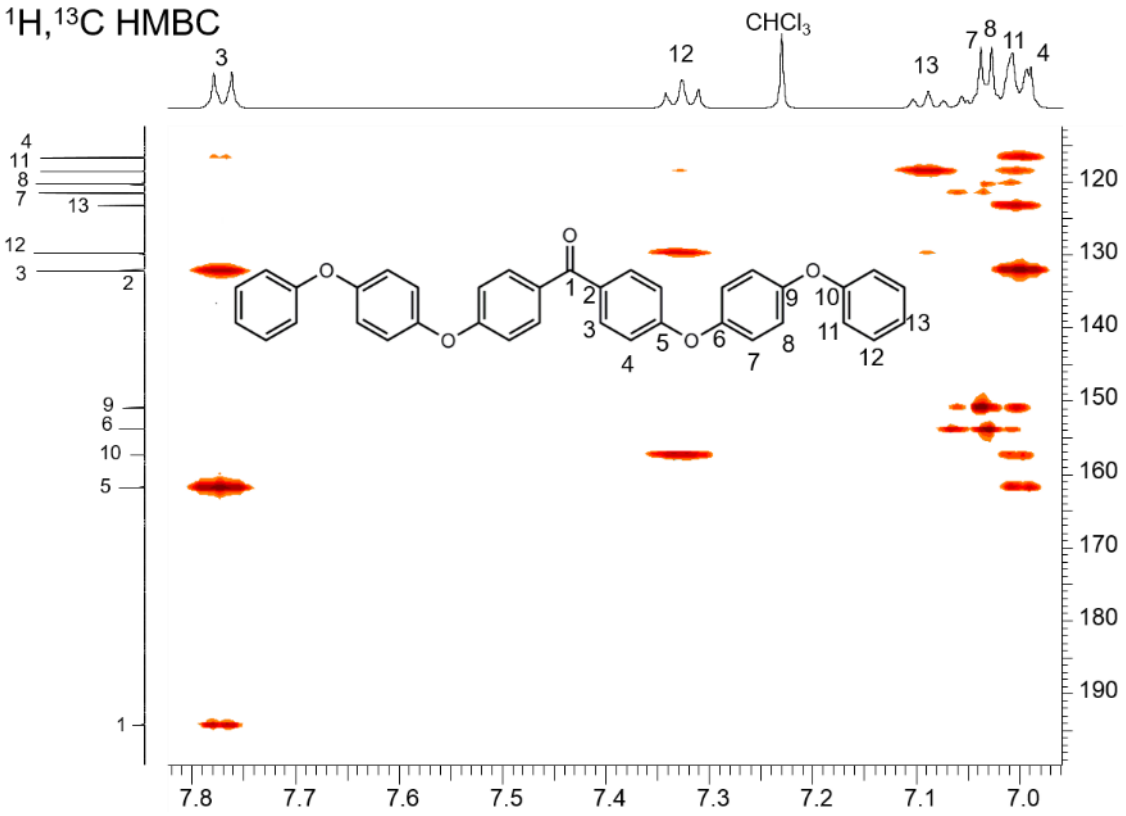

Bromo-PEEK ^{1}H NMR, ^{13}C NMR Signal Assignments

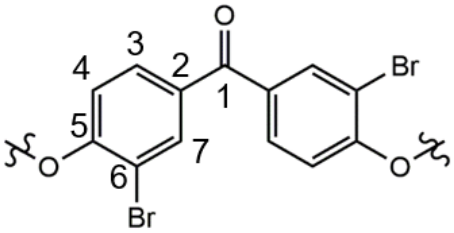

^{1}H NMR (500 MHz, $CDCl_3$): δ(ppm) 8.14 (H7); 7.70 (H3); 6.88 (H4). ^{13}C NMR (125 MHz, $CDCl_3$): δ (ppm) 191.1 (C1); 156.8 (C5); 135.9 (C7); 133.6 (C2); 130.8 (C3); 117.1 (C4); 113.5 (C6).

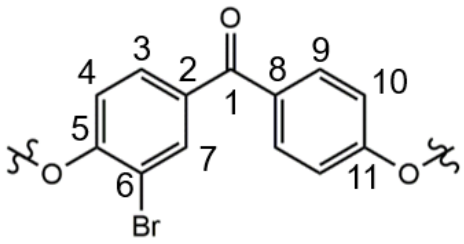

^{1}H NMR (500 MHz, $CDCl_3$): δ(ppm) 8.14 (H7); 7.86 (H9); 7.70 (H3); 7.06 (H10); 6.88 (H4). ^{13}C NMR (125 MHz, $CDCl_3$): δ (ppm) 192.5 (C1); 160.2 (C11); 156.8 (C5); 135.9 (C7); 133.6 (C2); 132.2 (C9); 132.2 (C8); 130.8 (C3); 117.1 (C4); 116.8 (C10); 113.5 (C6).

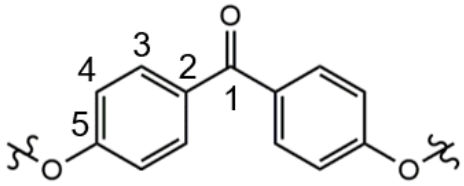

^{1}H NMR (500 MHz, $CDCl_3$): δ(ppm) 7.86 (H3); 7.06 (H4).^{13}C NMR (125 MHz, $CDCl_3$): δ (ppm) 193.8 (C1); 160.2 (C5); 132.2 (C3); 132.2 (C2); 116.8 (C4).

2D NMR Data for Bromo-PEEK

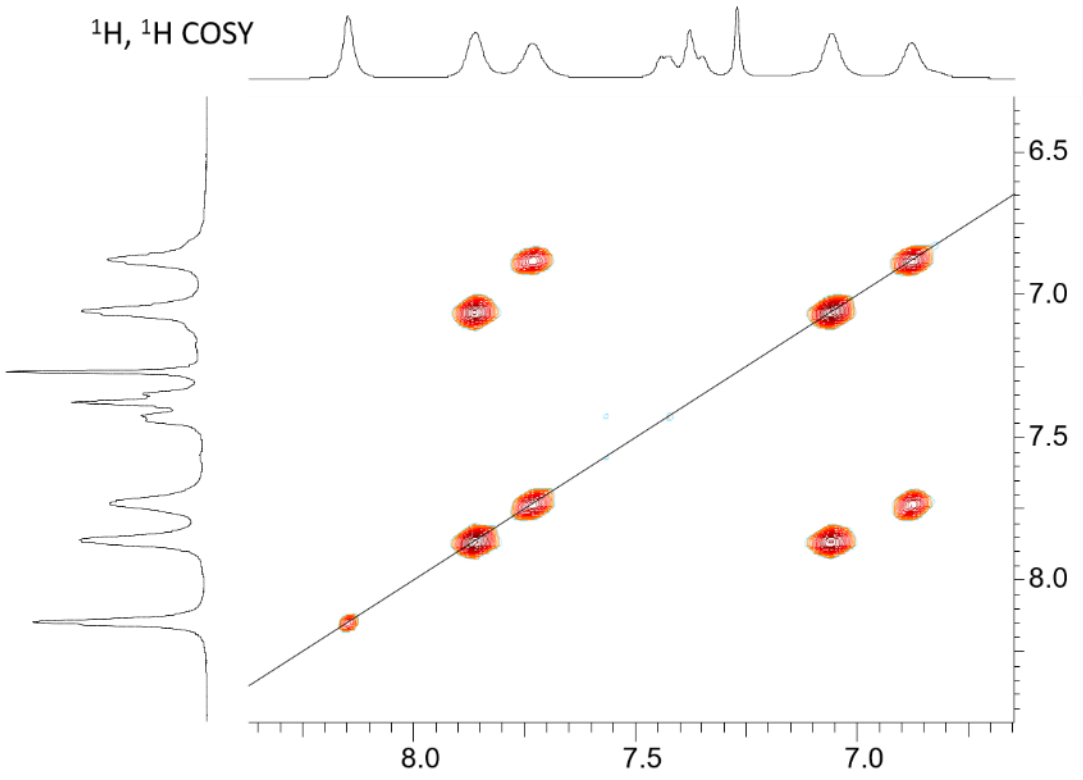

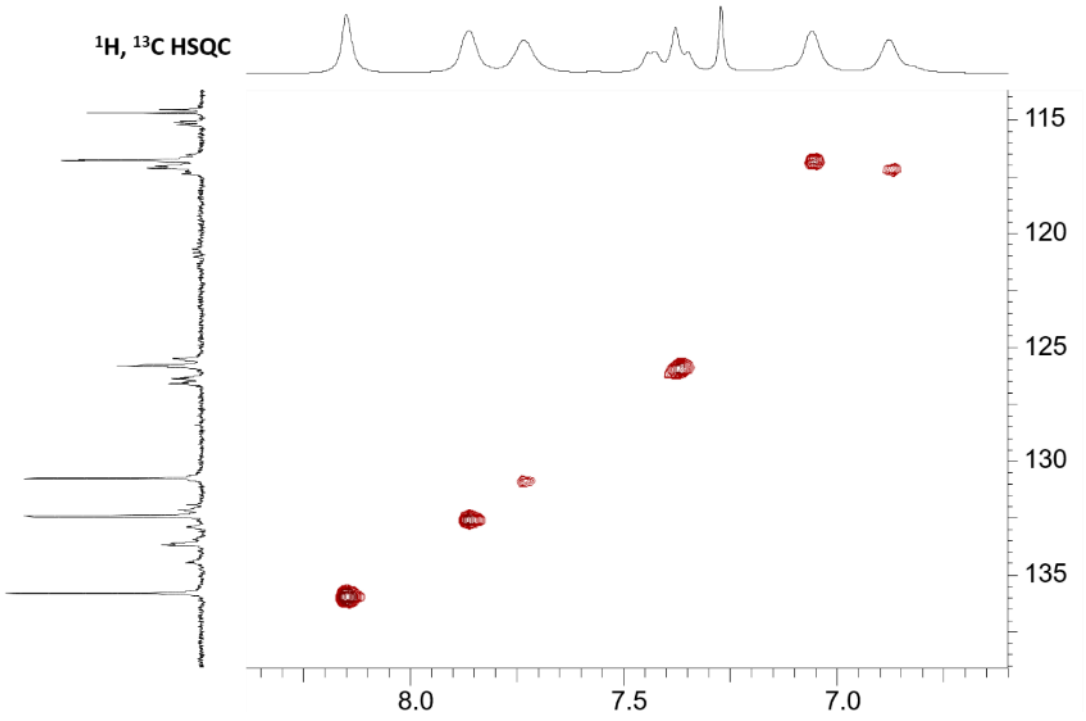
^{1}H, ^{13}C HSQC
115
120
125
130
135
8.0
7.5
7.0

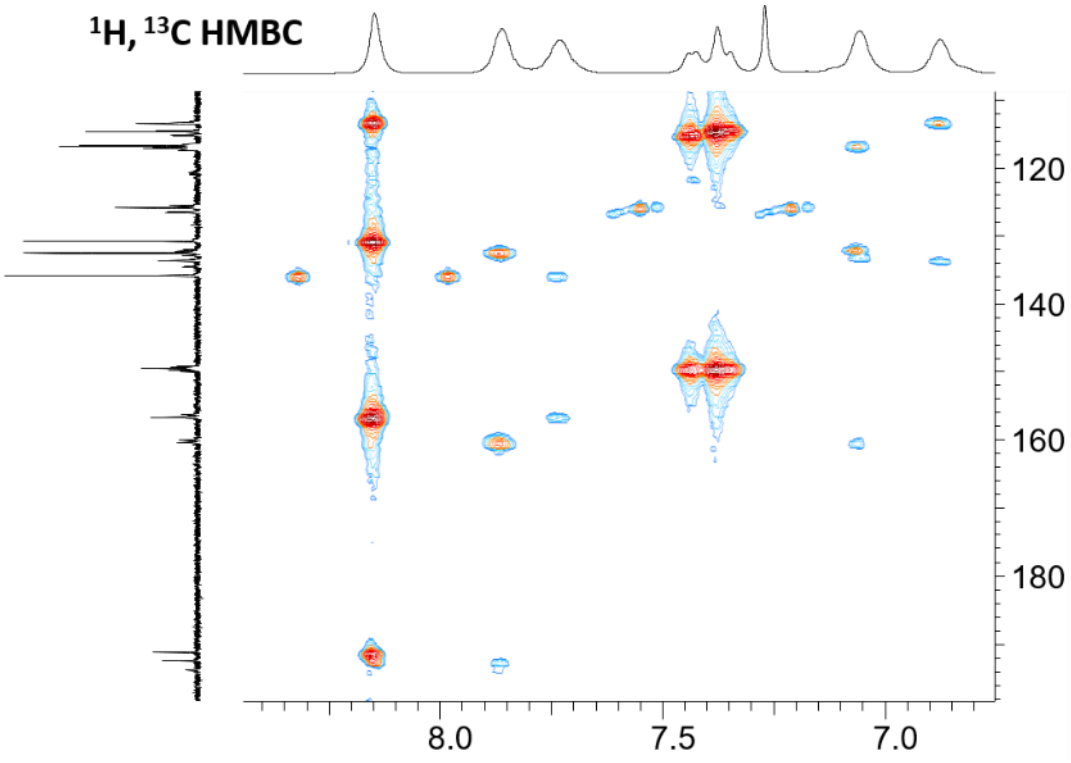
^{1}H, ^{13}C HMBC
120
140
160
180
8.0
7.5
7.0

APPENDIX C

SUPPLEMENTARY CHAPTER III

TGA of PEEK After Treatment in Different Fluids

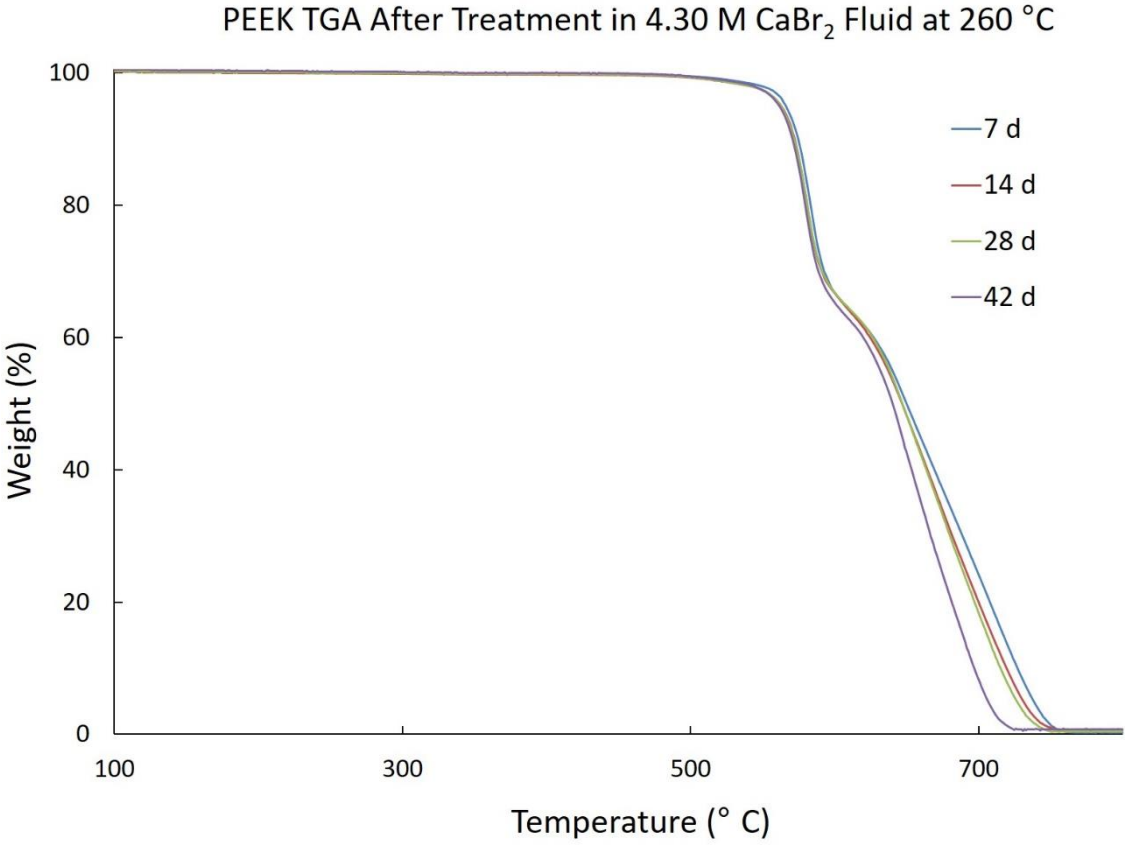

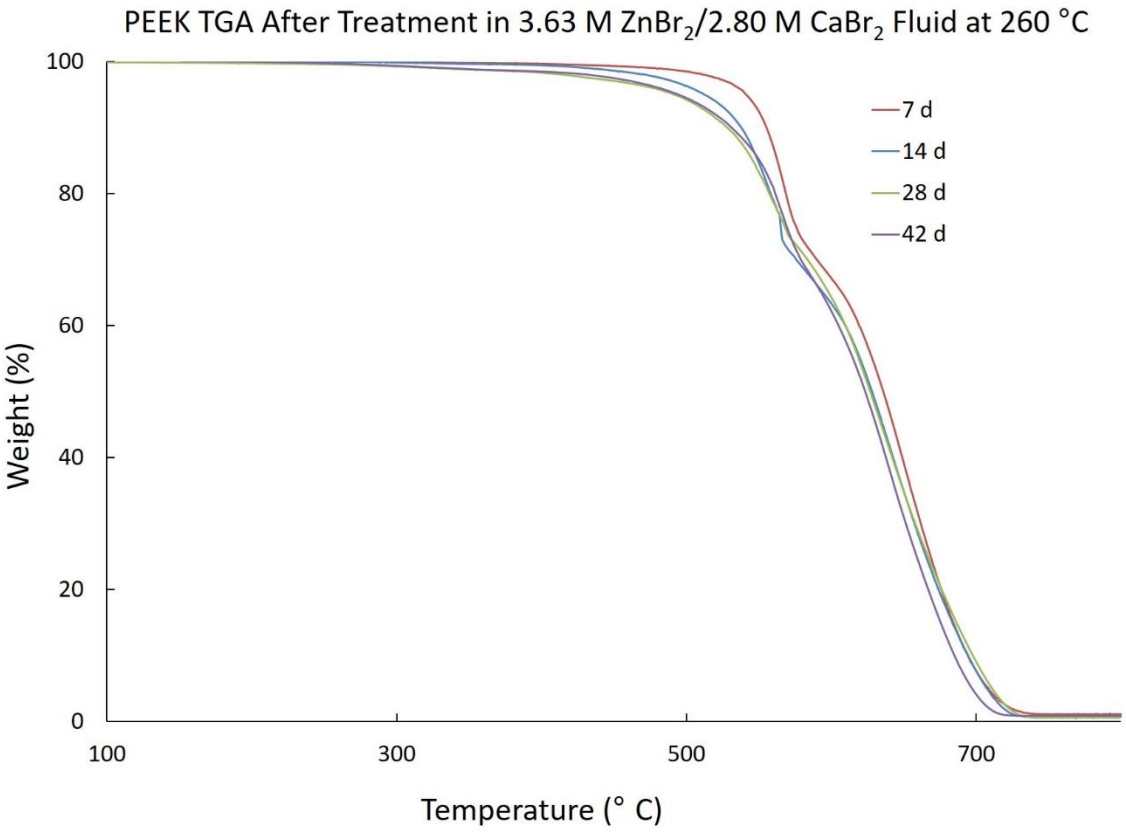
PEEK TGA After Treatment in 3.63 M ZnBr2/2.80 M CaBr2 Fluid at 260 °C
Weight (%)
100
80
60
40
20
0
100
300
500
700
Temperature (° C)
7 d
14 d
28 d
42 d

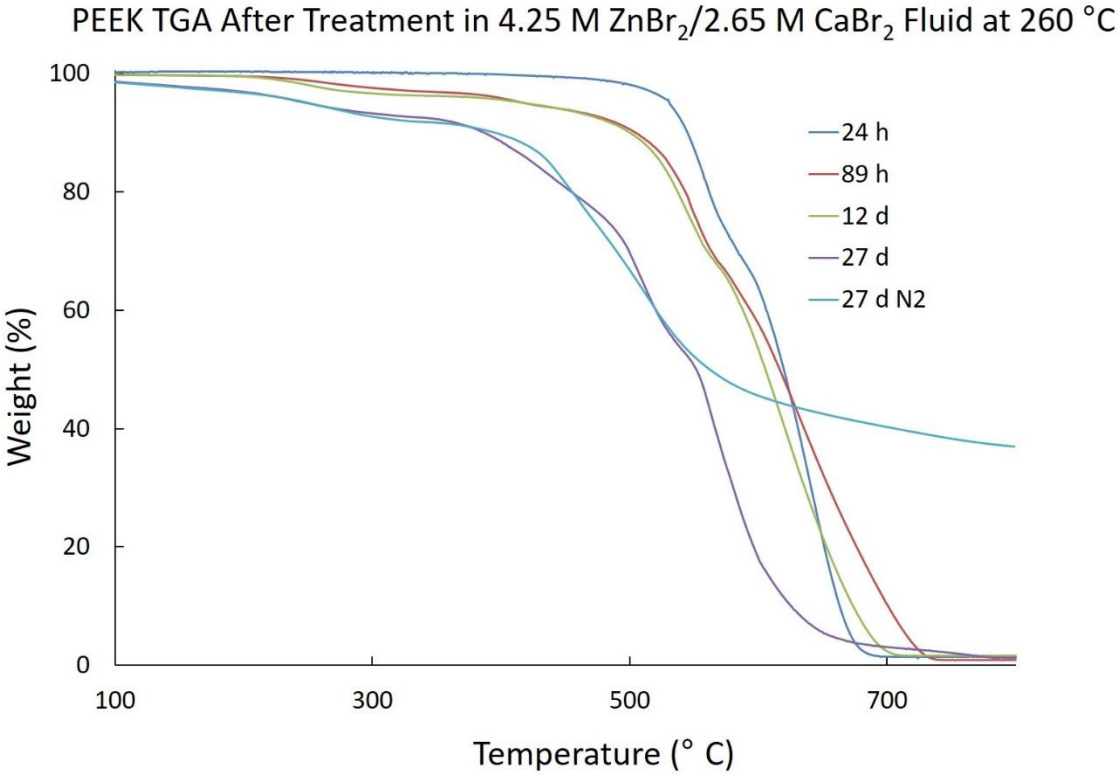

DSC of PEEK After Treatment in Different Fluids

Treatment Time	7 days	14 days	28 days	42 days
Completion Fluid	% Crystallinity Tm (°C)	% Crystallinity Tm (°C)	% Crystallinity Tm (°C)	% Crystallinity Tm (°C)
3.63 M $ZnBr_2$ 2.80 M $CaBr_2$	41.7 346.3	56.6 349.3	48.6 348.7	62.5 345.1
4.30 M $CaBr_2$	36.5 343.2	41.1 343.4	24.0 342.5	38.0 342.3

pH of Completion Fluid After Treatments at 260 °C

Treatment Time with PEEK 4.25 M $ZnBr_2$ / 2.65 M $CaBr_2$ Fluid	pH
Initial	1.29
24 h	1.22
89 h	1.32
12 d	1.33
27 d	1.47

Treatment Time with PEEK 4.09 $ZnBr_2$ / 2.69 M $CaBr_2$ Fluid	pH
Initial	1.37
21 h	1.34
89 h	1.38
11 d	1.44

Treatment Time with PEEK 3.63 $ZnBr_2$ / 2.80 M $CaBr_2$ Fluid	pH
As Received	1.98
7 d	2.14
14 d	2.06
28 d	2.10

Treatment Time with PEEK 4.30 M $CaBr_2$ Fluid	pH
Initial	7.17
7 d	4.46
14 d	4.82
28 d	4.89
42 d	4.66
63 d	5.77

Treatment Time No PEEK 4.30 M $CaBr_2$ Fluid	pH
Initial	7.17
4 d	4.29

NMR from Extraction of Fluid 1 after PEEK Treatment, 89 h, for Identification of Small Molecules

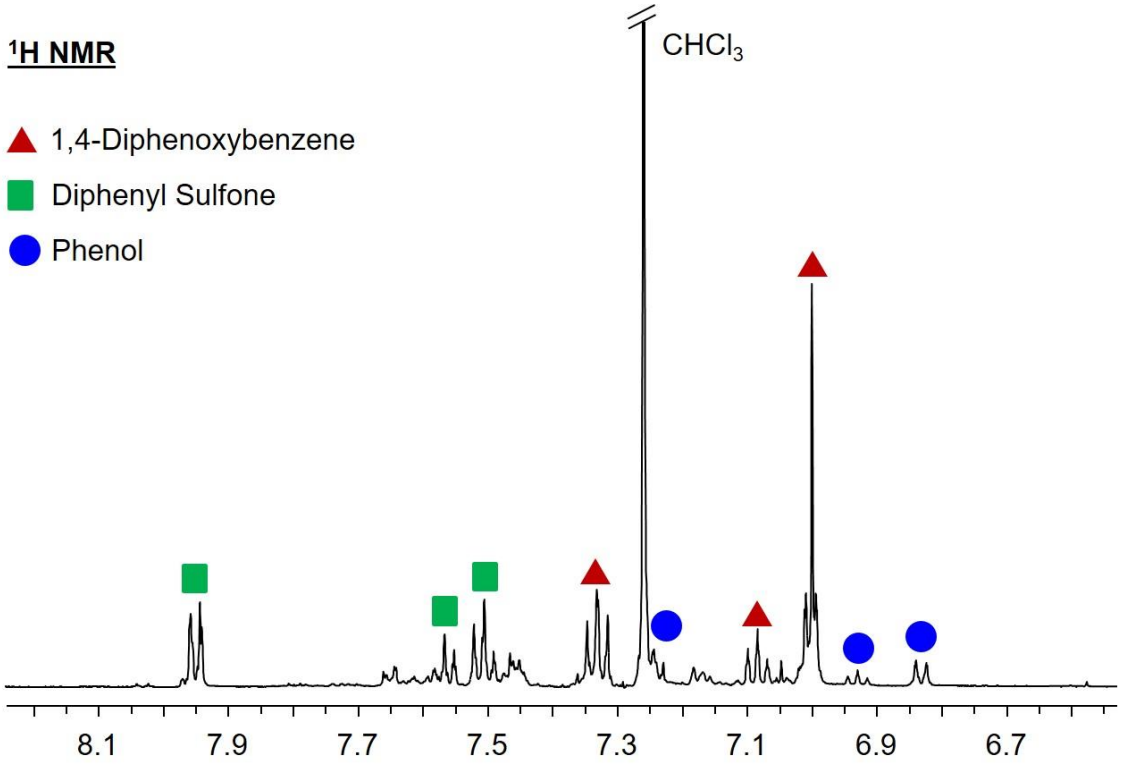

$^{1}H,^{1}H$ COSY

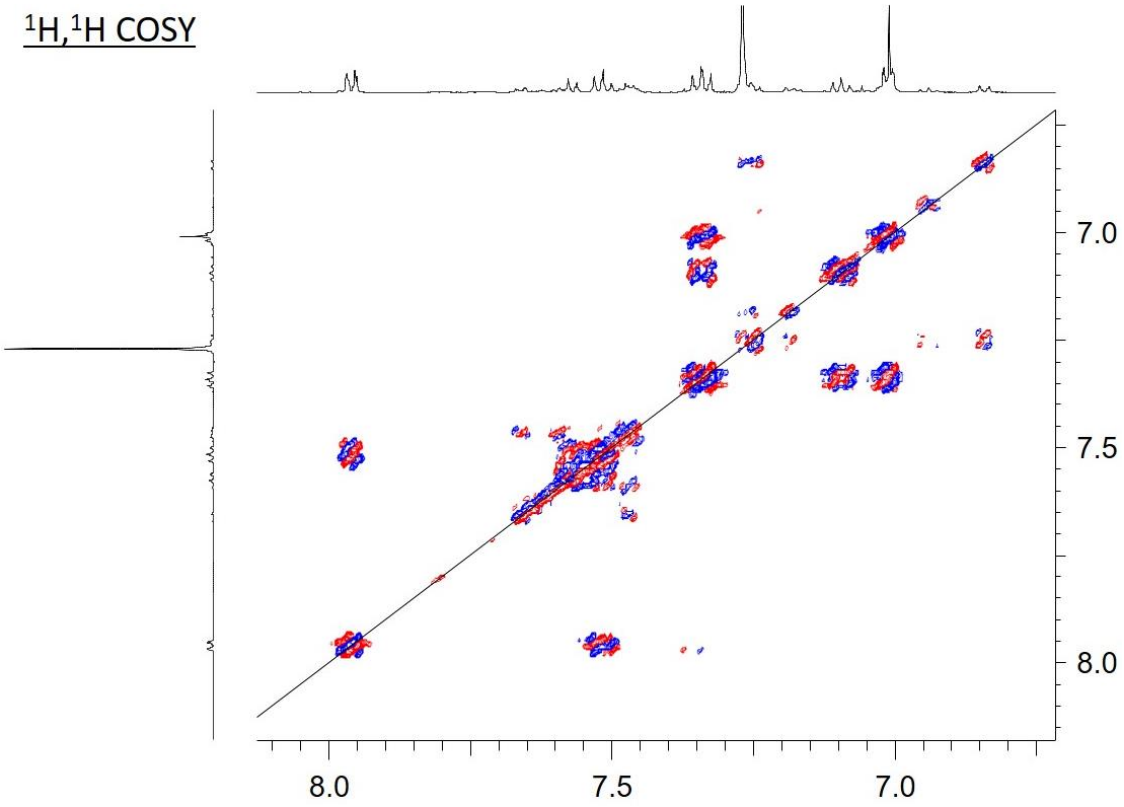

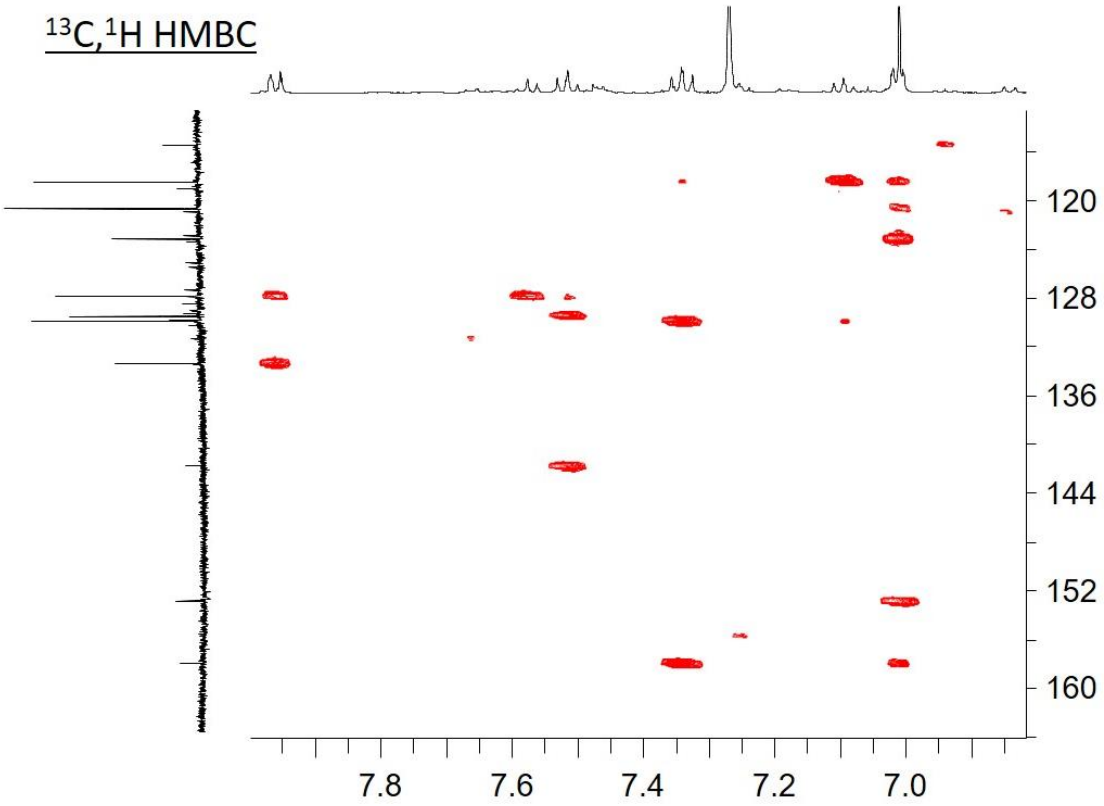
^{13}C,^{1}H HMBC
120
128
136
144
152
160
7.8
7.6
7.4
7.2
7.0